RICE UNIVERSITY

All-Conjugated Block Copolymers for Organic Photovoltaics

by

Yen-Hao Lin

A THESIS SUBMITTED
IN PARTIAL FULFILLMENT OF THE
REQUIREMENTS FOR THE DEGREE

Doctor of Philosophy

APPROVED, THESIS COMMITTEE

Rafael Verduzco, Assistant Professor
Chemical and Biomolecular Engineering

Michael S. Wong, Professor
Chemical and Biomolecular Engineering
and Chemistry

Andrew R. Barron
Charles W. Duncan, Jr. – Welch Chair of
Chemistry and Professor of Materials
Science and Nanoengineering

HOUSTON, TEXAS
May 2015

ABSTRACT

All-Conjugated Block Copolymers for Organic Photovoltaics

by

Yen-Hao Lin

Organic photovoltaics (OPVs) are a promising source of alternative energy due to cost effectiveness and process simplicity. However, the performance of OPVs must be improved to produce viable devices. This can be achieved by optimizing the optoelectronic properties of constituent materials, tuning the nanostructures of materials within active layer of OPVs and defining a well-defined interface between electron-donor materials and electron-acceptor materials. The above opportunities can potentially be addressed with using all-conjugated block copolymers in that self-assembly of block copolymers can lead to well-defined nanostructures driven by thermodynamics. The focus of this thesis is on the synthesis and development of all-conjugated block copolymers in which one block is an electron-donor polymer and the other is an electron-acceptor polymer. We focus primarily on poly(3-hexylthiophene) (P3HT)-based block copolymers in which the electron-donor P3HT is made from Grignard metathesis polymerization (GRIM) and the other block is synthesized by Suzuki-Miyaura polycondensation reaction for wide variety of electron-acceptor polymers. Subsequently, the nanostructures of polymers were studied on a model series of all-conjugated block copolymer: poly(3-hexylthiophene)—*block*—poly[2,7-(9′,9′-dioctyl-fluorene) (P3HT–*b*–PF) under different processing conditions with using differential scanning calorimetry (DSC) and grazing-incidence X-ray scattering (GIXS). This reveals strong process-structure-property relationships of all-conjugated block copolymers. Furthermore, using our two-step synthetic route, we prepared an all-conjugated block copolymer poly(3-

hexylthiophene)—*block*—poly[2,7-(9′,9′-dioctyl-fluorene)-*alt*-5,5-(4′,7′-di-2-thienyl-2′,1′,3′,-benzothiadiazole)] (P3HT–*b*–PFTBT) that exhibits over 3% PCEs as the active layer in a solution processed OPV due to the formation of lamellae of the block copolymers and preferential π-π stacking direction of the P3HT perpendicular to the substrate. In addition to covalently linked block copolymers, we applied a quadruple hydrogen group, 2-ureido-4[1H]-pyrimidinone (UPy), as polymeric end functionalities to reduce macro-phase separation in polymer blends. In the polymer blends OPVs comprised of P3HT and PFTBT, the UPy hydrogen bonding group reduces macro-phase separation in polymer blends and leads to improved power conversion efficiency of OPVs from 0.43% to 0.77% under 155 ^{o}C annealing condition. This thesis demonstrates that both the covalently linked and hydrogen bonding linked all-conjugated block copolymers are potential to enhance performance of OPVs. Furthermore, with the advancement in synthetic techniques and better understandings on structure-processing-property relationships of all-conjugated block copolymers, we are able to apply those into more emerging conjugated polymers and engineer molecules for efficient energy generation in OPVs.

Acknowledgments

I gratefully thank many people for support and guidance during my doctoral study. They are my thesis advisor, committee members, lab mates, collaborators from three National Laboratories, funding sources, friends and families. Their supports indeed make this thesis research accomplished.

I thank my thesis advisor Dr. Rafael Verduzco for his guidance and support. I am fortunate to be one of his first students at Rice. I learn a lot from him in hand-on experiments, writing and presentation skills and being a responsible researcher. The most important thing is his support and trust on research direction. Without these, I will not have these accomplishments.

I thank Professor Andrew R. Barron and Professor Michael S. Wong, for being my thesis committee members, contributing valuable perspectives and giving great scientific insights and inspiration from discussion with them.

All of my collaborators help me a lot in my thesis research with their technical support and scientific knowledge. I thank Dr. Kevin G. Yager, X-ray scientist at Brookhaven National Laboratory, and Dr. Joseph Strzalka, X-ray scientist at Argonne National Laboratory, for their abundant helps in X-ray experiments, data analyses and in-depth knowledge in X-ray physics. I thank Dr. Seth B. Darling, scientist at Argonne National Laboratory, for guidance in organic photovoltaics research. I thank Professor Enrique D. Gomez, professor at Pennsylvania State University, and his student Changhe Guo for supports in organic photovoltaics fabrication on our homemade polymers and achieve amazing results. I thank Dr. Aditya Mohite, scientist at Los Alamos National Laboratory, for offering me an opportunity to conduct researches for one year at Los

Alamos with his group, especially with Dr. Wanyi Nie, for coaching me electronics fabrication and electrical measurement.

I am lucky to work with such nice lab mates at Rice University, especially Kendall Smith, Aditya Agrawal, Xianyu Li and Stacy Pesek. I enjoyed a lot with working with these colleagues in discussing projects and building up best known methods for synthesis, testing and analysis.

Lastly, I truly thank my parents, Mr. Ruei-Sin Lin and Mrs. Yueh-Li Chen, my families for abundant cares and support, and all of my friends whom I've met with. Without the above mentioned people, I will not be able to reach this point and keep moving forward.

Contents

List of Figures

List of Tables

List of Equations

Nomenclatures

PV	Photovoltaic
OPV	Organic Photovoltaic
PCE	Power Conversion Efficiency
TW	Terawatts
DSSC	Dye-Sensitized Solar Cell
OFET	Organic Field-Effect Transistor
OLED	Organic Light Emitting Diode
TFT	Thin Film Transistor
HOMO	Highest Occupied Molecular Orbital
LUMO	Lowest Unoccupied Molecular Orbital
P3HT	Poly(3-hexylthiophene)
P3AT	Poly(3-alkylthiophene)
PF	Poly(9′,9′-dioctylfluorene)
BHJ	Bulk Heterojunction
ITO	Indium-Tin Oxide
V_{oc}	Open Circuit Voltage
Jsc	Short Circuit Current Density
FF	Fill Factor
EQE	External Quantum Efficiency
PCE	Power Conversion Efficiency
PCBM	Phenyl-C61-Butyric Acid Methyl Ester
GRIM	Grignard Metathesis
SEC	Size-Exclusion Chromatography
RI	Refractive Index
UV-VIS	Ultraviolet-Visible
PDI	Polydispersities
M_w	Weight average molecular weights
NMR	Nuclear Magnetic Resonance Spectroscopy

XRD	X-ray Diffraction
GIXS	Grazing-Incidence X-ray Scattering
DSC	Differential Scanning Calorimetry
POM	Polarized Optical Microscopy
PEDOT:PSS	Poly(3,4-ethylenedioxythiophene):poly(styrenesulfonate)
NEXAFS	Near-Edge X-ray Absorption Fine Structure
RSOXS	Resonant Soft X-ray Scattering
UPy	2-ureido-4[1H]-pyrimidinone
AFM	Atomic Force Microscopy
FTIR	Fourier Transform Infrared
IS	Impedance Spectroscopy
CV	Cyclic Voltammetery
PL	Photoluminescence
TA	Transient Absorption

Chapter 1

Introduction

1.1. Background

The present energy consumption heavily relies on fossil-based energies like coal, natural gas and petroleum. Renewable energy provides an alternative energy to fossil-based energy to reduce greenhouse gas and air pollutant emissions, create sustainable energy sources and meet growing demand in energy. The renewable sources including solar, wind, hydropower, biomass and geothermal energy presently contributed about 10% of total power supply in U.S.[1] Solar energy is one of the abundant energy resources that it reaches earth with energy about 120,000 TW. It is the energy much greater than world's energy consumption in a year (about 28 TW in 2012).[2,3] To collect endless energy from solar energy, different types of photovoltaics (PVs) have been developed over decades to improve the power conversion efficiency (PCE) and the records of PCEs of different PVs are summarized in Figure 1.1.

Among different PVs with various PCEs, although high efficiency multijunction cells (*eg.* InGaP/GaAs/InGaAs) have PCE up to 44%, silicon-based PVs still dominate the regular market with three major types: monocrystalline, polycrystalline and amorphous with record performance of 27.6%, 20.4% and 13.4%, respectively. However,

performance is not the only driving force for PV technologies in terms of cost-effectiveness. In addition to amorphous silicon solar cell, other relatively low cost PVs[4] manufactured from thin film technology such as copper-indium-gallium-diselenide (CIGS),[5] cadmium telluride (CdTe),[6] dye-sensitized solar cell (DSSC),[7] and organic photovoltaics (OPVs),[8] the last one being the subject in this thesis.

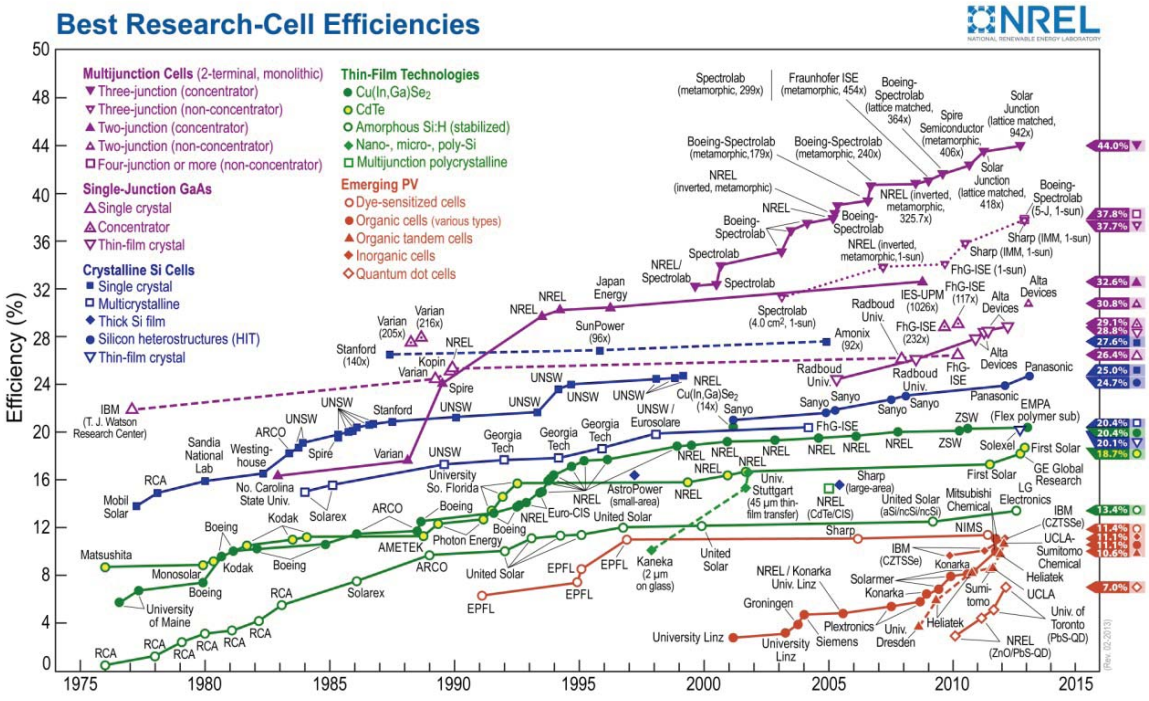

Figure 1.1 – Chart of best power conversion efficiencies in different PV technoligies, adapted from National Renewable Energy Laboratory.

Extensive research is required to pursue better performance with good stability of OPVs for low cost energy with great impact to society. In this thesis new types of polymers as known as conjugated polymers and all-conjugated block copolymers that one block is an electron donor polymer whereas the other one is an electron acceptor polymer

for OPVs are developed and their optical and thermal properties and the influences to OPVs are also investigated.

1.2. Conjugated polymers

Conjugated polymers have received enormous attention since their discovery in the late 70s, recognized by the Nobel Prize in Chemistry awarded in 2000.[9] Conjugated polymers are currently being investigated for organic electronic applications due to the electrical conductivity and optoelectrical properties, including field-effect transistors (OFETs),[10-13] light emitting diodes (OLEDs),[14-19] and photovoltaics (OPVs),[20-23] sensors,[24,25] and electrochromic devices[26] and they offer potentially low-cost solution processing strategies other benefits such as flexibility and transparency which are challenging to achieve in inorganic materials.[27-29]

The π-conjugated system in polymers offers unique physical properties to polymers and enables charge transport, electroluminescence and optical absorption.[30,31] The charge transporting property makes conjugated polymer be a suitable candidate for the semi-conductive layer between source and drain in thin film transistor (TFT) devices as an example shown in Figure 1.2(a). Upon applying voltage/electrical field via a metallic gate in the device (U_G), the conductivity of a conjugated polymer changes when the drain voltage (U_D) is greater than threshold voltage. The conjugated polymer can transport either electron or hole depending on its lowest unoccupied molecular orbital (LUMO) and highest occupied molecular orbital (HOMO) energy levels relative to the contact as described in Figure 1.2(b). OFET was first described in 1987 with a conjugated polymer poly(3-hexylthiophene) (P3HT) as a p-type (hole conducting) channel with mobility 2×10^{-5} $cm^2V^{-1}s^{-1}$ extracted from the slope of drain current versus drain voltage curve in saturation region (Figure 1.2(c)).[32,33] With further understanding in poly(3-

alkylthiophene) (P3AT) molecular weight dependent crystallinity, side-chain effect and nanostructure orientation, the mobility on P3HT can be pushed up to 0.1 $cm^2V^{-1}s^{-1}$. [34-38]

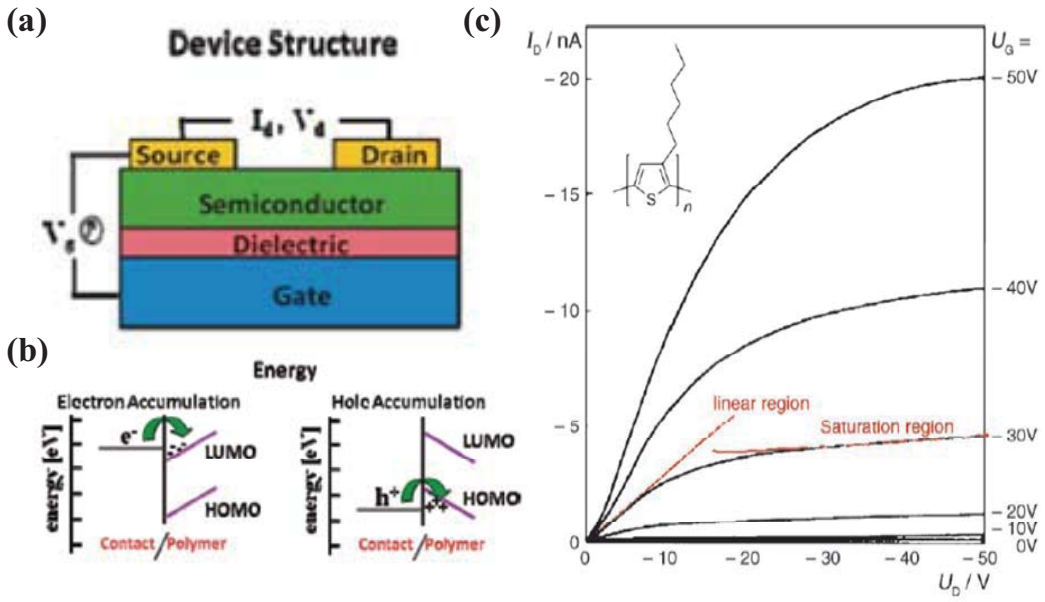

Figure 1.2 – (a) Scheme of a bottom-gate top-contact OFET,[13] (b) energy level of contact-polymer for representing charge transport between contact and polymer,[13] (c) Output characteristics plot an OFET device made from P3HT as semiconductive layler where the polymer is hole conductive.[32,33]

Although some other small organic molecules such as pentacene (5 $cm^2V^{-1}s^{-1}$)[39] already surpass the amorphous silicon TFT mobility of 0.5~1 $cm^2V^{-1}s^{-1}$, conjugated polymers are still competitive to amorphous silicon TFT with hole mobility up to 0.72 $cm^2V^{-1}s^{-1}$ from poly[2,5-bis(3-alkylthiophene-2-yl)thieno[3,2-b]thiophene] (PBTTT) (chemical structure is shown in Figure 1.3) as a p-channel polymer.[40,41] Several other conjugated polymers such as carbazole-based p-channel poly(indolo[3,2-*b*]carbazole-3,9-diyl) (PCB)[42] with hole mobility of 0.02 $cm^2V^{-1}s^{-1}$, thiophene-based p-channel poly(2,5-bis(thiophene-2-yl)-(3,7-ditridecanyltetrathienoacene) (P2TDC13FT4)[43] with hole mobility of 0.33 $cm^2V^{-1}s^{-1}$ have been developed. In addition, the first n-channel (electron

conductive) polymer poly(benzobisimidazobenzophenanthroline) (BBL)[44] with electron mobility 0.1 $cm^2V^{-1}s^{-1}$, BBL corresponding n-channel polymer BBB[44] with electron mobility 10^{-6} $cm^2V^{-1}s^{-1}$ and poly(*N,N'*-dialkylnaphthalenedicarboximidedithiophene) P(NDI2OD-T2)[45,46] with electron mobility 0.45~0.85 $cm^2V^{-1}s^{-1}$. The chemical structures for above conjugated polymers with the hole/electron mobility are provided in Figure 1.3. The details of these polymers can be found in the corresponding references.

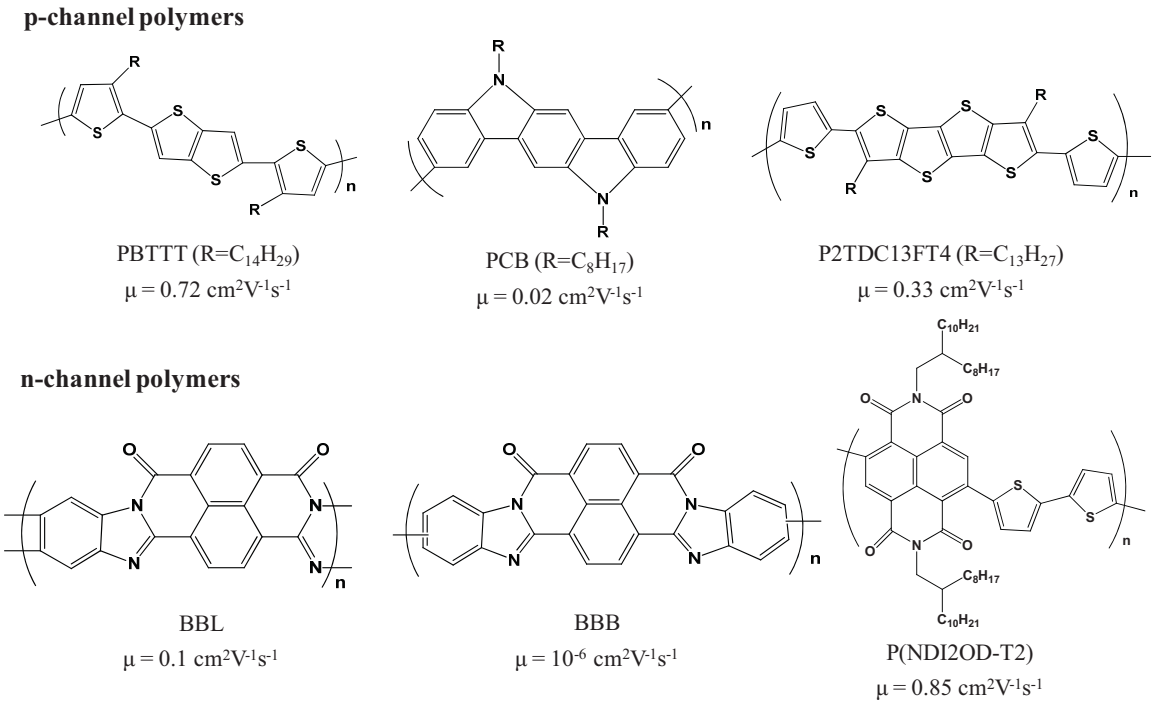

Figure 1.3 – Chemical structure of the p-channel and n-channel conjugated polymers and the reported hole/electron mobility.

In addition to the charge transporting property, conjugated polymers can be used in OLEDs for electroluminescence and OPVs for optical absorption and charge generation by incorporating two materials with compatible HOMO/LUMO levels as schemed in Figure 1.4(a) and Figure 1.4(b), respectively. In an OLED device (shown in

Figure 1.5(a)), the light is generated by excitation of electric current which is injected from electrodes and recombine in conjugated polymers. The electroluminescent characteristics of conjugated polymers directly decide the emitting wavelengths from the devices.[47] A few examples of conjugated polymers such as poly(9′,9′-dioctylfluorene) (PF)[48] and poly[2-methoxy-5-(2′-ethylhexyloxy)-*p*-phenylenevinylene] (MEH−PPV)[49] implemented in OLED and their emitting wavelengths are shown in Figure 1.5(b). Further material developments, processing and device structures are also important to improve the performance of OLED. Nonetheless, these will not be discussed in this thesis while conjugated polymers for OPVs are our focus and it will be separately discussed in the next section.

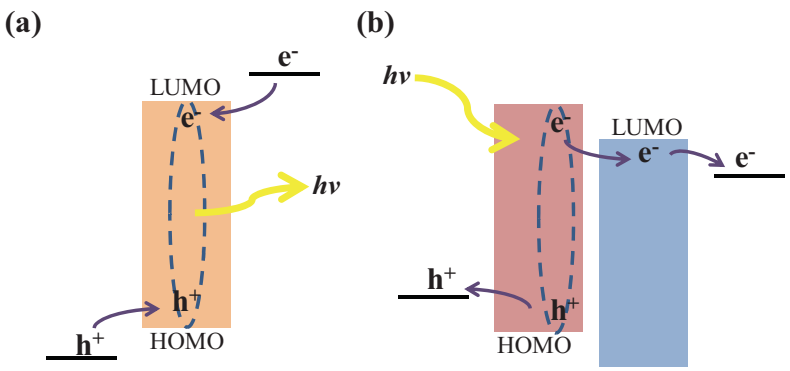

Figure 1.4 – (a) Representative energy diagram for an OLED that electron and hole recombine within a material after electron and hole are injected from cathode and anode, respectively. (b) Representative energy diagram for an OPV that an electron-hole pair is generated in an electorn-donor material upon photon excitation and after charge separation the electron transports through a electron-acceptor material to cathode while hole transports to anode.

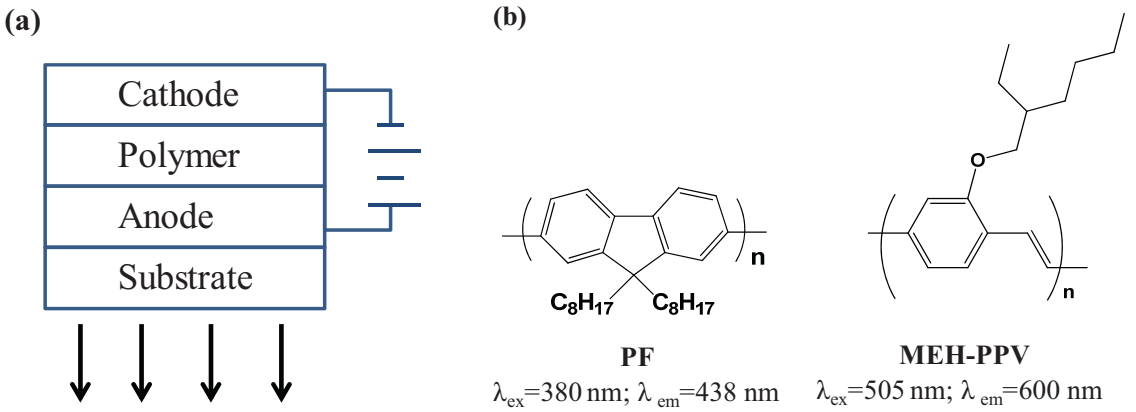

Figure 1.5 – (a) The basic structure of an OLED and (b) examples of conjugated polymers, PF and MEH-PPV and, for OLED with their emitting wavelength.

1.3. Organic photovoltaics (OPVs)

The need of renewable, environment-friendly and cheaper energy resources drives research for low-cost organic photovoltaic devices. Polymer-based solar cells represent potentially inexpensive and easily processible materials for converting light into electricity. OPVs have superior properties over silicon–based solar cells such as cheap synthetic materials, roll-to-roll process in thin film devices, and broad light absorption wavelength via combining several conjugated polymers,[20,50] The photo-conversion efficiency of organic solar cells has remarkable increase in recent years with reported certified efficiency values of up to 12% achieved by Heliatek and 8.4% for fullerene-free OPV.[51] This increase over decade has relied on understanding of synthetic discoveries, underlying physics, cell structures, and morphological improvement. Nonetheless, more works are needed to make OPVs viable for practical applications. In this section we give an overview on the device structure, process converting ray into electricity, optimization consideration, and obstacles that we have targeted to solve.

1.3.1. OPV device architectures and mechanism

Organic photovoltaics are made by depositing one of more semi-conductive organic molecules, oligomers, or polymers in a thin film (around 100 nm) between anode and cathode electrodes as depicted in Figure 1.6 for four different architectures of OPVs. Examples for these four device architectures will be discussed in the following paragraphs. The 100 nm thickness of organic solar cells is about 1,000 times thinner than that of crystalline silicon solar cells and roughly 10 times thinner than that in inorganic thin film cells.[52] Large area of polymer thin films can be deposited quickly and cheaply by spin-coating, screen-coating, spray coating, and ink jet printing, significantly reducing processing cost and guaranteeing thin, flexible devices.

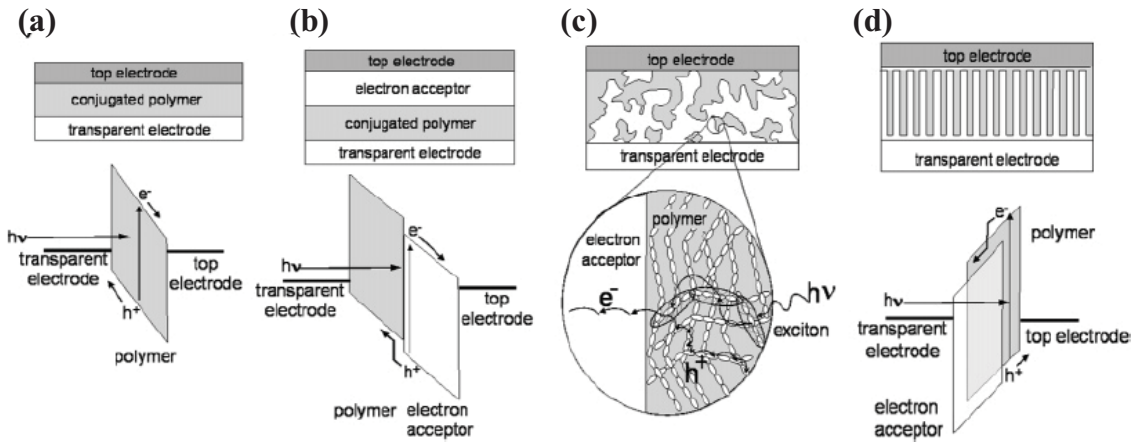

Figure 1.6 – Device architectures for OPVs: (a) single layer OPV, (b) bilayer heterojunction, (c) bulk heterojunction (BHJ) and (d) ordered bulk heterojunction.[53]

The function of conjugated polymers in active layer of devices involves four steps (as shown in Figure 1.7): (i) photon absorption by the active layer and exiton generation, (ii) exciton transportation to the interface of donor and acceptor, (iii) charge separation, (iv) transportation of charges to corresponding electrodes. Organic semiconductors have large absorption coefficient.[20] Thus an active layer of thickness around 100 nm is sufficient to absorb all the light at their peak absorption wavelength. A characteristic domain size about 10~20 nm is desired due to the penetration length of exiton.[52]

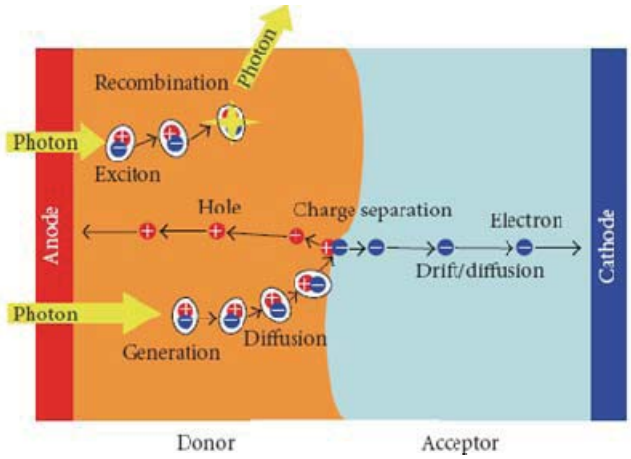

Figure 1.7 – Principle of charge separation in a solar cell.[52]

One of the first reported conjugated polymers for OPVs used poly(phenylene vinylene) (PPV) as the active layer sandwiched between indium-tin oxide (ITO) and metal for single layer OPV architecture.[54] This produced an open circuit voltage (V_{oc}) between 1.2V and 1.7 V depending on the metal used. However, the extremely low photocurrent with around 0.1 to 1% external quantum efficiency (EQE) which may attribute from the recombination of electron and hole after photon excitation. The importance of combining two distinct organic semiconductors in the active layer was recognized in 1986 with using bi-layer structures (Figure 1.6.(b)) and gives relatively high performance ~ 1%.[55] OPVs that combine an electron donor with an electron acceptor exhibit significant improved performance compared with OPVs with only one organic semiconductor. The direction of change transportation toward electrodes can be guaranteed in bi-layer structures and reduce the chances of charge recombination. However, the interfacial area between donor and acceptor materials is limited in bi-layer architecture, and the interfacial area plays an important role in separating excited state into positive and negative charges.[56,57]

Bulk heterojunction (BHJ) solar cells were developed to increase the interfacial area between donor and acceptor materials. In a BHJ architecture (Figure 1.6(c)) both electron donor and electron acceptor materials are uniformly mixed through the active layer, leading to a much larger interfacial area distributed through entire active layer. BHJ architectures were also considered to reduce the travel distance for excitons to reach charge separation interfaces.[58] The pathway for transporting hole and electron are demanded in that the separated charges can rapidly reach corresponding electrodes before recombination happens[50] Hence, an ideal type of BHJ has been proposed as shown in Figure 1.6.(d) with an average length scale of 10~20 nm equal to or less than the exciton diffusion length. This can possibly be achieved through self-assembly of block copolymers[59] and inorganic template nanostructures filled with organic materials[60] Our goal on BHJ solar cells is to prepare all-conjugated block copolymers and optimize morphologies under different processing conditions to understand the nanostructure dependent properties of materials and the resulting OPV device performance.

1.3.2. Performance parameters of OPVs

The current-voltage plot can be used to extract important information of photovoltaic devices. The power conversion efficiency (PCE, η_p) of a solar cell is defined as the ratio between the maximum deliverable electrical power $(V_m \times J_m)$ to the incident light power (P_{inc}), as well as in terms of the relevant parameters derived from the current–voltage plot (Figure1.8.). The η_p can be incorporated with three parameters of the short-circuit current density (J_{sc}), the open circuit voltage (V_{OC}), and fill factor (FF) for substitution of the current and voltage at the maximum power point (J_m and V_m, respectively).

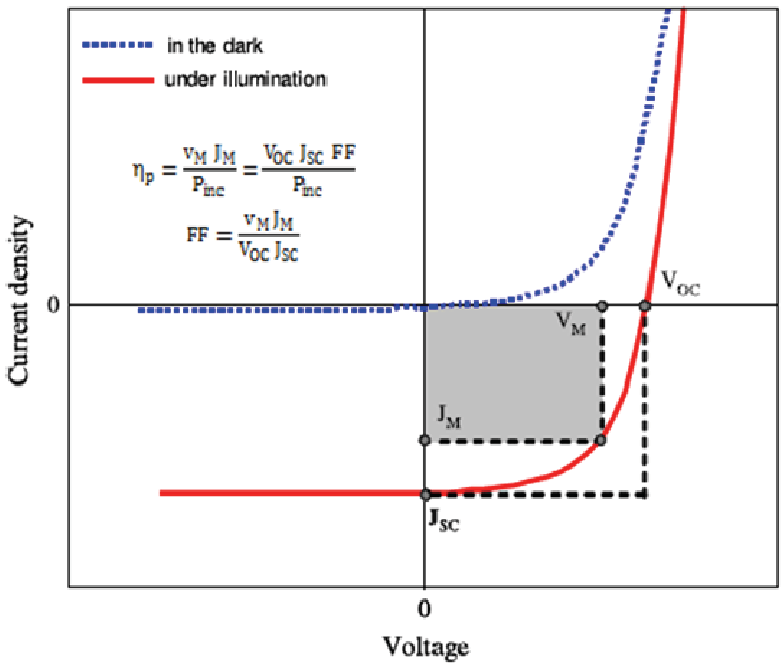

Figure 1.8 – Typical current–voltage characteristics for dark and light current in a solar cell. Embended equations are for calculation of power efficiency (η_p) conversion and fill factor (FF).[50]

1.3.3. Improving OPVs from material developments

A prototypical BHJ OPVs system of P3HT:PCBM (PCBM stands for phenyl-C61-butyric acid methyl ester) has been explored for the last decade.[61,62] The performance in these devices is almost optimal. For pursuing better efficiency of organic solar cell, the research on new materials is necessary. All-polymer solar cells in which n-type conjugated polymer is used as electron acceptor instead of fullerene show some advantages such as high absorption coefficient in the visible light region and tunable energy level owing to structural variety[63] The solar spectrum under AM 1.5 conditions (the sun being at 45^o above the horizon) is depicted in Figure 1.9. The photon flux is important in determining the number of electrons generated from solar cells. P3HT which

only absorb light at wavelength about 450 nm and most of photon flux is at wavelength above 500 nm. A common strategy to improve efficiency of OPV is to use low band gap polymers. Above 40% of photons from sun can be harvested while the absorption band of donor or donor-acceptor blend can extend the range of 350-826 nm[50,64] The enhancement of light absorption incorporated with well-defined nanostructures in active layer is considered to be the key toward higher efficiency.

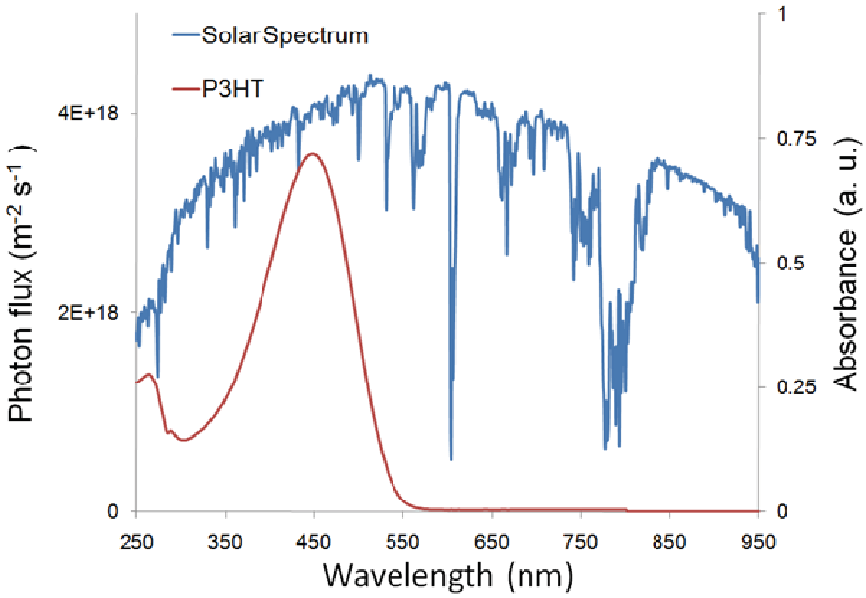

Figure 1.9 – Photon flux as function of wavelength with the example of P3HT UV-VIS absorbance as function of wavelength.

In addition, the fluorene based conjugated polymers as active materials in electronic devices become attractive due to tunable optoelectronic properties depending on chemical structures.[65] Polyfluorene is a wide bandgap material with good photo-fluorescence in blue region. The choice of co-monomer unit can determine the bandgap, HOMO and LUMO levels in materials. The candidates of co-monomers are generally the

materials emitting fluorescence colors at spectrum position higher than 500 nm as depicted in Figure 1.10. Several OPV researches have been conducted with using these fluorene based copolymers mixing with PCBM for improving OPV performance such as Bis-EH-PFDTBT[66] and PCDTBT.[67]

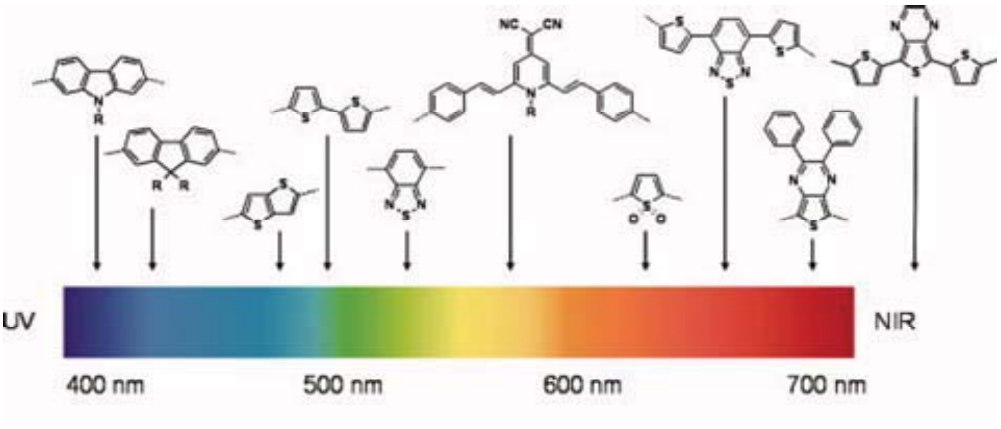

Figure 1.10 – Position of the fluorescence colors of several fluorene co-monomers in the visible spectrum.[65]

In addition to broadening light wavelength absorption, the use of low-bandgap polymers serving as n-type materials have potential to achieve larger V_{oc} (>1 V) while incorporating with p-type polymers such as P3HT. In this thesis research, we synthesized several fluorene-based copolymers which will be electron acceptor materials and be compatible with the energy levels of P3HT. Then, optimization of the nanostructures of these all-conjugated block copolymers will be the next task.

1.3.4. Improving OPVs from morphology of the active layer

The morphology in the active layer of BHJ OPVs is one of the key factors leading to efficient performance. A schematic for BHJ OPVs consisting of both conjugated polymer and fullerene is shown in Figure 1.11(left). In general, the final structure of

active layer is a result of various non-equilibrium processes, including polymer crystallization and phase separation that occur during film casting and annealing.[68,69] A variety of methods have been implemented to control the length scale interface structure and crystallinity of the active layers including the use of processing additives[70-72] and top-down approaches to patterning.[73-75] For OPVs that comprised of all polymers, the morphology and the optimization of devices have been studied by means of composition,[76] casting solvents,[77] annealing temperatures,[78] nanoimprint lithography[73] and block copolymer self-assembly,[59,79,80] Although all-conjugated block copolymers with p- and n- type blocks are considered an effective way to achieve optimal structures and superior performance, the simplicity of using polymer blends is still widely studied.[77,78,81,82]

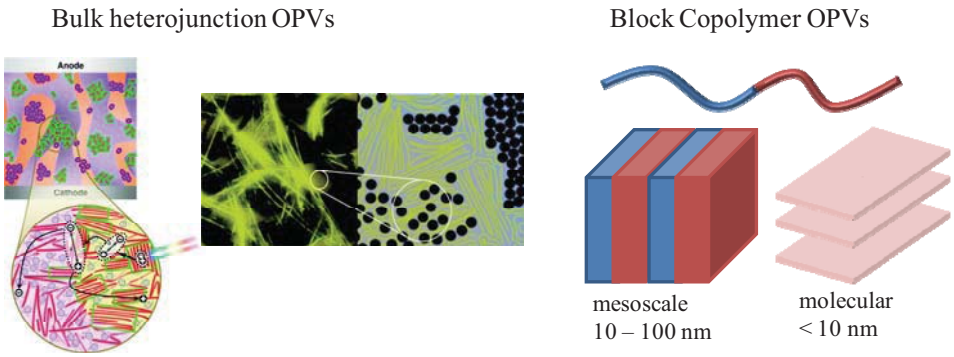

Figure 1.11 – Schematics for the active layer morphologies of bulk heterojunction OPVs (left)[83,84] and all-conjugated block copolymer OPVs (right).

The structure in BHJ device has been used to create more efficient polymeric photovoltaics in a relatively simple route that a solution of mixture of donor and acceptor is casted on substrate forming a blend film.[74,85] However, the resulting structure is in random orientation, phase separation due to thermodynamically favorable process (mainly dependent on Flory-Huggins parameter)[86] or high crystallinity in one component

such as P3HT.[87,88] Block copolymers can potentially be used to control the size and the orientation of the phase-separated domains through self-assembly into well-defined donor and acceptor domains as shown in Figure 1.11 (right).

Block copolymers comprised of two-conjugated polymer blocks, known as all-conjugated block copolymers,[89] can potentially address many of the current challenges in morphology and interfacial structure control for OPVs. All-conjugated block copolymers are an emerging class of materials comprised of two or more conjugated polymer chains. Such block copolymers combine the optoelectronic properties of semiconductive polymers with structure control through micro-phase segregation[90-92] and crystallization.[93,94] Donor-acceptor all-conjugated block copolymers comprised of both *p*-type and *n*-type polymer blocks are of particular interest for OPVs.[80,95] Selected examples of all-conjugated block copolymers are shown in Scheme 1.[89,93,96-106] The micro-phase segregation of diblock copolymer typically leads to domain sizes of 5-100 nm with various morphologies, depending on the volume fraction of block.[107,108] For the above reasons, in this thesis research we prepared all-conjugated block copolymers with varying block sizes for processing condition studies.

1.4. Thesis objectives and outlines

The key objective in this thesis is to develop all-conjugated block copolymers which comprise of an electron donor block and an electron acceptor block for the OPV application. Polymer synthesis, modification, processing-dependent morphology study in all-conjugated block copolymers and OPV device fabrication are studied in this thesis.

Chapter 2 presents development for synthesis of poly(3-alkylthiophene) (P3AT)-based all-conjugated block copolymers with a covalent linker between the electron donor polymer and the electron acceptor polymer. A two-step reaction with combination of

Grignard metathesis polymerization (GRIM) followed by Suzuki-Miyaura poly-condensation reaction for preparing three various all-conjugated block copolymers by incorporating different monomers in Suzuki-Miyaura poly-condensation step. This chapter is included in Yen-Hao Lin, Kendall A. Smith, Chloe N. Kempf, Rafael Verduzco, "Synthesis and Crystallinity of All-Conjugated Poly(3-hexylthiophene) Block Copolymers," *Polymer Chemistry,* 2013, **4(2)**, 229-232. Portions of this chapter are included in Yen-Hao Lin and Rafael Verduzco, "Synthesis and Process-Dependent Film Structure of All-conjugated Copolymers for Organic Photovoltaics," *The American Chemical Society Symposium of Polymer Composites for Energy Harvesting, Conversion and Storage*, 2014, Chapter 3, 49-70.

Chapter 3 provides a thorough investigation on the processing-dependent nanostructures on all-conjugated block copolymers with focus on a model example of poly(3-hexylthiophene) –*b*–poly(9′,9′-dioctylfluorene) (P3HT–*b*–PF) with varying block ratios. In contrast to previous researches that P3HT always dominates the nanostructures, here we provide rich processing dependence on the nanostructures of P3HT–*b*–PF as well as the resulting thermal and optical properties. This chapter is included in Yen-Hao Lin, Kevin G. Yager, Bridget Stewart, Rafael Verduzco, "Lamellar Structures of Solvent Annealed All-Conjugated Block Copolymers," *Soft Matter,* 2014, **4(2)**, 3817-3825. Portions of this chapter are included in Yen-Hao Lin and Rafael Verduzco, "Synthesis and Process-Dependent Film Structure of All-conjugated Copolymers for Organic Photovoltaics," *The American Chemical Society Symposium of Polymer Composites for Energy Harvesting, Conversion and Storage*, 2014, Chapter 3, 49-70.

Chapter 4 presents a breakthrough in non-fullerene OPV with using an all-conjugated block copolymer poly(3-hexylthiophene)–*b*–poly(2,7-(9′,9′-dioctyl-fluorene)-*alt*-5,5-(4′,7′-di-2-thienyl-2′,1′,3′,benzothiadiazole) (P3HT–*b*–PFTBT) which achieves a record ~3% performance. This chapter will discuss how nanostructures of this block

copolymer improve the device performance. This chapter is included in Changhe Guo, Yen-Hao Lin, Mathew D. Witman, Kendall A. Smith, Cheng Wang, Alexandar Hexemer, Joseph Strzalka, Enrique D. Gomez, Rafael Verduzco, "Conjugated Block Copolymer Photovoltaics with near 3% Efficiency through Microphase Separation," *Nano Letters,* 2013, **13 (6)**, 2957-2963.

Chapter 5 provides an unconventional method for all-conjugated block copolymer with using hydrogen bonding interaction to resolve macro-phase separation issue in polymer blends. We demonstrate the synthesis of a quadruple hydrogen bonding group, 2-ureido-4[1H]-pyrimidinone (UPy), and its impact to resolve the macro-phase separation issue in polymer blends together with the capability to enhance the energy transfer between an electron donor material and an electron acceptor material. This chapter is included in Yen-Hao Lin, Seth B. Darling, Maxim P. Nikiforov, Joseph Strzalka, Rafael Verduzco, "Supramolecular Conjugated Block Copolymers," *Macromolecules,* 2012, **45**, 6571-6579.

Chapter 6 studies the OPV devices with a quadruple hydrogen bonding mediation on P3HT and PFTBT polymer blends and blends with PCBM. Although the miscibility of blends is improved from the morphological study, there is no pronounced improvement for device performance probably because the improved miscibility surrenders the fill factor due to enlarged bulk resistance which is evidenced from impedance spectroscopy study.

The last, chapter 7 gives a few possibilities with preliminary results for future works which may lead to breakthrough in OPVs developments. This chapter also includes some notes for OPV device fabrication.

Appendix A lists publications associated with this thesis and Appendix B provides all reprints for the publications.

1.5. References

(1) Mai, T. W., R.; Sandor, D.; Brinkman, G.; Heath, G.; Denholm, P.; Hostick, D.J.; Darghouth, N.; Schlosser, A.; Strzepek, K., *Exploration of High-Penetration Renewable Electricity Futures. Vol. 1 of Renewable Electricity Futures Study.* **2012**, NREL/TP-6A20-52409-1. Golden, CO: National Renewable Energy Laboratory.

(2) *U.S. Energy Information Administration / Monthly Energy Review October 2013, Chapter 2: Energy Consumption by Sector* **2013**, http://www.eia.gov/totalenergy/.

(3) Darling, S. B.; You, F., *RSC Advances* **2013**, *3*, 17633-17648.

(4) Kalowekamo, J.; Baker, E., *Sol. Energy* **2009**, *83*, 1224-1231.

(5) Ramanathan, K.; Contreras, M. A.; Perkins, C. L.; Asher, S.; Hasoon, F. S.; Keane, J.; Young, D.; Romero, M.; Metzger, W.; Noufi, R.; Ward, J.; Duda, A., *Prog. Photovolt.: Res. Appl.* **2003**, *11*, 225-230.

(6) Wu, X., *Sol. Energy* **2004**, *77*, 803-814.

(7) O'Regan, B.; Gratzel, M., *Nature* **1991**, *353*, 737-740.

(8) Granstrom, M.; Petritsch, K.; Arias, A. C.; Lux, A.; Andersson, M. R.; Friend, R. H., *Nature* **1998**, *395*, 257-260.

(9) Shirakawa, H.; Louis, E. J.; MacDiarmid, A. G.; Chiang, C. K.; Heeger, A. J., *J. Chem. Soc., Chem. Commun.* **1977**, 578-580.

(10) Sirringhaus, H.; Tessler, N.; Friend, R. H., *Science* **1998**, *280*, 1741-1744.

(11) Hangarter, C. M.; Bangar, M.; Mulchandani, A.; Myung, N. V., *J. Mater. Chem.* **2010**, *20*, 3131-3140.

(12) Janata, J.; Josowicz, M., *Nat. Mater.* **2003**, *2*, 19-24.

(13) Facchetti, A., *Chem. Mater.* **2010**, *23*, 733-758.

(14) Gustafsson, G.; Cao, Y.; Treacy, G. M.; Klavetter, F.; Colaneri, N.; Heeger, A. J., *Nature* **1992**, *357*, 477-479.

(15) Gross, M.; Muller, D. C.; Nothofer, H.-G.; Scherf, U.; Neher, D.; Brauchle, C.; Meerholz, K., *Nature* **2000**, *405*, 661-665.

(16) Yang, Y.; Heeger, A. J., *Appl. Phys. Lett.* **1994**, *64*, 1245-1247.

(17) Gao, J.; Heeger, A. J.; Lee, J. Y.; Kim, C. Y., *Synth. Met.* **1996**, *82*, 221-223.

(18) Carter, S. A.; Angelopoulos, M.; Karg, S.; Brock, P. J.; Scott, J. C., *Appl. Phys. Lett.* **1997**, *70*, 2067-2069.

(19) Scott, J. C.; Carter, S. A.; Karg, S.; Angelopoulos, M., *Synth. Met.* **1997**, *85*, 1197-1200.

(20) Gunes, S.; Neugebauer, H.; Sariciftci, N. S., *Chem. Rev.* **2007**, *107*, 1324-1338.

(21) Thompson, B. C.; Fréchet, J. M. J., *Angew. Chem. Int. Ed.* **2008**, *47*, 58-77.

(22) Hoppe, H.; Sariciftci, N. S., *J. Mater. Res.* **2004**, *19*, 1924-1945.

(23) Peet, J.; Heeger, A. J.; Bazan, G. C., *Accounts Chem. Res.* **2009**, *42*, 1700-1708.

(24) Zhang, X.; Wei, S.; Haldolaarachchige, N.; Colorado, H. A.; Luo, Z.; Young, D. P.; Guo, Z., *J. Phys. Chem.C* **2012**, *116*, 15731-15740.

(25) Zhang, X.; Zhu, J.; Haldolaarachchige, N.; Ryu, J.; Young, D. P.; Wei, S.; Guo, Z., *Polymer* **2012**, *53*, 2109-2120.

(26) Wei, H.; Yan, X.; Li, Y.; Gu, H.; Wu, S.; Ding, K.; Wei, S.; Guo, Z., *J. Phys. Chem.C* **2012**, *116*, 16286-16293.

(27) Krebs, F. C.; Gevorgyan, S. A.; Alstrup, J., *J. Mater. Chem.* **2009**, *19*, 5442-5451.

(28) Nielsen, T. D.; Cruickshank, C.; Foged, S.; Thorsen, J.; Krebs, F. C., *Sol. Energy Mater. Sol. Cells* **2010**, *94*, 1553-1571.

(29) Krebs, F. C.; Jørgensen, M.; Norrman, K.; Hagemann, O.; Alstrup, J.; Nielsen, T. D.; Fyenbo, J.; Larsen, K.; Kristensen, J., *Sol. Energy Mater. Sol. Cells* **2009**, *93*, 422-441.

(30) Sirringhaus, H., *Nat. Mater.* **2003**, *2*, 641-642.

(31) Pron, A.; Rannou, P., *Prog. Polym. Sci.* **2002**, *27*, 135-190.

(32) Koezuka, H.; Tsumura, A.; Ando, T., *Synth. Met.* **1987**, *18*, 699-704.

(33) Allard, S.; Forster, M.; Souharce, B.; Thiem, H.; Scherf, U., *Angew. Chem. Int. Ed.* **2008**, *47*, 4070-4098.

(34) Zhang, R.; Li, B.; Iovu, M. C.; Jeffries-El, M.; Sauve, G.; Cooper, J.; Jia, S. J.; Tristram-Nagle, S.; Smilgies, D. M.; Lambeth, D. N.; McCullough, R. D.; Kowalewski, T., *J. Am. Chem. Soc.* **2006**, *128*, 3480-3481.

(35) Kline, R.; McGehee, M., *J. Macromol. Sci.-Pol. R.* **2006**, *46*, 27-45.

(36) Sauve, G.; Javier, A. E.; Zhang, R.; Liu, J. Y.; Sydlik, S. A.; Kowalewski, T.; McCullough, R. D., *J. Mater. Chem.* **2010**, *20*, 3195-3201.

(37) Zen, A.; Pflaum, J.; Hirschmann, S.; Zhuang, W.; Jaiser, F.; Asawapirom, U.; Rabe, J. P.; Scherf, U.; Neher, D., *Adv. Funct. Mater.* **2004**, *14*, 757-764.
(38) Kline, R. J.; McGehee, M. D.; Kadnikova, E. N.; Liu, J.; Fréchet, J. M. J., *Adv. Mater.* **2003**, *15*, 1519-1522.
(39) Baude, P. F.; Ender, D. A.; Haase, M. A.; Kelley, T. W.; Muyres, D. V.; Theiss, S. D., *Appl. Phys. Lett.* **2003**, *82*, 3964-3966.
(40) McCulloch, I.; Heeney, M.; Bailey, C.; Genevicius, K.; MacDonald, I.; Shkunov, M.; Sparrowe, D.; Tierney, S.; Wagner, R.; Zhang, W.; Chabinyc, M. L.; Kline, R. J.; McGehee, M. D.; Toney, M. F., *Nat. Mater.* **2006**, *5*, 328-333.
(41) Heeney, M.; Bailey, C.; Genevicius, K.; Shkunov, M.; Sparrowe, D.; Tierney, S.; McCulloch, I., *J. Am. Chem. Soc.* **2005**, *127*, 1078-1079.
(42) Li, Y.; Wu, Y.; Ong, B. S., *Macromolecules* **2006**, *39*, 6521-6527.
(43) He, M.; Li, J.; Tandia, A.; Sorensen, M.; Zhang, F.; Fong, H. H.; Pozdin, V. A.; Smilgies, D.-M.; Malliaras, G. G., *Chem. Mater.* **2010**, *22*, 2770-2779.
(44) Babel, A.; Jenekhe, S. A., *J. Am. Chem. Soc.* **2003**, *125*, 13656-13657.
(45) Chen, Z.; Zheng, Y.; Yan, H.; Facchetti, A., *J. Am. Chem. Soc.* **2008**, *131*, 8-9.
(46) Yan, H.; Chen, Z.; Zheng, Y.; Newman, C.; Quinn, J. R.; Dötz, F.; Kastler, M.; Facchetti, A., *Nature* **2009**, *457*, 679-686.
(47) AlSalhi, M. S.; Alam, J.; Dass, L. A.; Raja, M., *Int. J. Mol. Sci.* **2011**, *12*, 2036-2054.
(48) Chen, S. H.; Su, A. C.; Chen, S. A., *J. Phys. Chem. B* **2005**, *109*, 10067-10072.
(49) Sholin, V.; Lopez-Cabarcos, E. J.; Carter, S. A., *Macromolecules* **2006**, *39*, 5830-5835.
(50) Nicholson, P. G.; Castro, F. A., *Nanotechnology* **2010**, *21*.
(51) Cnops, K.; Rand, B. P.; Cheyns, D.; Verreet, B.; Empl, M. A.; Heremans, P., *Nat Commun* **2014**, *5*.
(52) Kietzke, T., *Advances in OptoElectronics* **2007**, 1-15.
(53) Coakley, K. M.; McGehee, M. D., *Chem. Mater.* **2004**, *16*, 4533-4542.
(54) Marks, R. N.; Halls, J. J. M.; Bradley, D. D. C.; Friend, R. H.; Holmes, A. B., *J. Phys.- Condens. Mat.* **1994**, *6*, 1379.
(55) Tang, C. W., *Appl. Phys. Lett.* **1986**, *48*, 183-185.
(56) Jenekhe, S. A.; Yi, S. J., *Appl. Phys. Lett.* **2000**, *77*, 2635-2637.

(57) Chen, L. C.; Godovsky, D.; Inganas, O.; Hummelen, J. C.; Janssens, R. A. J.; Svensson, M.; Andersson, M. R., *Adv. Mater.* **2000**, *12*, 1367-1370.
(58) Moon, J. S.; Takacs, C. J.; Sun, Y.; Heeger, A. J., *Nano Lett.* **2011**, *11*, 1036-1039.
(59) Guo, C.; Lin, Y.-H.; Witman, M. D.; Smith, K. A.; Wang, C.; Hexemer, A.; Strzalka, J.; Gomez, E. D.; Verduzco, R., *Nano Lett.* **2013**, *13*, 2957-2963.
(60) Olson, D. C.; Piris, J.; Collins, R. T.; Shaheen, S. E.; Ginley, D. S., *Thin Solid Films* **2006**, *496*, 26-29.
(61) Dang, M. T.; Hirsch, L.; Wantz, G., *Adv. Mater.* **2011**, *23*, 3597-3602.
(62) Dennler, G.; Scharber, M. C.; Brabec, C. J., *Adv. Mater.* **2009**, *21*, 1323-1338.
(63) Zhou, E.; Cong, J.; Wei, Q.; Tajima, K.; Yang, C.; Hashimoto, K., *Angew. Chem. Int. Ed.* **2011**, *50*, 2995-2998.
(64) Kroon, R.; Lenes, M.; Hummelen, J. C.; Blom, P. W. M.; de Boer, B., *Polym. Rev.* **2008**, *48*, 531-582.
(65) Abbel, R.; Schenning, A.; Meijer, E. W., *J. Polym. Sci., Part A: Polym. Chem.* **2009**, *47*, 4215-4233.
(66) Calabrese, A.; Schimperna, G.; Po, R.; Yohannes, T.; Debebe, S. E.; Tinti, F.; Camaioni, N., *J. Appl. Phys.* **2011**, *110*, 113106.
(67) Kingsley, J. W.; Marchisio, P. P.; Yi, H.; Iraqi, A.; Kinane, C. J.; Langridge, S.; Thompson, R. L.; Cadby, A. J.; Pearson, A. J.; Lidzey, D. G.; Jones, R. A. L.; Parnell, A. J., *Sci. Rep.* **2014**, *4*.
(68) Hoppe, H.; Sariciftci, N. S., *J. Mater. Chem.* **2006**, *16*, 45-61.
(69) Erb, T.; Zhokhavets, U.; Gobsch, G.; Raleva, S.; Stühn, B.; Schilinsky, P.; Waldauf, C.; Brabec, C. J., *Adv. Funct. Mater.* **2005**, *15*, 1193-1196.
(70) Peet, J.; Soci, C.; Coffin, R. C.; Nguyen, T. Q.; Mikhailovsky, A.; Moses, D.; Bazan, G. C., *Appl. Phys. Lett.* **2006**, *89*, 252105-3.
(71) Moon, J. S.; Takacs, C. J.; Cho, S.; Coffin, R. C.; Kim, H.; Bazan, G. C.; Heeger, A. J., *Nano Lett.* **2010**, *10*, 4005-4008.
(72) Perez, L. A.; Chou, K. W.; Love, J. A.; van der Poll, T. S.; Smilgies, D.-M.; Nguyen, T.-Q.; Kramer, E. J.; Amassian, A.; Bazan, G. C., *Adv. Mater.* **2013**, *25*, 6380-6384.
(73) He, X.; Gao, F.; Tu, G.; Hasko, D.; Hüttner, S.; Steiner, U.; Greenham, N. C.; Friend, R. H.; Huck, W. T. S., *Nano Lett.* **2010**, *10*, 1302-1307.

(74) Slota, J. E.; He, X. M.; Huck, W. T. S., *Nano Today* **2010**, *5*, 231-242.

(75) Moungthai, S.; Mahadevapuram, N.; Ruchhoeft, P.; Stein, G. E., *ACS Appl. Mater. Interfaces* **2012**, *4*, 4015-4023.

(76) Kim, Y.; Cook, S.; Choulis, S. A.; Nelson, J.; Durrant, J. R.; Bradley, D. D. C., *Chem. Mater.* **2004**, *16*, 4812-4818.

(77) Mori, D.; Benten, H.; Kosaka, J.; Ohkita, H.; Ito, S.; Miyake, K., *ACS Appl. Mater. Interfaces* **2011**, *3*, 2924-2927.

(78) McNeill, C. R.; Abrusci, A.; Hwang, I.; Ruderer, M. A.; Müller-Buschbaum, P.; Greenham, N. C., *Adv. Funct. Mater.* **2009**, *19*, 3103-3111.

(79) Segalman, R. A.; McCulloch, B.; Kirmayer, S.; Urban, J. J., *Macromolecules* **2009**, *42*, 9205-9216.

(80) Darling, S. B., *Energy Environ. Sci.* **2009**, *2*, 1266-1273.

(81) McNeill, C. R.; Abrusci, A.; Zaumseil, J.; Wilson, R.; McKiernan, M. J.; Burroughes, J. H.; Halls, J. J. M.; Greenham, N. C.; Friend, R. H., *Appl. Phys. Lett.* **2007**, *90*, 193506-3.

(82) Facchetti, A., *Mater. Today* **2013**, *16*, 123-132.

(83) Chen, W.; Xu, T.; He, F.; Wang, W.; Wang, C.; Strzalka, J.; Liu, Y.; Wen, J.; Miller, D. J.; Chen, J.; Hong, K.; Yu, L.; Darling, S. B., *Nano Letters* **2011**, *11*, 3707-3713.

(84) Yin, W.; Dadmun, M., *ACS Nano* **2011**, *5*, 4756-4768.

(85) McNeill, C. R.; Greenham, N. C., *Adv. Mater.* **2009**, *21*, 3840-3850.

(86) Kim, J.-S.; Ho, P. K. H.; Murphy, C. E.; Friend, R. H., *Macromolecules* **2004**, *37*, 2861-2871.

(87) Yang, X. N.; Loos, J.; Veenstra, S. C.; Verhees, W. J. H.; Wienk, M. M.; Kroon, J. M.; Michels, M. A. J.; Janssen, R. A. J., *Nano Lett.* **2005**, *5*, 579-583.

(88) Wu, P.-T.; Ren, G.; Li, C.; Mezzenga, R.; Jenekhe, S. A., *Macromolecules* **2009**, *42*, 2317-2320.

(89) Scherf, U.; Gutacker, A.; Koenen, N., *Accounts Chem. Res.* **2008**, *41*, 1086-1097.

(90) Tseng, Y.-C.; Darling, S. B., *Polymers* **2010**, *2*, 470-489.

(91) Bates, F. S.; Fredrickson, G. H., *Phys. Today* **1999**, *52*, 32-38.

(92) Park, C.; Yoon, J.; Thomas, E. L., *Polymer* **2003**, *44*, 6725-6760.

(93) Sommer, M.; Komber, H.; Huettner, S.; Mulherin, R.; Kohn, P.; Greenham, N. C.; Huck, W. T. S., *Macromolecules* **2012**, *45*, 4142-4151.
(94) Smith, K. A.; Lin, Y.-H.; Dement, D. B.; Strzalka, J.; Darling, S. B.; Pickel, D. L.; Verduzco, R., *Macromolecules* **2013**, *46*, 2636-2645.
(95) Sommer, M.; Huettner, S.; Thelakkat, M., *J. Mater. Chem.* **2010**, *20*, 10788-10797.
(96) Botiz, I.; Schaller, R. D.; Verduzco, R.; Darling, S. B., *J. Phys. Chem.C* **2011**, *115*, 9260-9266.
(97) Mulherin, R. C.; Jung, S.; Huettner, S.; Johnson, K.; Kohn, P.; Sommer, M.; Allard, S.; Scherf, U.; Greenham, N. C., *Nano Lett.* **2011**, *11*, 4846-4851.
(98) Woody, K. B.; Leever, B. J.; Durstock, M. F.; Collard, D. M., *Macromolecules* **2011**, *44*, 4690-4698.
(99) Wu, S.; Bu, L.; Huang, L.; Yu, X.; Han, Y.; Geng, Y.; Wang, F., *Polymer* **2009**, *50*, 6245-6251.
(100) Lai, Y.-C.; Ohshimizu, K.; Takahashi, A.; Hsu, J.-C.; Higashihara, T.; Ueda, M.; Chen, W.-C., *J. Polym. Sci., Part A: Polym. Chem.* **2011**, *49*, 2577-2587.
(101) Ouhib, F.; Khoukh, A.; Ledeuil, J.-B.; Martinez, H.; Desbrières, J.; Dagron-Lartigau, C., *Macromolecules* **2008**, *41*, 9736-9743.
(102) Ohshimizu, K.; Takahashi, A.; Higashihara, T.; Ueda, M., *J. Polym. Sci., Part A: Polym. Chem.* **2011**, *49*, 2709-2714.
(103) Sun, S.-S.; Zhang, C.; Ledbetter, A.; Choi, S.; Seo, K.; Carl E. Bonner, J.; Drees, M.; Sariciftci, N. S., *Appl. Phys. Lett.* **2007**, *90*, 043117.
(104) Chen, X. L.; Jenekhe, S. A., *Macromolecules* **1996**, *29*, 6189-6192.
(105) Xiao, X.; Fu, Y.; Sun, M.; Li, L.; Bo, Z., *J. Polym. Sci., Part A: Polym. Chem.* **2007**, *45*, 2410-2424.
(106) Verduzco, R.; Botiz, I.; Pickel, D. L.; Kilbey, S. M.; Hong, K.; Dimasi, E.; Darling, S. B., *Macromolecules* **2011**, *44*, 530-539.
(107) Orilall, M. C.; Wiesner, U., *Chem. Soc. Rev.* **2011**, *40*, 520-535.
(108) Matsen, M. W.; Bates, F. S., *Macromolecules* **1996**, *29*, 7641-7644.

Chapter 2

Synthesis and Crystallinity of All-Conjugated Poly(3-hexylthiophene) Block Copolymer

This chapter is included in Yen-Hao Lin, Kendall A. Smith, Chloe N. Kempf, Rafael Verduzco, "Synthesis and Crystallinity of All-Conjugated Poly(3-hexylthiophene) Block Copolymers," *Polymer Chemistry,* 2013, **4(2)**, 229-232. Portions of this chapter are included in Yen-Hao Lin and Rafael Verduzco, "Synthesis and Process-Dependent Film Structure of All-conjugated Copolymers for Organic Photovoltaics," *The American Chemical Society Symposium of Polymer Composites for Energy Harvesting, Conversion and Storage*, 2014, Chapter 3, 49-70.

A simplified approach towards the synthesis of high molecular weight (M_w > 50 kg/mol) poly(3-hexylthiophene) (P3HT)-based all-conjugated block copolymers is demonstrated and applied to prepare a series of all-conjugated block copolymers. Grazing-incidence X-ray scattering measurements show that P3HT crystallization is suppressed in all-conjugated block copolymers with low (< 25 wt%) P3HT content.

2.1. Introduction

Most approaches for making donor-acceptor all-conjugated block copolymers, which incorporate both *n*- and *p*-type polymer blocks, rely on distinct polymerization reactions for each polymer block, including GRIM, Suzuki-Miyaura, and Stille polymerization reactions.[1-6] All-conjugated block copolymers are generally synthesized from two general strategies depicted schematically in Figure 2.1: (a) through a macro-reagent approach involving sequential polymerization reactions; and (b) through the coupling of two conjugated polymers with controlled end-functionalities. Both strategies have advantages and limitations. While the macro-reagent approach is generally more straightforward and versatile, the coupling approach gives better control over the molecular weight of each polymer block separately. However, the coupling approach requires good end-group control for two separate conjugated polymer blocks.

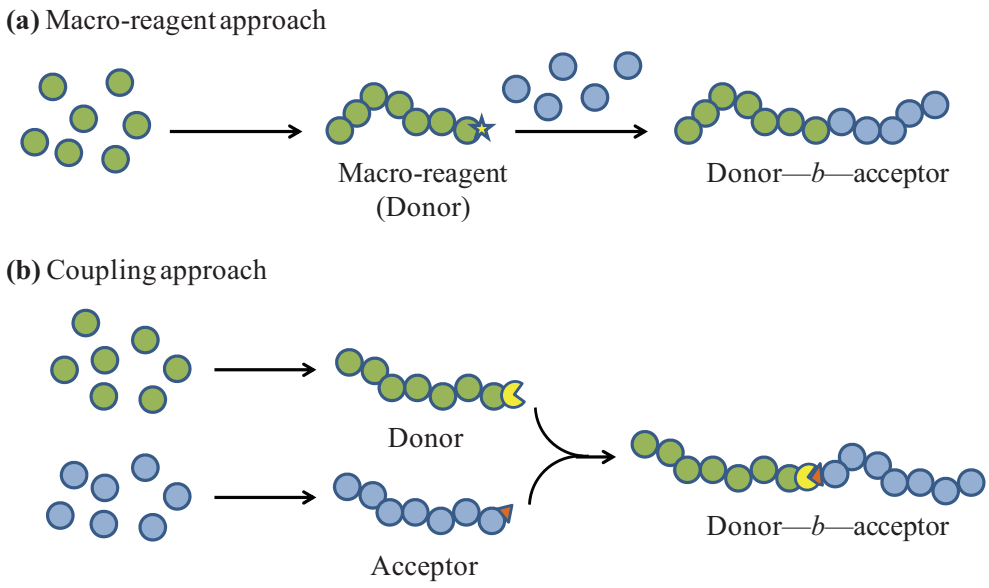

Figure 2.1 – Approaches for synthesis of all-conjugated block copolymers via (a) macro-reagent and (b) covalent/supramolecular coupling.

Alternative approaches to the two mentioned above are limited but include the "all-GRIM" approach which has been applied for the synthesis of block copolythiophenes[7-20] and P3HT–*b*–PF.[12] The advantage of "all-GRIM" is potentially improved control over the polymerization reaction of both blocks. However, "all-GRIM" is limited in terms of applicability to different monomeric repeat units. The reader is referred to recent reviews for more information on this synthetic approach.[21-23]

Studies on all-conjugated block copolymers are limited, due in large part to synthetic challenges.[1,3-5,10,16,24-30] Recent work has demonstrated the preparation of block copolythiophenes using Grignard metathesis polymerization (GRIM)[7-19] resulting in block copolymers with two p-type blocks and similar optoelectronic properties. Most approaches for making donor-acceptor all-conjugated block copolymers, which incorporate both n- and p-type polymer blocks, take advantage of distinct polymerization

reactions for each polymer block, including GRIM, Suzuki-Miyaura, and Stille polymerization reactions.[2-5] A drawback of these methods is that they typically result in relatively low molecular weight block copolymers with significant amounts of homopolymer impurities that can only be removed using tedious column purification techniques.[4,5,26]

In this work, we report an improved route to the synthesis of all-conjugated block copolymers *via* GRIM followed with Suzuki-Miyaura polycondensation as depicted in Figure 2.2. We show that the use of a LiCl additive during GRIM allows for the preparation of high molecular weight block copolymers with little or no homopolymer impurities. This improved synthetic method is applied to the preparation of three different P3HT block copolymers. The molecular weights, polydispersities, and block ratios are measured using a combination of size-exclusion chromatography with refractive index (SEC-RI) and UV-VIS absorbance (SEC-UVVIS) detection and nuclear magnetic resonance spectroscopy (NMR). The morphology and thermal properties of the materials are characterized using X-ray diffraction (XRD), grazing-incidence wide-angle X-ray scattering (GIWAXS), and differential scanning calorimetry (DSC). In contrast to previous work with P3HT-based block copolymers, we observe suppression of P3HT crystallinity in high molecular weight all-conjugated block copolymers, but at more balanced block ratios crystallization of both blocks is achieved. This work provides an improved synthetic method for preparing high-molecular weight all-conjugated block copolymers and the first examples of all-conjugated block copolymers with crystallinity determined by polymer block ratios.

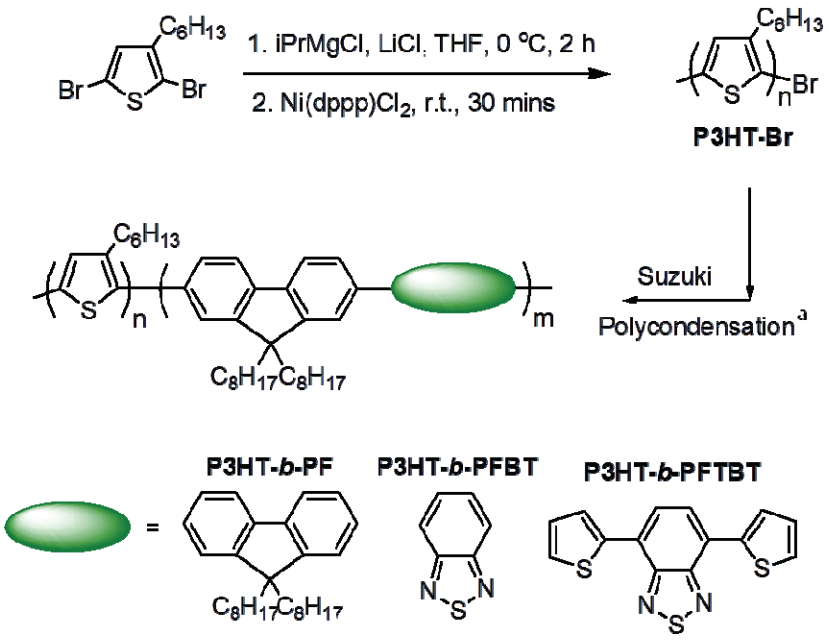

Figure 2.2 – Preparation of all-conjugated P3HT block copolymers *via* Grignard metathesis polymerization with LiCl additive followed by Suzuki-Miyaura Polycondensation. [a]conditions for Suzuki-Miyaura: $Pd(PPh_3)_4$, toluene, water, 90 °C. An equimolar ratio of 9′,9′-dioctylfluorene-2′,7′-diboronic acid ester and corresponding dibromo monomer is used.

2.2. Experimental methods

2.2.1. Materials

2,5-dibromo-3-hexylthiophene[31] and 4,7-di-2′-(5′-bromo)-thienyl-2′,1′,3′,-benzo-thiadiazole)[32] were synthesized as previously described. All other reagents were purchased from Sigma-Aldrich and used as received.

Poly(3-hexylthiophene) (P3HT-Br). The synthetic procedure is a slightly modified from a previous report.[33] In a 50 mL flask purged with nitrogen gas, 2,5-dibromo-3-hexylthiophene (1.9 g, 5.82 mmol) was dissolved in anhydrous THF (5 mL), and the solution was stirred under nitrogen at 0 °C for 15 minutes. A solution of isopropyl magnesium chloride and LiCl (1.3 M) in THF (4.48 mL, 5.82 mmol) was added, and the mixture was stirred for 2 hours. 25 mL of THF was then added before adding Ni(dppp)Cl_2 (105.15 mg, 0.194 mmol), and the mixture was stirred for 15 minutes. The reaction was quenched by adding 5 M HCl (2 mL, 10 mmol), and the solution was stirred for another 15 minutes. The final mixture was collected by precipitation in cold methanol and washed with hexanes and dried under vacuum. Yield: 92%. ^{1}H NMR (500 MHz, $CDCl_3$), δ (ppm): 6.95 (1H, Aryl—H), 2.82 (2H, C—CH_2—C_5H_{11}), 1.70 (2H, CH_2—CH_2—C_4H_9), 1.35 (6H, CH_2—C_3H_6—CH_3), 0.92 (3H, CH_2—CH_3). Molecular weight and PDI are provided in Table 2.1 in results and discussions section.

Poly(3-hexylthiophene)–*b*–poly(9′,9′-dioctylfluorene) (P3HT–*b*–PF) (P3HT36–*b*–PF100 and P3HT81–*b*–PF105). In a representative procedure, P3HT-Br (124 mg, 0.031 mmol), 9′,9′-dioctylfluorene-2′,7′-diboronic acid ester (781 mg, 1.4 mmol), 2′,7′-dibromo-9′,9′-dioctylfluorene (706 mg, 1.288 mmol), tetrakis-(triphenylphosphine) -palladium(0) (75 mg, 0.065 mmol), and aliquat 336 (3 drops) were added to a Schlenk tube loaded with nitrogen-purged toluene (25 mL) and an aqueous solution of Na_2CO_3 (2M, 10 mL). The reaction was stirred at 90 °C for 1 day. The final mixture was collected by precipitation in cold methanol, and the crude product was further purified by washing in a Soxhlet extractor with acetone and then hexanes. The undissolved residue was collected and dried under vacuum. Yield: 80%. ^{1}H NMR (500 MHz, $CDCl_3$) (see Figure 2.2), δ (ppm): 7.5-7.8 (6H; Aryl—H), 6.95 (1H, Aryl—H), 2.82 (2H, C—CH_2—C_5H_{11}), 2.1 (4H; CH_2—C_7H_{15}), 1.70 (2H, CH_2—CH_2—C_4H_9), 1.35

(6H, CH_2—$\underline{C_3H_6}$—CH_3), 1.13 (20H; CH_2—$\underline{C_5H_{10}}$—CH_3), 0.92 (3H, CH_2—$\underline{CH_3}$), 0.80 (6H; C_7H_{14}—$\underline{CH_3}$). Molecular weight and PDI are provided in Table 2.1 in results and discussions section.

Poly(3-hexylthiophene)–*b*–poly[(9′,9′-dioctylfluorene)-alt-(2′,3′,5′-benzothiadiazole)] (P3HT–*b*–PFBT) (P3HT51–*b*–PFBT66 and P3HT81–*b*–PFBT90). In a representative procedure, P3HT-Br (74.4 mg, 0.0062 mmol), 9′,9′-dioctylfluorene-2′,7′-diboronic acid ester (346 mg, 0.62 mmol), 4,7-dibromobenzo[1,2,5] thiadiazole (181 mg, 0.61 mmol), tetrakis-(triphenylphosphine)-palladium(0) (75 mg, 0.065 mmol), and aliquat 336 (3 drops) were added to a Schlenk tube loaded with nitrogen-purged toluene (25 mL) and an aqueous solution of Na_2CO_3 (2M, 10 mL). The reaction was stirred at 90 °C for 1 day. The final mixture was collected by precipitation in cold methanol, and the crude product was further purified by washing in a Soxhlet extractor with acetone and then hexanes. The undissolved residue was collected and dried under vacuum. Yield: 83%. ^{1}H NMR (500 MHz, $CDCl_3$) (see Figure 2.3.), δ (ppm): 7.3-8.2 (8H; Aryl—$\underline{H}$), 6.95 (1H, Aryl—$\underline{H}$), 2.82 (2H, C—$\underline{CH_2}$—C_5H_{11}), 2.1 (4H; $\underline{CH_2}$—C_7H_{15}), 1.70 (2H, CH_2—$\underline{CH_2}$—C_4H_9), 1.35 (6H, CH_2—$\underline{C_3H_6}$—CH_3), 1.13 (20H; CH_2—$\underline{C_5H_{10}}$—CH_3), 0.92 (3H, CH_2—$\underline{CH_3}$), 0.80 (6H; C_7H_{14}—$\underline{CH_3}$). Molecular weight and PDI are provided in Table 2.1 in results and discussions section.

Poly(3-hexylthiophene)–*b*–poly(2,7-(9′,9′-dioctyl-fluorene)-alt-5,5-(4′,7′-di-2-thienyl-2′,1′,3′,-benzothiadiazole) (P3HT–*b*–PFTBT) (P3HT51–*b*–PFTBT17 and P3HT81–*b*–PFTBT12). In a representative procedure, P3HT-Br (139 mg, 0.0116 mmol), 9′,9′-dioctylfluorene-2′,7′-diboronic acid ester (506 mg, 0.9 mmol), 4,7-di-2′-(5′-bromo)-thienyl-2′,1′,3′,-benzothiadiazole) (407 mg, 0.89 mmol), Tetrakis-(triphenylphosphine)-palladium(0) (75 mg, 0.065 mmol), and aliquat 336 (3 drops) were added to a Schlenk tube loaded with nitrogen-purged toluene (25 mL) and an aqueous solution of Na_2CO_3

(2M, 10 mL). The reaction was stirred at 90 °C for 1 day. The final mixture was collected by precipitation in cold methanol and the crude product was further purified by washing in a Soxhlet extractor with acetone and then hexanes. The undissolved residue was collected and dried under vacuum. Yield: 70%. ^{1}H NMR (500 MHz, $CDCl_3$) (see Figure S3), δ (ppm): 8.18 (2H), 7.94 (2H), 7.6-7.8 (6H; Aryl—H), 7.49 (2H) , 6.95 (1H, Aryl—H (P3HT)), 2.82 (2H, C—CH_2—C_5H_{11}), 2.1 (4H; CH_2—C_7H_{15}), 1.70 (2H, CH_2—CH_2—C_4H_9), 1.35 (6H, CH_2—C_3H_6—CH_3), 1.13 (20H; CH_2—C_5H_{10}—CH_3), 0.92 (3H, CH_2—CH_3), 0.80 (6H; C_7H_{14}—CH_3). Molecular weight and PDI are provided in Table 2.1 in results and discussions section.

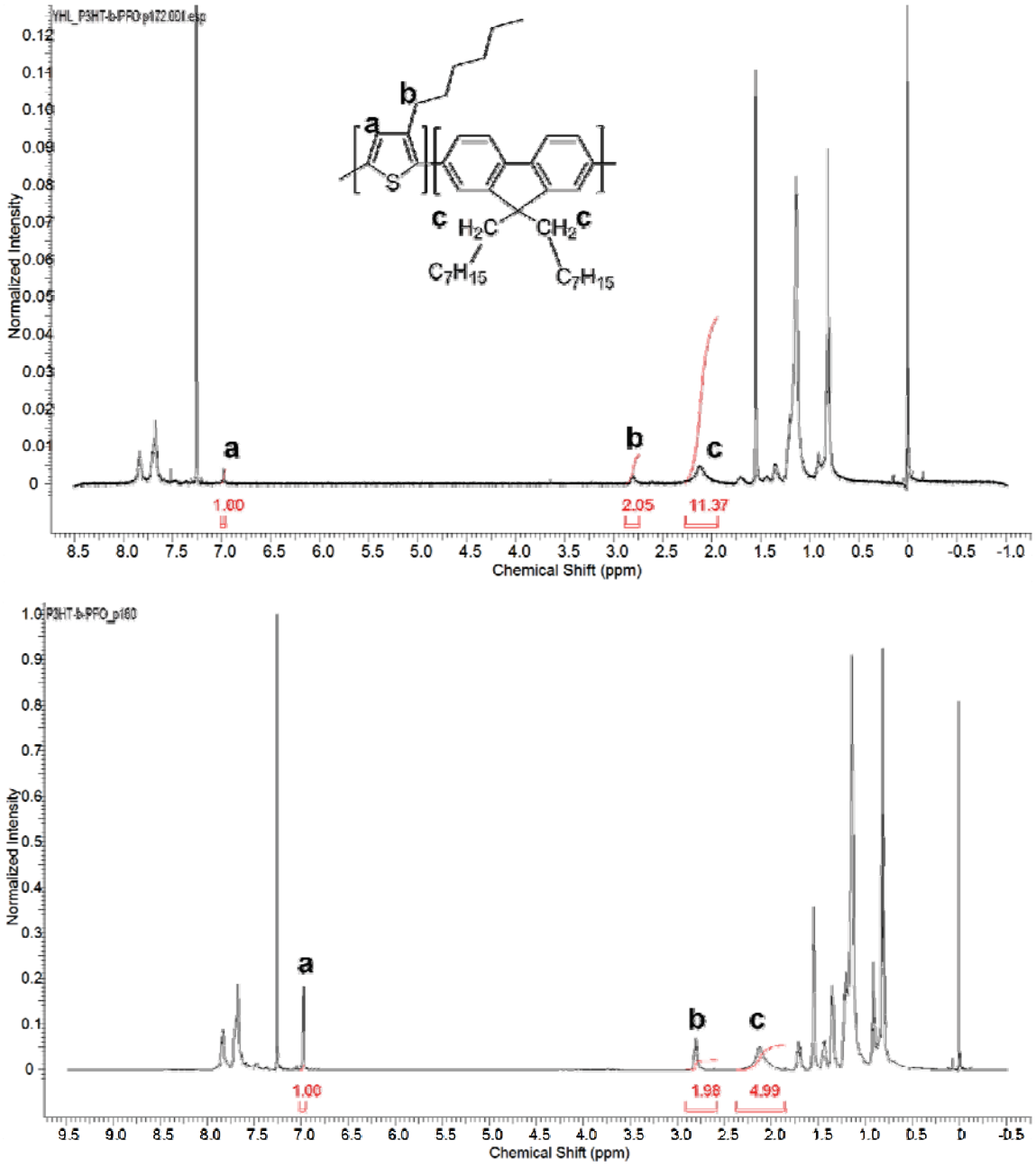

Figure 2.3 – ^{1}H NMR spectrum of P3HT36–*b*–PF100 (top) and P3HT81–*b*–PF105 (bottom).

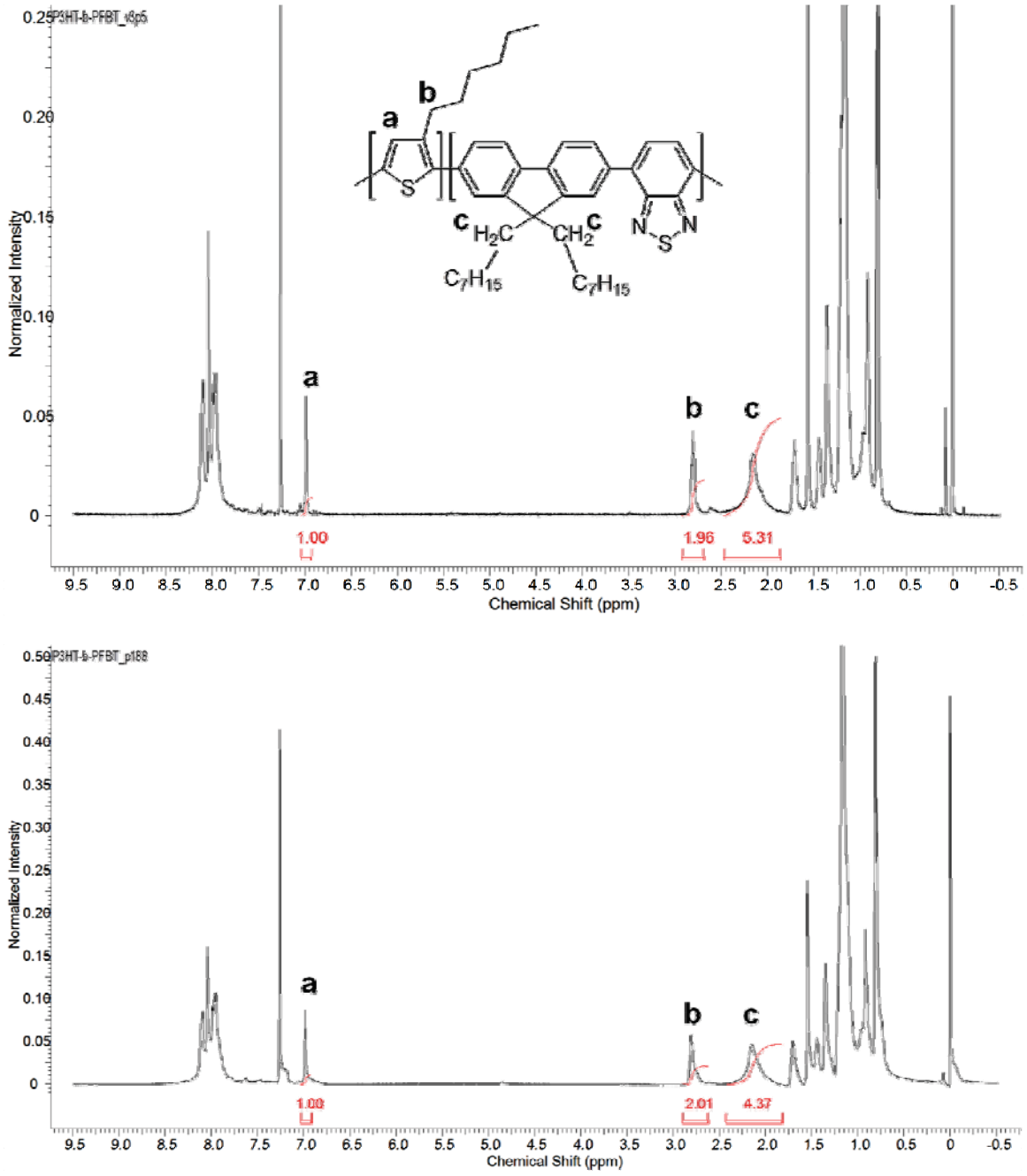

Figure 2.4 – ^{1}H NMR spectrum of P3HT51–*b*–PFBT 66 (top) and P3HT81–*b*–PFBT90 (bottom).

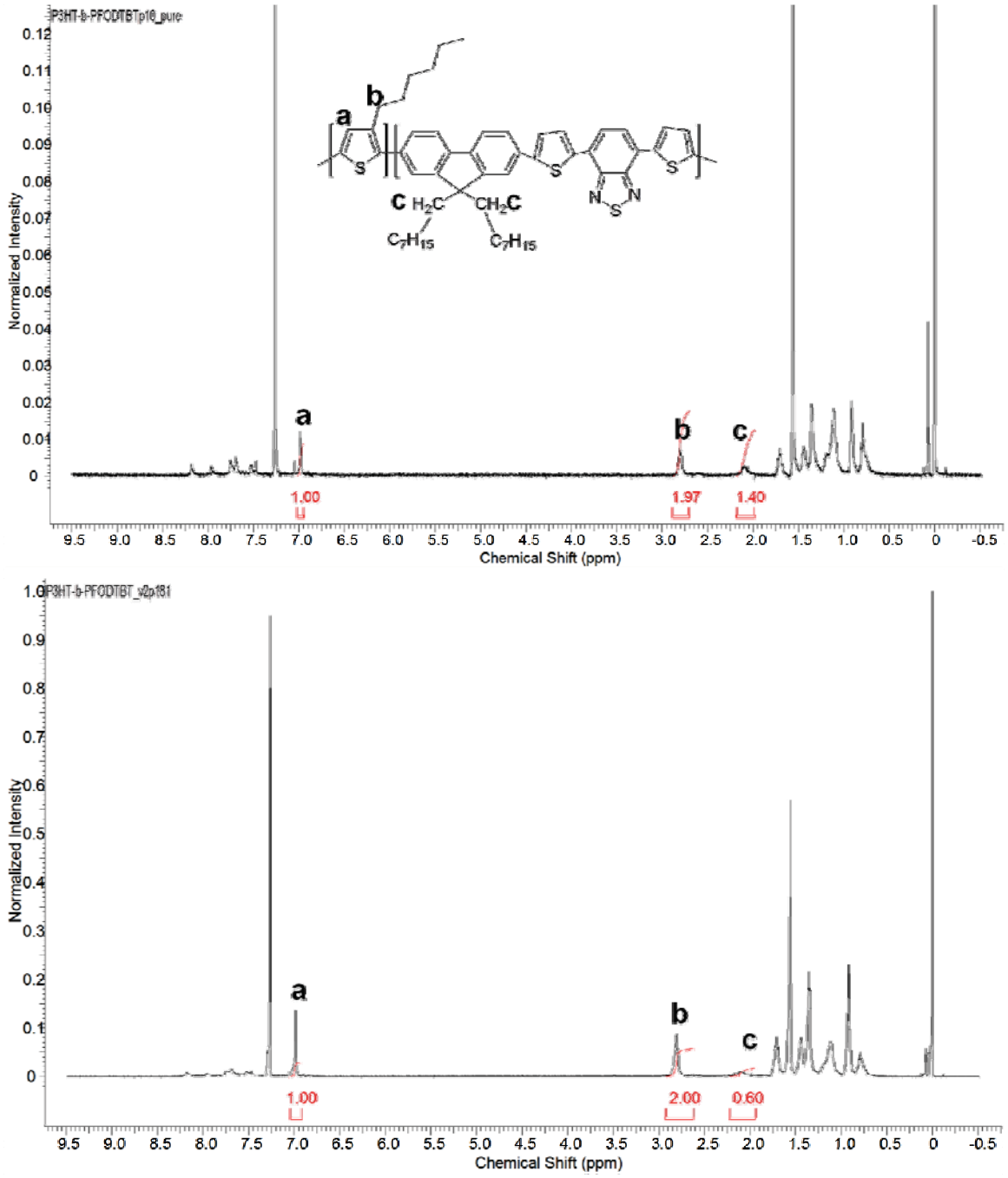

Figure 2.5 – ^{1}H NMR spectrum of P3HT51–*b*–PFTBT17 (top) and P3HT81–*b*–PFTBT12 (bottom).

2.2.2. Instrumentation

Size Exclusion Chromatography (SEC). Molecular weights and polydispersities were obtained by SEC using an Agilent 1200 module equipped with three PSS SDV columns in series (100, 1000, and 10 000 Å pore sizes), an Agilent variable wavelength UV/visible detector, and a Wyatt Technology Optilab reX RI detector. This system enables SEC with simultaneous refractive index (SEC-RI) and UV-VIS detection. THF was used as the mobile phase at a flow rate of 1mL/min at 40 °C. Polystyrene relative molecular weights are calculated using Astra Software Version 5.3.4.

The molecular weight distributions for each polymer block and corresponding homopolymer impurities can be obtained by SEC-UVVIS analysis at two distinct wavelengths. By using a wavelength specific to one polymer block, we first obtain the molecular weight distribution for one block. 450 nm (specific to P3HT), 500 nm (specific to P3HT), and 550 nm (specific to PFDTBT) were used for P3HT–*b*–PF, P3HT–*b*–PFBT, and P3HT–*b*–PFDTBT, respectively. PF and PFBT exhibit no measureable absorbance at 450 and 500 nm, respectively, while P3HT exhibits no measureable absorbance at 550 nm. Next, SEC-UVVIS analysis a second wavelength sensitive to both polymer blocks can be corrected to obtain the molecular weight distribution of the second block. In the case of P3HT–*b*–PF, analysis at 380 nm is sensitive to both blocks, but the contribution of P3HT to the signal is subtracted using the 450 nm SEC-UVVIS trace and the absorbance ratio for P3HT at 450nm relative to 380 nm, measured independently to be 1.82. The 380 nm absorbance trace presented in Figure S5 is the result of this subtraction and reflects the molecular weight distribution of the PF block only. Similar analysis was carried out for P3HT–*b*–PFBT and P3HT–*b*–PFDTBT. 300 nm and 500 nm were used for analysis of P3HT–*b*–PF, with a measured absorbance ratio of 0.12 for P3HT at 500nm

relative to 300 nm. 550 nm and 450 nm were used for P3HT–*b*–PFDTBT, with a measured absorbance ratio of 3.2 for PFODTBT at 550 nm relative to 450 nm

Nuclear Magnetic Resonance Spectroscopy (NMR). ^{1}H NMR spectroscopy was performed on Varian 500 MHz. Samples were placed in 5 mm o.d. tubes with sample concentrations of about 5 mg/mL. Solvents contain 0.05% TMS as an internal standard. Spectra were processed using 1D NMR Processor in ACDLABS 12.0.

Ultraviolet-Visible Absorbance Spectroscopy (UV-VIS). UV-VIS measurements were carried out with a Varian Cary 50 spectrophotometer with scan range of 190 nm – 1100 nm at the Center for Functional Nanomaterials at Argonne National Laboratory. Samples were prepared by stirring 1 mg/mL solutions in $CHCl_3$ and diluted to a concentration of approximately 1 μg/mL immediately before measurement.

Differential Scanning Calorimetry (DSC). Differential scanning calorimetry measurements were performed using a TA Instrument DSC Q10 with a ramp rate of 5 °C/min under N_2 flow. Samples about 3 mg were placed in hermetic pans from Thermal Support Inc.

Wide-angle X-ray diffraction (XRD). X-ray diffraction was performed with Rigaku D/Max Ultima II with Cu Kα radiation source. Samples were prepared by drop casting 6 mg/mL polymer $CHCl_3$ solution on glass slide and dried under a stream of air. Then, samples were annealed to 220 °C and cooled to room temperature twice before measurement.

Grazing-Incidence Wide Angle X-ray scattering (GIWAXS). Grazing incidence wide angle X-ray scattering measurements were carried out on Sector 8-ID-E at the Advanced Photon Source, Argonne National Laboratory.[34] Beamline 8-ID-E operates at an energy of 7.35 keV and images were collected from a Pilatus 1MF camera (Dectris),

with two exposures for different vertical position of the detector. After flatfield correction for detector nonuniformity, the images are combined to fill in the gaps for rows at the borders between modules, leaving dark only the columns of inactive pixels at the center. Using the GIXSGUI package[35] for Matlab (Mathworks), data are corrected for X-ray polarization, detector sensitivity and geometrical solid-angle. The beam size is 200 μm (h) x 20 μm (v). Sample detector distance is 204 mm. Sample measurement and thermal annealing were carried out under vacuum which is in the range of $2\sim3 \times 10^{-6}$ bar, with the sample stage interfaced with a Lakeshore 340 unit.

Couple samples (P3HT81–*b*–PFBT90 and P3HT51–*b*–PFTBT17) were carried out on X9 at National Synchrotron Light Source, Brookhaven National Laboratory. Beamline X9 operates at an energy of 14 keV and images were collected from a Pilatus 1MF camera (Dectris). Using the GIXSGUI package[35] for Matlab (Mathworks), data are corrected for X-ray polarization, detector sensitivity and geometrical solid-angle. Sample detector distance is 370 mm for wide-angle detector and 3091 mm for small-angle detector. Sample measurement and thermal annealing were carried out under vacuum which is in the range of $2\sim3 \times 10^{-6}$ bar.

2.3. Results and discussions

Our synthetic strategy involves a combination of GRIM and Suzuki-Miyaura polymerizations as shown in Figure 2.2. GRIM is first carried out to synthesize a Br end-functionalized P3HT (P3HT-Br) macroreagent, and P3HT-Br is subsequently utilized in a Suzuki-Miyaura polymerization reaction to make all-conjugated P3HT block copolymers. A high degree of end functionali zation of the P3HT-Br macroreagent is required to avoid residual P3HT homopolymer impurities, and this was accomplished using LiCl as an additive for the preparation of bromo-chloromagnesio-hexylthiophene monomer. LiCl

has been shown to be an effective additive for accelerating Grignard formation and producing P3HT with a high degree of end-group functionality.[33,36,37] P3HT-Br was prepared using standard methods by the addition of Ni(dppp)Cl_2 catalyst to the monomer solution to initiate GRIM.[38] Three different sizes of P3HT were synthesized with relatively low PDI and regioregularity higher than 93%. Next, P3HT-Br was reacted in a Suzuki-Miyaura polycondensation reaction to prepare three different types block copolymers, each with a P3HT block and a second conjugated polymer block: poly(9′,9′-dioctyl fluorene) (PF), poly(9′,9′-dioctyl fluorene-*alt*-benzothiadiazole) (PFBT), and poly(2,7-(9′,9′-dioctyl-fluorene)-*alt*-5,5-(4′,7′-di-2-thienyl-2′,1′,3′,benzothiadiazole) (PFTBT). PF, PFBT, and PFTBT have been previously studied for use in bulk-heterojunction OPVs and OLEDs,[39-41] and PFTBT may be particularly promising for use in block copolymer OPVs because it exhibits a broad absorbance and a low-lying HOMO level.[42,43] A high and low molecular weight P3HT-Br macroreagent was used for each type of block copolymer, resulting in a total of six different block copolymers, as shown in Table 2.1. The formation of triblock copolymers is unlikely due to a low content of P3HT-Br macroreagent used in the Suzuki-Miayura polycondensation step (roughly 1 mole % relative to monomers).

Polymers	P3HT[a] M_w (PDI)	BCP[a] M_w (PDI)	DP ratios[b] (P3HT wt%)
P3HT36–*b*–PF100	6.1 (1.16)	48.4 (1.86)	36:100 (13%)
P3HT81–*b*–PF105	13.5 (1.32)	60.6 (1.87)	81:105 (25%)
P3HT51–*b*–PFBT66	8.5 (1.19)	168 (3.61)	51:66 (20%)
P3HT81–*b*–PFBT90	13.5 (1.32)	81.5 (2.24)	81:90 (22%)
P3HT51–*b*–PFTBT17	8.5 (1.19)	19.7 (1.49)	51:17 (42%)
P3HT81–*b*–PFTBT12	13.5 (1.32)	N/A[c]	81:12 (62%)

[a] M_w (kg/mol) and PDI for P3HT and block copolymers determined by comparison to a set of monodisperse polystyrene standards. Head-to-tail regioregularity of P3HT is greater than 93% for all samples as determined from ^{1}H NMR. [b]DP ratios and P3HT content were determined by ^{1}H NMR *via* comparison of the integrated intensity of P3HT aromatic peak (6.9 ppm) and fluorene alkyl peaks (2.2 ppm). [c]P3HT81–*b*–PFTBT12 contains primarily homopolymer impurities, and therefore an estimate for block copolymer molecular weight is not provided.

Table 2.1 – Characteristics of all-conjugated P3HT block copolymers.

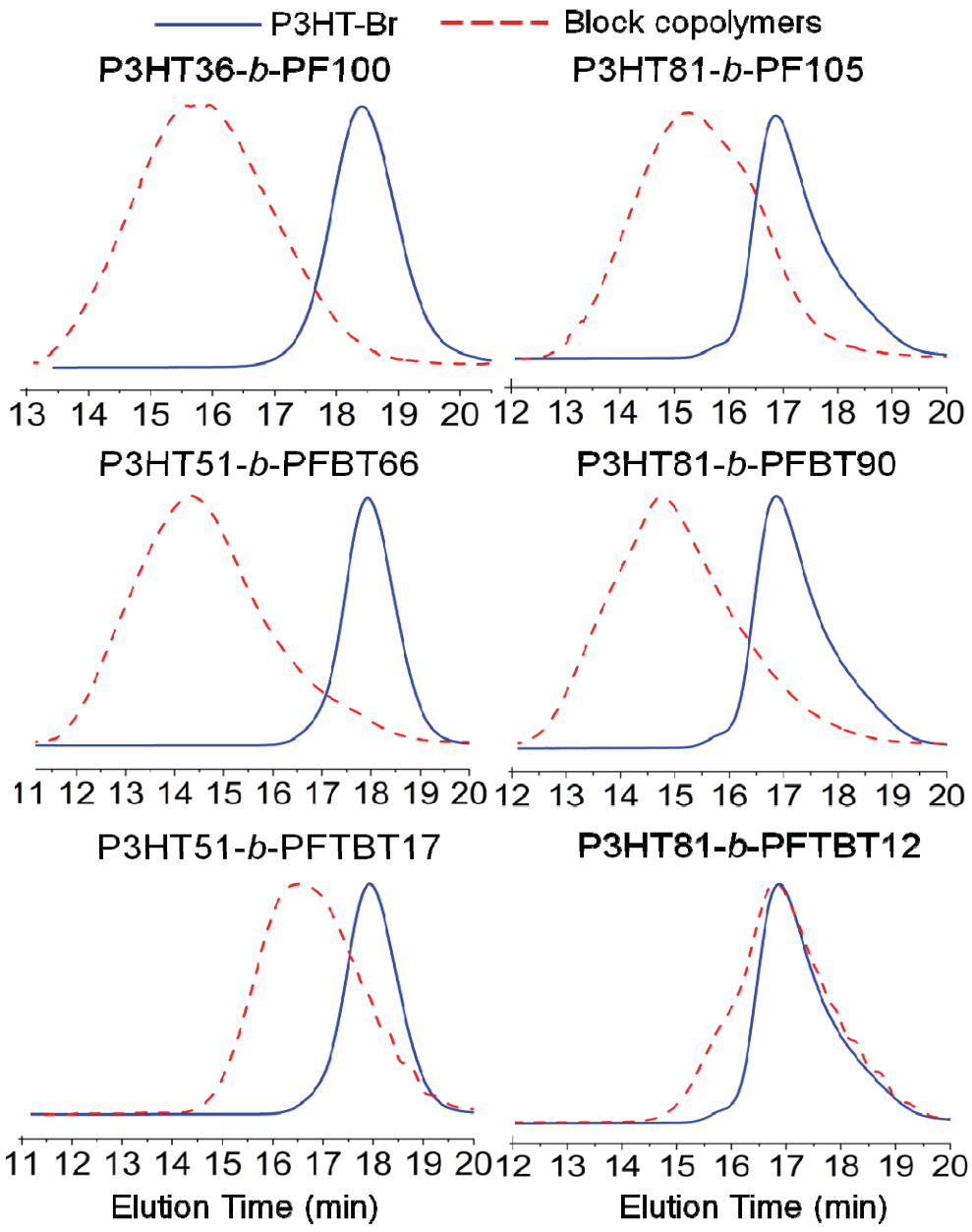

Figure 2.6 – SEC-RI analysis of block copolymers and corresponding P3HT-Br macroreagents. Intensities are normalized for clarity.

A comparison of the characteristics of final block copolymer products produced (Figure 2.6 and Table 2.1) with previous reports using similar methods[4-5] indicates that

the use of an LiCl additive enables the preparation of much cleaner and higher molecular weight block copolymers. With the exception of P3HT81–*b*–PFTBT12, a clear shift in the molecular weight distribution of the final products is observed relative to the starting P3HT homopolymers. For comparison, our previous attempts at making similar all-conjugated block copolymers using similar methods (but without the LiCl additive) resulted in only modest shifts in the molecular weight distribution along with homopolymer impurities.[5] Other reports using similar synthetic methods report the presence of significant homopolymer impurities or relatively low molecular weights for the second polymer block.[6,26] The clear shift in the molecular weight distributions of the block copolymer products shown in Figure 2.6 indicates that little or no residual P3HT homopolymer remains, and all-conjugated block copolymers with a mass-averaged molecular weight M_w as high as 168 kg/mol (relative to polystyrene) are produced. Number-averaged molecular weights for each block estimated by SEC-RI are in relatively good agreement with ^{1}H NMR estimates of P3HT content of the final block copolymers (see Table 2.1 and Figure 2.3, 2.4, and 2.5). In the case of P3HT81–*b*–PFTBT12, the synthesis failed to produce significant amounts of block copolymer due to poor solubility of the PFTBT block and the resulting block copolymer. However, the use of a lower molecular weight P3HT macroreagent in the polycondensation reaction of PFTBT resulted in product with majority block copolymer in P3HT51–*b*–PFTBT17.

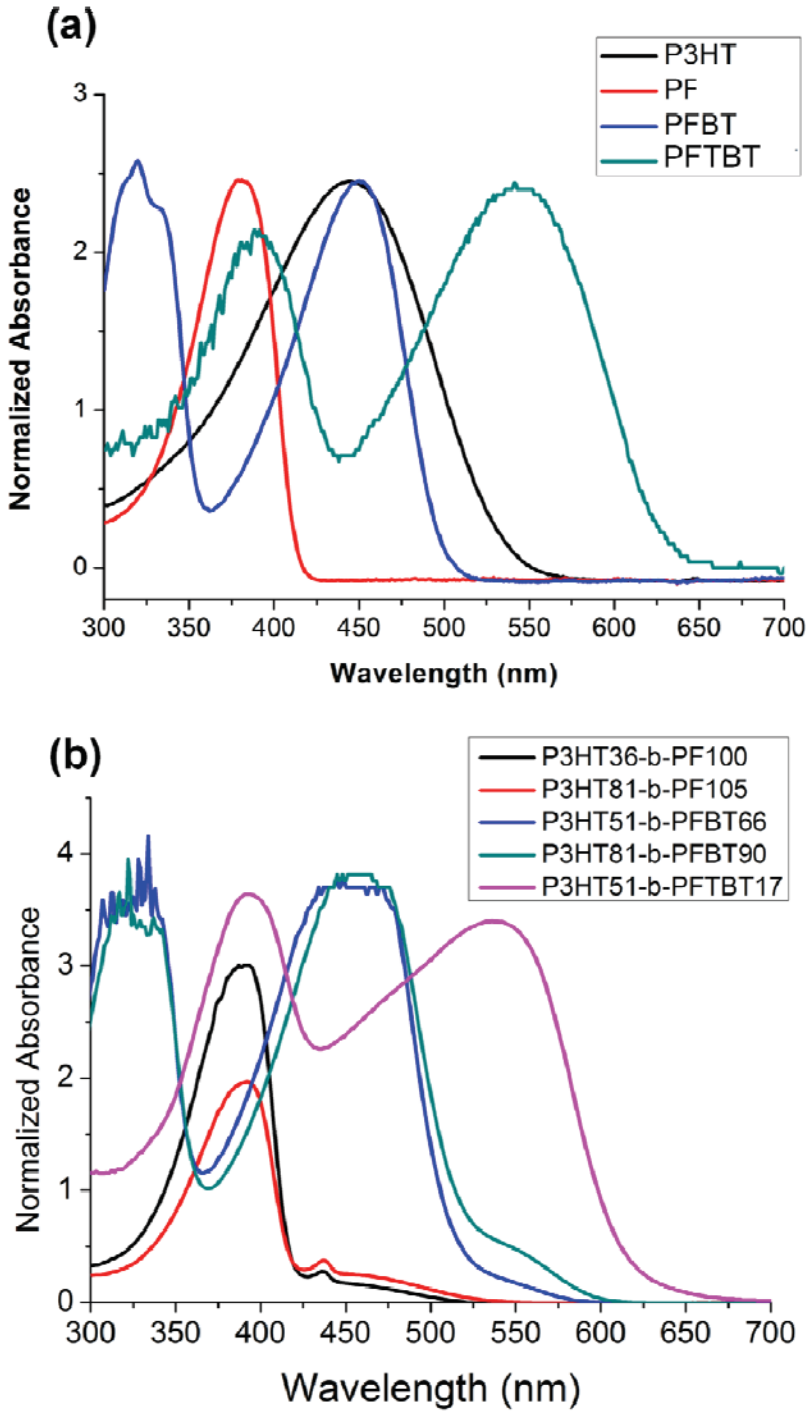

Figure 2.7 – (a) UV-VIS absorbance spectra for P3HT, PF, PFBT, and PFTBT homopolymers and (b) UV-VIS absorbance spectra for block copolymers.

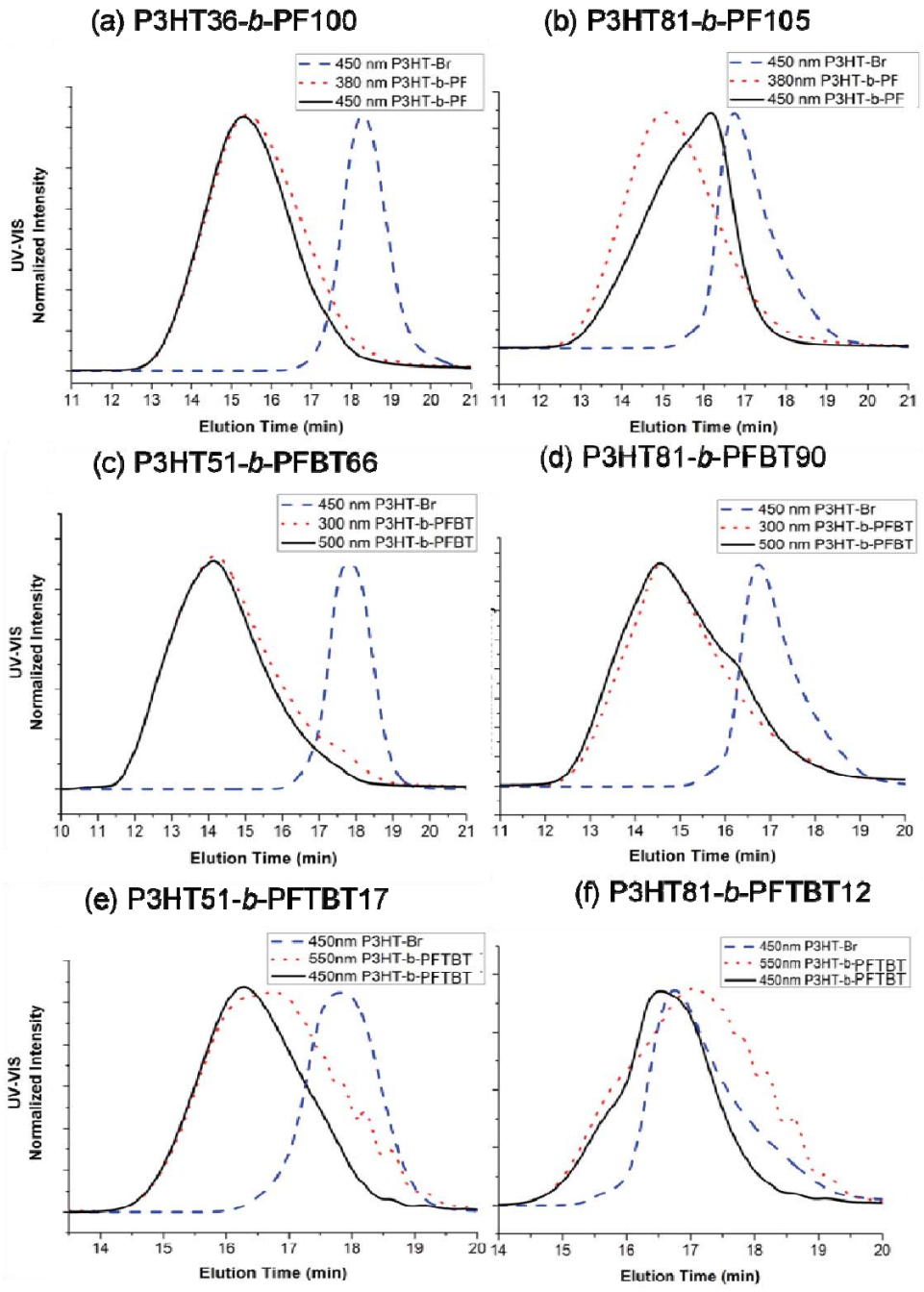

Figure 2.8 – SEC-UVVIS traces for block copolymers and P3HT macroreagents. All traces are normalized for clarity. SEC-UVVIS traces at 380 nm for P3HT–*b*–PF, 300 nm for P3HT–*b*–PFBT, and 450 nm for P3HT–*b*–PFTBT were corrected as described in Experimental Methods. SEC-UVVIS traces for block copolymers reflect the molecular weight distribution of one polymer block only.

Analysis of the final product using SEC with UV-VIS absorbance detection (SEC-UVVIS) provides additional information on homopolymer impurities (see Figure 2.7 and 2.8). By using two different wavelengths for analysis, the molecular weight distributions for each polymer block can be obtained (see experimental methods for details of this analysis). For all BCP samples except for P3HT81–*b*–PFTBT12, SEC-UVVIS analysis indicates clean block copolymer product - a clear shift in the SEC-UVVIS traces corresponding to P3HT is observed as well a good match between SEC-UVVIS traces at both wavelengths. The purity of the final product is better for block copolymers with shorter P3HT blocks; both P3HT36–*b*–PF100 and P3HT51–*b*–PFBT66 exhibit excellent overlap between SEC-UVVIS traces corresponding to both polymer blocks, while some high molecular weight P3HT homopolymer may be present in P3HT81–*b*–PF105 and P3HT81–*b*–PFBT90. In the case of P3HT51–*b*–PFTBT17, some high molecular weight PFTBT homopolymer is present, but the product is primarily block copolymer. Deconvolution of the SEC-RI trace gives an estimate of approximately 15% for PFTBT homopolymer impurities in the final P3HT51–*b*–PFTBT17 product.

Altogether, SEC-RI and SEC-UVVIS indicate the formation of clean all-conjugated block copolymer products. The synthetic method enables the preparation of all-conjugated block copolymers with high molecular weights (M_w up to 168 kg/mol) and with varying molecular weight of the P3HT block. Importantly, the synthetic method is straightforward to implement, scalable, and provides the final product in good overall yield.

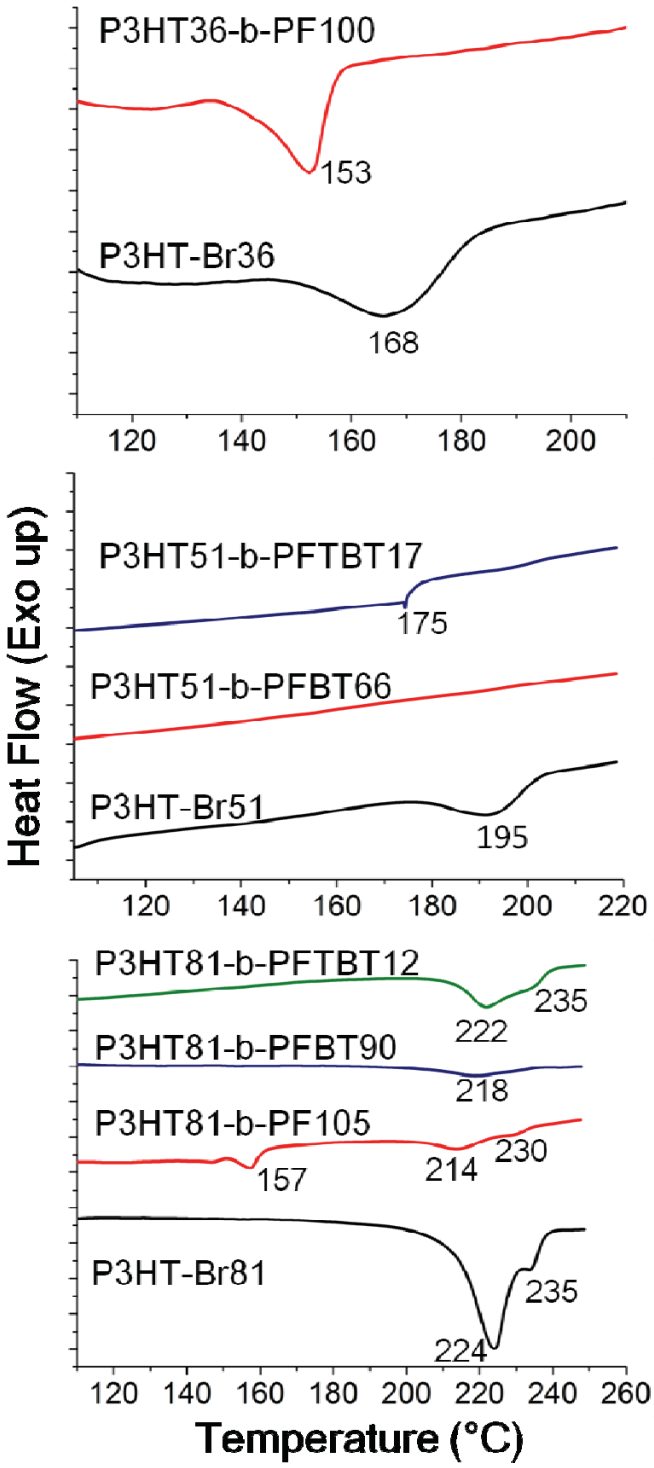

Figure 2.9 – DSC data for all-conjugated block copolymers and P3HT-Br macroreagents. Third heating cycles are shown for all samples, and a heating rate of 5 °C/min is used.

Prior studies on P3HT block copolymers have found that P3HT crystallization can dominate the morphology, suppressing micro-phase segregation and crystallization of the second block.[9,44-46] Here, we are able to test whether this holds true in large (M_w > 50 kg/mol) all-conjugated block copolymers with a semi-crystalline polymer block attached to a minority P3HT block. For all block copolymers, DSC indicates that the crystallization of P3HT is suppressed or shifted to lower temperatures, and as expected the effect is more pronounced in block copolymers with lower P3HT block ratios (Figure 2.9). For block copolymers with larger P3HT blocks, P3HT81–*b*–PF105 and P3HT81–*b*–PFBT90, a crystallization transition is observed at approximately 214 °C, a roughly 10 °C decrease in the crystallization temperature relative to the corresponding P3HT-Br macroreagent. P3HT crystallization is not observed for P3HT51–*b*–PFBT66 while the decrease in the crystallization temperature is approximately 15 and 20 °C for P3HT36–*b*–PF100 and P3HT51–*b*–PFTBT17, respectively. P3HT81–*b*–PFTBT12 exhibits a transition near 224 °C matching that of the corresponding P3HT-Br homopolymer, as expected due to the presence of P3HT homopolymer impurities. In the case of P3HT36–*b*–PF100, as discussed below, GIWAXS analysis indicates that the observed transition at 153 °C corresponds primarily to crystallization of the PF block. Only P3HT81–*b*–PF105 exhibits two transitions; one at 214 °C corresponding to P3HT crystallization and a second near 150 °C, corresponding to PF crystallization.

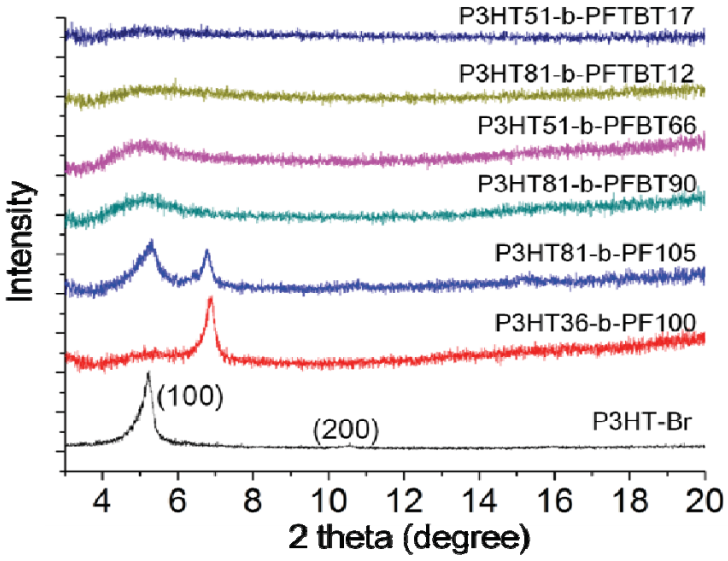

Figure 2.10 – XRD analysis of all-conjugated block copolymers and P3HT-Br.

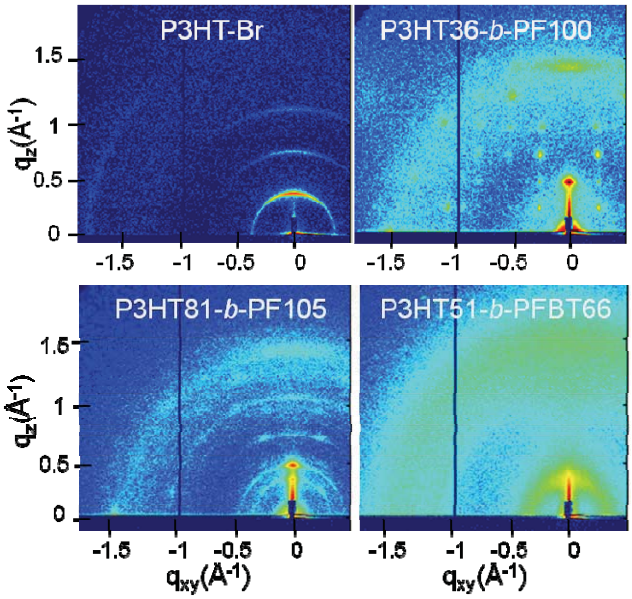

Figure 2.11 – GIWAXS measurement for P3HT-Br, P3HT36–*b*–PF100, P3HT81–*b*–PF105, and P3HT51–*b*–PFBT66. All samples were thermally annealed at 230 °C and measured at 80 °C. Samples were measured at an incident angle of 0.25° and 20 second exposure time. All images plotted using the same color scale for the scattered intensity.

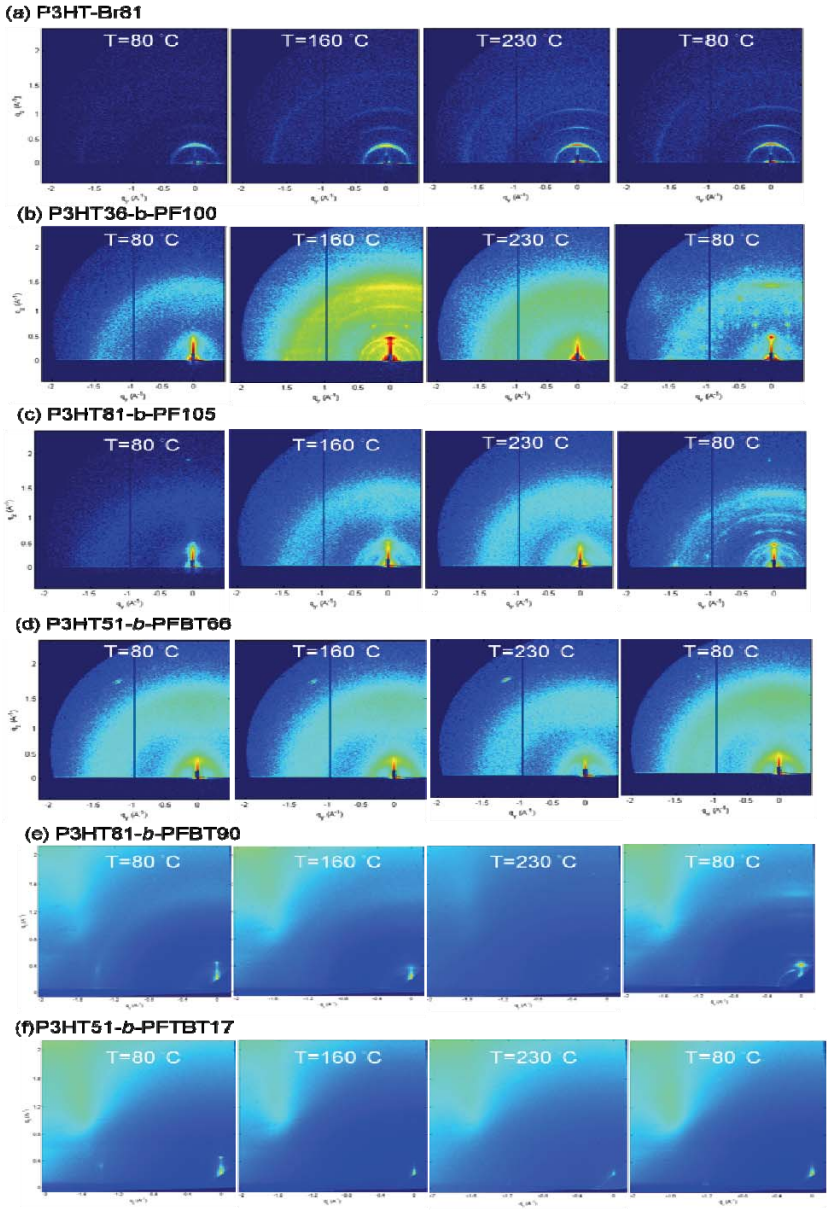

Figure 2.12 – Temperature-dependent GIWAXS measurements for block copolymer polymer thin films. (a) P3HT-Br81, (b) P3HT36–*b*–PF100, (c) P3HT81–*b*–PF105, (d) P3HT51–*b*–PFBT66, (e) P3HT81–*b*–PFBT90, (f) P3HT51–*b*–PFTBT17. Samples were heated from room temperature and measured at 80 °C, 160 °C and 230 °C before cooling and measuring again at 80 °C, as indicated for each sample from left to right. All samples were measured at an incident angle of 0.25° and 20 second exposure time.

XRD (Figure 2.10) and GIWAXS (Figure 2.11 and Figure 2.12) analysis confirms the low content of P3HT crystallinity in the block copolymer samples. P3HT–*b*–PFBT and P3HT–*b*–PFTBT block copolymers show only broad scattering peaks, while P3HT–*b*–PF block copolymers exhibit crystalline peaks corresponding primarily to PF crystallites. Highly oriented crystallites are observed in P3HT36–*b*–PF100 films with features characteristic of the PF phase,[47] confirming that the DSC transition near 150 °C reflects PF crystallization. In the case of P3HT81–*b*–PF105, both P3HT and PF crystallinites are observed, but P3HT crystallite peaks are less pronounced. Quantitative analysis of the GIWAXS pattern for P3HT81–*b*–PF105 shows scattering peaks at q_z = 0.38, 0.75, and 1.12 Å^{-1} corresponding to the (100), (200), and (300) reflections for P3HT crystallites and a scattering peak at q_z = 0.50 Å^{-1} corresponding to PF crystallites (see Figure 2.12b). This is consistent with DSC measurements that show both a PF and a P3HT crystallization transition for P3HT81–*b*–PF105, the latter which is shifted to lower temperatures relative to the corresponding P3HT-Br macroreagent. Altogether, DSC, XRD, and GIWAXS results show that P3HT crystallization is reduced or suppressed in high molecular weight all-conjugated P3HT block copolymers, and at more balanced block ratios both blocks can crystallize.

2.4. Conclusions

We demonstrate a straightforward, versatile, and scalable synthetic route to prepare block copolymers comprised of a poly(alkyl thiophene) block and second polymer block made *via* Suzuki-Miyaura polycondensation, and block copolymers with M_w > 50 kg/mol are achieved. Analysis of different all-conjugated block copolymers indicates that P3HT crystallinity is reduced or completely suppressed in all-conjugated

P3HT block copolymers. These results indicate that proper balance of block ratios is important for the development of all-conjugated block copolymers for use in OPVs.

2.5. References

(1) Scherf, U.; Gutacker, A.; Koenen, N., *Accounts Chem. Res.* **2008**, *41*, 1086-1097.

(2) Tu, G.; Li, H.; Forster, M.; Heiderhoff, R.; Balk, L. J.; Sigel, R.; Scherf, U., *Small* **2007**, *3*, 1001-1006.

(3) Mulherin, R. C.; Jung, S.; Huettner, S.; Johnson, K.; Kohn, P.; Sommer, M.; Allard, S.; Scherf, U.; Greenham, N. C., *Nano Lett.* **2011**, *11*, 4846-4851.

(4) Sommer, M.; Komber, H.; Huettner, S.; Mulherin, R.; Kohn, P.; Greenham, N. C.; Huck, W. T. S., *Macromolecules* **2012**, *45*, 4142-4151.

(5) Verduzco, R.; Botiz, I.; Pickel, D. L.; Kilbey, S. M.; Hong, K.; Dimasi, E.; Darling, S. B., *Macromolecules* **2011**, *44*, 530-539.

(6) Scherf, U.; Adamczyk, S.; Gutacker, A.; Koenen, N., *Macromol. Rapid Commun.* **2009**, *30*, 1059-1065.

(7) Gutacker, A.; Adamczyk, S.; Helfer, A.; Garner, L. E.; Evans, R. C.; Fonseca, S. M.; Knaapila, M.; Bazan, G. C.; Burrows, H. D.; Scherf, U., *J. Mater. Chem.* **2010**, *20*, 1423-1430.

(8) Ku, S.-Y.; Brady, M. A.; Treat, N. D.; Cochran, J. E.; Robb, M. J.; Kramer, E. J.; Chabinyc, M. L.; Hawker, C. J., *J. Am. Chem. Soc.* **2012**, *134*, 16040-16046.

(9) Yu, X.; Yang, H.; Wu, S.; Geng, Y.; Han, Y., *Macromolecules* **2012**, *45*, 266-274.

(10) Lai, Y.-C.; Ohshimizu, K.; Takahashi, A.; Hsu, J.-C.; Higashihara, T.; Ueda, M.; Chen, W.-C., *J. Polym. Sci., Part A: Polym. Chem.* **2011**, *49*, 2577-2587.

(11) Wu, P.-T.; Ren, G.; Kim, F. S.; Li, C.; Mezzenga, R.; Jenekhe, S. A., *J. Polym. Sci., Part A: Polym. Chem.* **2010**, *48*, 614-626.

(12) Javier, A. E.; Varshney, S. R.; McCullough, R. D., *Macromolecules* **2010**, *43*, 3233-3237.

(13) Hollinger, J.; Jahnke, A. A.; Coombs, N.; Seferos, D. S., *J. Am. Chem. Soc.* **2010**, *132*, 8546-8547.

(14) Ge, J.; He, M.; Qiu, F.; Yang, Y., *Macromolecules* **2010**, *43*, 6422-6428.
(15) Zhang, Y.; Tajima, K.; Hashimoto, K., *Macromolecules* **2009**, *42*, 7008-7015.
(16) Wu, S.; Bu, L.; Huang, L.; Yu, X.; Han, Y.; Geng, Y.; Wang, F., *Polymer* **2009**, *50*, 6245-6251.
(17) Wu, P.-T.; Ren, G.; Li, C.; Mezzenga, R.; Jenekhe, S. A., *Macromolecules* **2009**, *42*, 2317-2320.
(18) Zhang, Y.; Tajima, K.; Hirota, K.; Hashimoto, K., *J. Am. Chem. Soc.* **2008**, *130*, 7812-7813.
(19) Chueh, C.-C.; Higashihara, T.; Tsai, J.-H.; Ueda, M.; Chen, W.-C., *Org. Electron.* **2009**, *10*, 1541-1548.
(20) He, M.; Zhao, L.; Wang, J.; Han, W.; Yang, Y.; Qiu, F.; Lin, Z., *ACS Nano* **2010**, *4*, 3241-3247.
(21) Kiriy, A.; Senkovskyy, V.; Sommer, M., *Macromol. Rapid Commun.* **2011**, *32*, 1503-1517.
(22) Okamoto, K.; Luscombe, C. K., *Polym. Chem.* **2011**, *2*, 2424-2434.
(23) Verswyvel, M.; Verstappen, P.; De Cremer, L.; Verbiest, T.; Koeckelberghs, G., *J. Polym. Sci., Part A: Polym. Chem.* **2011**, *49*, 5339-5349.
(24) Botiz, I.; Schaller, R. D.; Verduzco, R.; Darling, S. B., *J. Phys. Chem.C* **2011**, *115*, 9260-9266.
(25) Woody, K. B.; Leever, B. J.; Durstock, M. F.; Collard, D. M., *Macromolecules* **2011**, *44*, 4690-4698.
(26) Ouhib, F.; Khoukh, A.; Ledeuil, J.-B.; Martinez, H.; Desbrières, J.; Dagron-Lartigau, C., *Macromolecules* **2008**, *41*, 9736-9743.
(27) Ohshimizu, K.; Takahashi, A.; Higashihara, T.; Ueda, M., *J. Polym. Sci., Part A: Polym. Chem.* **2011**, *49*, 2709-2714.
(28) Sun, S.-S.; Zhang, C.; Ledbetter, A.; Choi, S.; Seo, K.; Carl E. Bonner, J.; Drees, M.; Sariciftci, N. S., *Appl. Phys. Lett.* **2007**, *90*, 043117.
(29) Chen, X. L.; Jenekhe, S. A., *Macromolecules* **1996**, *29*, 6189-6192.
(30) Xiao, X.; Fu, Y.; Sun, M.; Li, L.; Bo, Z., *J. Polym. Sci., Part A: Polym. Chem.* **2007**, *45*, 2410-2424.

(31) Han, Y.-K. L., Y-J; and Huang, P-C, *J. Electrochem. Soc.* **2009**, *156*, k37-k43.
(32) Svensson, M.; Zhang, F.; Veenstra, S. C.; Verhees, W. J. H.; Hummelen, J. C.; Kroon, J. M.; Inganäs, O.; Andersson, M. R., *Adv. Mater.* **2003**, *15*, 988-991.
(33) Lohwasser, R. H.; Thelakkat, M., *Macromolecules* **2011**, *44*, 3388-3397.
(34) Jiang, Z.; Li, X. F.; Strzalka, J.; Sprung, M.; Sun, T.; Sandy, A. R.; Narayanan, S.; Lee, D. R.; Wang, J., *J. Synchrot. Radiat.* **2012**, *19*, 627-636.
(35) Jiang, Z., *GIXSGUI is available for download: http://www.aps.anl.gov/Sectors/Sector8/Operations/GIXSGUI.html*.
(36) Kochemba, W. M.; Kilbey, S. M.; Pickel, D. L., *J. Polym. Sci., Part A: Polym. Chem.* **2012**, *50*, 2762-2769.
(37) Takahashi, A.; Rho, Y.; Higashihara, T.; Ahn, B.; Ree, M.; Ueda, M., *Macromolecules* **2010**, *43*, 4843-4852.
(38) Loewe, R. S.; Ewbank, P. C.; Liu, J. S.; Zhai, L.; McCullough, R. D., *Macromolecules* **2001**, *34*, 4324-4333.
(39) Herguth, P.; Jiang, X.; Liu, M. S.; Jen, A. K. Y., *Macromolecules* **2002**, *35*, 6094-6100.
(40) Kim, Y.; Cook, S.; Choulis, S. A.; Nelson, J.; Durrant, J. R.; Bradley, D. D. C., *Chem. Mater.* **2004**, *16*, 4812-4818.
(41) Calabrese, A.; Schimperna, G.; Po, R.; Yohannes, T.; Debebe, S. E.; Tinti, F.; Camaioni, N., *J. Appl. Phys.* **2011**, *110*, 113106.
(42) Lee, W.-Y.; Cheng, K.-F.; Wang, T.-F.; Chueh, C.-C.; Chen, W.-C.; Tuan, C.-S.; Lin, J.-L., *Macromol. Chem. Phys.* **2007**, *208*, 1919-1927.
(43) Lee, W.-Y.; Cheng, K.-F.; Wang, T.-F.; Chen, W.-C.; Tsai, F.-Y., *Thin Solid Films* **2010**, *518*, 2119-2123.
(44) Choi, S. Y.; Lee, J. U.; Lee, J. W.; Lee, S.; Song, Y. J.; Jo, W. H.; Kim, S. H., *Macromolecules* **2011**, 1771-1774.
(45) Dai, C. A.; Yen, W. C.; Lee, Y. H.; Ho, C. C.; Su, W. F., *J. Am. Chem. Soc.* **2007**, *129*, 11036-11038.
(46) Lee, Y. J.; Kim, S. H.; Yang, H.; Jang, M.; Hwang, S. S.; Lee, H. S.; Baek, K.-Y., *J. Phys. Chem.C* **2011**, *115*, 4228-4234.

(47) Chen, S. H.; Chou, H. L.; Su, A. C.; Chen, S. A., *Macromolecules* **2004**, *37*, 6833-6838.

Chapter 3

Lamellar and Liquid Crystal Ordering in Solvent-Annealed All-Conjugated Block Copolymers

This chapter is included in Yen-Hao Lin, Kevin G. Yager, Bridget Stewart, Rafael Verduzco, "Lamellar Structures of Solvent Annealed All-Conjugated Block Copolymers," *Soft Matter,* 2014, **4(2)**, 3817-3825. Portions of this chapter are included in Yen-Hao Lin and Rafael Verduzco, "Synthesis and Process-Dependent Film Structure of All-conjugated Copolymers for Organic Photovoltaics," *The American Chemical Society Symposium of Polymer Composites for Energy Harvesting, Conversion and Storage*, 2014, Chapter 3, 49-70.

All-conjugated block copolymers are an emerging class of polymeric materials promising for organic electronic applications, but further progress requires a better understanding of their microstructure including crystallinity and self-assembly through micro-phase segregation. Here, we demonstrate remarkable changes in the thin film structure of a model series of all-conjugated block copolymers with varying processing conditions. Under thermal annealing, poly(3-hexylthiophene)–*b*–poly(9′,9′-

dioctylfluorene) (P3HT–*b*–PF) all-conjugated block copolymers exhibit crystalline features of P3HT or PF, depending on the block ratio, and poor π-π stacking. Under chloroform solvent annealing, the block copolymers exhibit lamellar ordering, as evidenced by multiple reflections in grazing incidence wide- and small-angle X-ray scattering (GIWAXS and GISAXS), including an in-plane reflection indicative of order along the π-π stacking direction for both P3HT and PF blocks. The lamellae have a characteristic domain size of 4.2 nm, and this domain size is found to be independent of block copolymer molecular weight and block ratio. This suggests that lamellar self-assembly arises due to a combination of polymer block segregation and π-π stacking of both P3HT and PF polymer blocks. Strategies for predicting the microstructure of all-conjugated block copolymers must take into account intermolecular π-π stacking and liquid crystalline interactions not typically found in flexible coil block copolymers.

3.1. Introduction

All-conjugated block copolymers are an emerging class of materials comprised of two or more covalently linked conjugated polymer chains. This class of block copolymers is of interest for organic electronic applications because they combine the optoelectronic properties of semiconductive polymers with structure control through micro-phase segregation[1,2] and crystallization.[3,4] As an example, recent work demonstrated significant performance enhancement in block copolymer organic photovoltaics (OPVs) compared with polymer-polymer blends.[5] However, further progress in the development of all-conjugated block copolymers requires a better understanding of the microstructure of all-conjugated block copolymers and how their crystallinity, micro-phase segregation, and domain orientation can be controlled by applying different processing strategies.

Comprehensive theoretical and experimental studies of rod-coil diblock copolymers (containing one conjugated polymer block and one flexible coil polymer block) have revealed an interplay between relative block size, polymer crystallinity, liquid crystal ordering, and micro-phase segregation.[6-11] Processing conditions have been demonstrated to give some control over the microstructure of rod-coil block copolymers, including aligned domains through the application of a magnetic field[12-15] or the formation of micellar assemblies using a selective solvent.[16] This work has led to the development of a quantitative model to describe the phase behavior of rod-coil block copolymers, including self-assembly and liquid crystal ordering.[17] Comparable predictive models are unavailable for all-conjugated block copolymers due in part to limited experimental studies on structure-processing relationships. Previous work with P3HT-based all-conjugated block copolymers have found that P3HT crystallization dominates the film morphology, suppressing micro-phase segregation and crystallization of the second polymer block.[18,19] Evidence for micro-phase segregation in rod-rod all-conjugated block copolymer has been inconclusive, potentially due to polymer crystallization, slow dynamics, stiff polymer backbones, and/or low enthalpic driving force for micro-phase segregation.[20] Improved control over the microstructure of all-conjugated block copolymers and a broader understanding of structure-processing-property relationships could benefit their development for and use in organic electronic devices and applications.

Here, we report remarkable changes in the thin film structure of a model series of all-conjugated block copolymers under different annealing conditions. Thermally annealed, poly(3-hexylthiophene)–*b*–poly(9′,9′-dioctylfluorene) (P3HT–*b*–PF) (Figure 3.1) all-conjugated block copolymers exhibit crystalline features characteristic of P3HT or PF, but poor order along the π-π stacking direction. The same block copolymers, under

solvent annealing, self-assemble into a lamellar phase, as evidenced by multiple reflections in grazing incidence wide- and small-angle X-ray scattering (GIWAXS and GISAXS). The degree of face-to-face π-π stacking substantially increases in solvent-annealed compared with unannealed films. We present a detailed analysis of the structure of P3HT–*b*–PF block copolymer films and the self-assembled lamellar phase, including paracrystallinity measurement, spectroscopic properties, and phase behaviour with temperature. These results indicate that all-conjugated block copolymers have a rich, processing-dependent microstructure determined by a combination of π-π stacking, crystallization, and micro-phase segregation of the polymer blocks.

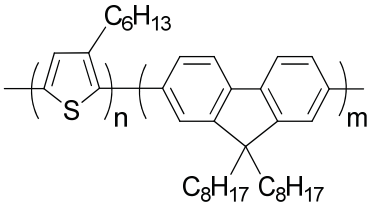

Figure 3.1 – Chemical structure of poly(3-hexylthiophene)–*b*–poly(9′,9′-dioctylfluorene) (P3HT–*b*–PF).

3.2. Experimental methods

3.2.1. Synthesis of P3HT–*b*–PF

P3HT–*b*–PF block copolymers were synthesized with using the method shown in chapter 2.[21] Characteristics of P3HT–*b*–PF block copolymers reported in this study are listed in Table 3.1. ^{1}H NMR spectra are provided below in Figure 3.2.

Polymers	P3HT[a] M_w (PDI)	BCP[a] M_w (PDI)	DP ratios[b] (P3HT wt%)
P3HT36–*b*–PF100	6.1 (1.16)	48.4 (1.86)	36:100 (13%)
P3HT81–*b*–PF105	13.5 (1.32)	60.6 (1.87)	81:105 (25%)
P3HT84–*b*–PF80	14.1 (1.10)	42.5 (1.58)	84:80 (33%)
P3HT84–*b*–PF13	14.1 (1.10)	22.8 (1.39)	84:13 (74%)

[a] M_w (kg/mol) and PDI for P3HT and block copolymers determined by comparison to a set of monodisperse polystyrene standards. Head-to-tail regioregularity of P3HT is greater than 93% for all samples as determined from ^{1}H NMR. [b]DP ratios and P3HT content were determined by ^{1}H NMR *via* comparison of the integrated intensity of P3HT aromatic peak (6.9 ppm) and fluorene alkyl peaks (2.2 ppm).

Table 3.1 – Characteristics of all-conjugated P3HT–*b*–PF block copolymers.

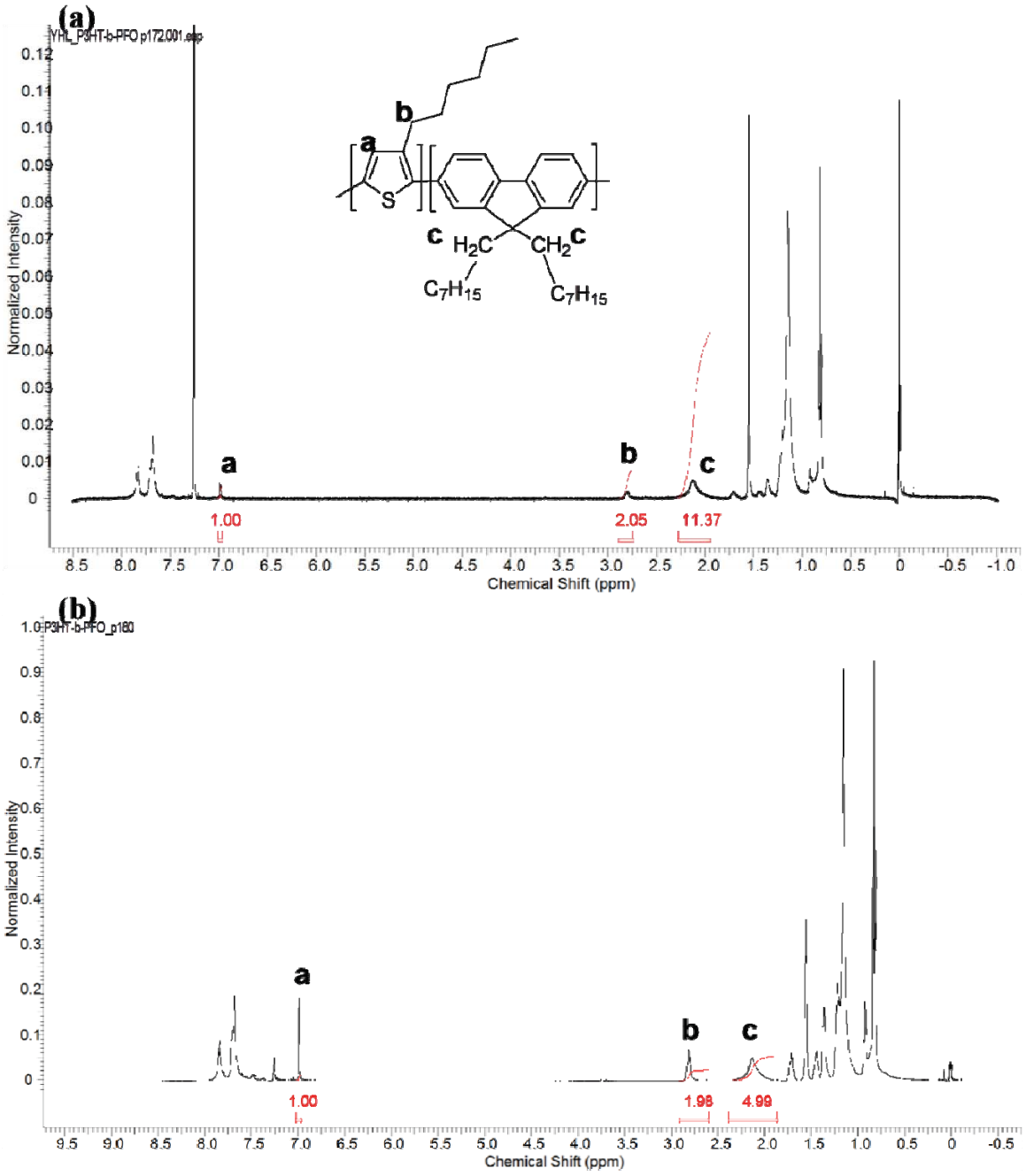
(a)
YHL_P3HT-b-PFO p172.001.esp
Normalized Intensity
Chemical Shift (ppm)
a
b
c
1.00
2.05
11.37
(b)
1.0-P3HT-b-PFO_p180
Normalized Intensity
Chemical Shift (ppm)
a
b
c
1.00
1.98
4.99

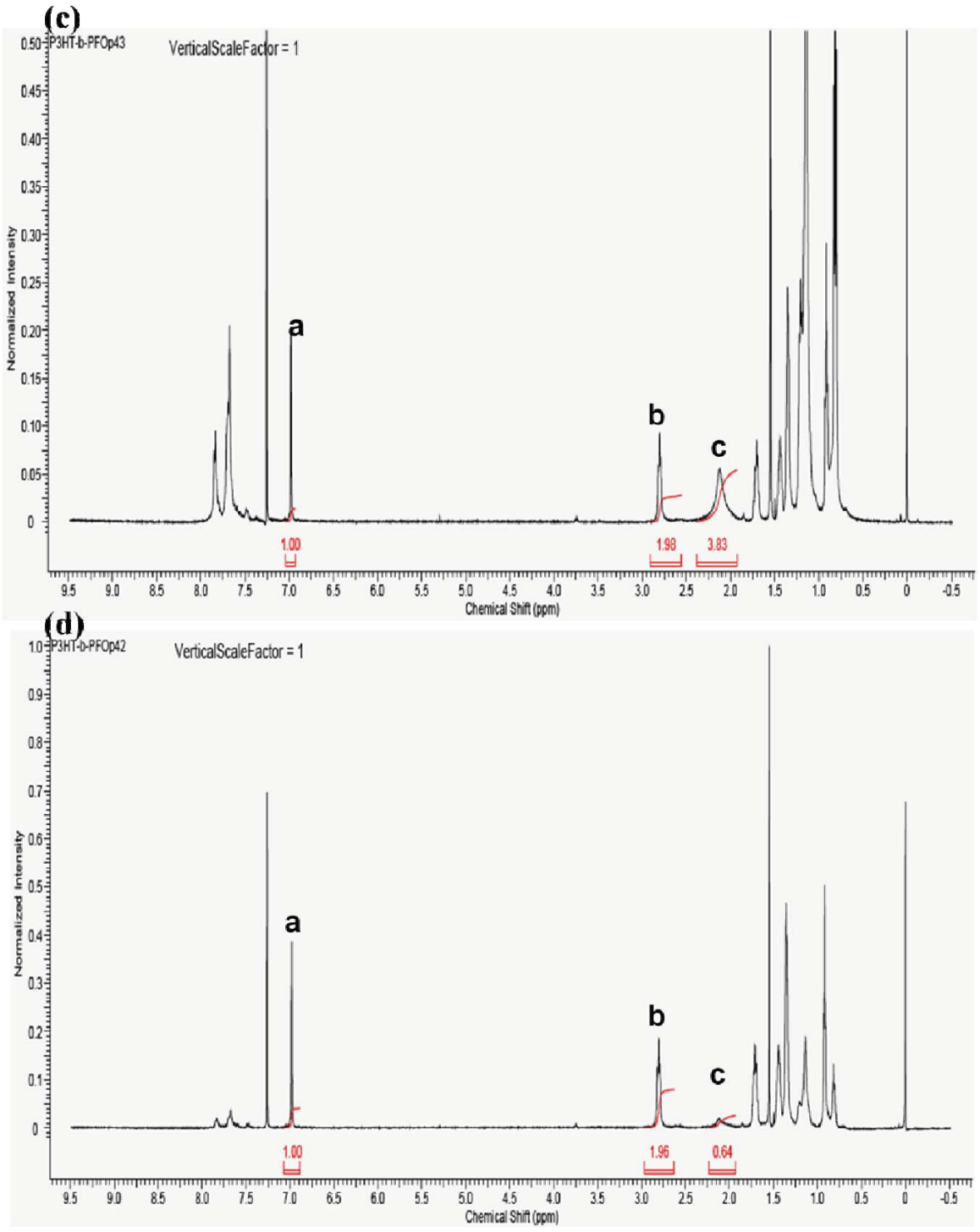

Figure 3.2 – ^{1}H NMR spectrum of (a) P3HT36–*b*–PF100, (b) P3HT81–*b*–PF105 (c) P3HT84–*b*–PF80 and (d) P3HT84–*b*–PF13.

3.2.2. Sample preparation and measurements

Sample films were prepared by drop casting from 0.05 wt% chloroform solutions onto silicon substrates and quartz substrates. Evaporation of chloroform under ambient conditions gives films with a thickness of approximately 350 nm as measured by X-ray reflectivity. Samples were solvent annealed in a closed chamber saturated with chloroform at ambient temperature and pressure for 5 days. Samples were dried under vacuum for at least 12 hours prior to measurement.

Grazing incident small- and wide-angle X-ray scattering (GIWAXS and GISAXS) measurements were carried out on the X9 beamline at the National Synchrotron Light Source, Brookhaven National Laboratory. The undulator beamline was operated at an energy of 14 keV; two-dimensional images were collected using CCD area detectors. The beam size was 100 μm (h) × 50 μm (v). Sample detector distance was 370 mm for the wide-angle detector and 3091 mm for the small-angle detector. Sample measurements were carried out under vacuum which was in the range of 2~3 × 10^{-6} bar, with a temperature-controlled sample stage interfaced with a Lakeshore 340 unit.

GIXS measurement at Argonne National Laboratory. The measurements were carried out on Sector 8-ID-E at the Advanced Photon Source, Argonne National Laboratory.[22] Beamline 8-ID-E operates at an energy of 7.35 keV and images were collected from a Pilatus 1MF camera (Dectris), with two exposures for different vertical position of the detector. After flatfield correction for detector nonuniformity, the images are combined to fill in the gaps for rows at the borders between modules, leaving dark only the columns of inactive pixels at the center. Using the GIXSGUI package[23] for Matlab (Mathworks), data are corrected for X-ray polarization, detector sensitivity and geometrical solid-angle. The beam size is 200 μm (h) x 20 μm (v). Sample detector

distance is 204 mm. Sample measurement and thermal annealing were carried out under vacuum which is in the range of 2~3 × 10^{-6} bar, with the sample stage interfaced with a Lakeshore 340 unit.

Differential Scanning Calorimetry (DSC) measurements were performed using a TA Instrument DSC Q10 with a ramp rate of 5 °C/min under N_2. Samples were placed in hermetic pans from Thermal Support, Inc. Solvent annealed samples were solvent annealed as described above for one month and dried under vacuum before measurement. All samples were subjected to at least two heating and cooling cycles between 10 °C to 250 °C.

Ultraviolet-Visible Absorbance Spectroscopy (UV-VIS) measurements were carried out with a Shimadzu UV-3101PC spectrophotometer with scan range of 200 nm – 900 nm. All films were cast on quartz substrates.

Polarized Optical Microscopy (POM) images of polymer films were acquired using an Axioplan 2 imaging microscope in reflective mode. Films were the same as films for GIXS measurements. Images were processed using Axio Vision version 4.8.

3.3. Results and discussions

P3HT–*b*–PF is an all-conjugated block copolymer comprised of two semi-crystalline conjugated polymer blocks (crystal melting temperatures 220 °C and 150 °C for P3HT and PF, respectively). Prior work with P3HT–*b*–PF thin films has found a morphology dominated primarily by crystallization of the P3HT or PF block but no evidence for liquid crystal ordering or micro-phase segregation.[19,21,24,25] We hypothesized that long-term solvent annealing in a good solvent for both blocks would increase chain mobility, yielding improved crystallinity, new phases and/or micro-phase segregation.

Similar strategies applied to flexible coil block copolymers can result in improved long-range ordering of block copolymer domains and, in some cases, new phases through micro-phase segregation.[26]

As detailed by prior work, the microstructure of P3HT and PF homopolymers is influenced by processing. Regioregular P3HT organizes into lamellar crystalline domains with face-to-face π-π stacking between chains and lamellar stacking through the hexyl side-chains.[27] In solution processed thin films, the preferred orientation of P3HT crystallites can be dictated to some extent by varying processing conditions.[28] PF exhibits crystalline, liquid crystalline, or amorphous phases depending on its processing history.[29-31]

To investigate the role of processing and annealing conditions, the microstructure of a series of P3HT–*b*–PF films with varying P3HT contents after solvent and/or thermal annealing were analyzed by grazing-incidence X-ray scattering, microscopy, UV-VIS absorbance measurements, and differential scanning calorimetry (DSC). P3HT–*b*–PF all-conjugated block copolymers with varying block ratios were synthesized *via* a combination of Grignard metathesis and Suzuki-Miyaura polycondensation. The P3HT–*b*–PF block copolymers studied have varying compositions ranging from 13 wt% of P3HT to 74 wt% of P3HT, as shown in Table 1. Samples films were drop cast from chloroform and analyzed by grazing-incidence wide- and small-angle scattering (GIWAXS and GISAXS) without annealing (as-cast), after thermal annealing, and with long-time solvent annealing (5 days at room temperature, $CHCl_3$).

3.3.1. Grazing Incidence X-ray Scattering (GIXS) Analysis of P3HT–*b*–PF under varying processing conditions

Small- and wide-angle X-ray scattering (GISAXS and GIWAXS) measurements provide information on both the in-plane (q_{xy}, direction parallel to substrate) and out-of-plane (q_z, direction perpendicular to the substrate) structure of the films. Peaks or reflections in the spectra indicate periodicities in the film microstructure, which may arise due to crystallinity or self-assembly processes. More information on the application of GIWAXS and GISAXS to study block copolymer films is provided by Lee et al.[32]

GIWAXS measurements of P3HT–*b*–PF films are shown in Figure 3.3, 3.4 and 3.5. As-cast P3HT–*b*–PF films are amorphous and exhibit a weak in-plane reflection at q~1.45 Å^{-1} (see Figure 3.3, 3.4 and 3.5). This in-plane reflection matches the π-π stacking reflection observed in PF homopolymer films,[33] and we therefore conclude this reflection indicates some π-π stacking of the PF polymer block in as-cast films. P3HT84–*b*–PF13 additionally exhibits weak scattering peaks characteristic of P3HT crystallites: an in-plane π-π stacking (010) peak at q ~ 1.65 Å^{-1} and out-of-plane (100), (200), and (300) peaks.[4,27,34]

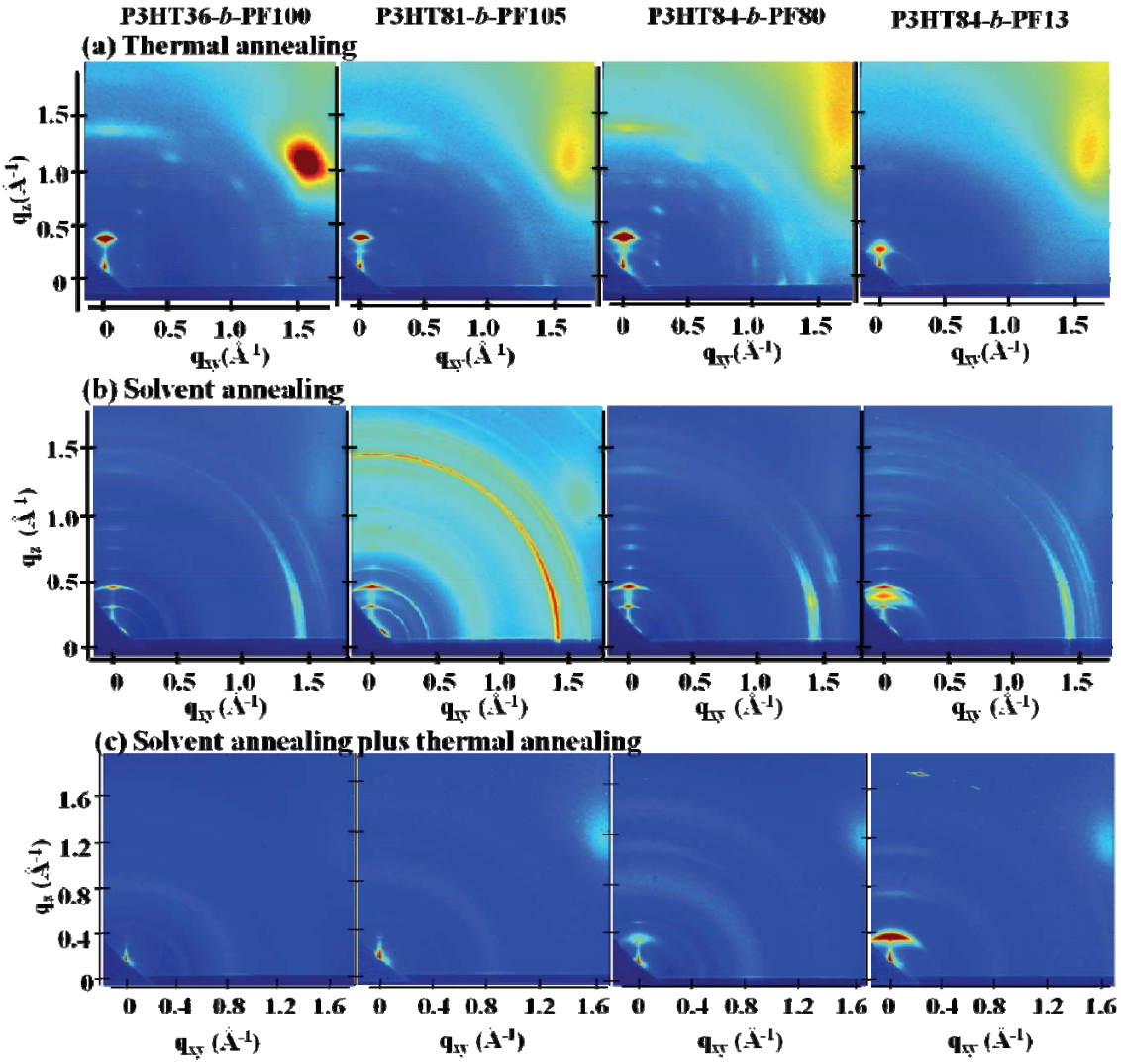

Figure 3.3 – GIWAXS measurements for P3HT36–*b*–PF100, P3HT81–*b*–PF105, P3HT84–*b*–PF80, P3HT84–*b*–PF13 with varying processing histories, as indicated. (a) and (b) were acquired at room temperature and (c) was acquired at 150 ^{o}C. All samples were measured at an incident angle of 0.25° and 30 seconds exposure time.

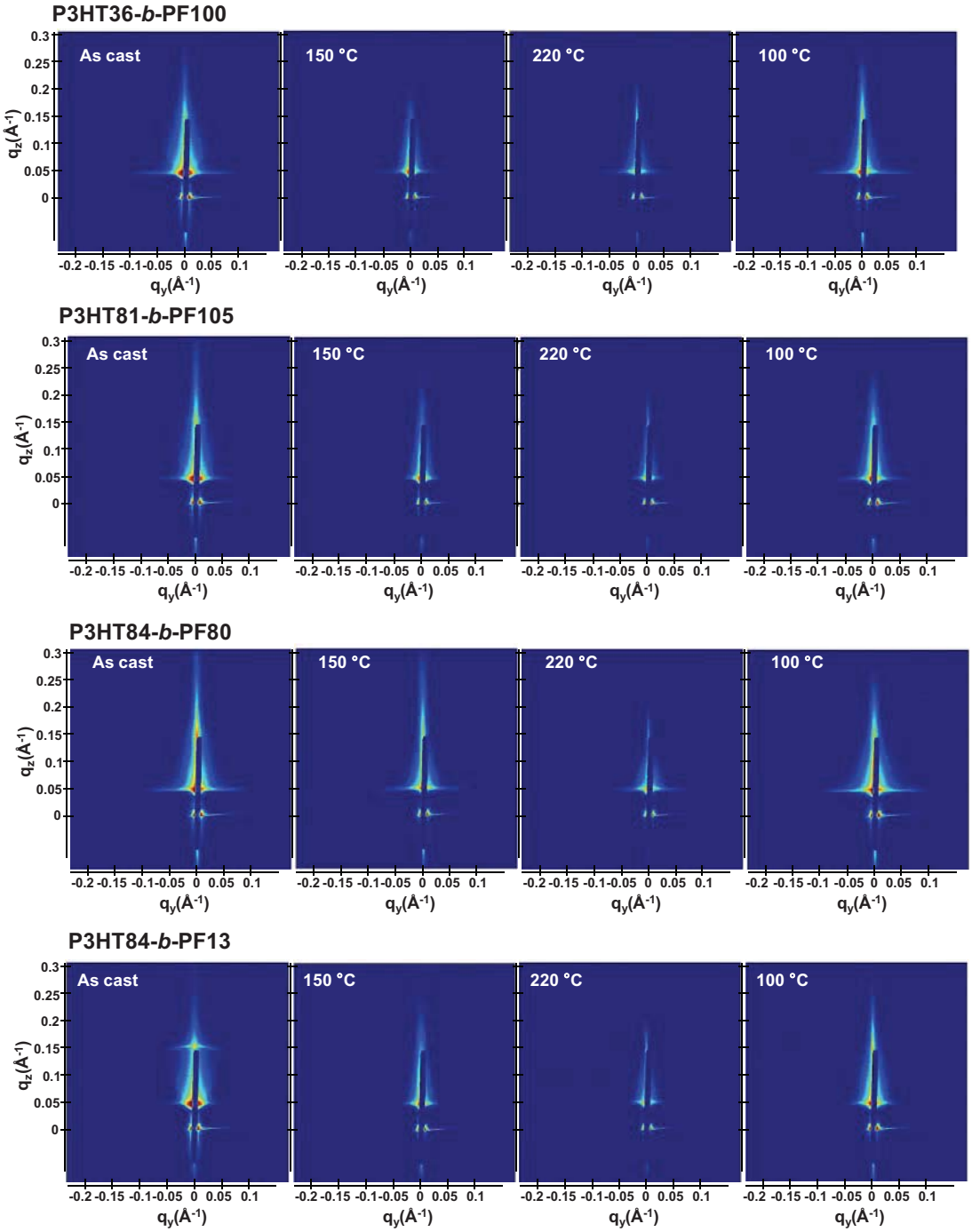

Figure 3.4 – GISAXS measurement for P3HT36–*b*–PF100, P3HT81–*b*–PF105, P3HT84–*b*–PF80, P3HT84–*b*–PF13. All samples were in-situ thermally annealed and measured at various temperatures. Samples were measured at an incident angle of 0.25° and 5 seconds exposure time. All images plotted using the same color scale for the scattered intensity.

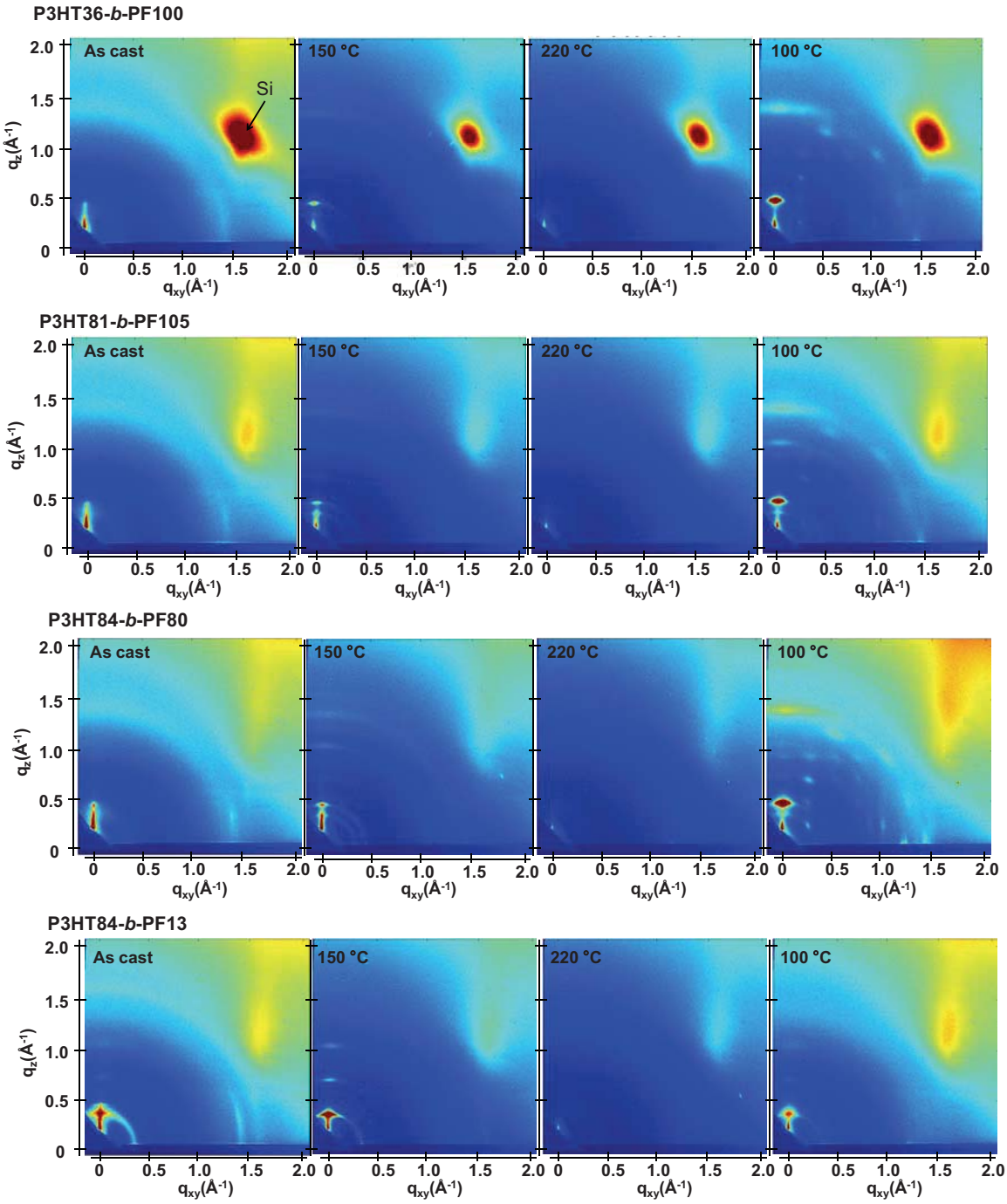

Figure 3.5 – GIWAXS measurement for P3HT36–*b*–PF100, P3HT81–*b*–PF105, P3HT84–*b*–PF80, P3HT84–*b*–PF13. All samples were in-situ thermally annealed and measured at various temperatures. Samples were measured at an incident angle of 0.25° and 30 seconds exposure time. All images plotted using the same color scale for the scattered intensity.

After thermal annealing at 220 °C - beyond the crystal melting temperatures for both blocks - and cooling to 100 °C, the films exhibit characteristics of pure P3HT or PF crystallites, or both, depending on the block ratio (Figure 3.3a). Thermally annealed P3HT36–*b*–PF100 films exhibit characteristics of PF α-phase crystals[34] while thermally annealed P3HT84–*b*–PF13 films show (100), (200), and (300) P3HT crystal reflections. Block copolymers with intermediate P3HT compositions, P3HT81–*b*–PF105 and P3HT84–*b*–PF80, show primarily reflections consistent with PF α-phase and some crystallization of the P3HT block. In contrast to thermally annealed P3HT homopolymer films, reflections corresponding to π-π stacking (q ~ 1.45 $Å^{-1}$ and 1.65 $Å^{-1}$ for PF and P3HT, respectively) are absent for all thermally annealed block copolymer films.

Block copolymer films subjected to 5 days of solvent annealing in a good solvent for both blocks (chloroform) exhibit multiple out-of-plane reflections indicative of long-range, lamellar ordering (Figure 3.3b, 3.6 and 3.7). A primary GISAXS reflection is observed at ~0.15 $Å^{-1}$, which corresponds to a spacing between lamellae of approximately 4.2 nm (Figure 3.6). As shown in Figure 3.7, the observed peaks are separated by integral multiples of q. These reflections reveal long-range lamellar ordering in solvent annealed P3HT–*b*–PF films not present in solvent or thermally annealed pristine P3HT or PF films. By contrast, solvent annealed P3HT homopolymer exhibits a (100) crystal peak while solvent-annealed PF films exhibit a metastable liquid crystal β mesophase[35] (Figure 3.8, 3.9 and 3.10).

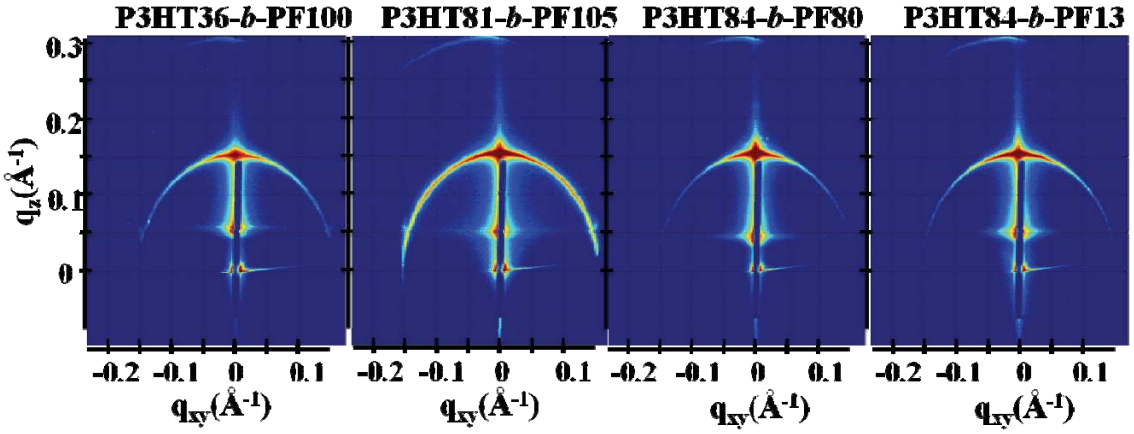

Figure 3.6 – GISAXS measurements for solvent-annealed P3HT36–*b*–PF100, P3HT81–*b*–PF105, P3HT84–*b*–PF80, P3HT84–*b*–PF13. Samples were analyzed at room temperature.

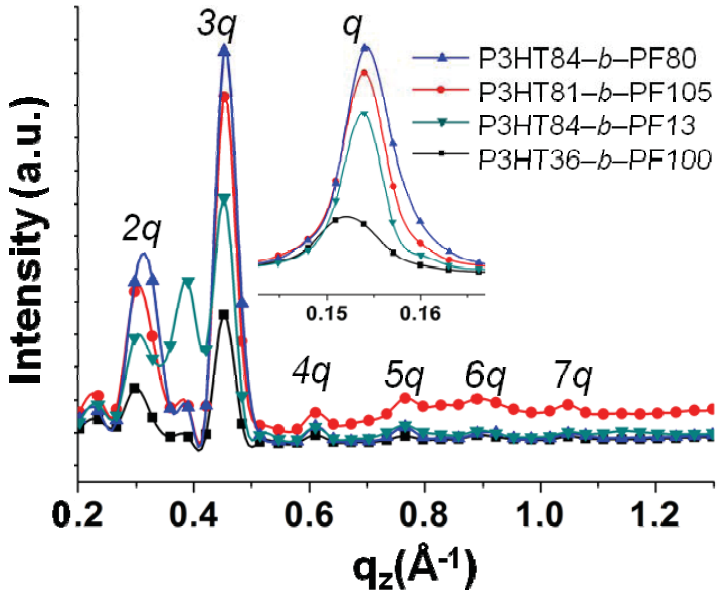

Figure 3.7 – Linecuts of GISAXS (imbedded figure) and GIWAXS measurements along $q_{xy} \sim 0$ Å^{-1} for solvent annealed samples.

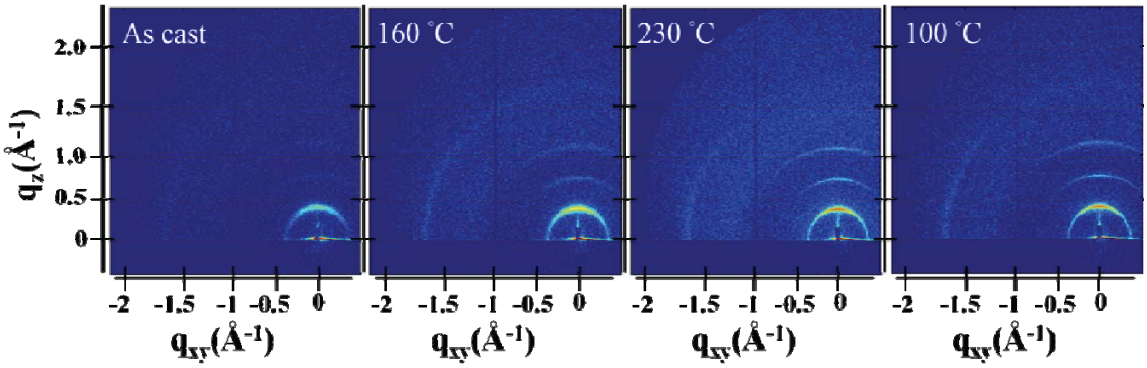

Figure 3.8 – GIWAXS patterns of a P3HT-Br thin films cast at room temperature and thermally annealed in-situ. All samples were measured at an incident angle of 0.25° and 20 seconds exposure time, and all images have the same color scale.

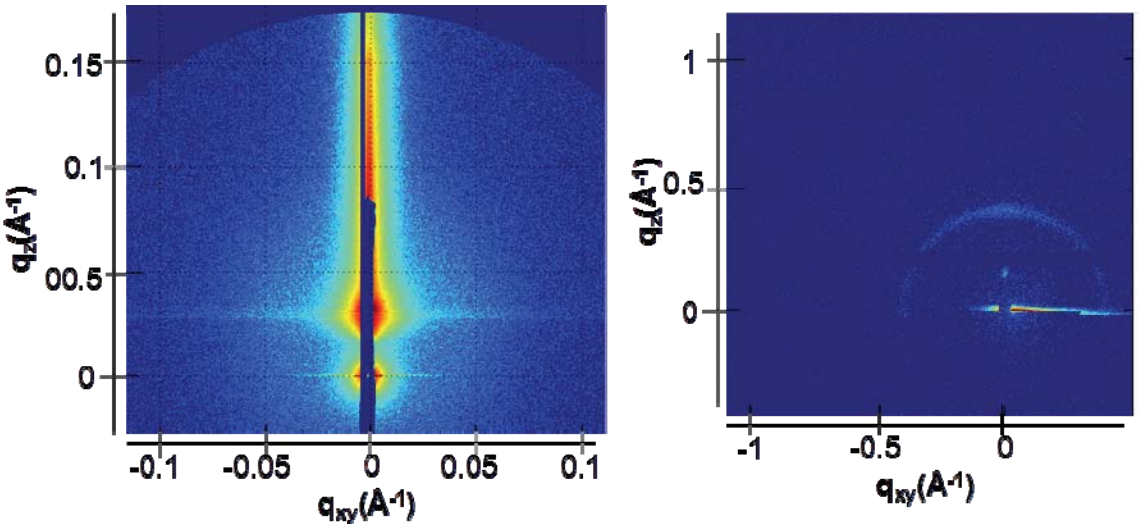

Figure 3.9 – GISAXS and GIWAXS measurement for P3HT homopolymer. Samples were annealed at room temperature with $CHCl_3$ vapors for 5 days.

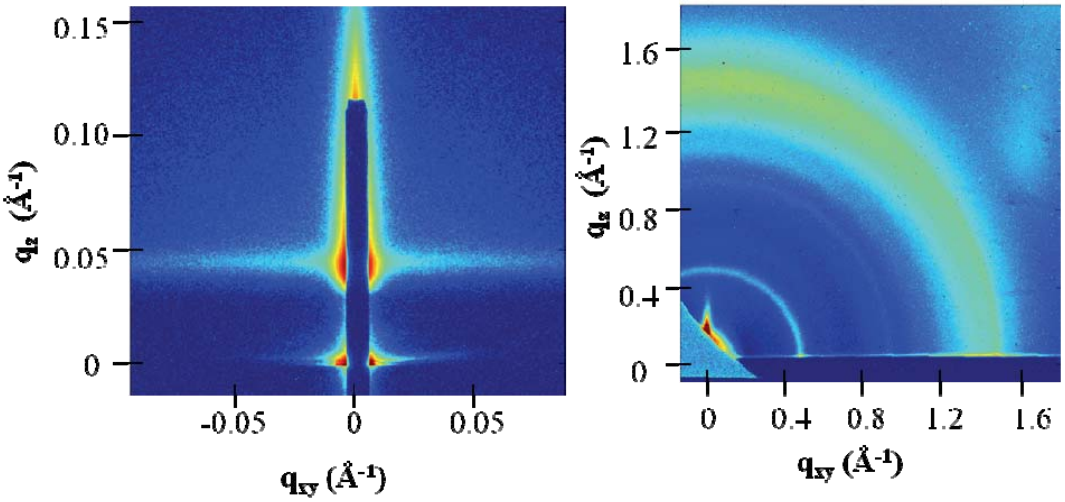

Figure 3.10 – GISAXS and GIWAXS measurement for β mesophase PF homopolymer. Samples were annealed at room temperature with $CHCl_3$ vapors for 5 days.

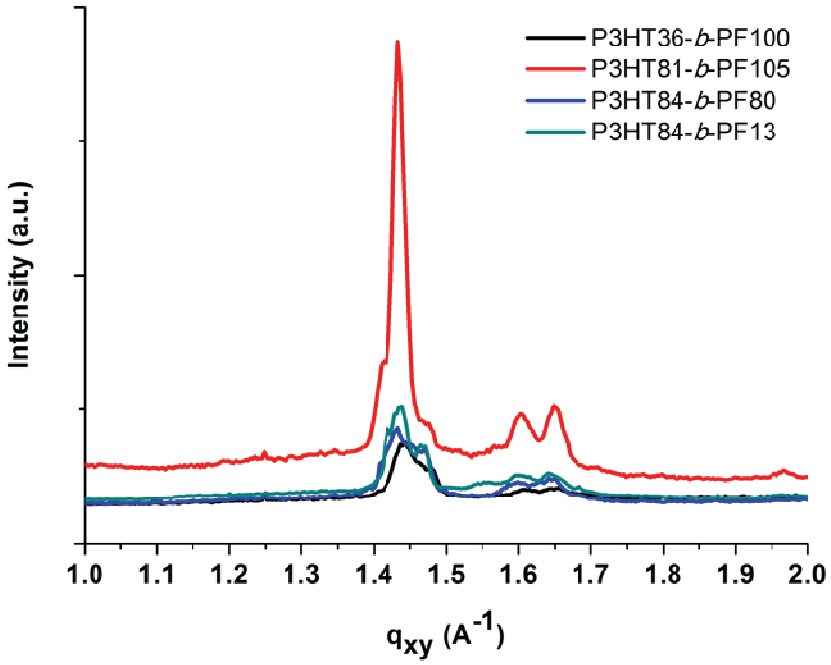

Figure 3.11 – Linecuts of GIWAXS measurements along $q_z \sim 0$ Å^{-1} for solvent annealed samples.

Solvent-annealed block copolymer films also display strong in-plane reflections at q~1.45 $Å^{-1}$ and q~1.65 $Å^{-1}$ (see Figure 3.11). These reflections are characteristic of face-to-face π-π stacking for PF and P3HT, respectively. Other crystal reflections characteristic of PF or P3HT homopolymers are absent in solvent annealed films, except for P3HT84–*b*–PF13. A peak corresponding to the (100) P3HT crystal spacing (q~0.39 $Å^{-1}$) is clearly evident in solvent-annealed P3HT84–*b*–PF13 (see linecut in Figure 3.7). A quantitative analysis of crystalline disorder through measurements of a paracrystallinity parameter is provided below.

On heating the solvent-annealed films from room temperature to 150 °C, lamellar GISAXS and GIWAXS reflections disappear and P3HT–*b*–PF films, with the exception of P3HT84–*b*–PF13, show only diffuse scattering, with no sharp reflections or peaks. This is indicative of an amorphous or liquid crystal nematic phase (Figure 3.3c). Note that 150 °C is below the crystal melting temperatures for both P3HT and PF blocks.

The presence of nematic liquid crystal ordering is confirmed by inspection of the films by polarized optical microscopy (POM), which reveals a birefringent Schlieren texture characteristic of a nematic phase for P3HT36–*b*–PF100, P3HT81–*b*–PF105, and P3HT84–*b*–PF80 (Fig. 3.12a, 3.12b, and 3.12c). The block copolymer with the highest P3HT content, P3HT84–*b*–PF13, (comprised of 85 wt% P3HT) does not exhibit a nematic phase. Instead, as shown in Figure 3.3c, some P3HT crystallization is evident. POM analysis of all solvent-annealed and solvent+thermal-annealed block copolymer films are provided in the Electronic Supplementary Information Figure 3.13.

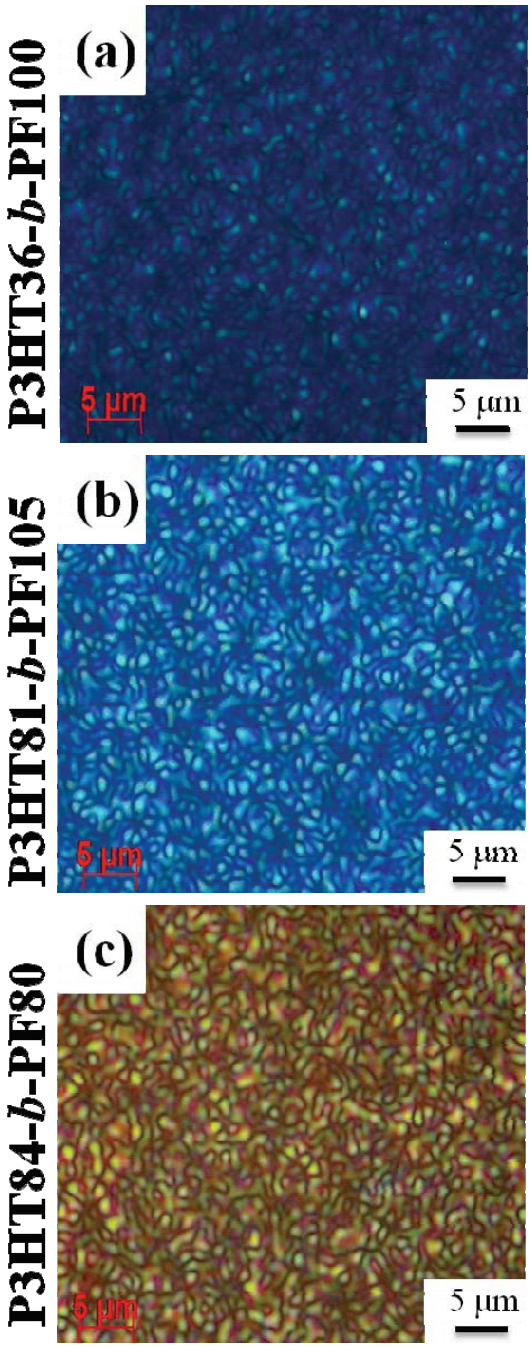

Figure 3.12 – Polarized optical microscopy images of P3HT–*b*–PF block copolymer thin films subjected to solvent-annealing followed by thermal annealing at 150 °C. Images were acquired at room temperature.

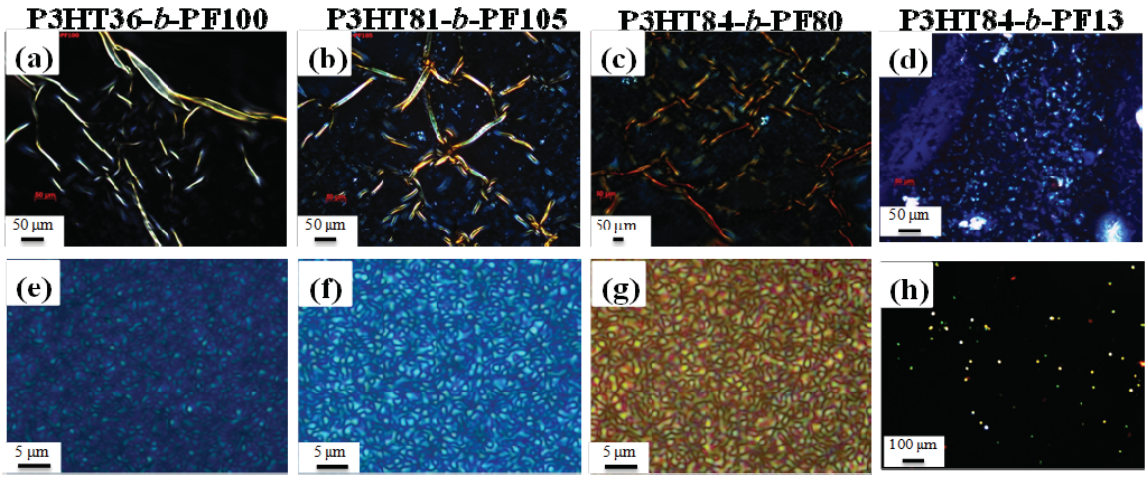

Figure 3.13 – Polarized optical microscopy images: (a)-(d) chloroform vapor induced smectic phases. (e)-(g) Additional thermal induced nematic phases. All measurements were carried out at room temperature.

P3HT–*b*–PF films, with the exception of P3HT84–*b*–PF13, thus form a nematic phase after solvent annealing followed by heating to 150 °C and slowly cooling to room temperature. PF homopolymers exhibit a nematic phase only at temperatures higher than the crystal melting temperature[36] or at room temperature after rapid quenching.[30,37] The enhanced stability of the nematic phase in block copolymers may be due to poor chain mobility resulting from the rigidity of polymer chains or close π-π stacking in the self-assembled lamellar phase.[38] The results also suggest that the lamellae of P3HT–*b*–PF is metastable and can be affected by elevated temperature as well as the crystallization of P3HT as shown in P3HT84–*b*–PF13.

P3HT–*b*–PF films thus exhibit remarkable changes depending on the processing history. Thermally annealed films show characteristics of P3HT or PF crystallites, but with poor order along the π-π stacking direction. Solvent-annealed films exhibit a self-assembled lamellar phase along with ordering along the π-π stacking direction. Solvent-

annealed films subsequently heated to 150 °C transition to a nematic liquid crystal phase, which is stable on cooling back down to room temperature. This phase behaviour is distinct from that of P3HT or PF homopolymers. Below, we provide a proposed structure of the lamellar phase, detail the optical and thermal properties of the materials, and quantify disorder in solvent-annealed films through quantitative analysis of peak spacings and widths.

3.3.2. Schematic for Lamellar Assembly in Solvent-Annealed Films

A schematic for the film microstructure consistent with the features of GISAXS and GIWAXS is shown in Figure 3.14. P3HT and PF lamellar domains are oriented parallel to the substrate, and the primary lamellar peak reflection (q_z ~ 0.15 Å^{-1}) (Figure 3.6 and inset Figure 3.7) corresponds to a domain spacing of 4.2 nm. Peaks at q~1.45 Å^{-1} and q~1.65 Å^{-1} correspond to face-to-face (π-π) packing for PF and P3HT, respectively, and indicate π-π stacking along the in-plane direction, as shown schematically in Figure 3.14. The orientation of the face-to-face π-π stacking is perpendicular to the lamellar domains but free to rotate 180 degrees within the plane parallel to the substrate. For clarity, only one possible orientation is shown in the schematic.

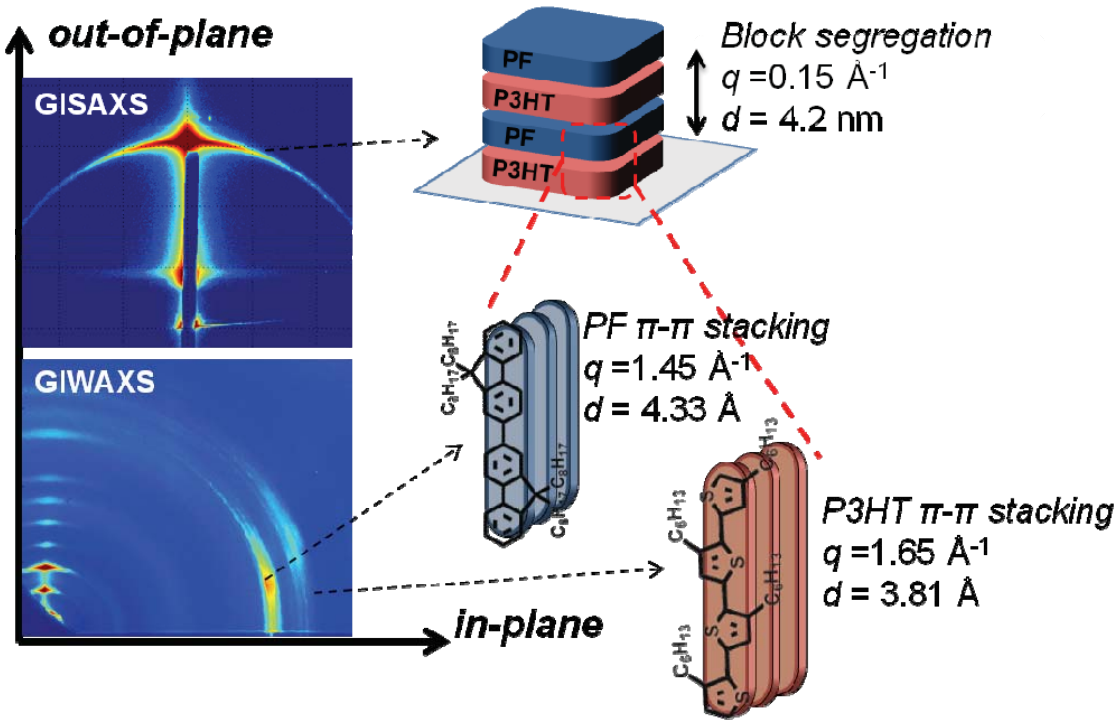

Figure 3.14 – Representative GISAXS and GIWAXS reflections and schematic for lamellar ordering in solvent-annealed P3HT–*b*–PF all-conjugated block copolymers.

The size of the lamellar domains formed after solvent annealing is invariant with block copolymer molecular weight and composition. All solvent-annealed block copolymers exhibit lamellar ordering with a characteristic domain spacing of 4.2 nm. The underlying mechanism for the formation of lamellar domains cannot be attributed to conventional micro-phase segregation as in coil-coil block copolymers, in which the domain spacing is dependent on the block copolymer molecular weight.[39] Instead, we propose that self-assembled lamellae arise due to a combination of polymer block segregation and π-π interactions of both P3HT and PF polymer blocks. The lamellae are expected to consist of both ordered and amorphous regions, consistent with the structure of P3HT and other semicrystalline, conjugated polymers.[40] Prior work has shown that

P3HT polymer chains can be folded in amorphous regions and between crystalline domains, even with very sharp turns and folds of the P3HT backbone.[41] This allows for a single chain to occupy both ordered and amorphous domains and pass in and out of relatively small domains. As a result, the lamellar domain size (4.2 nm) is determined primarily by π-π stacking associations and is relatively unaffected by block copolymer molecular weight and composition.

An alternative possibility for the structure of solvent-annealed block copolymer films is shown schematically in the Figure 3.15. In this proposed schematic, polymer backbones are oriented in-plane rather than out-of-plane. As a result, the domain spacing is determined by the fully extended length of the alkyl side-chains. While this structure is consistent with the features observed by GISAXS and GIWAXS, we believe this type of ordering is unlikely due to the relatively large spacing between polymers, 4.2 nm. This would require stretching of the P3HT and PF alkyl side-chains. Additionally, the hypothetical ordering is not volume conserving due to the large space (4.2 nm) between polymer chains and close π-π stacking. As a result, the structure in Figure 3.14 is the more likely possibility, but acknowledge the potential for an alternative configuration shown in Figure 3.15.

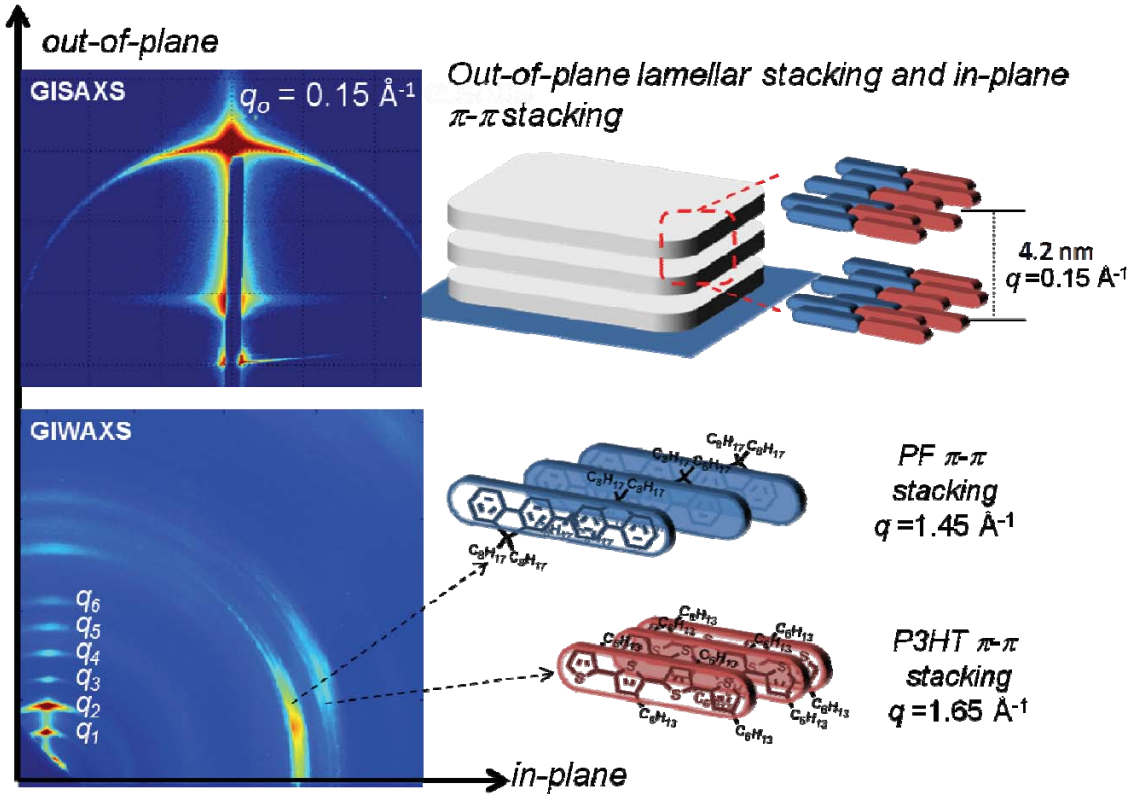

Figure 3.15 – Alternative schematic for lamellar ordering in solvent-annealed all-conjugated block copolymer films. The lamellar domain size in this schematic is determined by stacking through the alkyl side-chains of P3HT and PF polymers.

3.3.3. Optical and Thermal Properties of P3HT–*b*–PF Films

UV-VIS absorbance analysis of block copolymer films can provide information about ordering and crystallinity, particularly along the π-π stacking direction. UV-VIS analysis has previously been used to study conformational changes in PF[35,37] and P3HT.[42-44] High-temperature thermally annealed block copolymer films, which exhibit a morphology dominated by crystallinity of either P3HT or PF (Figure 3.3a), show only broad absorbance peaks at λ ~ 390 and 500 nm, indicative of poor π-π stacking (Figure

3.16a). Similar broad peaks by UV-VIS are observed in the PF crystalline α-phase[35] and nematic phases.[35]

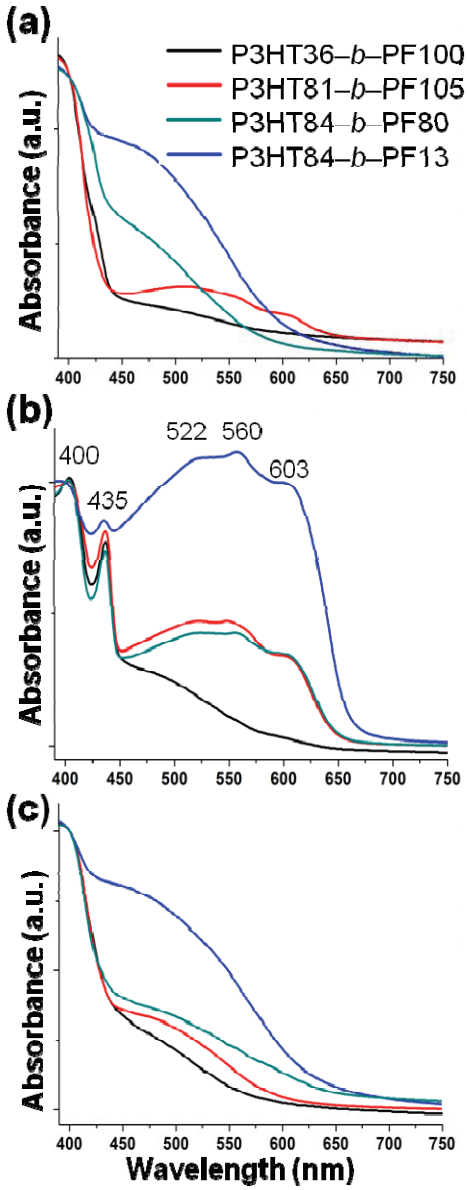

Figure 3.16 – UV-VIS spectra for P3HT–*b*–PF block copolymers after: (a) high-temperature thermal annealing, (b) long-term solvent annealing, and (c) long-term solvent annealing followed by 150 °C thermal annealing. All spectra were acquired at room temperature.

After solvent annealing, UV-VIS measurements reveal peaks at λ ~ 522, 560 and 603 nm in the absorption spectra, reflecting P3HT π-π stacking in all solvent annealed films. Regioregular P3HT homopolymer, ordered in the π-π stacking direction, exhibits similar peaks by UV-VIS analysis.[42-44] UV-VIS analysis also reveals peaks at λ ~ 400 and 435 nm in the absorption spectra for lamellar block copolymer films, similar to what is seen for the PF β phase.[33] This suggests that face-to-face π-π of PF and P3HT polymer blocks is enhanced in solvent-annealed films, compared with thermally annealed films.

After heating to 150 °C resulting in nematic liquid crystal ordering, sharp absorbance features characteristic of π-π stacking disappear. Nematic block copolymer films show only broad peaks in the absorption spectra at λ ~ 390 and 500 nm, similar to thermally annealed block copolymer films and corresponding to poor face-to-face ordering of PF and P3HT blocks. The observed transformations in the UV-VIS spectra are thus consistent with GIWAXS measurements that indicate poor π-π stacking in crystalline and nematic block copolymer films and enhanced π-π stacking in the lamellar block copolymer phase.

Differential scanning calorimetry (DSC) reveals differences in the crystal melting temperatures for samples with different processing histories. With the exception of P3HT84–*b*–PF13, DSC measurements detect a phase transition at 145 °C in solvent-annealed block copolymer on the first heating cycle (Figure 3.17a). This transition temperature is consistent with the transition to the nematic liquid crystal phase observed by GIWAXS.

For thermally annealed samples, melting transitions at roughly 157 °C and 215 °C are detected. These temperatures correspond approximately to the crystal melting temperatures of PF and P3HT, respectively.

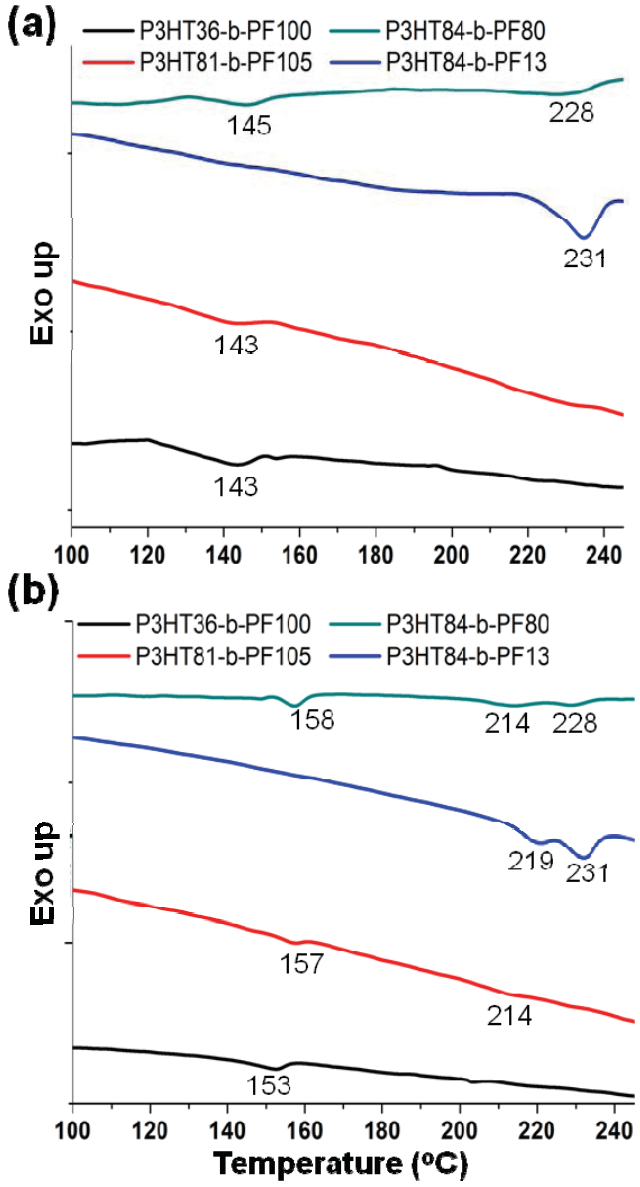

Figure 3.17 – DSC analysis of P3HT–*b*–PF block copolymers after (a) long-term solvent annealing and (b) thermal annealing above 220 °C.

DSC measurements thus indicate that the self-assembled lamellar phase melts near 150 °C, while thermally annealed samples exhibit crystal melting temperatures comparable to the constituent homopolymers. Similar results for thermally annealed films

have been previously reported for P3HT–*b*–PF[4,21] and other all-conjugated block copolymers.[3,18,45-47] For P3HT84–*b*–PF13, only one thermal transition near 220 °C (near the crystal melting temperature of P3HT) is detected by DSC on both first and second heating cycles, suggesting that PF crystallization is suppressed in this sample due to the much higher content of P3HT in the block copolymer.

3.3.4. Paracrystallinity Disorder Analysis on Lamellar Ordering

Peak width analysis can provide information on disorder within crystalline or semicrystalline regions. Disorder is quantified through calculation of a paracrystallinity disorder parameter *g*,[48] calculated using the center (q_0) and breadth (Δq) of a peak, as shown in Eqn. (1).[40,49] A larger value of *g* indicates greater disorder. Here, we present an analysis of *g* for block copolymer films under different processing histories and for P3HT and PF homopolymer films. The paracrystallinity disorder parameter was measured for the out-of-plane primary lamellar spacing (Figure 3.6) in GISAXS and the in-plane π-π stacking reflection (Figure 3.14) in GIWAXS in solvent-annealed films.

$$g = \sqrt{\Delta q / 2\pi q_0}$$

Equation 3.1 – Paracrystallinity disorder parameter *g* for information on disorder within crystalline or semicrystalline regions.

As shown in Table 3.2, the paracrystallinity disorder parameter *g* measured for P3HT π-π stacking in thermally-annealed films is in agreement with literature values (g ~ 6-8%[40]). The disorder for π-π stacking of the P3HT block is slightly higher for solvent-annealed P3HT–*b*–PF compared with thermally annealed P3HT homopolymer. This is expected due to connectivity to a PF block which can increase disorder in the P3HT π-π stacking.

Spacings[a]	Samples	g (%)
π-π stacking, P3HT	P3HT36–*b*–PF100	9.68
	P3HT81–*b*–PF105	7.58
	P3HT84–*b*–PF80	9.54
	P3HT84–*b*–PF13	8.42
	Solvent ann. P3HT[b]	8.82
	Thermal ann. P3HT[b]	8.19
π-π stacking, PF	P3HT36–*b*–PF100	8.23
	P3HT81–*b*–PF105	5.18
	P3HT84–*b*–PF80	8.81
	P3HT84–*b*–PF13	7.59
	Solvent ann. PF	17.84
Primary lamellar reflection	P3HT36–*b*–PF100	9.38
	P3HT81–*b*–PF105	9.05
	P3HT84–*b*–PF80	9.44
	P3HT84–*b*–PF13	8.89

[a]π-π stacking of P3HT and PF was analyzed on GIWAXS patterns whereas 1st lamellar ordering was analyzed on GISAXS patterns. [b]commercially available P3HT homopolymer has M_w~60 kg/mol.

Table 3.2 – Paracrystallinity disorder (*g*) analysis on solvent annealed films.

The paracrystallinity disorder parameter has similar values, roughly 8 – 10 %, for PF π-π stacking and for ordering of the self-assembled lamellae. We also note that PF is more ordered along π-π direction in solvent-annealed BCPs compared with solvent annealed PF homopolymer β phase (g ~ 17.84%).

Quantitative paracrystallinity disorder analysis thus indicates that ordering along the π-π stacking direction is substantially improved for solvent-annealed films compared with thermally-annealed block copolymers.

3.4. Conclusions

A combination of analytical techniques—GIXS, UV-VIS, POM and DSC—reveal novel lamellar ordering in all-conjugated P3HT–*b*–PF block copolymers after long-term solvent annealing. We observe enhanced π-π stacking in the lamella compared with either the crystal or nematic phases. These results demonstrate that all-conjugated block copolymers exhibit a rich, processing-dependent microstructure, and a quantitative description will have to account for various intermolecular interactions including π-π stacking, steric repulsions of the alkyl side-chains, and chain rigidity. The presence of a liquid crystal phase with enhanced π-π stacking may lead to block copolymer films with superior optoelectronic properties or the use of new processing strategies, such as the application of magnetic fields,[13-15] to achieve improved alignment. The results reported for rod-rod all-conjugated block copolymers contrast with previous studies of coil-coil and rod-coil diblock copolymers. In the case of rod-coil block copolymers, self-assembly can be described through a mean field theory that includes Flory-Huggins interactions and Maier-Saupe parameter to account for liquid crystal ordering.[17] Here, we observe a qualitatively different self-assembly process driven by both π-π stacking interactions and polymer block segregation.

3.5. References

(1) Bates, F. S.; Fredrickson, G. H., *Phys. Today* **1999**, *52*, 32-38.

(2) Park, C.; Yoon, J.; Thomas, E. L., *Polymer* **2003**, *44*, 6725-6760.

(3) Sommer, M.; Komber, H.; Huettner, S.; Mulherin, R.; Kohn, P.; Greenham, N. C.; Huck, W. T. S., *Macromolecules* **2012**, *45*, 4142-4151.

(4) Smith, K. A.; Lin, Y.-H.; Dement, D. B.; Strzalka, J.; Darling, S. B.; Pickel, D. L.; Verduzco, R., *Macromolecules* **2013**, *46*, 2636-2645.

(5) Guo, C.; Lin, Y.-H.; Witman, M. D.; Smith, K. A.; Wang, C.; Hexemer, A.; Strzalka, J.; Gomez, E. D.; Verduzco, R., *Nano Lett.* **2013**, *13*, 2957-2963.
(6) Moon, H. C.; Bae, D.; Kim, J. K., *Macromolecules* **2012**, *45*, 5201-5207.
(7) Dai, C. A.; Yen, W. C.; Lee, Y. H.; Ho, C. C.; Su, W. F., *J. Am. Chem. Soc.* **2007**, *129*, 11036-11038.
(8) Olsen, B. D.; Segalman, R. A., *Macromolecules* **2005**, *38*, 10127-10137.
(9) Lohwasser, R. H.; Gupta, G.; Kohn, P.; Sommer, M.; Lang, A. S.; Thurn-Albrecht, T.; Thelakkat, M., *Macromolecules* **2013**, *46*, 4403-4410.
(10) Choi, S. Y.; Lee, J. U.; Lee, J. W.; Lee, S.; Song, Y. J.; Jo, W. H.; Kim, S. H., *Macromolecules* **2011**, 1771-1774.
(11) Lee, Y. J.; Kim, S. H.; Yang, H.; Jang, M.; Hwang, S. S.; Lee, H. S.; Baek, K.-Y., *J. Phys. Chem.C* **2011**, *115*, 4228-4234.
(12) McCulloch, B.; Portale, G.; Bras, W.; Pople, J. A.; Hexemer, A.; Segalman, R. A., *Macromolecules* **2013**, *46*, 4462-4471.
(13) Gopinadhan, M.; Majewski, P. W.; Beach, E. S.; Osuji, C. O., *ACS Macro Lett.* **2011**, *1*, 184-189.
(14) Gopinadhan, M.; Majewski, P. W.; Choo, Y.; Osuji, C. O., *Phys. Rev. Lett.* **2013**, *110*, 078301.
(15) Tran, H.; Gopinadhan, M.; Majewski, P. W.; Shade, R.; Steffes, V.; Osuji, C. O.; Campos, L. M., *ACS Nano* **2013**, *7*, 5514-5521.
(16) Tung, Y.-C.; Wu, W.-C.; Chen, W.-C., *Macromol. Rapid Commun.* **2006**, *27*, 1838-1844.
(17) Olsen, B. D.; Shah, M.; Ganesan, V.; Segalman, R. A., *Macromolecules* **2008**, *41*, 6809-6817.
(18) Yu, X.; Yang, H.; Wu, S.; Geng, Y.; Han, Y., *Macromolecules* **2012**, *45*, 266-274.
(19) Verduzco, R.; Botiz, I.; Pickel, D. L.; Kilbey, S. M.; Hong, K.; Dimasi, E.; Darling, S. B., *Macromolecules* **2011**, *44*, 530-539.
(20) He, M.; Qiu, F.; Lin, Z., *J. Mater. Chem.* **2011**, *21*, 17039-17048.
(21) Lin, Y.-H.; Smith, K. A.; Kempf, C. N.; Verduzco, R., *Polym. Chem.* **2013**, *4*, 229-232.

(22) Jiang, Z.; Li, X. F.; Strzalka, J.; Sprung, M.; Sun, T.; Sandy, A. R.; Narayanan, S.; Lee, D. R.; Wang, J., *J. Synchrot. Radiat.* **2012**, *19*, 627-636.

(23) Jiang, Z., *GIXSGUI is available for download: http://www.aps.anl.gov/Sectors/Sector8/Operations/GIXSGUI.html*.

(24) Scherf, U.; Gutacker, A.; Koenen, N., *Accounts Chem. Res.* **2008**, *41*, 1086-1097.

(25) Tu, G.; Li, H.; Forster, M.; Heiderhoff, R.; Balk, L. J.; Sigel, R.; Scherf, U., *Small* **2007**, *3*, 1001-1006.

(26) Sinturel, C.; Vayer, M.; Morris, M.; Hillmyer, M. A., *Macromolecules* **2013**, *46*, 5399-5415.

(27) Sirringhaus, H.; Brown, P. J.; Friend, R. H.; Nielsen, M. M.; Bechgaard, K.; Langeveld-Voss, B. M. W.; Spiering, A. J. H.; Janssen, R. A. J.; Meijer, E. W.; Herwig, P.; de Leeuw, D. M., *Nature* **1999**, *401*, 685-688.

(28) Kline, R. J.; McGehee, M. D.; Kadnikova, E. N.; Liu, J.; Fréchet, J. M. J.; Toney, M. F., *Macromolecules* **2005**, *38*, 3312-3319.

(29) Chen, S. H.; Su, A. C.; Chen, S. A., *J. Phys. Chem. B* **2005**, *109*, 10067-10072.

(30) Grell, M.; Bradley, D. D. C.; Ungar, G.; Hill, J.; Whitehead, K. S., *Macromolecules* **1999**, *32*, 5810-5817.

(31) Peet, J.; Brocker, E.; Xu, Y.; Bazan, G. C., *Adv. Mater.* **2008**, *20*, 1882-1885.

(32) Lee, B.; Park, I.; Yoon, J.; Park, S.; Kim, J.; Kim, K.-W.; Chang, T.; Ree, M., *Macromolecules* **2005**, *38*, 4311-4323.

(33) Tseng, K.-L.; Ruan, J.; Lan, Y.-K.; Wang, W.-Z.; Su, A.-C., *Macromolecules* **2013**, *46*, 1820-1831.

(34) Chen, S. H.; Chou, H. L.; Su, A. C.; Chen, S. A., *Macromolecules* **2004**, *37*, 6833-6838.

(35) Chen, S. H.; Su, A. C.; Su, C. H.; Chen, S. A., *Macromolecules* **2005**, *38*, 379-385.

(36) Teetsov, J.; Anne Fox, M., *J. Mater. Chem.* **1999**, *9*, 2117-2122.

(37) Misaki, M.; Ueda, Y.; Nagamatsu, S.; Yoshida, Y.; Tanigaki, N.; Yase, K., *Macromolecules* **2004**, *37*, 6926-6931.

(38) Lin, Y.-H.; Darling, S. B.; Nikiforov, M. P.; Strzalka, J.; Verduzco, R., *Macromolecules* **2012**, *45*, 6571-6579.

(39) Matsen, M. W.; Bates, F. S., *Macromolecules* **1996**, *29*, 1091-1098.
(40) Noriega, R.; Rivnay, J.; Vandewal, K.; Koch, F. P. V.; Stingelin, N.; Smith, P.; Toney, M. F.; Salleo, A., *Nat. Mater.* **2013**, *12*, 1038-1044.
(41) Grévin, B.; Rannou, P.; Payerne, R.; Pron, A.; Travers, J. P., *Adv. Mater.* **2003**, *15*, 881-884.
(42) He, M.; Zhao, L.; Wang, J.; Han, W.; Yang, Y.; Qiu, F.; Lin, Z., *ACS Nano* **2010**, *4*, 3241-3247.
(43) Kiriy, N.; Jähne, E.; Adler, H.-J.; Schneider, M.; Kiriy, A.; Gorodyska, G.; Minko, S.; Jehnichen, D.; Simon, P.; Fokin, A. A.; Stamm, M., *Nano Lett.* **2003**, *3*, 707-712.
(44) Samitsu, S.; Shimomura, T.; Heike, S.; Hashizume, T.; Ito, K., *Macromolecules* **2008**, *41*, 8000-8010.
(45) Ku, S.-Y.; Brady, M. A.; Treat, N. D.; Cochran, J. E.; Robb, M. J.; Kramer, E. J.; Chabinyc, M. L.; Hawker, C. J., *J. Am. Chem. Soc.* **2012**, *134*, 16040-16046.
(46) Wang, J.; Ueda, M.; Higashihara, T., *ACS Macro Lett.* **2013**, *2*, 506-510.
(47) Nakabayashi, K.; Mori, H., *Macromolecules* **2012**, *45*, 9618-9625.
(48) Hindeleh, A. M.; Hosemann, R., *J. Phys. C Solid State* **1988**, *21*, 4155.
(49) Rivnay, J.; Noriega, R.; Kline, R. J.; Salleo, A.; Toney, M. F., *Phys. Rev. B* **2011**, *84*, 045203.

Chapter 4

Conjugated Block Copolymer Photovoltaics with Near 3% Efficiency Through Microphase Separation

This chapter is included in Changhe Guo, Yen-Hao Lin, Mathew D. Witman, Kendall A. Smith, Cheng Wang, Alexandar Hexemer, Joseph Strzalka, Enrique D. Gomez, Rafael Verduzco, "Conjugated Block Copolymer Photovoltaics with near 3% Efficiency through Microphase Separation," *Nano Letters,* 2013, **13 (6)**, 2957-2963.

Organic electronic materials have the potential to impact almost every aspect of modern life including how we access information, light our homes, and power personal electronics. Nevertheless, weak intermolecular interactions and disorder at junctions of different organic materials limit the performance and stability of organic interfaces and hence the applicability of organic semiconductors to electronic devices. Here, we demonstrate control of donor-acceptor heterojunctions through microphase-separated conjugated block copolymers. When utilized as the active layer of photovoltaic cells, block copolymer-based devices demonstrate efficient photoconversion well beyond devices composed of homopolymer blends. The 3% block copolymer device efficiencies

are achieved without the use of a fullerene acceptor. X-ray scattering results reveal that the remarkable performance of block copolymer solar cells is due to self-assembly into mesoscale lamellar morphologies with primarily face-on crystallite orientations. Conjugated block copolymers thus provide a pathway to enhance performance in excitonic solar cells through control of donor-acceptor interfaces.

4.1. Introduction

Excitonic photovoltaics are a class of devices where donor-acceptor interfaces are critical for photogeneration of charges and efficient device performance.[1-4] In contrast to many inorganic semiconductors where optical excitations generate delocalized free charge carriers, current generation in organic photovoltaics depends on dissociation of tightly bound charge transfer states near donor-acceptor interfaces. For instance, a recent model by Giebink et al. suggests that tuning the electronic coupling at donor/acceptor interfaces is crucial to minimizing the recombination rate of charge transfer states while maintaining yields of exciton dissociation near unity.[5] It follows that tuning the chemical structure and local order at organic heterojunctions is a requirement to access the full potential of organic solar cell materials. Unfortunately, organic solar cells rely on kinetically-trapped, partially phase-separated structures of donor/acceptor mixtures to create a high surface area for exciton dissociation and networks of bicontinuous phases for charge extraction.[6-12] As a consequence, molecular control of the interface in state-of-the-art organic photovoltaics is nearly impossible.

Microphase-separated block copolymers comprised of electron donor and electron acceptor polymers can address many of the current challenges in morphology and interfacial structure control for photovoltaics. The equilibrium self-assembly of block copolymers into mesoscale (5-500 nm) well-ordered morphologies where interfaces are

governed by moieties near the junction between blocks[13,14] is ideal for the active layer of organic solar cells. While several examples of block copolymers with donor and acceptor blocks have been reported, the majority contain a non-conjugated insulating backbone in at least one polymer block and consequently do not directly control donor/acceptor interfaces.[15-20] Recent work has demonstrated significant progress in the design, synthesis, and characterization of fully conjugated block copolymers,[21-23] but it remains a challenge to achieve efficient charge photogeneration in photovoltaic device architectures.

We demonstrate that poly(3-hexylthiophene)–*block*–poly((9′,9′-dioctylfluorene)-2,7-diyl-alt-[4,7-bis(thiophen-5-yl)-2,1,3-benzothiadiazole]-2′,2″-diyl) (P3HT–*b*–PFTBT) block copolymers can be utilized as the active layer for efficient photovoltaic device operation. These block copolymers self-assemble to form in-plane lamellar morphologies with alternating electron donor and acceptor domains and a dominant face-on orientation in the crystalline P3HT block. Even without the use of fullerene, we obtain efficiencies near 3%, remarkable open-circuit voltages of 1.2 V, and short-circuit currents above 5 mA/cm^2 from block copolymer devices. These results demonstrate that conjugated block copolymers are a viable strategy for morphology and interfacial control for high performance organic solar cells.

4.2. Experimental Section

4.2.1. Materials

Regioregular P3HT (96% H-T regioregular, M_n = 26 kg/mol, polydispersity = 2.0) was purchased from Merck. All other reagents and solvents were purchased from Sigma-Aldrich and used as received. P3HT–*b*–PFTBT block copolymers were synthesized using a procedure similar to that previously described[23] and the synthesis is briefly discussed in

the next section. The chemical structures of polymers and block copolymer are shown in Figure 4.1.

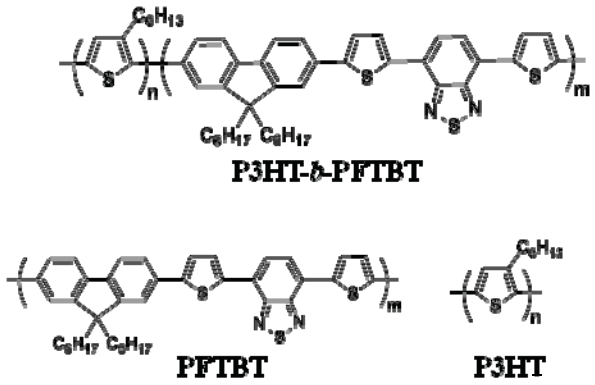

Figure 4.1 – Chemical structures of P3HT–*b*–PFTBT, PFTBT, and P3HT.

4.2.2. Synthesis and size-exclusion chromatography of block copolymers

P3HT–*b*–PFTBT block copolymers were synthesized using a procedure similar to that previously described.[23] Briefly, Br end capped P3HT (M_w = 16.1 kg/mol, polydispersity = 1.12, 685 mg, 0.042 mmol), 9′,9′-dioctylfluorene-2′,7′-diboronic acid ester (455 mg, 0.82 mmol), 4,7-bis-2′-(5′-bromo)-thienyl-2′,1′,3′,- benzothiadiazole) (309 mg, 0.68 mmol), tetrakis-(triphenylphosphine)-palladium(0) (38 mg, 0.033 mmol), 5 mL of tetraethyl ammonium hydroxide (20% in H_2O) and aliquat 336 (3 drops) were added to a Schlenk tube loaded with nitrogen-purged toluene (25 mL). The flask was purged with three freeze-pump-thaw cycles, backfilled with nitrogen, and stirred overnight at 90 °C. Next, 5mL bromobenzene was added and stirred at 90°C for 1 h before cooling the reaction mixture. The polymer was precipitated in cold methanol and collected by filtration. The powder was then loaded into a Soxhlet thimble and washed with acetone,

hexanes, and then chloroform to recover the polymer. The yield of block copolymer was 740 mg (M_w = 28.5 kg/mol, polydispersity = 1.3).

Polymer molecular weights and polydispersities (PDIs) were obtained by size-exclusion chromatography (SEC) as described below. Refractive index (RI) SEC analyses for the P3HT macroreagent and the final P3HT–*b*–PFTBT are shown in Figure 4.2.

Polymer molecular weights and polydispersities (PDIs) were obtained by size-exclusion chromatography (SEC) using an Agilent 1200 module equipped with three PSS SDV columns in series (100, 1000, and 10 000 Å pore sizes), an Agilent variable wavelength UV/visible detector, and a Wyatt Technology Optilab reX RI detector. Tetrahydrofuran was used as the mobile phase at a flow rate of 1 mL/min at 40 °C. Weight average molecular weights (M_w) and polydispersities (PDIs) are determined relative to a set of monodisperse polystyrene standards (Astra Software Version 5.3.4). SEC-RI analysis for the P3HT macroreagent and the final P3HT–*b*–PFTBT is shown in Figure 4.2. Deconvolution of the constituent peaks in the block copolymer trace reveals 14 wt% of P3HT homopolymer impurities.

SEC analysis shows a clear shift of the molecular weight distribution for the final P3HT–*b*–PFTBT block copolymer compared with the starting P3HT macroreagent. The shoulder in the molecular weight distribution at long times indicates that some residual P3HT macroreagent is present (14 wt%).

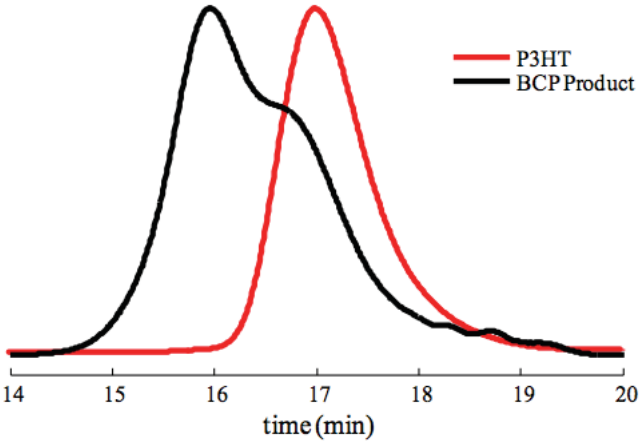

Figure 4.2 – Size-Exclusion Chromatography (SEC) analysis of P3HT macroreagent and final block copolymer product.

4.2.3. Photovoltaic device fabrication and measurement

Photovoltaic devices were prepared with the conventional architecture of ITO/PEDOT:PSS (65 nm)/active layer (60-70 nm)/Al (75 nm). ITO-coated glass substrates (20 ohm/sq, Xin Yan Technology, Hong Kong) were cleaned by soap, followed by 20 min of sonication in acetone, then isopropanol, and finally 15 min of ultraviolet light ozonation. Poly(3,4-ethylenedioxythiophene) poly(styrenesulfonate), PEDOT:PSS (Clevios P, Heraeus), was spin-coated on top of ITO at 4000 rpm for 2 min yielding a thickness of about 65 nm. The PEDOT:PSS/ITO substrates were dried for 10 min at 165 °C in air and then transferred to a nitrogen-filled glovebox. Solutions of P3HT/PFTBT mixtures (15 mg/ml, weight ratio 1:2) and P3HT–*b*–PFTBT (5 mg/ml) were made with anhydrous chloroform (≥ 99%, amylenes as stabilizer, Sigma-Aldrich) and stirred at 95 °C for about 20-22 hrs in a tightly sealed container prior to casting in a N_2 glovebox. The active layers of P3HT/PFTBT and P3HT–*b*–PFTBT devices were cast onto PEDOT:PSS layers from prepared hot solutions (95 °C) at various spin speeds for 1

min to maintain thicknesses around 60-70 nm. The film thicknesses were determined on a TENCOR P-10 surface profiler. Samples were then transferred immediately onto a calibrated digital hot plate at 100 or 165 °C and dried for 5 min. The devices were completed by vacuum thermal evaporation of 75 nm aluminum at 10^{-6} torr on top of the active layer through a shadow mask. The device area is 16.2 mm^2. Integrated solar cells were further annealed at 100 or 165 °C for various annealing times.

Photovoltaic measurements were performed in a N_2 atmosphere under simulated AM 1.5G illumination (97 mW/cm^2) from a xenon lamp solar simulator (Newport Model SP92250A-1000). The illumination intensity was calibrated using an optical power meter and NREL certified Si reference photocell (Newport). A Keithley 2636A Sourcemeter was used to measure the current-voltage characteristics of solar cells. External quantum efficiencies (EQE) were measured in air. The photocurrents as a function of wavelength were recorded by a multifunction optical power meter (Model 70310) using 300W xenon lamp and Cornerstone monochromator (Newport Model 74100) illumination. The absorption spectra of films were measured using an ultraviolet/visible/near-infrared spectrophotometer (Beckman DU Series 500).

Samples for RSOXS, XRD, GISAXS and GIWAXS measurements were prepared on PEDOT:PSS/Si substrates in the same manner as for device fabrication. For RSOXS experiments, as-cast films were floated-off in deionized water and picked up with 5 mm × 5 mm silicon frames supporting a 1 mm × 1 mm, 100 nm thick Si_3N_4 window. Samples were then dried for 24 hrs at room temperature under vacuum and subsequently annealed on a hot plate in the N_2 glovebox. RSOXS measurements were carried out at beam line 11.0.1.2 at the Advanced Light Source, Lawrence Berkeley National Laboratory.[24] Scattering was performed in the transmission geometry in vacuum at X-ray energies at

the carbon absorption edge (285.4 eV) with linearly polarized X-rays. Data were corrected for dark currents and azimuthally integrated.

XRD experiments were conducted at the Materials Characterization Lab of Pennsylvania State University, on a Rigaku DMAX Rapid Micro-diffractometer. The X-ray wavelength, λ, was 1.54 Å. Rocking curves were obtained by rocking the sample (±0.5°) around the Bragg angle and images were collected with a curved image plate detector. Data were azimuthally integrated. GISAXS and GIWAXS measurements were carried out at Beamline 8-ID-E of the Advanced Photon Source, Argonne National Laboratory (λ = 1.6868 Å).[25] Scattering data were acquired at an incident angle of 0.2°. Data are corrected for X-ray polarization, detector sensitivity and geometrical solid-angle.

4.2.4. Absorption spectra of P3HT–*b*–PFTBT block copolymers

The absorption spectra of P3HT, PFTBT, and P3HT–*b*–PFTBT are shown in Figure 4.3. All films were cast from chloroform solutions and not annealed. The absorption coefficients are calculated from the absorbance and film thickness. PFTBT demonstrates two absorption peaks around 390 and 540 nm with a similar absorption edge and optical bandgap (~ 2 eV) as P3HT. P3HT–*b*–PFTBT block copolymers approximately preserve the features of the constituent P3HT and PFTBT homopolymers. Hence, the absorption coefficient is enhanced at longer wavelengths (450-600 nm) due to the overlapping absorption bands of P3HT and PFTBT, while absorption at short wavelengths (300-420 nm) is mainly attributed to the PFTBT block.

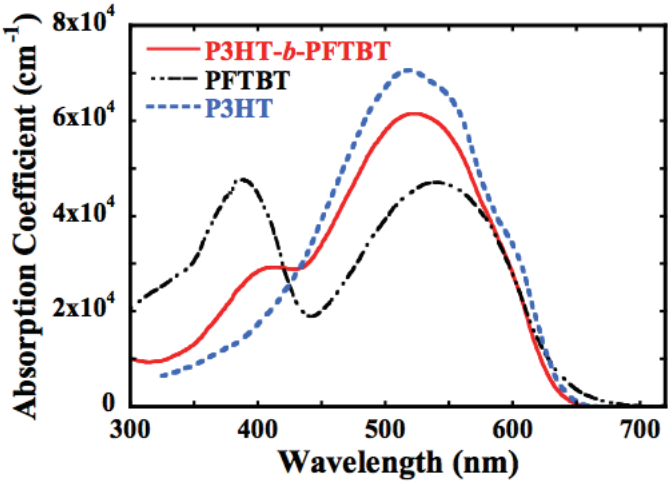

Figure 4.3 – UV-VIS absorption spectra of pristine P3HT, PFTBT and P3HT–*b*–PFTBT films.

4.2.5. X-ray absorption spectra

Near-edge X-ray absorption fine structure (NEXAFS) studies of neat P3HT and neat PFTBT films are shown in Figure 4.4. Both films are annealed at optimized conditions (165 °C) for device performance. The absorption spectra were normalized to 1 at 320 eV to account for thickness variations in different samples. NEXAFS spectra show that the absorption in organic materials is sensitive to small changes of the X-ray energy near the carbon absorption edge (280-320 eV). For example, significant contrast exists at 285.4 eV, where the C 1s to π* transition differs in P3HT and PFTBT.

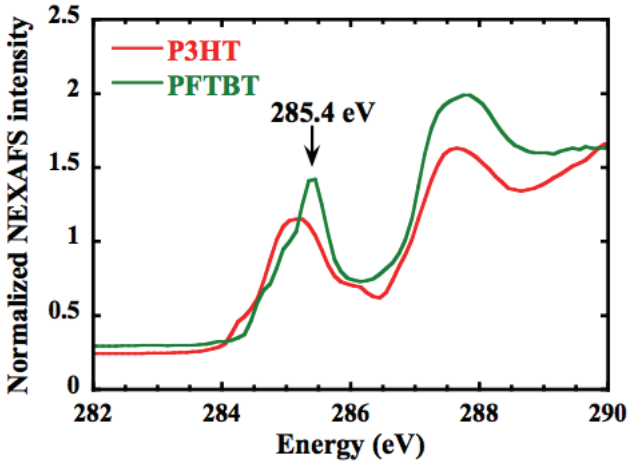

Figure 4.4 – NEXAFS absorption spectra of neat P3HT and PFTBT films. NEXAFS spectra were normalized to 1 at 320 eV to account for thickness variations. Significant contrast is observed at 285.4 eV, where the X-ray absorption of P3HT and PFTBT differ.

4.2.6. Morphological characterization through RSOXS and GISAXS

Figure 4.5 presents resonant soft X-ray scattering (RSOXS) profiles of P3HT/PFTBT and P3HT–*b*–PFTBT thin films at various annealing conditions. RSOXS experiments were carried out at beamline 11.0.1.2 of the Advanced Light Source, Lawrence Berkeley National Laboratory.[24] The X-ray energy was 285.4 eV, such that the absorption contrast between P3HT and PFTBT is significant (Figure 4.4). Scattering intensities are offset for clarity. Figure 4.5 shows the RSOXS scattering data as I vs q, where I is the scattering intensity and q is the scattering vector. Figure 4.5(b) shows the data as Kratky plots of Iq^2 vs q.

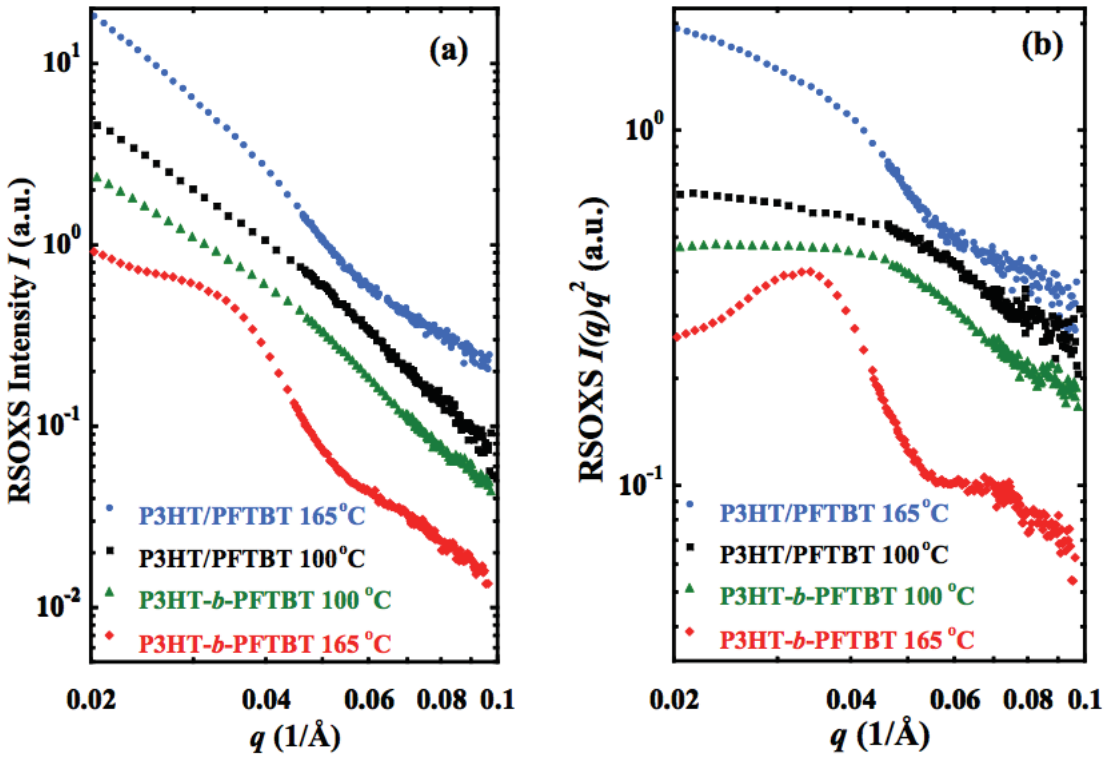

Figure 4.5 – RSOXS intensities of P3HT–*b*–PFTBT and P3HT/PFTBT thin films under various processing conditions. (a) I vs q and (b) Iq^2 vs q. Profiles are offset for clarity. Scattering data were acquired at 285.4 eV, azimuthally integrated, and presented as a Kratky plot of $I(q)q^2$ vs q.

The broad peak or shoulder in the RSOXS data for blends or the block copolymer annealed at 100 °C is similar to the scattering data obtained from P3HT mixtures with fullerene derivatives,[10] suggesting that this scattering feature corresponds to the spacing between P3HT fibrils. Annealing blends at 165 °C instead of 100 °C leads to a shift in the scattering to lower *q* suggesting that the microstructure coarsens upon annealing. In contrast, a well-defined primary peak at 0.035 $Å^{-1}$ and its second-order reflection are identified only in block copolymer films annealed at 165 °C, suggesting the existence of alternating lamellar microdomains on a length scale of around 10 nm.

Grazing-incidence small-angle X-ray scattering (GISAXS) experiments were performed to characterize the morphology in block copolymer thin films annealed at 165 °C, as shown in Figure 4.6. GISAXS measurements were carried out at Beamline 8-ID-E of the Advanced Photon Source, Argonne National Laboratory (λ = 1.6868 Å).[25] Scattering data were acquired at an incident angle of 0.2°. Using the GIXSGUI package[26] for Matlab (Mathworks), data were corrected for X-ray polarization, detector sensitivity and geometrical solid-angle. A line cut along the in-plane direction was used to present scattering data as a function of the in-plane scattering vector, q_y. The GISAXS data clearly show that a periodic structure is present with an average domain spacing of around 16 nm, consistent with RSOXS results (Figure 4.5 and Figure 4.9). No such structure is evident from the out-of-plane GISAXS scattering data.

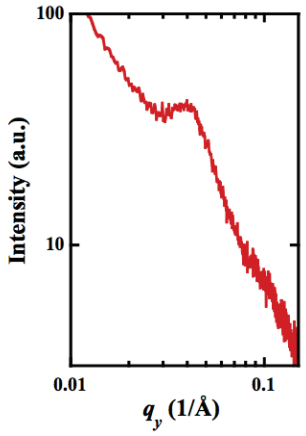

Figure 4.6 – GISAXS intensities vs scattering vector, q_y, for a P3HT–*b*–PFTBT film annealed at 165 °C.

4.3. Results and Discussions

The structure of P3HT, PFTBT and P3HT–*b*–PFTBT are shown in Figure 4.1. P3HT–*b*–PFTBT is roughly symmetric in composition, with 56 wt% P3HT and a total

weight-averaged molecular weight of 29 kg/mol. The energy levels of PFTBT as an electron acceptor are well aligned with those of P3HT as an electron donor, such that the difference between the lowest unoccupied molecular orbital of PFTBT (~ 3.5 eV)[27] and the highest occupied molecular orbital of P3HT (~ 4.9 eV)[28] can yield open-circuit voltages above 1 V. High open-circuit voltages have indeed been demonstrated for solar cells where the active layer is comprised of blends of P3HT and other dioctylfluorene bisthienyl-benzothiadiazole alternating copolymers,[28] ternary blends composed of similar conjugated block copolymers as P3HT–*b*–PFTBT with donor and acceptor homopolymers,[29] or polymer blends with fluorene benzothiadiazole alternating copolymers as acceptor molecules.[30-32]

Solar cell devices with P3HT/PFTBT blends as active layers are compared with devices comprised of P3HT–*b*–PFTBT block copolymers in Figure 4.7. All devices have an active layer thickness of 60-70 nm and were thermally annealed after deposition of the cathode (Al). As shown in Table 4.1, devices made from P3HT/PFTBT blends exhibited a maximum power conversion efficiency of 1.0%, which is comparable to the performance reported previously for devices which utilize blends of P3HT and PFTBT-based polymers as the active layer.[28] Solar cells made from P3HT/PFTBT blends were optimized at 1:2 weight ratios of P3HT:PFTBT after annealing at 100 °C for 20 min. Longer annealing times or higher annealing temperatures lead to a drop in performance, potentially due to macroscopic phase separation.

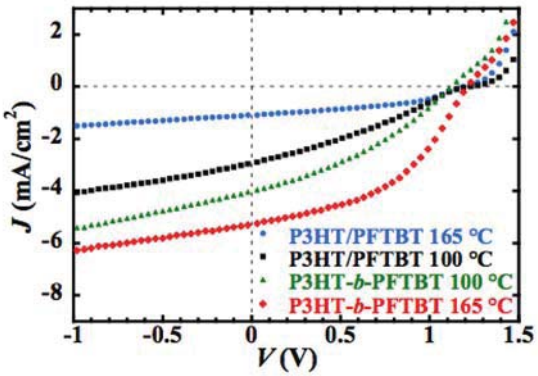

Figure 4.7 – Current-voltage characteristics of P3HT/PFTBT (1:2 by mass) and P3HT–*b*–PFTBT photovoltaic devices annealed at 100 °C for 20 min and 165 °C for 10 min, respectively. P3HT/PFTBT solar cells are optimized at 100 °C for 20 min, while P3HT–*b*–PFTBT devices are optimized at 165 °C for 10 min. Devices were measured under simulated AM 1.5G irradiation with intensity of 97 mW/cm^2.

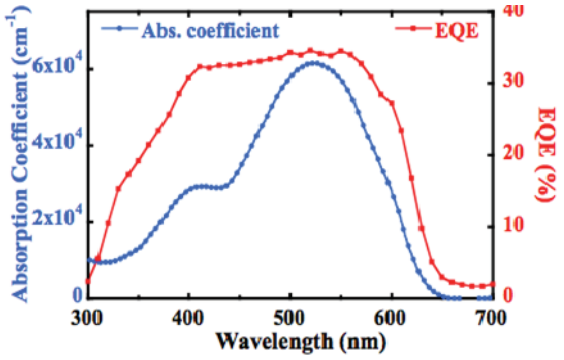

Figure 4.8 – UV-Visible absorption spectrum of a P3HT–*b*–PFTBT film and EQE characteristics of a P3HT–*b*–PFTBT solar cell annealed at optimized conditions (165 °C for 10 min).

If the active layer is comprised of P3HT–*b*–PFTBT block copolymers, devices yielded average efficiencies of 1.5% under annealing conditions optimal for polymer blend devices (100 °C for 20 min) and higher efficiencies of around 1.7% with an

extended annealing time of 90 min at 100 °C (Table 4.1). Optimal performance, however, was achieved at higher annealing temperatures. After annealing for 10 minutes at 165 °C, average power conversion efficiencies of 2.7 ±0.4% with short-circuit currents (J_{sc}) of 5.0 ±0.3 mA/cm^2, open-circuit voltages (V_{oc}) of 1.14 ±0.08 V and fill factors of 0.45 ±0.02 were measured for devices under simulated solar conditions made from block copolymers. The nearly three-fold increase in device performance with respect to optimized devices comprised of polymer blends is due to enhancements of the short-circuit currents and fill factors. Nevertheless, fill factors in all of our devices do not exceed 0.5, a result of the inflection point near open-circuit conditions visible in the current-voltage characteristics shown in Figure 4.7. We attribute the presence of an inflection point to problems in charge extraction due to either an imbalance in charge transport or accumulation of charge at an interface.[33,34] As shown in Table 4.2, the best overall efficiency among our devices was recorded at 3.1% with an open-circuit voltage of 1.23 V. This device performance is remarkable for solar cells based on donor-acceptor block copolymers[15-17,35,36] and for non-fullerene solution-processed organic solar cells.[37-40]

	efficiency (%)	short-circuit current (mA/cm^2)	open-circuit voltage (V)	fill factor
100 ^oC 20 min polymer blend	1.0 ±0.1	2.6 ±0.3	1.22 ±0.02	0.33 ±0.02
165 ^oC 10 min polymer blend	0.5 ±0.1	1.0 ±0.1	1.16 ±0.03	0.42 ±0.02
100 ^oC 20 min block copolymer	1.5 ±0.1	3.7 ±0.2	1.13 ±0.04	0.35 ±0.01
100 ^oC 90 min block copolymer	1.7 ±0.1	4.1 ±0.1	1.14 ±0.02	0.35 ±0.01
165 ^oC 10 min block copolymer	2.7 ±0.4	5.0 ±0.3	1.14 ±0.08	0.45 ±0.02

Note: Devices are measured under simulated AM 1.5G irradiation with intensity of 97 mW/cm^2.

Table 4.1 – Device characteristics of P3HT/PFTBT blend and P3HT–*b*–PFTBT block copolymer solar cells at different annealing conditions.

	efficiency (%)	short-circuit current (mA/cm^2)	open-circuit voltage (V)	fill factor
Best device , block copolymer	3.1	5.2	1.23	0.47
Best device, blend	1.1	2.9	1.22	0.30

Note: Devices are measured under simulated AM 1.5G irradiation with intensity of 97 mW/cm^2.

Table 4.2 – Device characteristics of P3HT/PFTBT polymer blend and P3HT–*b*–PFTBT block copolymer solar cells with highest efficiencies.

The absorption spectrum of pristine P3HT–*b*–PFTBT films and external quantum efficiency (EQE) of P3HT–*b*–PFTBT devices annealed at 165 °C are shown in Figure 4.8. The absorption profiles of P3HT–*b*–PFTBT films preserve the features of the constituent homopolymers and a similar optical bandgap (~ 2 eV) as P3HT is deduced from the absorption edge (see Figure 4.3 in experimental session). Optimized block copolymer devices display relatively high photoconversion efficiencies over a broad range of wavelengths (namely 350-610 nm) with EQE values of 20-35%, which are significant for thin-film photovoltaics based on only polymeric materials. Interestingly, an EQE value of 31% was recorded at 400 nm where the exciton generation is mostly attributed to the optical absorption of PFTBT, suggesting efficient exciton dissociation from photoexcitations in the acceptor domains. Integrating the EQE results predicts a J_{sc} of 4.7 mA/cm^2 with an AM 1.5G reference spectrum. This is consistent with a measured J_{sc} of 5.0 mA/cm^2 under AM 1.5G simulated solar conditions for the same device (~ 5% error). We attribute the small discrepancy to degradation in air, as EQE measurements took

place in ambient. Indeed, devices which have undergone EQE measurements exhibit reduced J_{SC} (< 4 mA/cm^2) when tested under 1 sun conditions in a N_2 atmosphere.

Resonant soft X-ray scattering (RSOXS) and grazing-incidence X-ray scattering measurements were carried out to elucidate the basis for the enhanced performance of block copolymer devices compared to devices made from polymer blends. RSOXS is a powerful tool for characterizing the phase separation in polymer thin films with limited phase contrast or in complicated multiphase systems.[41-44] Differences in the core electronic transitions of organic materials in the soft X-ray regime greatly enhance scattered intensities over hard X-ray scattering, enabling transmission X-ray scattering experiments of thin polymer films. As shown in Figure 4.4, the X-ray absorptions of P3HT and PFTBT differ at 285.4 eV, which enables RSOXS experiments.

Figure 4.9 presents RSOXS intensities as a function of scattering vector, q (q = $4\pi\sin(\theta/2)/\lambda$, λ is the X-ray wavelength and θ is the scattering angle), taken at 285.4 eV X-ray energy for P3HT/PFTBT polymer blend and P3HT–*b*–PFTBT block copolymer thin films annealed at 100 and 165 °C, respectively. The film annealing conditions match the optimum for the active layer of devices. Scattering data from polymer blends show little structure. Scattering profiles from P3HT–*b*–PFTBT block copolymer films are distinct from scattering data from polymer blends (Figure 4.9. and Figure 4.5.) or polymer/fullerene mixtures.[10,45] A primary scattering peak at q^* = 0.035 Å^{-1} and a weak second-order peak at $2q^*$ = 0.070 Å^{-1} are evident in data from thin films of block copolymers annealed at 165 °C. The positions of the scattering peaks at q^* and $2q^*$ are a signature of self-assembly into block copolymer lamellar microdomains[46,47] with a domain spacing of approximately 18 nm. The individual domain sizes are therefore roughly 9 nm, comparable to the exciton diffusion length in organic semiconductors (~ 10 nm).[48]

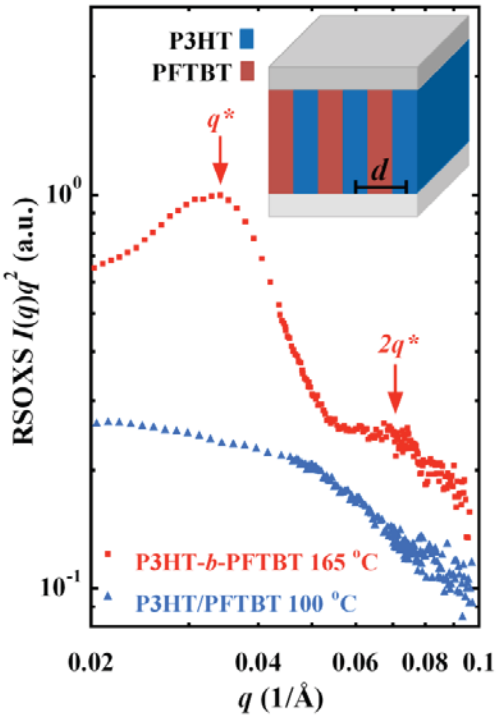

Figure 4.9 – Comparison of the morphology in the active layers of optimized P3HT–*b*–PFTBT and P3HT/PFTBT photovoltaic devices using RSOXS. RSOXS data were acquired at the carbon absorption edge (285.4 eV) of a P3HT–*b*–PFTBT film annealed at 165 °C and a P3HT/PFTBT (1:2 by mass) blend annealed at 100 °C. RSOXS intensities are offset for clarity. Scattering data are presented as a Kratky plot of $I(q)q^2$ vs q, where $I(q)$ is the scattering intensity, and q is the scattering vector. In optimized P3HT–*b*–PFTBT samples, a well-defined primary peak, q^* (~ 0.035 Å^{-1}), and second-order reflection, $2q^*$, are identified. Schematic illustration of the lamellar morphology is shown in the inset, with the average domain spacing indicated as d.

RSOXS experiments in the transmission geometry exclusively explore the in-plane film structure and consequently demonstrate the presence of P3HT–*b*–PFTBT lamellae oriented perpendicular to the substrate, as shown in the inset of Figure 4.9. Grazing incidence small-angle X-ray scattering (GISAXS) measurements shown in Figure 4.6 similarly suggest in-plane microdomains with roughly 16 nm spacing (q^* = 0.04 Å^{-1}), in reasonable agreement with the length scales extracted from RSOXS data.

Consequently, RSOXS and GISAXS data demonstrate a thin-film lamellar morphology that not only establishes an equilibrium microstructure amenable for exciton dissociation but also provides pathways for electron and hole transport to the corresponding electrodes. We note that the appearance of a lamellar microstructure in P3HT–*b*–PFTBT films only occurs at 165 ^{o}C and not 100 ^{o}C (see Figure 4.5.), and device efficiencies exhibit a roughly two-fold increase when films are annealed at 165 ^{o}C versus 100 ^{o}C (Table 4.1). Thus, we attribute the significant improvement in photovoltaic device performance to the self-assembly of block copolymers into well-defined mesostructures in the active layer.

We examined the molecular order in block copolymer thin films using conventional X-ray diffraction (XRD) and grazing-incidence wide-angle X-ray scattering (GIWAXS). Measurements were performed on P3HT–*b*–PFTBT films deposited on top of PEDOT:PSS-coated Si substrates and processed in an analogous manner to optimized devices (165 °C annealing for 10 min). XRD results show that PFTBT is amorphous while P3HT forms crystalline structures in both blend and block copolymer films with the same (100) spacing as that in the pristine P3HT films (Figure 4.10(a)). Complementary 2-D GIWAXS measurements provide the preferred orientation of these crystallites through analysis of both the in-plane (along q_y) and out-of-plane (along q_z) scattering data. As shown in Figure 4.10(b), the (100), (200), and (300) reflections of P3HT (q ~ 0.4, 0.8, and 1.2 Å^{-1}, respectively) - corresponding to spacing between the polymer backbone through the alkyl side-chains - are strongly in-plane with the substrate (along q_y). The (010) peak (q ~ 1.65 Å^{-1}), which corresponds to π-π stacking between chains, is only evident in the out-of-plane direction (along q_z). This indicates that P3HT assumes a predominantly face-on orientation, with π-stacking primarily out-of-plane with the substrate. Face-on P3HT crystallites likely enhance the hole extraction efficacy because the fast charge transport direction is along the π-π stacking direction.[49] The

orientation of P3HT crystals in P3HT–*b*–PFTBT block copolymer films differs qualitatively from previously reported studies on P3HT crystallization in homopolymers,[50] polymer/fullerene mixtures[51,52] or polymer/polymer blends[53] where edge-on orientations are strongly preferred. To first order, there is no reason for the lamellar block copolymer morphology to constrain the P3HT block into either a face-on or edge-on orientation. Instead, we hypothesize that interactions between PFTBT and the substrate lead to preferred face-on orientations for the PFTBT block at the substrate interface. Consequently, the connectivity between blocks nucleates crystals with face-on orientations within the P3HT domains.

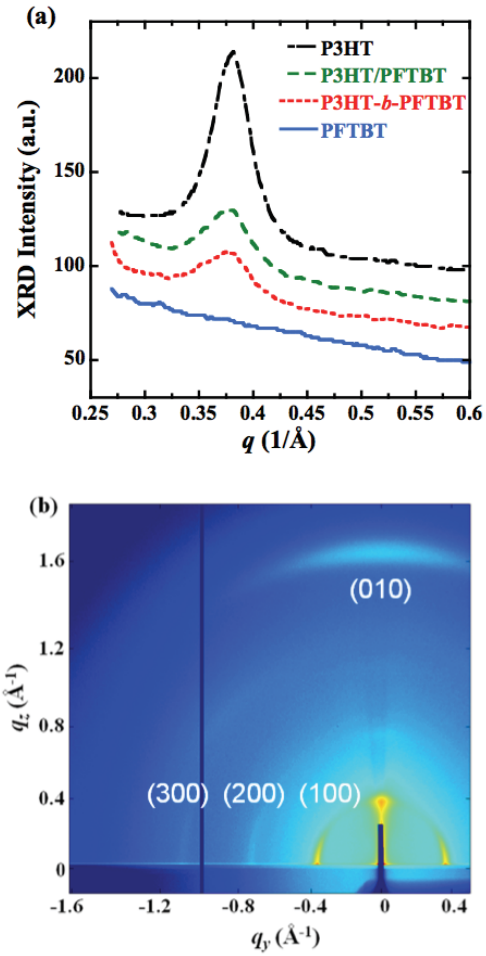

Figure 4.10 – Molecular organization in P3HT–*b*–PFTBT thin films. (a) X-ray diffraction (XRD) patterns of neat P3HT, neat PFTBT, P3HT/PFTBT blend, and P3HT–*b*–PFTBT block copolymer films annealed at 165 °C. (b) Two-dimensional GIWAXS pattern for thin films of P3HT–*b*–PFTBT annealed at optimized conditions (165 °C) for device performance. The (100), (200), and (300) diffraction peaks of regioregular P3HT are strongly biased in the in-plane direction (q_y) and the (010) peak is apparent in the out-of-plane direction (q_z), suggesting face-on crystallites.

The combination of our device results and structural characterization on multiple length scales demonstrates the unique strengths of block copolymer architectures for efficient organic photovoltaics. In addition to controlling the mesoscale structure, conjugated block copolymers provide control of the donor-acceptor interface and of crystallite orientations. Covalent bonding across the donor-acceptor interface has the potential to control charge separation and charge recombination rates,[54,55] opening the possibility of achieving the near unit efficiencies for charge separation from charge transfer states observed in photosynthetic systems.[56] In our studies, the device performance increases when the active layer is composed of block copolymers instead of polymer blends even when the morphology is roughly invariant between the two systems; for example, after annealing at 100 ^{o}C the device efficiencies improve by 50% when block copolymers are used as active layers even though the RSOXS data and mesoscale structure are similar for block copolymer and blend films (Table 4.1 and Figure 4.5).

A possible explanation for the difference in the device performance between blend and block copolymer devices is that the connectivity between blocks provides donor/acceptor interfaces within length scales of the order of chain dimensions (ca. 10 nm) and consequently promotes charge separation. The size of domains, however, in P3HT/PFTBT blends at optimum conditions is near 10-20 nm, as evident from the inflection point in the scattering data from blends shown in Figure 4.9 or the data in reference.[57] Another possible explanation, changes in charge extraction efficacy, is ruled out given that the current at reverse bias scales with the short-circuit current in Figure 1b.[45] Thus, we hypothesize that conjugation across the donor-acceptor interface is responsible for enhancing device performance in block copolymer devices even when the microstructure of the active layer is similar to blends, suggesting that covalent control of

donor-acceptor interfaces is a route for controlling interfacial molecular order, exciton dissociation and charge recombination to enhance excitonic solar cell performance.

4.4. Conclusions

Establishing exceptional performance in P3HT–*b*–PFTBT solar cells provides a clear pathway for enhancing efficiencies in fully conjugated block copolymers devices. The choice of P3HT and PFTBT as constituent blocks is motivated by previous work on optimizing polymer blends composed of P3HT and PFTBT derivatives for the active layer of solar cells.[28,58-61] As a consequence, combinations of polymer blocks with complementary absorbance could lead to significant enhancements in short-circuit currents beyond P3HT–*b*–PFTBT because the absorption spectra of P3HT and PFTBT overlap significantly (Figure 4.3.). Broad-band light absorption can be achieved in combination with open-circuit voltages beyond 1 V with careful design of the HOMO/LUMO levels of the constituent blocks, as demonstrated with P3HT–*b*–PFTBT. Previous work has also demonstrated the presence of exciplex or bound charge transfer states at polymer-polymer interfaces which are unlikely to contribute to the photocurrent at room temperature.[62-64] These strongly bound states are localized, in many cases intermolecularly to the benzothiadiazole group in the acceptor polymer.[65,66] Nevertheless, recent photophysical studies of conjugated donor-acceptor molecules have shown that the presence of charge transfer states and consequently the degree of recombination depends strongly on the linking chemistry.[67] As such, fully conjugated block copolymers provide a path to achieve unprecedented combinations of light absorption, high photovoltages and control of electronic coupling at donor-acceptor interfaces in single-component active layers of organic solar cells.

4.5. References

(1) Brédas, J.-L.; Norton, J. E.; Cornil, J.; Coropceanu, V., *Accounts Chem. Res.* **2009**, *42*, 1691-1699.

(2) Forrest, S. R., *Nature* **2004**, *428*, 911-918.

(3) Shaheen, S. E.; Ginley, D. S.; Jabbour, G. E., *MRS Bull.* **2005**, *30*, 10-19.

(4) Mayer, A. C.; Scully, S. R.; Hardin, B. E.; Rowell, M. W.; McGehee, M. D., *Mater. Today* **2007**, *10*, 28-33.

(5) Giebink, N. C.; Wiederrecht, G. P.; Wasielewski, M. R.; Forrest, S. R., *Phys. Rev. B* **2010**, *82*, 155305.

(6) Thompson, B. C.; Fréchet, J. M. J., *Angew. Chem. Int. Ed.* **2008**, *47*, 58-77.

(7) Chen, W.; Nikiforov, M. P.; Darling, S. B., *Energy Environ. Sci.* **2012**, *5*, 8045-8074.

(8) Kim, J. B.; Allen, K.; Oh, S. J.; Lee, S.; Toney, M. F.; Kim, Y. S.; Kagan, C. R.; Nuckolls, C.; Loo, Y.-L., *Chem. Mater.* **2010**, *22*, 5762-5773.

(9) Vakhshouri, K.; Kozub, D. R.; Wang, C.; Salleo, A.; Gomez, E. D., *Phys. Rev. Lett.* **2012**, *108*, 026601.

(10) Kozub, D. R.; Vakhshouri, K.; Orme, L. M.; Wang, C.; Hexemer, A.; Gomez, E. D., *Macromolecules* **2011**, *44*, 5722-5726.

(11) Brabec, C. J.; Gowrisanker, S.; Halls, J. J. M.; Laird, D.; Jia, S. J.; Williams, S. P., *Adv. Mater.* **2010**, *22*, 3839-3856.

(12) Xin, H.; Reid, O. G.; Ren, G.; Kim, F. S.; Ginger, D. S.; Jenekhe, S. A., *ACS Nano* **2010**, *4*, 1861-1872.

(13) Bates, F. S.; Fredrickson, G. H., *Phys. Today* **1999**, *52*, 32-38.

(14) Leibler, L., *Macromolecules* **1980**, *13*, 1602-1617.

(15) Sary, N.; Richard, F.; Brochon, C.; Leclerc, N.; Lévêque, P.; Audinot, J.-N.; Berson, S.; Heiser, T.; Hadziioannou, G.; Mezzenga, R., *Adv. Mater.* **2010**, *22*, 763-768.

(16) Zhang, Q.; Cirpan, A.; Russell, T. P.; Emrick, T., *Macromolecules* **2009**, *42*, 1079-1082.

(17) Tao, Y.; McCulloch, B.; Kim, S.; Segalman, R. A., *Soft Matter* **2009**, *5*, 4219-4230.

(18) Sivula, K.; Ball, Z. T.; Watanabe, N.; Fréchet, J. M. J., *Adv. Mater.* **2006**, *18*, 206-210.

(19) Sun, S.-S.; Zhang, C.; Ledbetter, A.; Choi, S.; Seo, K.; Carl E. Bonner, J.; Drees, M.; Sariciftci, N. S., *Appl. Phys. Lett.* **2007**, *90*, 043117.
(20) Hadziioannou, G., *MRS Bull.* **2002**, *27*, 456-460
(21) Ku, S.-Y.; Brady, M. A.; Treat, N. D.; Cochran, J. E.; Robb, M. J.; Kramer, E. J.; Chabinyc, M. L.; Hawker, C. J., *J. Am. Chem. Soc.* **2012**, *134*, 16040-16046.
(22) Sommer, M.; Komber, H.; Huettner, S.; Mulherin, R.; Kohn, P.; Greenham, N. C.; Huck, W. T. S., *Macromolecules* **2012**, *45*, 4142-4151.
(23) Lin, Y.-H.; Smith, K. A.; Kempf, C. N.; Verduzco, R., *Polym. Chem.* **2013**, *4*, 229-232.
(24) Gann, E.; Young, A. T.; Collins, B. A.; Yan, H.; Nasiatka, J.; Padmore, H. A.; Ade, H.; Hexemer, A.; Wang, C., *Rev. Sci. Instrum.* **2012**, *83*, 045110.
(25) Jiang, Z.; Li, X. F.; Strzalka, J.; Sprung, M.; Sun, T.; Sandy, A. R.; Narayanan, S.; Lee, D. R.; Wang, J., *J. Synchrot. Radiat.* **2012**, *19*, 627-636.
(26) Jiang, Z., *GIXSGUI is available for download: http://www.aps.anl.gov/Sectors/Sector8/Operations/GIXSGUI.html*.
(27) Zhang, F.; Perzon, E.; Wang, X.; Mammo, W.; Andersson, M. R.; Inganäs, O., *Adv. Funct. Mater.* **2005**, *15*, 745-750.
(28) McNeill, C. R.; Halls, J. J. M.; Wilson, R.; Whiting, G. L.; Berkebile, S.; Ramsey, M. G.; Friend, R. H.; Greenham, N. C., *Adv. Funct. Mater.* **2008**, *18*, 2309-2321.
(29) Mulherin, R. C.; Jung, S.; Huettner, S.; Johnson, K.; Kohn, P.; Sommer, M.; Allard, S.; Scherf, U.; Greenham, N. C., *Nano Lett.* **2011**, *11*, 4846-4851.
(30) Ramsdale, C. M.; Barker, J. A.; Arias, A. C.; MacKenzie, J. D.; Friend, R. H.; Greenham, N. C., *J. Appl. Phys.* **2002**, *92*, 4266-4270.
(31) Barker, J. A.; Ramsdale, C. M.; Greenham, N. C., *Phys. Rev. B* **2003**, *67*, 075205.
(32) Snaith, H. J.; Greenham, N. C.; Friend, R. H., *Adv. Mater.* **2004**, *16*, 1640-1645.
(33) Tress, W.; Petrich, A.; Hummert, M.; Hein, M.; Leo, K.; Riede, M., *Appl. Phys. Lett.* **2011**, *98*, 063301.
(34) Wang, J. C.; Ren, X. C.; Shi, S. Q.; Leung, C. W.; Chan, P. K. L., *Org. Electron.* **2011**, *12*, 880-885.

(35) Miyanishi, S.; Zhang, Y.; Tajima, K.; Hashimoto, K., *Chem. Commun.* **2010**, *46*, 6723-6725.
(36) Topham, P. D.; Parnell, A. J.; Hiorns, R. C., *J. Polym. Sci., Part B: Polym. Phys.* **2011**, *49*, 1131-1156.
(37) Anthony, J. E., *Chem. Mater.* **2010**, *23*, 583-590.
(38) Sonar, P.; Fong Lim, J. P.; Chan, K. L., *Energy Environ. Sci.* **2011**, *4*, 1558-1574.
(39) Mikroyannidis, J. A.; Suresh, P.; Sharma, G. D., *Synth. Met.* **2010**, *160*, 932-938.
(40) Ahmed, E.; Ren, G.; Kim, F. S.; Hollenbeck, E. C.; Jenekhe, S. A., *Chem. Mater.* **2011**, *23*, 4563-4577.
(41) Virgili, J. M.; Tao, Y.; Kortright, J. B.; Balsara, N. P.; Segalman, R. A., *Macromolecules* **2007**, *40*, 2092-2099.
(42) Wang, C.; Lee, D. H.; Hexemer, A.; Kim, M. I.; Zhao, W.; Hasegawa, H.; Ade, H.; Russell, T. P., *Nano Lett.* **2011**, *11*, 3906-3911.
(43) Swaraj, S.; Wang, C.; Yan, H.; Watts, B.; Lüning, J.; McNeill, C. R.; Ade, H., *Nano Lett.* **2010**, *10*, 2863-2869.
(44) Guo, C.; Kozub, D. R.; Vajjala Kesava, S.; Wang, C.; Hexemer, A.; Gomez, E. D., *ACS Macro Lett.* **2013**, *2*, 185-189.
(45) Kozub, D. R.; Vakhshouri, K.; Kesava, S. V.; Wang, C.; Hexemer, A.; Gomez, E. D., *Chem. Commun.* **2012**, *48*, 5859-5861.
(46) Bendejacq, D.; Ponsinet, V.; Joanicot, M.; Loo, Y. L.; Register, R. A., *Macromolecules* **2002**, *35*, 6645-6649.
(47) Hamley, I. W., *The Physics of Block Copolymers. Oxford University Press: Oxford* **1998**.
(48) Haugeneder, A. a. N., M. and Kallinger, C. and Spirkl, W. and Lemmer, U. and Feldmann, J. and Scherf, U. and Harth, E. and Gugel, A. and Mullen, K., *Phys. Rev. B* **1999**, *59*, 15346-15351.
(49) Sirringhaus, H.; Brown, P. J.; Friend, R. H.; Nielsen, M. M.; Bechgaard, K.; Langeveld-Voss, B. M. W.; Spiering, A. J. H.; Janssen, R. A. J.; Meijer, E. W.; Herwig, P.; de Leeuw, D. M., *Nature* **1999**, *401*, 685-688.

(50) Yang, H.; Shin, T. J.; Yang, L.; Cho, K.; Ryu, C. Y.; Bao, Z., *Adv. Funct. Mater.* **2005**, *15*, 671-676.
(51) Woo, C. H.; Thompson, B. C.; Kim, B. J.; Toney, M. F.; Fréchet, J. M. J., *J. Am. Chem. Soc.* **2008**, *130*, 16324-16329.
(52) Li, G.; Yao, Y.; Yang, H.; Shrotriya, V.; Yang, G.; Yang, Y., *Adv. Funct. Mater.* **2007**, *17*, 1636-1644.
(53) Nam, S.; Shin, M.; Park, S.; Lee, S.; Kim, H.; Kim, Y., *Phys. Chem. Chem. Phys.* **2012**, *14*, 15046-15053.
(54) Bu, L.; Guo, X.; Yu, B.; Qu, Y.; Xie, Z.; Yan, D.; Geng, Y.; Wang, F., *J. Am. Chem. Soc.* **2009**, *131*, 13242-13243.
(55) Guo, Z.; Jenekhe, S. A.; Prezhdo, O. V., *Phys. Chem. Chem. Phys.* **2011**, *13*, 7630-7636.
(56) Blankenship, R. E., *Molecular Mechanisms of Photosynthesis. Blackwekk Science: Oxford, U. K.* **2002**.
(57) Yan, H.; Collins, B. A.; Gann, E.; Wang, C.; Ade, H.; McNeill, C. R., *ACS Nano* **2011**, *6*, 677-688.
(58) McNeill, C. R.; Abrusci, A.; Zaumseil, J.; Wilson, R.; McKiernan, M. J.; Burroughes, J. H.; Halls, J. J. M.; Greenham, N. C.; Friend, R. H., *Appl. Phys. Lett.* **2007**, *90*, 193506-3.
(59) McNeill, C. R.; Westenhoff, S.; Groves, C.; Friend, R. H.; Greenham, N. C., *J. Phys. Chem.C* **2007**, *111*, 19153-19160.
(60) McNeill, C. R.; Abrusci, A.; Hwang, I.; Ruderer, M. A.; Müller-Buschbaum, P.; Greenham, N. C., *Adv. Funct. Mater.* **2009**, *19*, 3103-3111.
(61) McNeill, C. R.; Greenham, N. C., *Adv. Mater.* **2009**, *21*, 3840-3850.
(62) Morteani, A. C.; Dhoot, A. S.; Kim, J. S.; Silva, C.; Greenham, N. C.; Murphy, C.; Moons, E.; Ciná, S.; Burroughes, J. H.; Friend, R. H., *Adv. Mater.* **2003**, *15*, 1708-1712.
(63) Friend, R. H.; Phillips, M.; Rao, A.; Wilson, M. W. B.; Li, Z.; McNeill, C. R., *Faraday Discussions* **2012**, *155*, 339-348.
(64) Yin, C.; Kietzke, T.; Kumke, M.; Neher, D.; Hörhold, H.-H., *Sol. Energy Mater. Sol. Cells* **2007**, *91*, 411-415.

(65) Huang, Y.-s.; Westenhoff, S.; Avilov, I.; Sreearunothai, P.; Hodgkiss, J. M.; Deleener, C.; Friend, R. H.; Beljonne, D., *Nat. Mater.* **2008**, *7*, 483-489.
(66) Bakulin, A. A.; Rao, A.; Pavelyev, V. G.; van Loosdrecht, P. H. M.; Pshenichnikov, M. S.; Niedzialek, D.; Cornil, J.; Beljonne, D.; Friend, R. H., *Science* **2012**, *335*, 1340-1344.
(67) Johnson, K.; Huang, Y.-S.; Huettner, S.; Sommer, M.; Brinkmann, M.; Mulherin, R.; Niedzialek, D.; Beljonne, D.; Clark, J.; Huck, W. T. S.; Friend, R. H., *J. Am. Chem. Soc.* **2013**, *135*, 5074-5083.

Chapter 5

Supramolecular Conjugated Block Copolymers

This chapter is included in Yen-Hao Lin, Seth B. Darling, Maxim P. Nikiforov, Joseph Strzalka, Rafael Verduzco, "Supramolecular Conjugated Block Copolymers," *Macromolecules,* 2012, **45**, 6571-6579.

While the performance of polymer-polymer bulk heterojunction organic photovoltaics (OPVs) is poor compared with polymer-fullerene OPVs, reducing or eliminating micron-scale phase separation in all-polymer OPVs may dramatically improve performance. Herein, we demonstrate that 2-ureido-4[1H]-pyrimidinone (UPy) quadruple hydrogen bonding interactions can be used to prevent micron-scale phase separation at temperatures and processing conditions typically used to prepare bulk heterojunction OPVs. UPy-terminated polymers are synthesized by coupling hydroxyl or primary amine terminated polymers to a reactive isocyanate-UPy group in a one-step reaction. Polymer blend films are subsequently prepared by solution blending, casting onto a surface, and thermal and/or solvent annealing. Film microstructure including the presence of phase-separated domains and polymer crystallinity is analyzed by optical

microscopy, atomic force microscopy (AFM), and grazing-incidence wide-angle X-ray scattering (GIWAXS). In contrast to unmodified polymer blends, blends of UPy-terminated polymers do not exhibit micron-scale phase separation after extended thermal annealing. AFM reveals the presence of crystalline nanofibers and, in some cases, 100 - 300 nm phase-separated domains in UPy-mediated polymer blends. Fluorescence measurements indicate that UPy modification increases fluorescence quenching in solutions of donor and acceptor polymers, due to hydrogen-bonding associations which reduce the average distance for energy and/or electron transfer. These results show that UPy-mediated interactions can suppress micron-scale phase separation in bulk heterojunction polymer blends at temperatures and processing conditions typically used to prepare bulk-heterojunction OPVs. As a result, UPy functionalization may be a powerful route for improving the performance of all-polymer OPVs.

5.1. Introduction

The nanoscale structure of the active layer plays a key role in determining the efficiency of photon-to-electricity conversion in bulk heterojunction (BHJ) organic photovoltaics (OPVs), which are typically comprised of a blend of p-type (hole-conductive) and n-type (electron-conductive) organic semiconductors. While some degree of phase separation is desired for creating continuous charge transport pathways, micron-scale phase separated domains are unfavorable due to reduced interfacial area and decreased charge separation efficiencies.[1-4] This presents significant challenges for all-polymer OPVs, which are made up of a blend of a p-type and n-type conjugated polymers; micron-scale phase separation is commonly observed due to the reduced entropy of mixing for polymer blends.[5-8] While the best performance in all-polymer OPVs (~ 2%)[9-13] is significantly lower compared with state-of-the art polymer-fullerene BHJs, reducing

or eliminating large-scale phase separation in all-polymer OPVs may dramatically improve performance. Advantages of all-polymer OPVs over polymer-fullerene OPVs include a typically higher V_{oc}, a broader absorbance, and tunability of the absorption profile due to the presence of two polymeric semiconductors in the active layer.

All-conjugated block copolymers with p- and n-type blocks represent a promising approach to improving the performance of all-polymer OPVs. Phase separation can be avoided and block copolymer self-assembly may lead to ideal structures for charge dissociation and transport.[14,15] However, studies on donor-acceptor all-conjugated block copolymers are limited, due in large part to synthetic challenges,[16-28] and non-covalent interactions may provide a more accessible approach to construct materials that exhibit the desirable properties of all-conjugated block copolymers.[29-31] Non-covalent associations such as hydrogen bonds,[32,33] ionic bonds,[34,35] and metal-ligand coordination[36] give rise to persistent intermolecular associations between monomeric or polymeric units resulting in supramolecular polymers. These associations potentially provide a straightforward method to reduce phase separation in all-polymer OPVs, resulting in improved performance and model materials for understanding the structure of conjugated polymer blends.

The ureidopyrimidone (UPy) group forms self-complementary quadrupole hydrogen bonding interactions with high dimerization constants (up to 10^7 M^{-1} in non-polar solvents such as chloroform).[37-39] Supramolecular polymers based on UPy interactions have been widely studied, and recent work with coil-like (non-conjugated) polymers has shown that hydrogen bonding interactions can reduce phase separation in polymer blends.[32,38,40-42] The UPy group is also effective in mediating the microstructure and optoelectronic properties of organic semiconductors. For example, UPy hydrogen bonding interactions can enhance energy transfer between electron donor and acceptor

molecules[43] and improve interfacial contact and ionic conductivity when incorporated in the polymer electrolyte of a dye-sensitized solar cell.[44] Also, white-light emitting diodes have been demonstrated using UPy-mediated supramolecular interactions between semiconductive oligomers.[45]

Herein, we present a study of the structure, optoelectronic properties, and crystallization of blends of polymers modified with UPy groups. Conjugated and non-conjugated polymers are functionalized with UPy in a one-step coupling reaction and solution blended to form supramolecular conjugated block copolymers. A practical advantage of UPy interactions compared with all-conjugated block copolymers is a greatly simplified synthetic route and straightforward preparation through solution blending. The structure of blend films is analyzed under a variety of annealing conditions using a combination of polarized optical microscopy (POM), atomic force microscopy (AFM), and grazing-incidence wide-angle X-ray scattering (GIWAXS). We find that UPy quadruple hydrogen bonding interactions can prevent micron-scale phase separation in polymer blend thin films and increase fluorescence quenching in solution due to a reduced average distance between donor and acceptor polymers.

5.2. Experimental Section

5.2.1. Materials

Methyl isocytosine (MIC) was purchased from Sigma-Aldrich and dried under vacuum at 100 °C overnight before use. Styrene (purchased from Sigma-Aldrich) was purified by passing through an Al_2O_3 column. Poly(ethylene glycol) methyl ether (PEG-OH, 5,000 g/mol) was purchased from Sigma-Aldrich. 2(6-isocyanatohexylaminocarbonylamino)-6-methyl-4[1H]-pyrimidinone (UPy-isocyanate),[38]

2,5-dibromo-3-hexylthiophene,[46] 9′,9′-dioctylfluoren-2′,7′-diboronic pinacol ester, and 7′-bromo-9′,9′-dioctylfluoren-2′-yl-4,4,5,5-tetramethyl[1,3,2]dioxaborolane[47] were synthesized as previously described. Tetrahydrofuran (THF) and chloroform ($CHCl_3$) were dried over molecular sieves (4Å). All other reagents were purchased from Sigma-Aldrich and used as received. Silicon Wafers were purchased from El-Cat, washed by sonication in DI water and isopropyl alcohol, and dried under a stream of compressed air before use.

5.2.2. Syntheses

Aniline-end functionalized poly(3-hexylthiophene), P3HT-NH_2. P3HT-NH_2 was prepared using a procedure adapted from a previous report.[35] In a 50 mL flask purged with nitrogen gas, 2,5-dibromo-3-hexylthiophene (1.9 g, 5.82 mmol) was dissolved in anhydrous THF (5 mL), and the solution was stirred under nitrogen at 0 °C for 15 minutes. A solution of isopropyl magnesium chloride and LiCl (1.3 M) in THF (4.48 mL, 5.82 mmol) was added, and the mixture was stirred for 2 hours. 25 mL of THF was then added before adding Ni(dppp)Cl_2 (105.15 mg, 0.194 mmol), and the mixture was stirred for 15 minutes. The reaction was quenched by adding a 1M THF solution of 3-[bis-(trimethylsilyl)amino] phenylmagnesium chloride (6 mL, 6mmol) and stirring for 15 minutes. 5 M HCl (8 mL, 40 mmol) was then added, and the solution was stirred for another 15 minutes. The final mixture was collected by precipitation in cold methanol and water and then by washing with $CHCl_3$ in a Soxhlet apparatus. The $CHCl_3$ solution was stirred with 2 M Na_2CO_3 solution to neutralize the aniline end group. The resulting product was precipitated in cold methanol and dried at 50 °C under vacuum. Yield: 0.86g (88%). M_w (GPC): 4986 g/mol, d*n*/d*c* = 0.250, polydispersity (PDI) = 1.17, Degree of polymerization (DP) (NMR) = 30. ^{1}H NMR (400 MHz, $CDCl_3$, see Figure 5.1), δ (ppm):

6.95 (30H; Aryl-H), 3.75 (2H; NH_2), 2.82 (60H; C-CH_2-C_5H_{11}), 1.70 (60H; CH_2-CH_2-C_4H_9), 1.35 (180H; CH_2-C_3H_6-CH_3), 0.92 (90H; CH_2-CH_3).

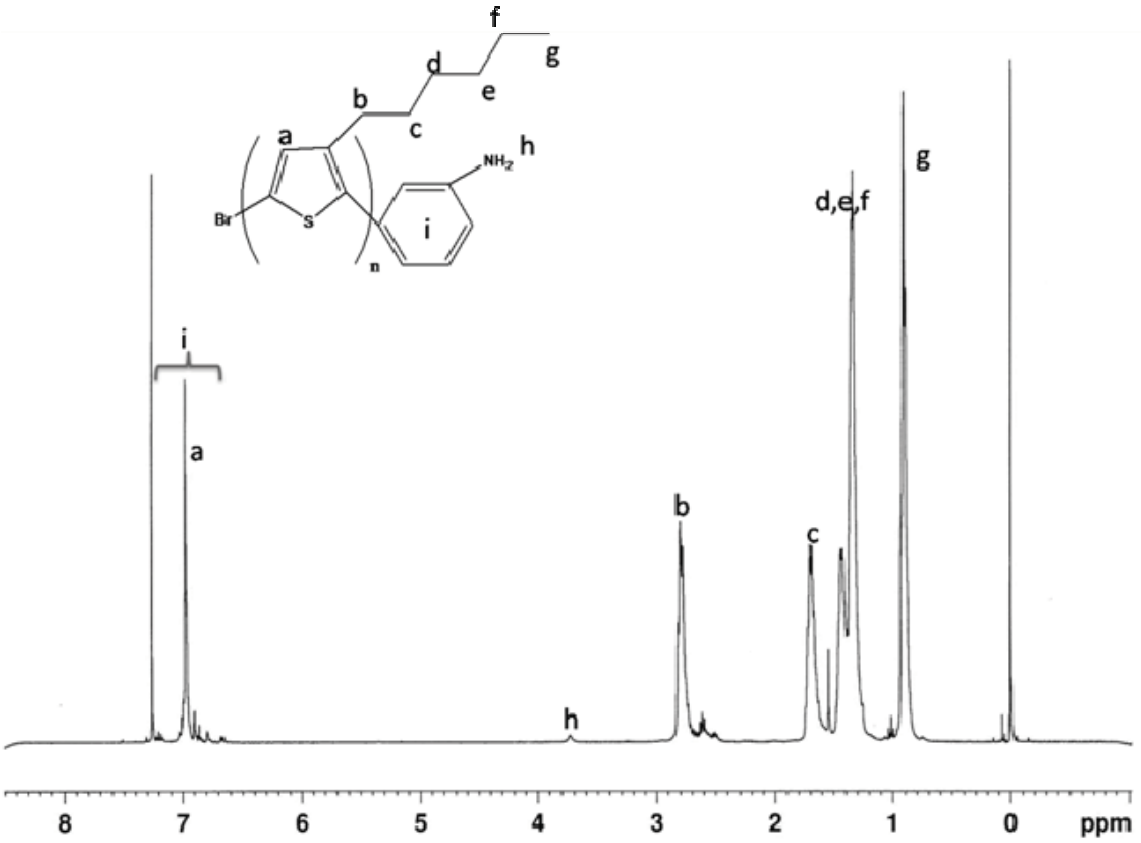

Figure 5.1 – ^1H NMR spectrum of P3HT-NH_2.

Hydroxyl-end functionalized poly(9,9-dioctylfluorenyl-2,7-diyl), PFO-OH. 7′-bromo-9′,9′-dioctylfluoren-2′-yl-4,4,5,5-tetramethyl[1,3,2]dioxaborolane (1 g, 1.68 mmol), 4-(Hydroxymethyl)phenylboronic acid pinacol ester (19.6 mg, 0.08 mmol), Tetrakis-(triphenylphosphine)-palladium(0) (75 mg, 0.065 mmol), and aliquat 336 (3 drops) were added to a Schlenk tube loaded with nitrogen-purged toluene (25 mL) and 2 M Na_2CO_3 aqueous solution (10 mL). The reaction was stirred in 90 °C oil bath for 1 day.

4-(Hydroxymethyl)phenylboronic acid pinacol ester (157 mg, 0.67mmol) was added to the reaction tube and the solution was stirred for 1 day at 90 °C. Bromobenzene (large excess) was added to the reaction and stirred for an additional day before collecting the product by precipitation in methanol. The polymer was subsequently washed with copious amounts of methanol and acetone and dried under vacuum. Yield: 520 mg (84%). M_w (GPC): 5860 g/mol, d*n*/d*c* = 0.234, PDI = 1.31, DP (NMR) = 13. ^{1}H NMR (400 MHz, $CDCl_3$, see Figure 5.2), δ (ppm): 7.5-7.8 (87H; -Ph), 4.78 (2H; Ar-C$\underline{H_2}$-OH), 2.1 (52H; C$\underline{H_2}$-C_7H_{15}), 1.13 (260H; CH_2-$C_5\underline{H_{10}}$-CH_3), 0.80 (78H; C_7H_{14}-C$\underline{H_3}$).

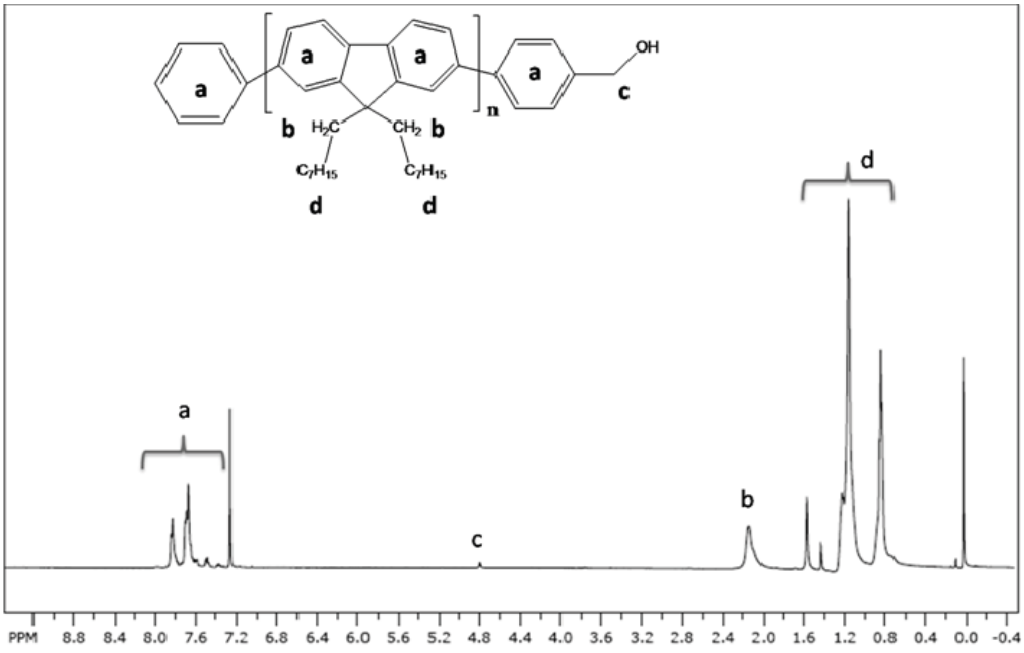

Figure 5.2 – ^{1}H NMR spectrum of PFO-OH.

Hydroxyl-end functionalized poly(9,9-dioctylfluorenyl-2,7-diyl)-co-(2,3,5-benzothiadiazole), PFBT-OH. 9′,9′-dioctylfluorene-2′,7′-diboronic pinacol ester (812 mg, 1.265 mmol), 4,7-dibromobenzo[1,2,5]thiadiazole (370 mg, 1.265 mmol), 4-

(hydroxymethyl)phenylboronic acid pinacol ester (14.8 mg, 0.063 mmol), tetrakis-(triphenylphosphine)-palladium(0) (75 mg, 0.065 mmol), and aliquat 336 (3 drops) were added to a Schlenk tube loaded with nitrogen-purged toluene (25 mL) and 2 M Na_2CO_3 aqueous solution (10 mL). The reaction was stirred in 90 °C oil bath for 1 day. 4-(hydroxymethyl)phenylboronic acid pinacol ester (118 mg) was added to the reaction tube, and the solution was stirred for 1 day at 90 °C. 4-bromobenzyl alcohol (283 mg) was added to the reaction, and the solution was stirred for 1 day at 90 °C. The polymer was recovered by precipitation in methanol, washed with copious amounts of methanol and acetone, and dried under vacuum. Yield: 620 mg (81%). M_w (GPC): 15320 g/mol, d*n*/d*c* = 0.263, PDI = 1.37, DP (NMR) = 22. ^{1}H NMR (400 MHz, $CDCl_3$, see Figure 5.3), δ (ppm): 7.3-8.2 (184H; -Ph), 4.78 (4H; Ar-C$\underline{H_2}$-OH), 2.1 (88H; C$\underline{H_2}$-C_7H_{15}), 1.13 (440H; CH_2-$C_5\underline{H_{10}}$-CH_3), 0.80 (132H; C_7H_{14}-C$\underline{H_3}$).

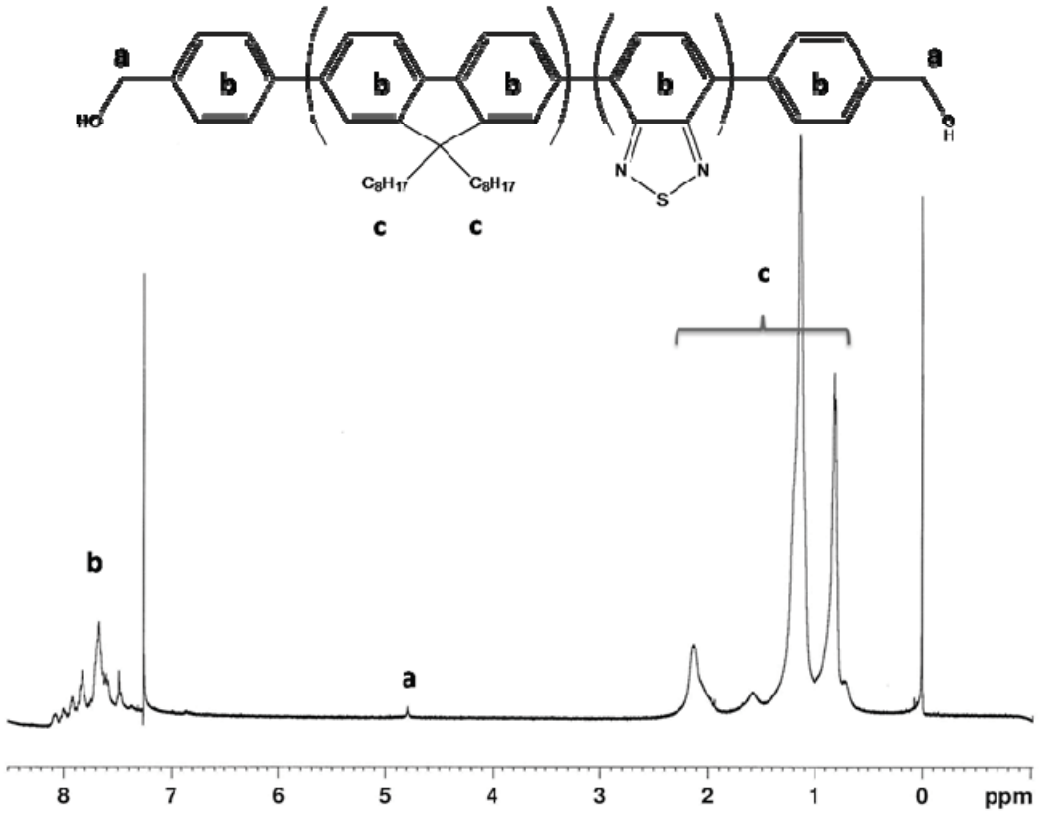

Figure 5.3 – ^{1}H NMR spectrum of PFBT-OH.

Hydroxyl-end functionalized polystyrene, PS-OH. Bromine-terminated polystyrene (PS-Br) was first synthesized by mixing styrene (12g, 115.2 mmol), Cu(I)Br (200 mg, 1.38 mmol), PMDETA (0.29 mL), and ethyl α-bromoisobutyrate (0.127 mL, 0.86 mmol) under nitrogen and reacting at 65 °C. The polystyrene product was precipitated in cold methanol and dried at 50 °C under vacuum. Next, PS-Br (M_w~10,000, 1.6 g, 0.16 mmol), ethanolamine (0.5 mL), and Et_3N (1 mL) were dissolved in DMF (25 mL) and stirred at room temperature overnight. The product was precipitated in cold methanol and dried at 50 °C under vacuum. Yield: 5g (50%). M_w (GPC): 9851, d*n*/d*c* = 0.173, PDI = 1.04. DP (NMR) = 97. ^{1}H NMR (400 MHz, $CDCl_3$, see Figure 5.4), δ (ppm):

6.45-7.08 (490H; -ph), 3.42 (2H; O-C<u>H</u>$_2$-CH$_3$), 3.36 (2H; -C<u>H</u>$_2$-OH), 3.10 (1H; NH-C<u>H</u>-Ph), 2.10 (2H; NH-C<u>H</u>$_2$-CH-OH), 1.84 (194H; C<u>H</u>$_2$-CH-Ph), 1.42 (97H; CH$_2$-C<u>H</u>-Ph), 0.99(6H; C-(C<u>H</u>$_3$)$_2$), 0.83 (3H; O-CH$_2$-C<u>H</u>$_3$).

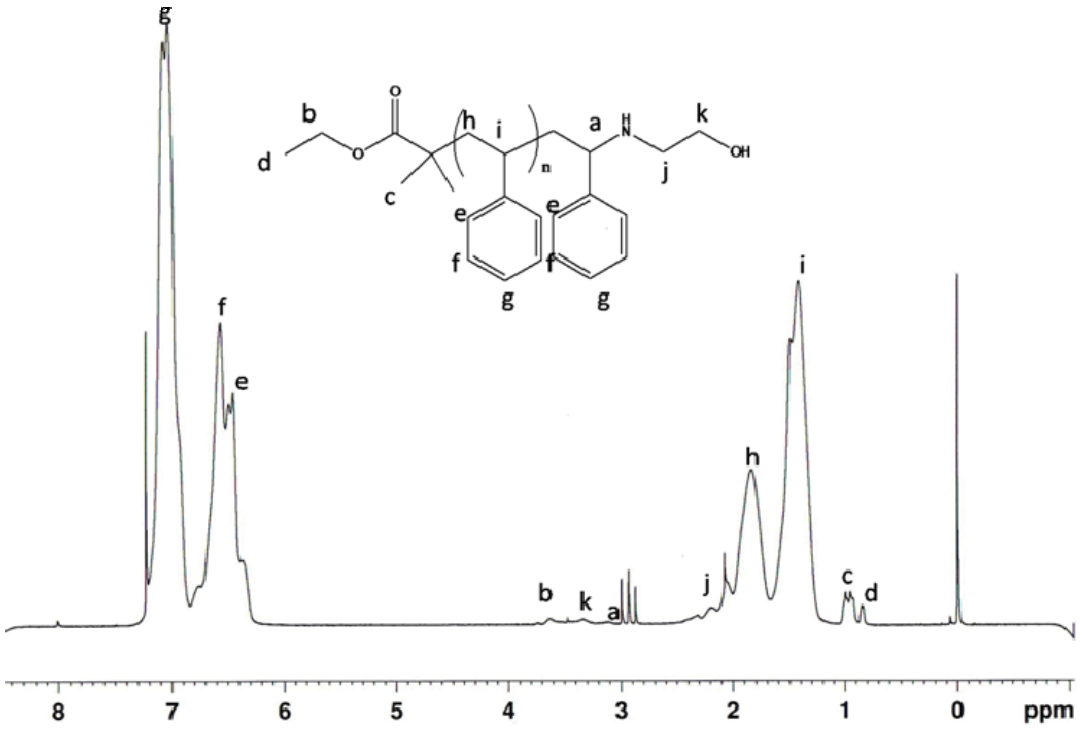

Figure 5.4 – ^{1}H NMR spectrum of PS-OH.

General procedure for the preparation of UPy-end functionalized polymers. All UPy-end terminated polymers were prepared using the same procedure, except where indicated otherwise. In a representative procedure, P3HT-NH$_2$ (300 mg, 0.075 mmol), UPy-isocyanate (65.9 mg, 0.225 mmol) and 3 drops of dibutyltin dilaurate (DBDTL) were dissolved in dry CHCl$_3$ and stirred at 50 °C for 24 hours. Silica gel (240 mesh, 10 mg) was subsequently added, and the solution was stirred at 60 °C for 24 hours. The crude product was precipitated in cold methanol (PEG-UPy was precipitated from cold

diethyl ether), loaded into a Soxhlet apparatus, and washed with $CHCl_3$ to collect the final product, which was concentrated under reduced pressure and dried under vacuum. Recovered yield: 261 mg, 87%. ^{1}H NMR data for each polymer is provided in the text below and in the Figure 5.5 – Figure 5.9.

UPy-functionalized Polystyrene (PS-UPy): Yield (recovered): 90%. ^{1}H NMR (500 MHz, $CDCl_3$, see Figure 5.5), δ (ppm): 13.15 (1H; -N<u>H</u>), 11.88 (1H; -N<u>H</u>), 10.18 (1H, -N<u>H</u>), 5.82 (1H; -C<u>H</u>), 6.45-7.08 (490H; -ph), 3.42 (2H; O-C<u>H$_2$</u>-CH$_3$), 3.21 (2H; -C<u>H$_2$</u>-O-isocyanate-UPy), 3.10 (1H; NH-C<u>H</u>-Ph), 2.10 (2H; NH-C<u>H$_2$</u>-CH-OH), 1.84 (194H; C<u>H$_2$</u>-CH-Ph), 1.42 (97H; CH$_2$-C<u>H</u>-Ph), 0.99(6H; C-(C<u>H$_3$</u>)$_2$), 0.83 (3H; O-CH$_2$-C<u>H$_3$</u>).

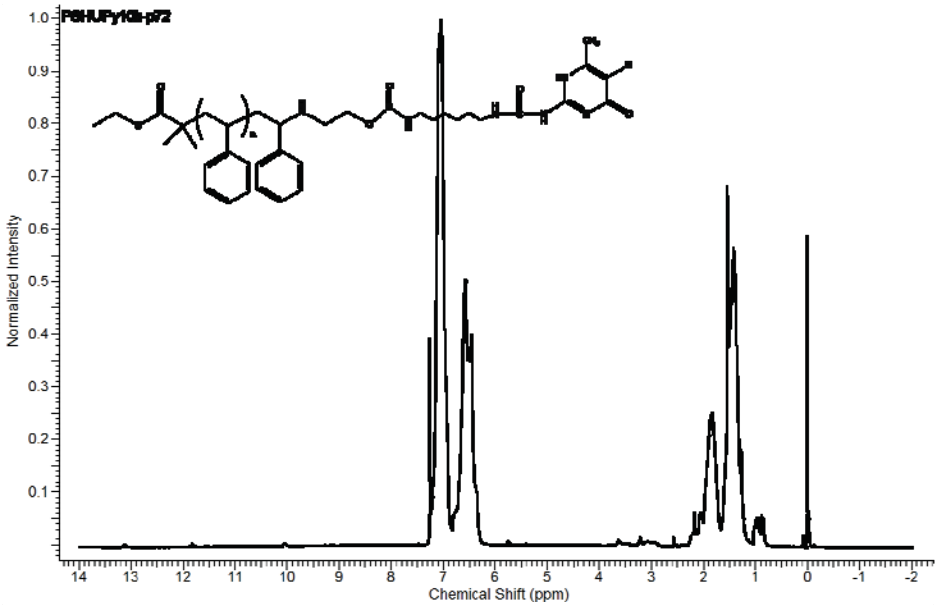

Figure 5.5 – ^{1}H NMR spectrum of PS-UPy.

UPy-functionalized Poly(ethylene glycol) (PEG-UPy): Yield (recovered): 92%. ^{1}H NMR (400 MHz, $CDCl_3$, see Figure 5.6), δ (ppm): 13.15 (1H; -NH), 11.88 (1H; -NH), 10.18 (1H, -NH), 5.82 (1H; -CH), 3.4-3.8 (452H; O-CH_2-CH_2-O-), 3.35 (3H; O-CH_3), 3.21 (4H; NH-CH_2), 2.20 (3H; NH-C-CH_3); 1.63 (4H; -CH_2-CH_2-), 1.35 (4H; NH-CH_2-CH_2).

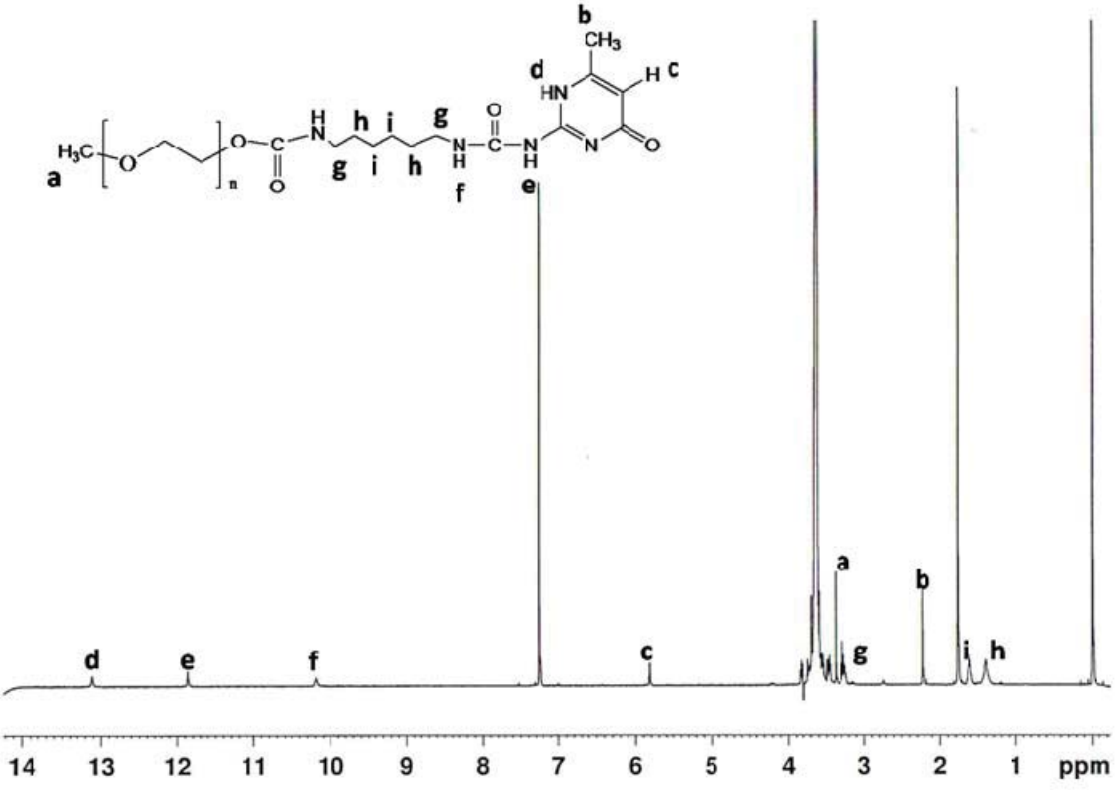

Figure 5.6 – ^{1}H NMR spectrum of PEG-UPy.

UPy-functionalized Poly(3-hexyl thiophene) (P3HT-UPy): Yield (recovered): 87%. ^{1}H NMR (500 MHz, $CDCl_3$, see Figure 5.7), δ (ppm): 13.15 (1H; -N<u>H</u>), 11.88 (1H; -N<u>H</u>), 10.18 (1H, -N<u>H</u>), 5.82 (1H; -C<u>H</u>), 6.95 (30H; Aryl-<u>H</u>), 3.75 (1H; N<u>H</u>-UPy), 2.82 (60H; C-C<u>H$_2$</u>-C_5H_{11}), 1.70 (60H; CH_2-C<u>H$_2$</u>-C_4H_9), 1.35 (180H; CH_2-C_3<u>H$_6$</u>-CH_3), 0.92 (90H; CH_2-C<u>H$_3$</u>).

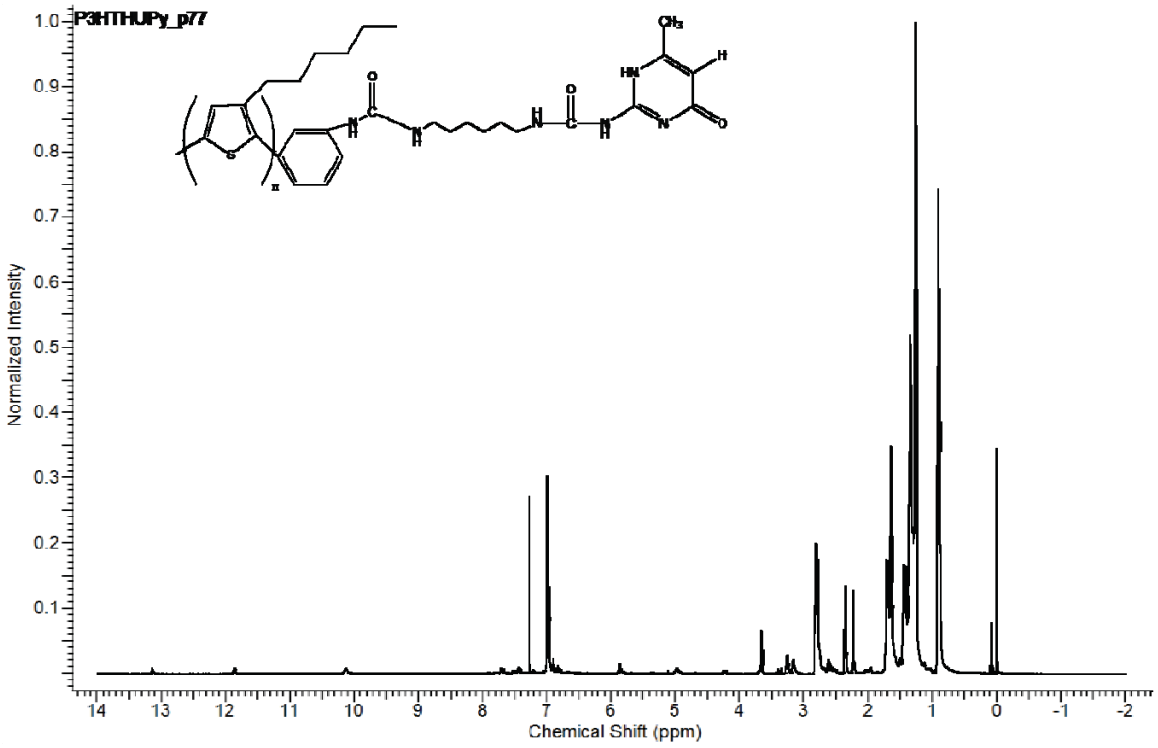

Figure5.7 – ^{1}H NMR spectrum of P3HT-UPy.

UPy-functionalized Poly(9,9-dioctyl fluorene) (PFO-UPy): Yield (recovered): 85%. ^{1}H NMR (500 MHz, $CDCl_3$, see Figure 5.8), δ (ppm): 13.15 (1H; -N<u>H</u>), 11.88 (1H;

-N<u>H</u>), 10.18 (1H, -N<u>H</u>), 5.82 (1H; -C<u>H</u>), 7.5-7.8 (87H; -Ph), 5.12 (2H; Ar-C<u>H</u>$_2$-O-UPy), 2.1 (52H; C<u>H</u>$_2$-C$_7$H$_{15}$), 1.13 (260H; CH$_2$-C$_5$<u>H</u>$_{10}$-CH$_3$), 0.80 (78H; C$_7$H$_{14}$-C<u>H</u>$_3$).

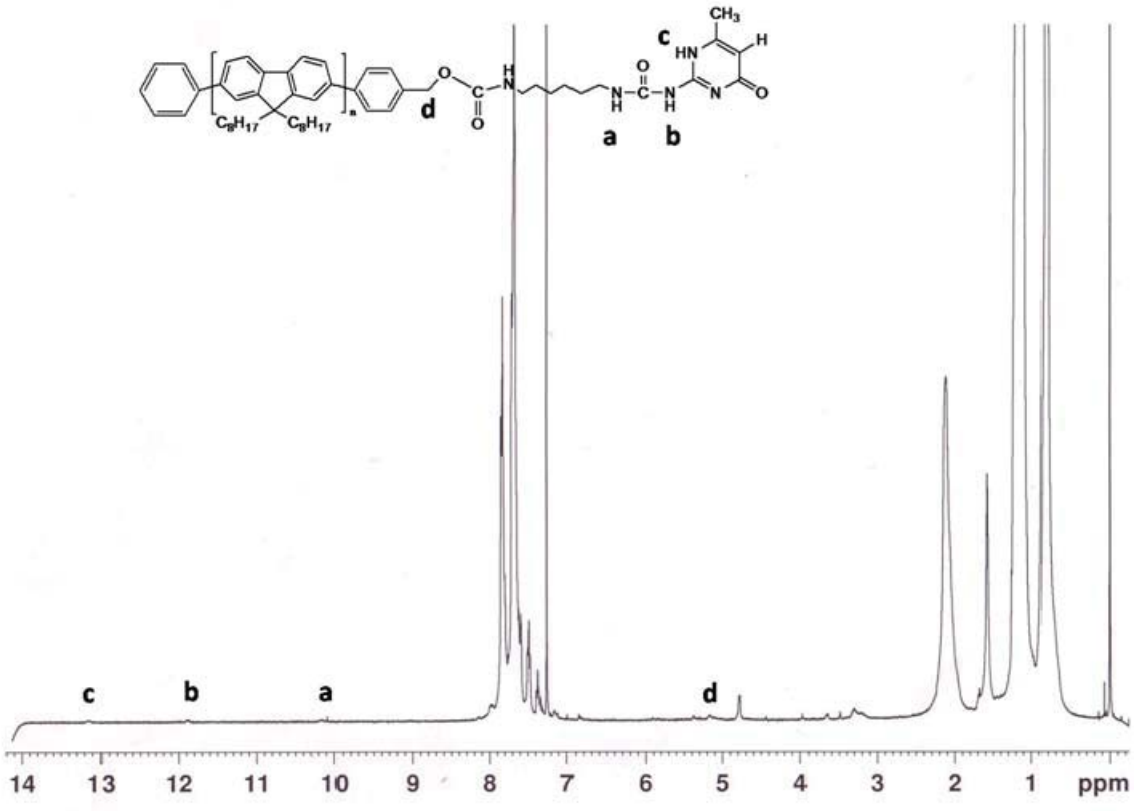

Figure 5.8 – ^{1}H NMR spectrum of PFO-UPy.

UPy-functionalized Poly(9,9-dioctyl fluorene-*alt*-benzothiadiazole) (PFBT-UPy): Yield (recovered): 87%. ^{1}H NMR (500 MHz, $CDCl_3$, see Figure 5.9), δ (ppm): 13.15 (2H; -N<u>H</u>), 11.88 (2H; -N<u>H</u>), 10.18 (2H, -N<u>H</u>), 5.82 (2H; -C<u>H</u>), 7.3-8.2 (184H; -Ph), 5.12 (4H; Ar-C<u>H</u>$_2$-OH), 2.1 (88H; C<u>H</u>$_2$-C$_7$H$_{15}$), 1.13 (440H; CH$_2$-C$_5$<u>H</u>$_{10}$-CH$_3$), 0.80 (132H; C$_7$H$_{14}$-C<u>H</u>$_3$).

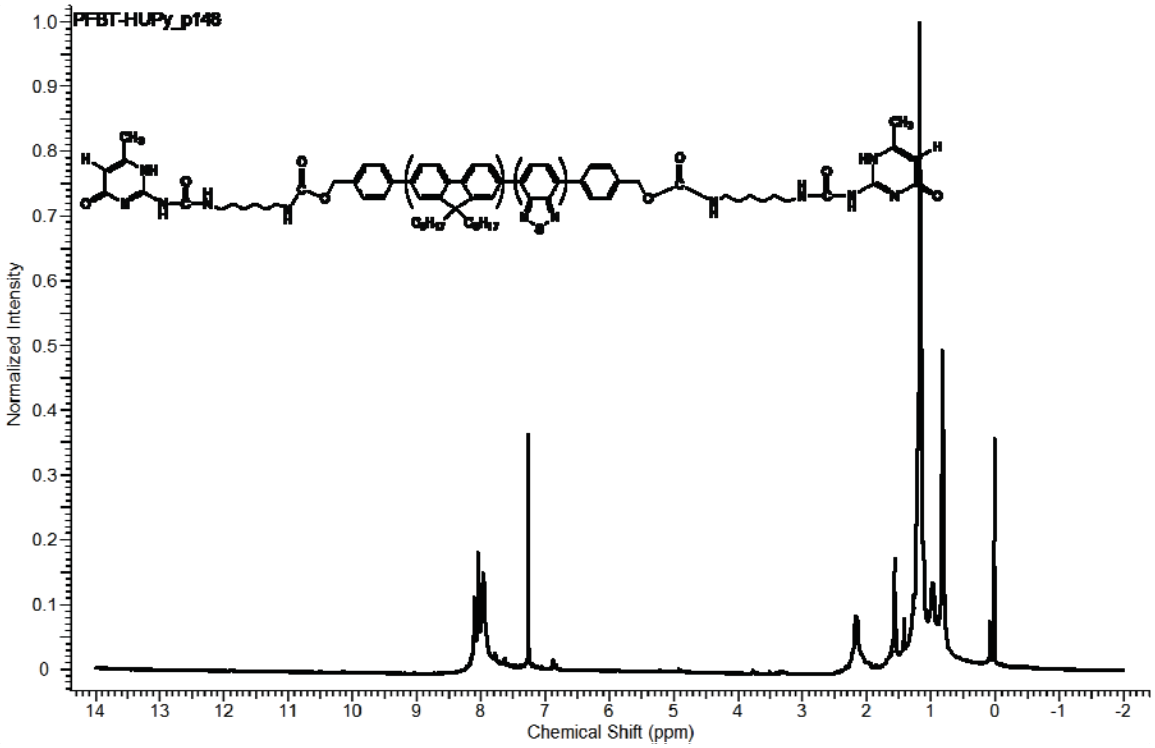

Figure 5.9 – ^{1}H NMR spectrum of PFBT-UPy.

5.2.3. Characterizations

Size Exclusion Chromatography (SEC). Molecular weights and polydispersities were obtained by SEC using an Agilent 1200 module equipped with three PSS SDV columns in series (100, 1000, and 10000 Å pore sizes), an Agilent variable wavelength UV/VIS detector, a Wyatt Technology HELEOS II multi-angle laser light scattering (MALLS) detector (λ = 658 nm), and a Wyatt Technology Optilab reX RI detector. This system enables SEC with simultaneous refractive index (SEC-RI), UV/VIS (SEC-UV/VIS), and MALLS detection. THF was used as the mobile phase at a flow rate of 1 mL/min at 40 °C.

Nuclear Magnetic Resonance (NMR). ^{1}H NMR spectroscopy was performed on Bruker 400 MHz spectrometers for all OH- and NH_2-terminated polymers and Varian 500 MHz for all UPy-terminated polymers. Samples were placed in 5 mm o.d. tubes with sample concentrations of about 5 mg/mL. Solvents contain 0.05% TMS as an internal standard.

Polarizing Optical Microscopy. Optical microscopy images of polymer blend films were acquired using an Axioplan 2 imaging microscope in reflective mode. Films were prepared by spin casting 6 mg/mL solutions onto a silicon wafer cleaned by sonication in DI water and isopropyl alcohol. Images were processed using Axio Vision version 4.8.

Fourier Transform Infrared (FTIR). FTIR analysis was carried out using a Thermo-Nicolet Nexus 670 instrument operated via the OMNIC program. Samples were prepared by depositing approximately 1 mg of bulk polymer on the sample holder.

Atomic force microscopy (AFM). AFM analysis was performed using a Veeco Multimode 8 with NanoScope V Controller (instruments located at the Center for Nanoscale Materials at Argonne National Laboratory and the Center for Functional Nanomaterials at Brookhaven National Laboratory) and a Multimode with Nanoscope IIIA controller at Rice University. Sample topography was recorded using Tapping™ and PeakForce™ modes. 2^{nd} order flattening has been used for compensation of sample tilt and enhancement of image's contrast. Sample films were prepared by spin-casting a 6 mg/mL solution onto a silicon substrate and thermally annealing on a temperature controlled hotplate.

Ultraviolet-visible (UV-VIS) absorbance and Luminescence spectrometer. UV-VIS absorbance measurements were carried out with a Varian Cary 50 spectrophotometer with scan range of 190 nm – 1100 nm, and fluorescence quenching measurements were

carried out on a Jobin-Yvon Horiba NanoLog spectrofluorimeter. Samples for fluorescence measurements were prepared by stirring 1 mg/mL solutions in $CHCl_3$ overnight before diluting to a concentration of approximately 1 g/mL P3HT or P3HT-UPy. The actual P3HT or P3HT-UPy concentration in the sample was estimated by measuring the optical density at 510 nm, and normalized fluorescence data were obtained by scaling the raw fluorescence measurement by the actual concentration of P3HT or P3HT-UPy in solution.

Grazing incidence wide angle X-ray scattering (GIWAXS). Grazing incidence wide angle X-ray scattering measurements were carried out on Sector 8-ID-E at Advanced Photon Source, Argonne National Laboratory.[48] Beamline 8-ID-E operates at an energy of 7.35 keV and images were collected from a Pilatus 1MF camera (Dectris), with two exposures for different vertical position of the detector. After flatfield correction for detector nonuniformity, the images are combined to fill in the gaps for rows at the borders between modules, leaving dark only the columns of inactive pixels at the center. Using the GIXSGUI package[49] for Matlab (Mathworks), data are corrected for X-ray polarization, detector sensitivity and geometrical solid-angle. The beam size is 200 μm (h) x 20 μm (v). Sample detector distance is 204 mm. Sample measurement and thermal annealing were carried out under vacuum which is in the range of $2\sim3 \times 10^{-6}$ bar, with the sample stage interfaced with a Lakeshore 340 unit.

5.3. Results and Discussions

Synthesis of UPy-functionalized polymers. Supramolecular block polymers can be prepared by blending UPy-functionalized homopolymers. UPy is a self-complementary

group, and as a result the blend is expected to consist of A-A, A-B, and B-B associations (Figure 5.10(b)). To investigate phase-separation, crystallinity, and optoelectronic properties of supramolecular block copolymers, both conjugated and non-conjugated UPy-functionalized polymers were prepared. Specifically, three conjugated polymers - poly(3-hexylthiophene) (P3HT), poly(9',9'-dioctyl fluorene) (PFO), and poly(9',9'-dioctyl fluorene-*alt*-benzothiadiazole) (PFBT) - and two coil-like polymers - poly(ethylene glycol) (PEG) and polystyrene (PS) were studied. P3HT is a widely studied p-type polymer in bulk-heterojunction OPVs. PFO has been utilized in both OPVs and OLEDs, and a variety of PFO copolymers exhibit broad absorbance, low bandgap, and, in some cases, electron transport.[50] PFBT has measurable electron mobility,[42] and bulk heterojunction blends of PFBT and P3HT exhibit a 0.13 % power conversion efficiency.[51] PS and PEG are chosen as model coil-like polymers for their ease of preparation and relevance to a number of block copolymer systems.

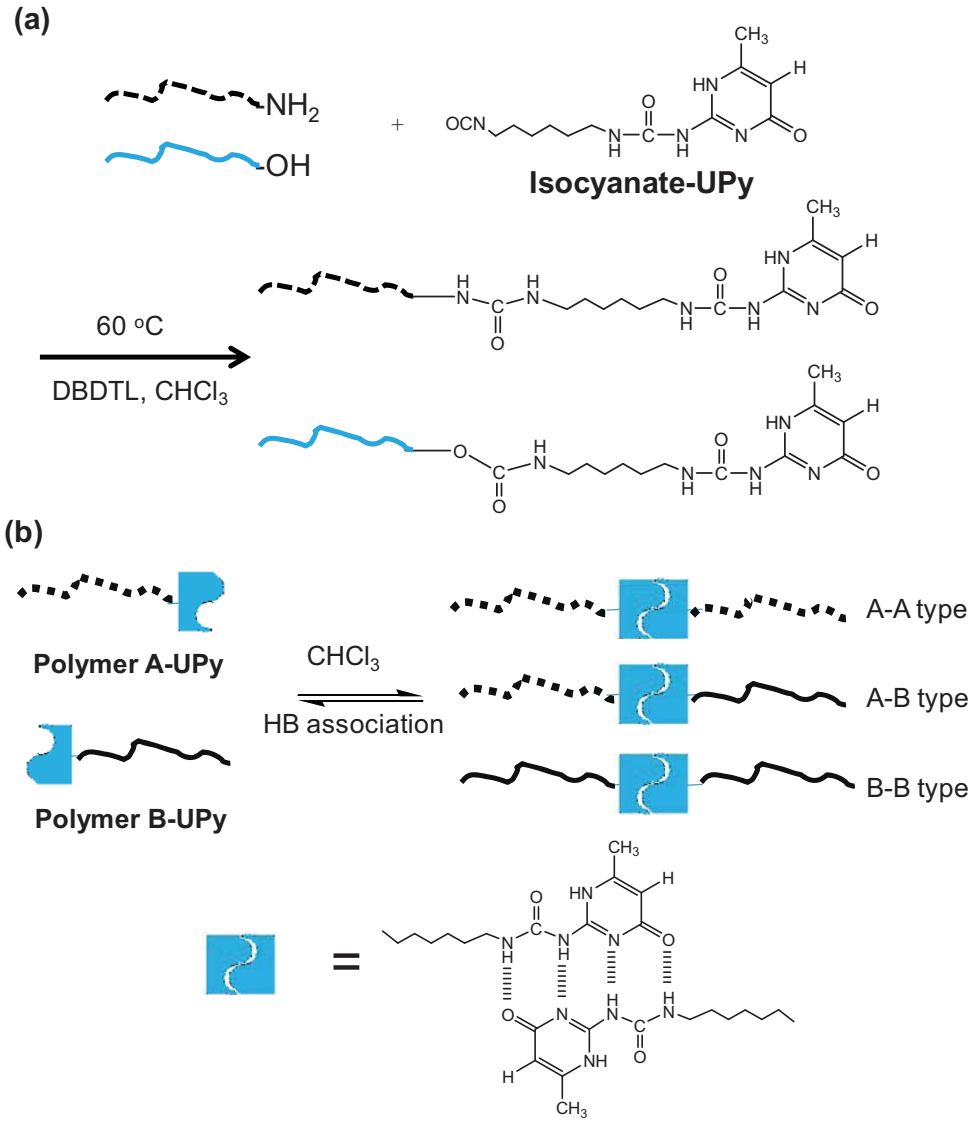

Figure 5.10 – Schematic of (a) the synthetic scheme for preparation of UPy-terminated polymers and (b) quadruple hydrogen bonding (HB) associations between different UPy-terminated polymers to form supramolecular block copolymers.

As shown schematically in Figure 5.10(a), UPy-terminated polymers can be prepared through a one-step coupling reaction involving hydroxyl or primary amine-functionalized polymers and isocyanate-functionalized UPy.[38] As evidenced by ^{1}H NMR

and FTIR, this enables the preparation of UPy-terminated polymers with a high degree of functionalization due to the reactivity of isocyanate groups towards primary hydroxyl and amine functionalities (Figures 5.11 and 5.12). All UPy-functionalized polymers prepared exhibited four distinct NMR peaks corresponding to the terminal UPy group - δ (ppm) =13.15 (-NH), 11.88 (-NH), 10.18 (-NH), and 5.82 (-CH) (Figure 5.11(a) and Figure 5.5-Figure 5.9). PS, PFO, and PFBT also exhibit a clear shift in the ^{1}H NMR peak corresponding to CH_2 adjacent to the terminal hydroxyl group (Figure 5.11). For PS-OH, the ^{1}H NMR peak corresponding to terminal CH_2 shifts from δ (ppm) = 3.36 to 3.21 after the coupling reaction (Figure 5.11(b)). In the case of PFO-OH and PFBT-OH (see Figure 5.2 and Figure 5.3), the terminal CH_2 ^{1}H NMR peak shifts from δ (ppm) = 4.78 to 5.12 (Figure 5.11(c)).

FTIR spectroscopy (Figure 5.12) provides further evidence for UPy functionalization of P3HT and PFO. MIC, a precursor to the UPy endgroup, exhibits a sharp primary amine ($-NH_2$) peak at 3330 cm^{-1} and a peak at 1655 cm^{-1} corresponding to the carbonyl group (C=O). After reaction with hexyl diisocyanate, the primary amine peak vanishes and a peak at 2282 cm^{-1} corresponding to free isocyanate (N=C=O) appears. A new peak near 3235 cm^{-1} corresponding to a secondary amine also appears, and split peaks at 1655 cm^{-1} reflect hydrogen bonding interactions between the carbonyl group and the secondary amine functionality. P3HT-NH_2 exhibits two weak signals at around 3400 and 3500 cm^{-1}, and after functionalization with UPy a broad peak at 3380 cm^{-1} appears, indicative of a secondary amine functional group. PFO-OH has a small peak at around 3450 cm^{-1} corresponding to the primary hydroxyl group, and the peak disappears after functionalization with UPy. FTIR was less reliable for analyzing end-group functionalization of PEG-OH, PS-OH, and PFBT-OH (see Figure 5.13).

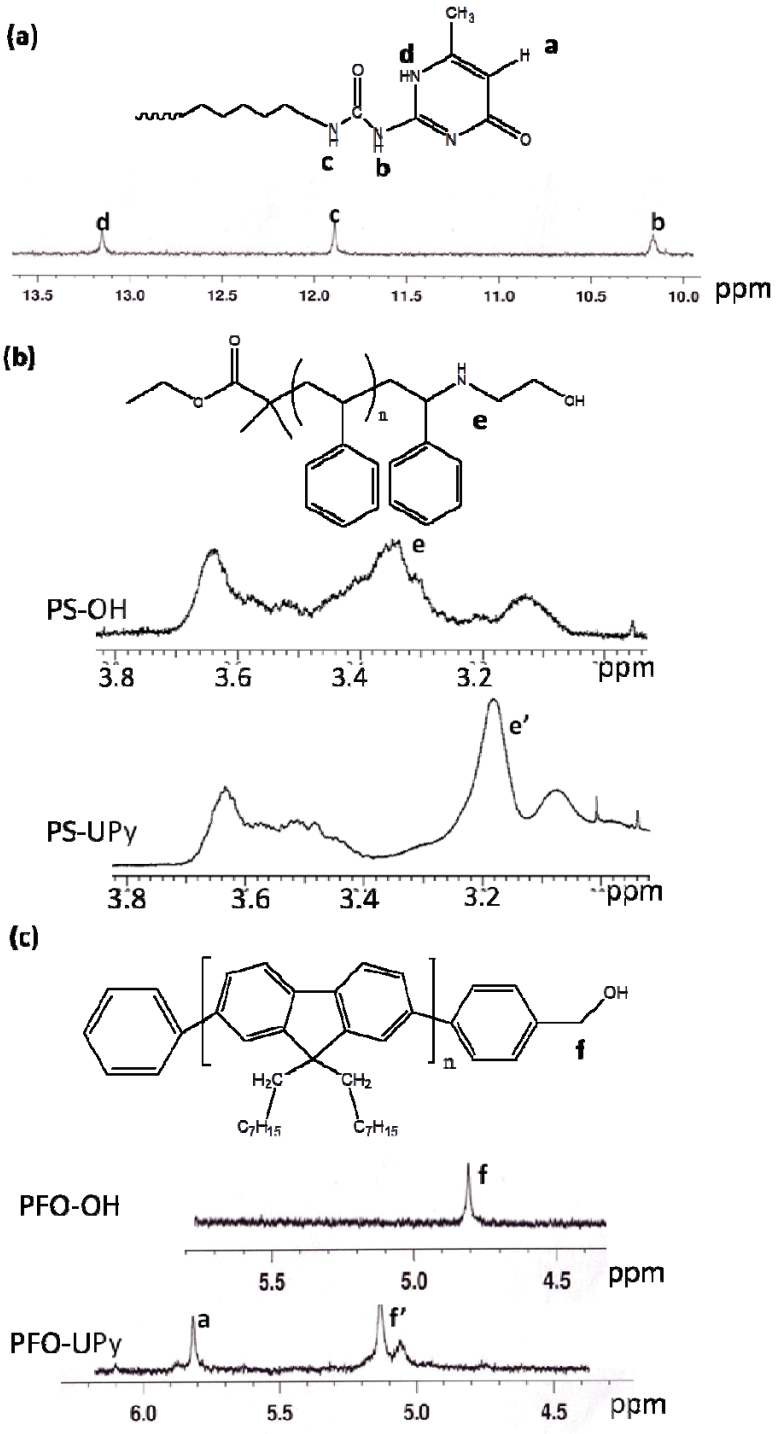

Figure 5.11 – ^{1}H NMR data for (a) the UPy end group, (b) polystyrene before and after coupling to UPy, and (c) poly(9,9-dioctyl fluorene) before and after coupling to UPy.

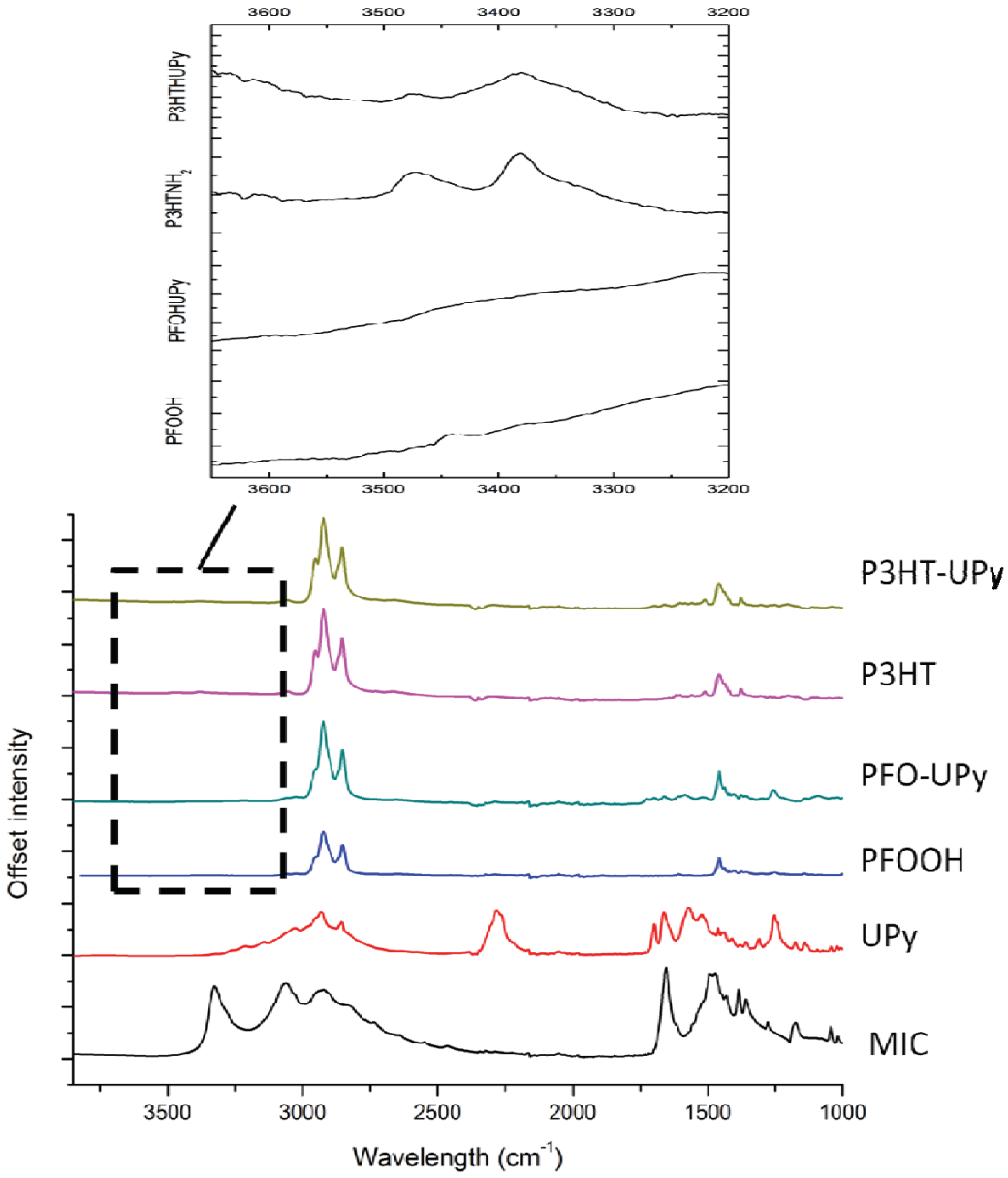

Figure 5.12 – FTIR spectra for various end-functionalized polymers as well as the reactive UPy-isocyanate group (UPy) and methyl isocytosine (MIC).

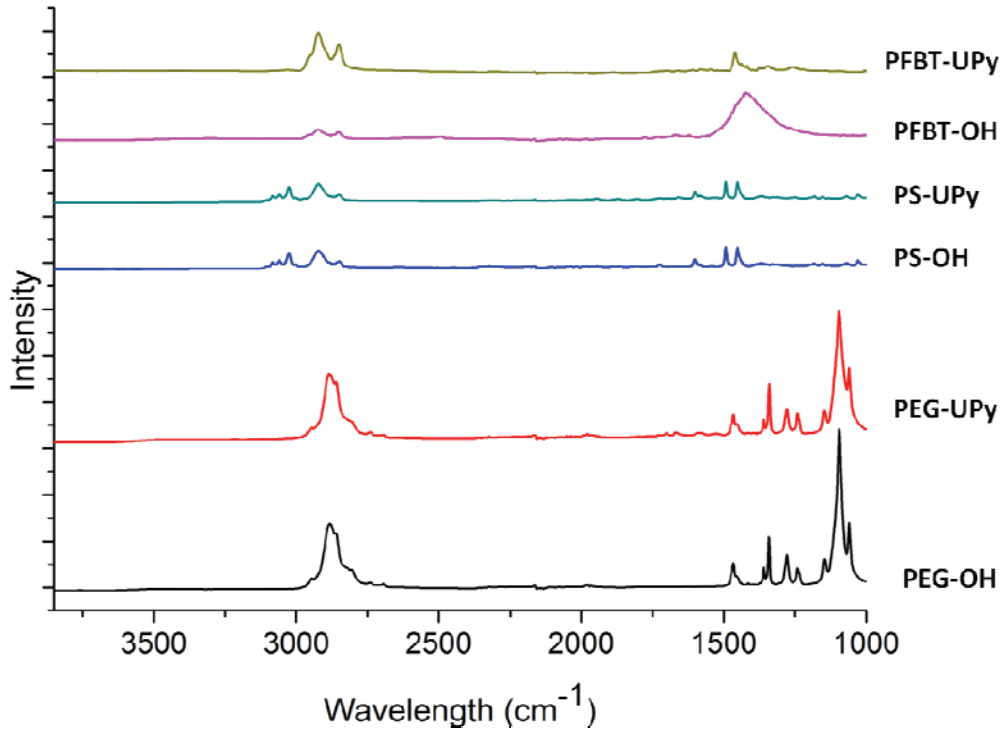

Fgure 5.13 – FTIR spectra of UPy-modified and hydroxyl-terminated PFBT, PS, and PEG.

Phase behavior of polymer blends in thin films In order to test the effect of UPy associations on phase behavior, blend films were cast on a surface and analyzed by optical microscopy and AFM. Samples were thermally annealed near but below the highest crystallization temperatures (180 °C and 110 °C for 5K P3HT and PFO, respectively) before analysis by POM. These annealing conditions were chosen because a clear difference was observed in the phase behavior of UPy and non-UPy polymer blends. POM analysis shows that UPy-mediated hydrogen bonding interactions suppress micron-scale phase separation at these annealing conditions (Figure 5.14). For example, in the case of P3HT/PS blends mixed at a 50/50 ratio by mass, clear evidence for micron-scale

phase separation is observed after annealing overnight at 160 °C (Figure 5.14(a)). By contrast, no micron-scale phase separation is observed for P3HT-UPy/PS-UPy blend films (Figure 5.14(b)). Similar results are observed for PFO/PEG blend films annealed at 100 °C (Figures 5.14(c) and 5.14(d)), P3HT/PEG blend films annealed at 160 °C (see Figure 5.15), and P3HT/PFO blend annealed at 160 °C (Figures 5.14(e) and 5.14(f)). Results for PS/PFO blend films were inconclusive since no phase separation was observed for both PS/PFO and PS-UPy/PFO-UPy blends (Figure 5.16). Altogether, these results indicate that UPy-functionalized conjugated polymer blends have a reduced tendency for micron-scale phase separation.

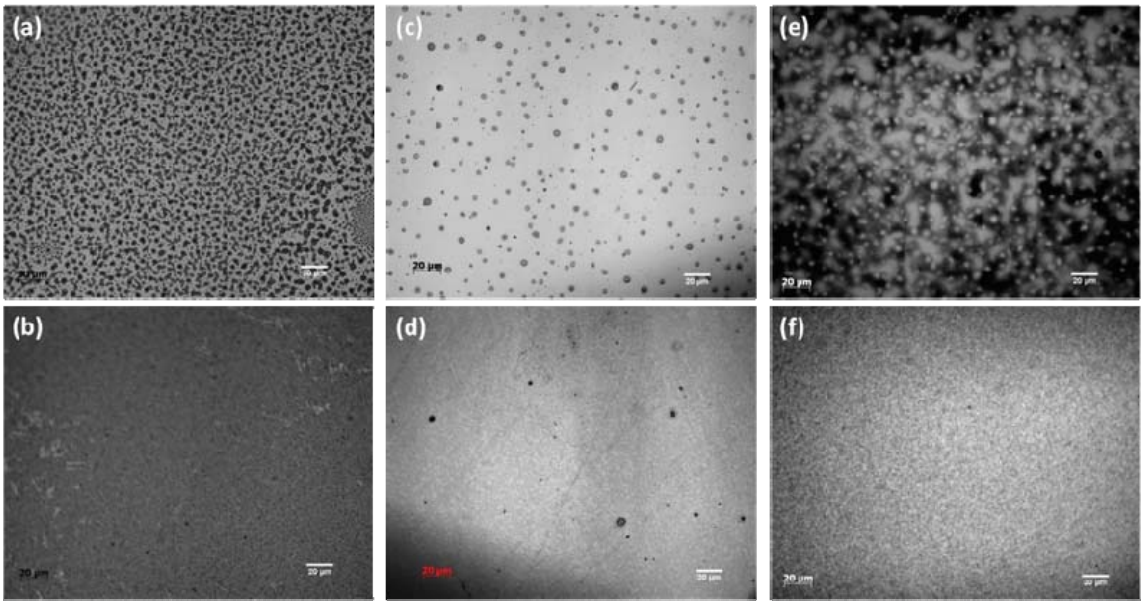

Figure 5.14 – Optical microscopy images of thermally annealed polymer blends: (a) 50/50 wt% P3HT/PS, (b) 50/50 wt% P3HT-UPy/PS-UPy, (c) 50/50 wt% PFO/PEG, (d) 50/50 wt% PFO-UPy/PEG-UPy, (e) 50/50 wt% P3HT/PFO, and (f) 50/50 wt% P3HT-UPy/PFO-UPy. Scale bar: (a) 50 μm, and (b)-(f) 20 μm. Thermal annealing conditions: (a), (b), (e), and (f): 160 °C, 16 hours. (c) and (d): 100 °C, 16 hours.

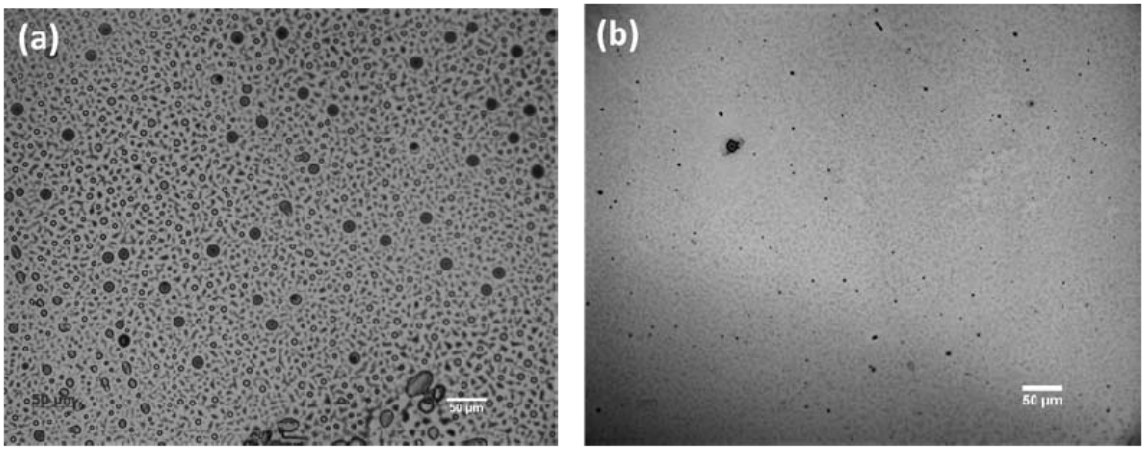

Figure 5.15 – Polarizing optical microscopy images of thermally annealed polymer blends: (a) 50/50 wt% P3HT/PEG, (b) 50/50 wt% P3HT-UPy/PEG-UPy. Annealing temperature: 160 °C. Scale bars: 50 µm.

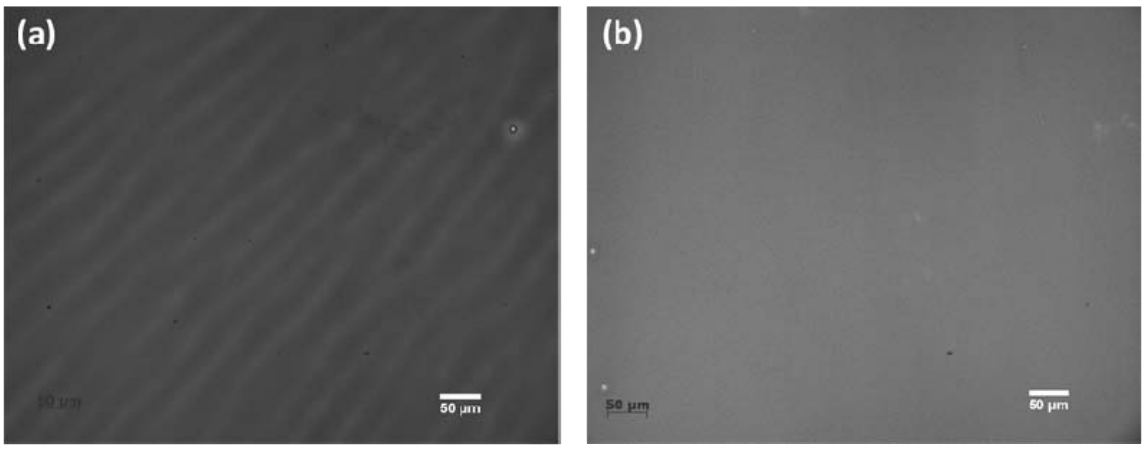

Figure 5.16 – Polarizing optical microscopy images of thermally annealed polymer blends: (a) 50/50 wt% PFO/PS, (b) 50/50 wt% PFO-UPy/PS-UPy. Annealing temperature: 100 °C. Scale bars: 50 µm.

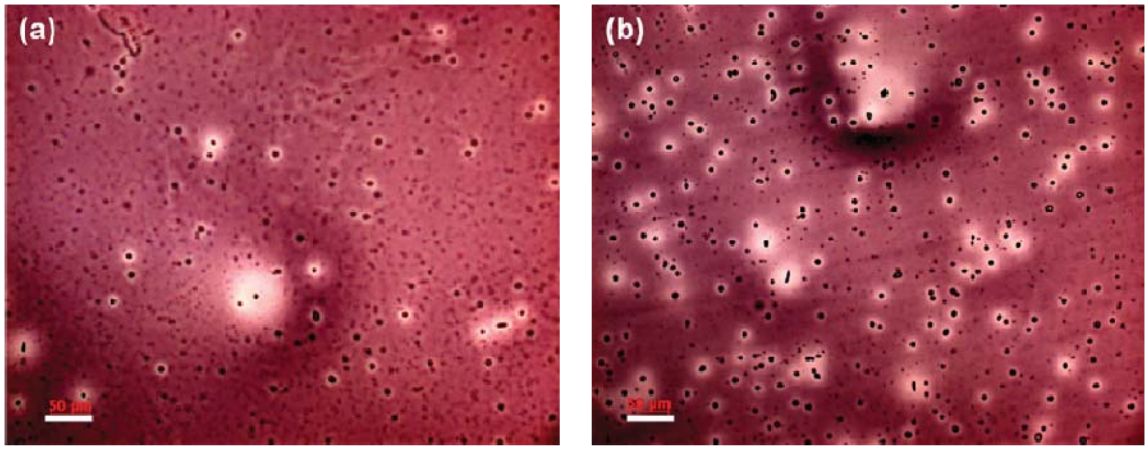

Figure 5.17 – Polarizing optical microscopy images of solvent annealed polymer blends: (a) 50/50 wt% P3HT/PFO, (b) 50/50 wt% P3HT-UPy/PFO-UPy. Annealing temperature: 170 °C in the presence of dichlorobenzene. Scale bars: 50 μm.

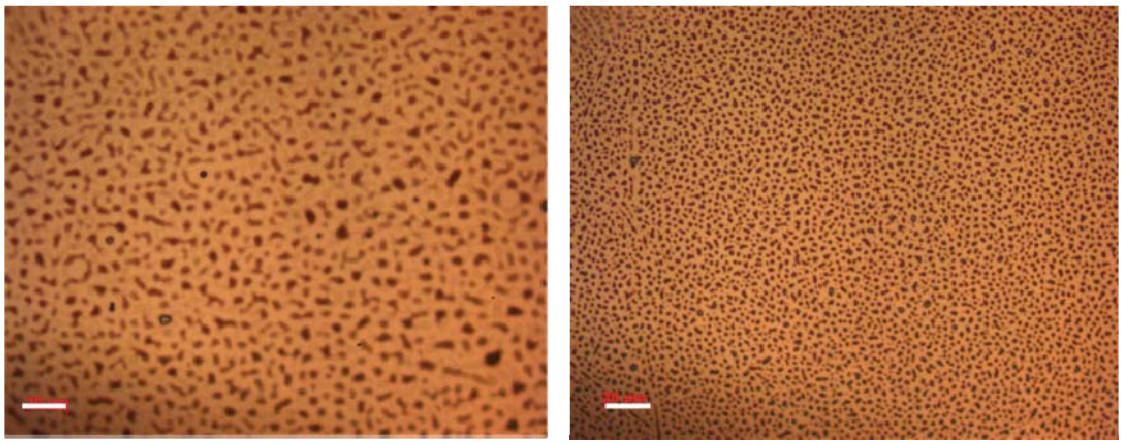

Figure 5.18 – Polarizing optical microscopy images of thermally annealed polymer blends: (a) 50/50 wt% P3HT/PEG, (b) 50/50 wt% P3HT-UPy/PEG-UPy. Annealing temperature: 190 °C. Scale bars: 20 μm.

While a clear difference between UPy and non-UPy-terminated polymers was observed for the specific annealing conditions described above, higher temperature

treatment conditions were tested to explore the limit of miscibility of UPy-terminated polymer blends. All blend films studied, including UPy polymer blends, showed micron-scale phase separation when solvent annealed at 170 °C in the presence of dichlorobenzene (See Figure 5.17) or when thermally annealed (without solvent present) at 190 °C (higher than the crystalline temperature of the present P3HT sample) (see Figure 5.18). On the other hand, no phase separation was observed by POM after annealing overnight at 100 °C for any polymer blend (see Figure 5.16 for an example). These results indicate that thermal annealing at 190 °C or at 170 °C in the presence of dichlorobenzene is required to induce micron-scale phase separation in P3HT-UPy blends. By comparison, other studies on UPy-functionalized molecules have shown that associations are disrupted at a temperature of approximately 80 °C when solvent is present,[52,53] and a report on star-shaped UPy end-functionalized polymers found associations persist only to temperatures as high as 130 °C.[54] A recent study on UPy-functionalized non-conjugated polymers reported micron-scale phase separation in polymer blend films thermally annealed at just 100 °C.[32] Thus, the results in the present study indicate that blends consisting of one or more conjugated polymers can increase the temperature required for phase separation. This may be due to a combination of thermodynamic and kinetic effects, as discussed below.

GIWAXS measurements were carried out on pristine P3HT-UPy films, P3HT films, and P3HT blend films to investigate crystallization in UPy-modified polymers and polymer blends (Figures 5.19 and 5.20). In the case of P3HT-UPy, as-cast films show little or no crystallinity, but on heating to 80 °C characteristic P3HT-crystallite peaks appear and persist up to temperatures of 160 °C (Figure 5.19). The positions and intensity of crystalline peaks is qualitatively similar to those of P3HT films prepared similarly and measured at an elevated temperature (Figure 5.20a). Furthermore, thermally annealed

(160 °C, 16 h) P3HT-UPy/PFO-UPy and P3HT-UPy/PS-UPy blend films exhibit similar crystalline peaks (Figures 5.20b and 5.20c), but the intensity of the crystal peaks is significantly weaker for blend films compared with pristine P3HT films. These measurements indicate that crystallization is still present but reduced in UPy-modified polymer blend films.

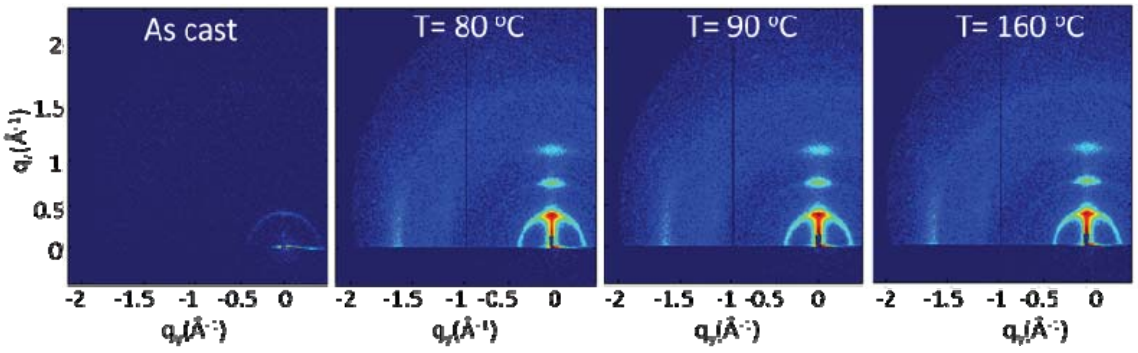

Figure 5.19 – GIWAXS patterns of a P3HT-UPy thin films cast at room temperature and thermally annealed in-situ. All samples were measured at an incident angle of 0.25° and 20 second exposure time, and all images have the same color scale.

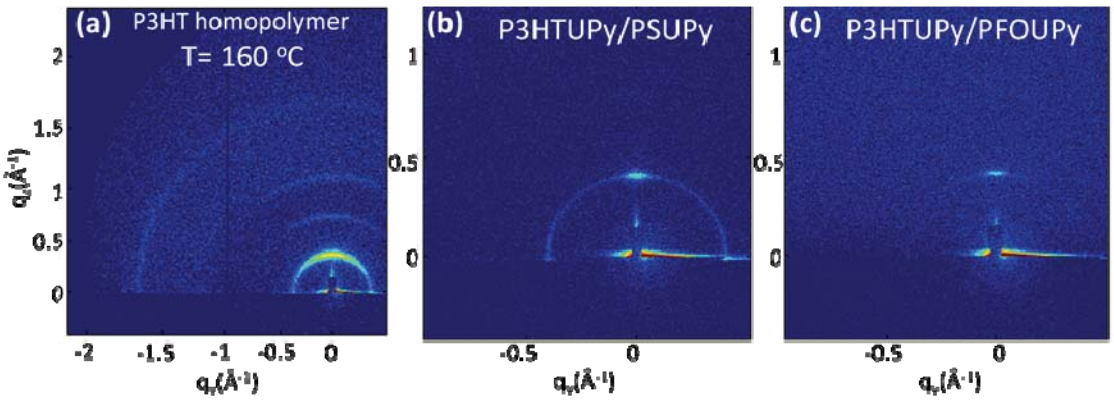

Figure 5.20 – GIWAXS patterns of (a) P3HT homopolymer annealed in-situ at 160 °C, (b) P3HT-UPy/PS-UPy and (c) P3HT-UPy/PFO-UPy measured at r.t. after thermal annealing for 16 h at 160 °C. All samples were measured at an incident angle of 0.25° and 20 second exposure time, and all images have the same color scale.

AFM measurements were carried out to investigate the mesoscale structure of UPy polymer blend films.[55] AFM images show clear evidence for crystallization in pristine P3HT, pristine PFO, and their blend films with UPy-mediated interactions. For example, AFM topography images of P3HT-UPy/PS-UPy blend films reveals crystalline nanowires characteristic of P3HT with fiber dimensions approximately 10 nm in width and lengths up to 100 nm after 16 hours of thermal annealing at 160 °C (Figure 5.21b). Pristine PFO films also exhibit crystalline fibers after thermal annealing at 100 °C for 16 h (Figure 5.21c), with fiber dimensions of about 50 nm in width and lengths up to 1 μm. In the case of PFO-UPy/PEG-UPy annealed at 100 °C for 16 h, both crystallization and sub-micron-scale phase separation are observed, with phase-separated domains roughly 300 nm in size (Figure 5.21d-e). Crystalline fibers are only present in the PFO-rich domains and have fiber dimensions approximately 20 nm in width and lengths up to 200 nm. Similar fibril structures with dimensions of about 30 nm in width and 700 nm in length were observed in P3HT-UPy/PFO-UPy blends annealed at 160 °C for 16 h with no

evidence of phase separation. Sub-micron phase separation was also observed in P3HT-UPy/PEG-UPy and PFO-UPy/PS-UPy blends (Figure 5.22). Furthermore, for P3HT-UPy/PFO-UPy and P3HT-UPy/PS-UPy, solvent annealing at room temperature for 4 days gives rise to nanoscale phase-separated domains with P3HT crystallinity (see Figure 5.23).

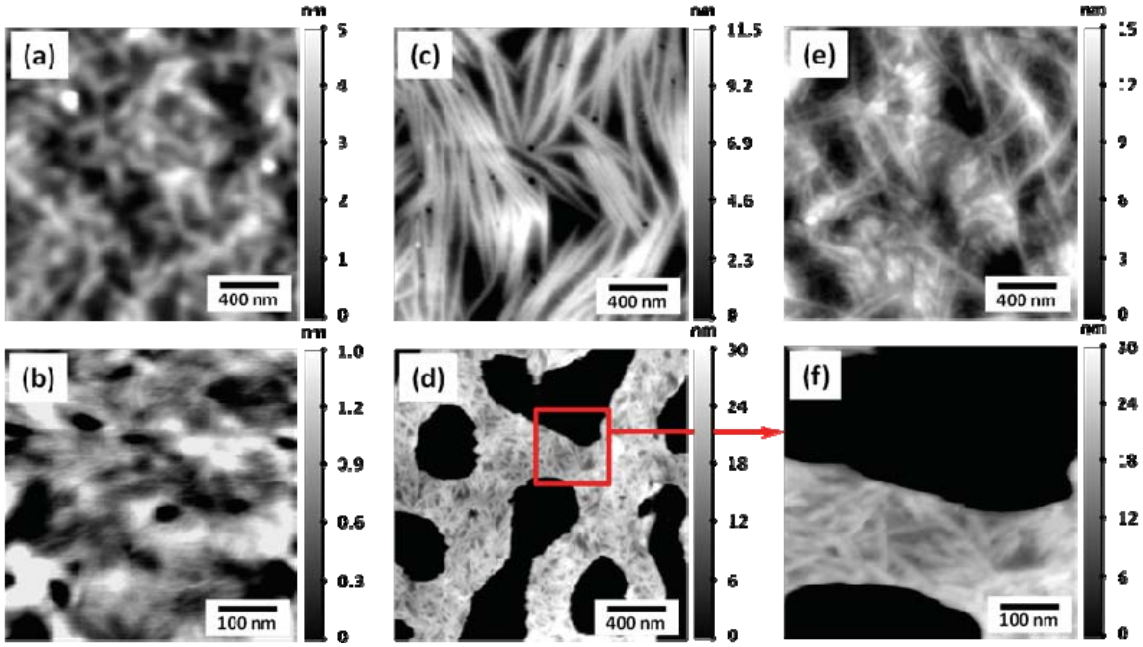

Figure 5.21 – Atomic force microscopy height images of thermally annealed polymer films: (a) pristine P3HT-NH_2, (b) 50/50 wt% P3HT-UPy/PS-UPy, (c) PFO, (d) 50/50 wt% PFO-UPy/PEG-UPy, (f) 50/50 wt% PFO-UPy/PEG-UPy in smaller scale, and (e) 50/50 wt% P3HT-UPy/PFO-UPy. Thermal annealing conditions: (a), (b), and (e): 160 °C, 16 hours. (c) (d), and (f): 100 °C, 16 hours.

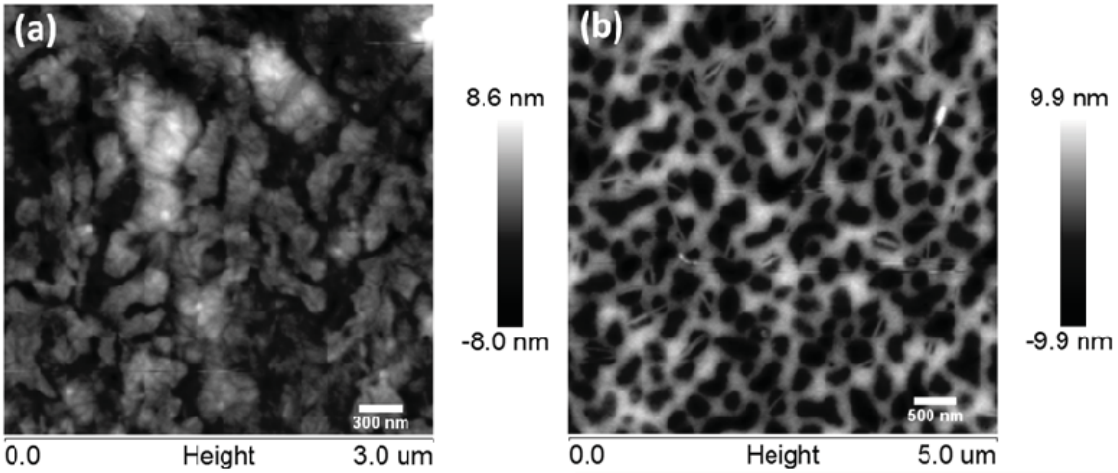

Figure 5.22 – Atomic Force Microscopy height images of thermally annealed UPy modified polymer blends: (a) 50/50 wt% P3HT-UPy/PEG-UPy thermally annealed at 160 °C for 16 hours, (b) 50/50 wt% PFO-UPy/PS-UPy, thermally annealed at 100 °C for 16 hours.

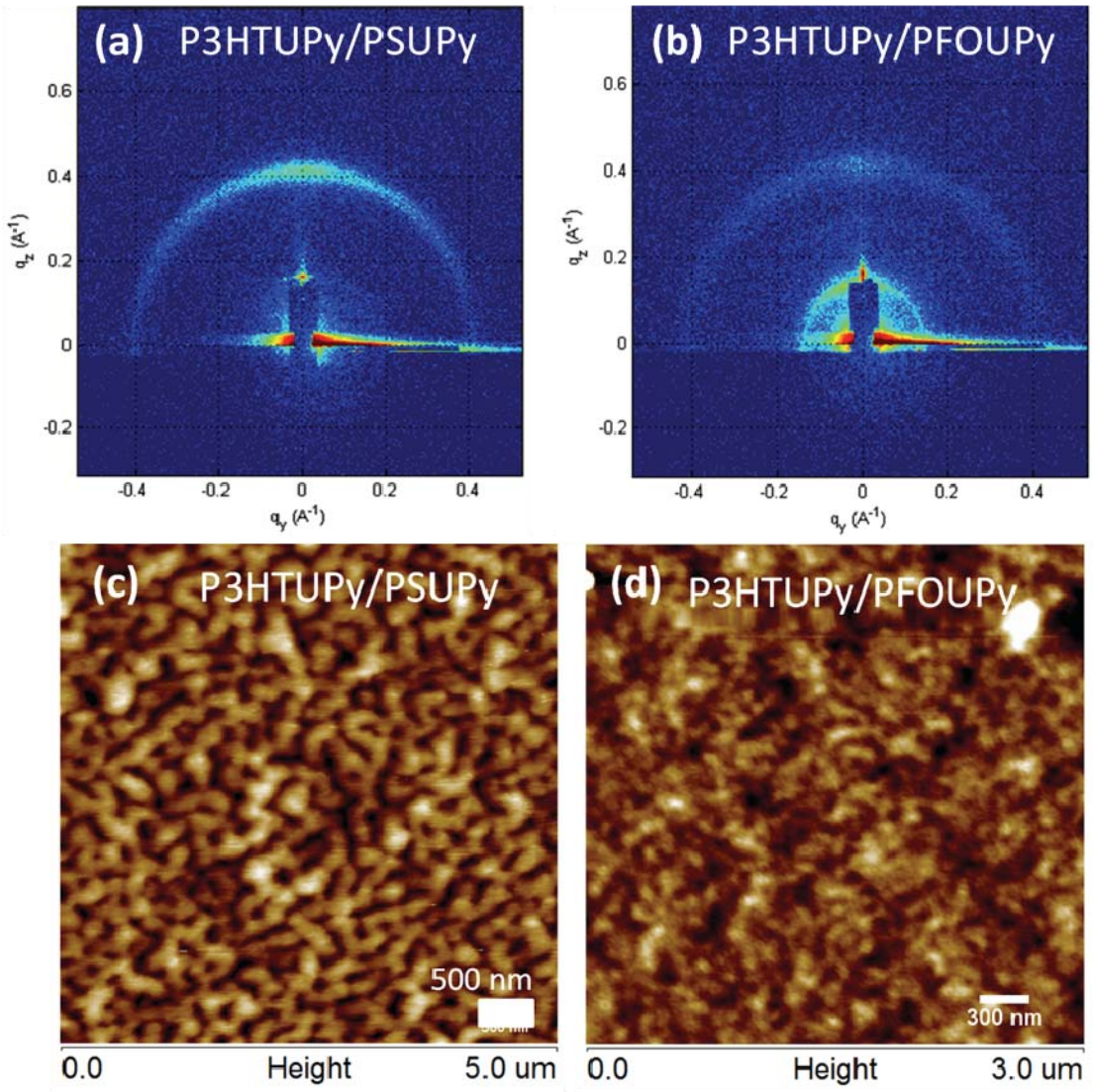

Figure 5.23 – GIWAXS patterns of a (a) P3HTUPy/PSUPy and (b) P3HTUPy/PFOUPy toluene solvent annealed thin film at room temperatures for 4 days. All samples were measured with incident angle 0.25° and 20 seconds exposure time. AFM height images of (c) P3HTUPy/PSUPy and (d) P3HTUPy/PFOUPy toluene solvent annealed thin film at room temperatures for 4 days.

Altogether, AFM and POM measurements of thermally annealed polymer blend films indicate that UPy-mediated interactions can suppress micron-scale phase separation

in conjugated polymer blend films thermally annealed at temperatures up to 160 °C. The reduced tendency for micron-scale phase separation may be due to a combination of thermodynamic and kinetic effects. Previous work indicates that UPy-mediated hydrogen bonding interactions are weak above 100 °C,[52,53] but crystallization in P3HT-UPy blends persists up to 180 °C and may lead to reduced chain mobility and slower kinetics for phase-separation. This is consistent with the GIWAXS data that show significant crystallinity present in P3HT-UPy at 160 °C and AFM images, which indicate that phase separation occurs at a reduced length scale in some UPy-terminated polymer blend films (e.g. PFO-UPy/PEG-UPy). On the other hand, UPy-modification may also affect the thermodynamics of polymer blends, resulting in a homogeneous phase for some UPy-polymer blends. This is supported by mean-field theories for supramolecular block copolymers that indicate complete miscibility under some conditions[56,57] and may explain the absence of micro-phase segregated structures in UPy polymer blends.

Fluorescence quenching in conjugated polymer blends. Fluorescence measurements were carried out on P3HT/PFO and P3HT/PFBT solution blends to determine if UPy-mediated interactions between donor and acceptor polymers affect fluorescence quenching. UPy associations are expected to decrease the average distance between polymers compared with unmodified polymer blends, resulting in increased fluorescence quenching. PFBT has a more compatible LUMO level for energy transfer with P3HT and is therefore expected to exhibit more significant quenching compared with PFO.[28]

Fluorescence quenching measurements were carried out by selectively exciting P3HT; this is accomplished by choosing an excitation wavelength greater than 510 nm, above which PFO and PFBT exhibit no absorbance (Figure 5.24a). The measurements therefore probe energy and/or electron transfer from P3HT to PFO or PFBT, and a

quantitative comparison can be made by preparing solutions with approximately the same P3HT content (1 - 5 μg/mL) and normalizing fluorescence spectra by the overall P3HT concentration, estimated by the measured absorbance at 510 nm.

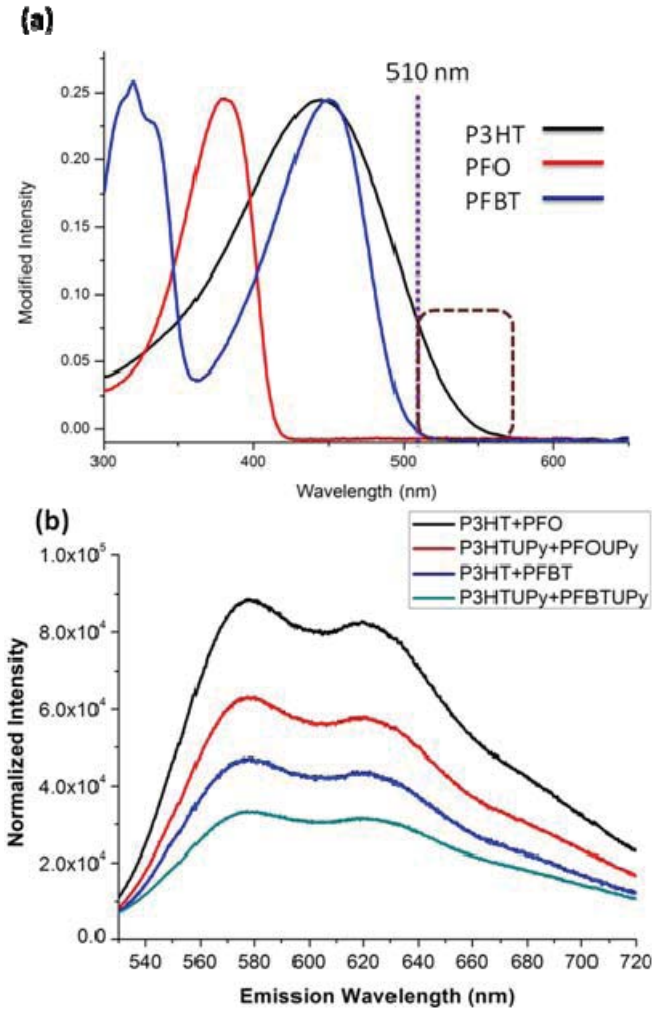

Figure 5.24 – (a) UV-VIS absorbance spectra of P3HT, PFO, and PFBT. The dotted line indicates the excitation wavelength used for fluorescence measurements; note that only P3HT exhibits significant absorbance at 510 nm. (b) Fluorescence spectra for conjugated polymer blends in solution under 525 nm excitation wavelength.

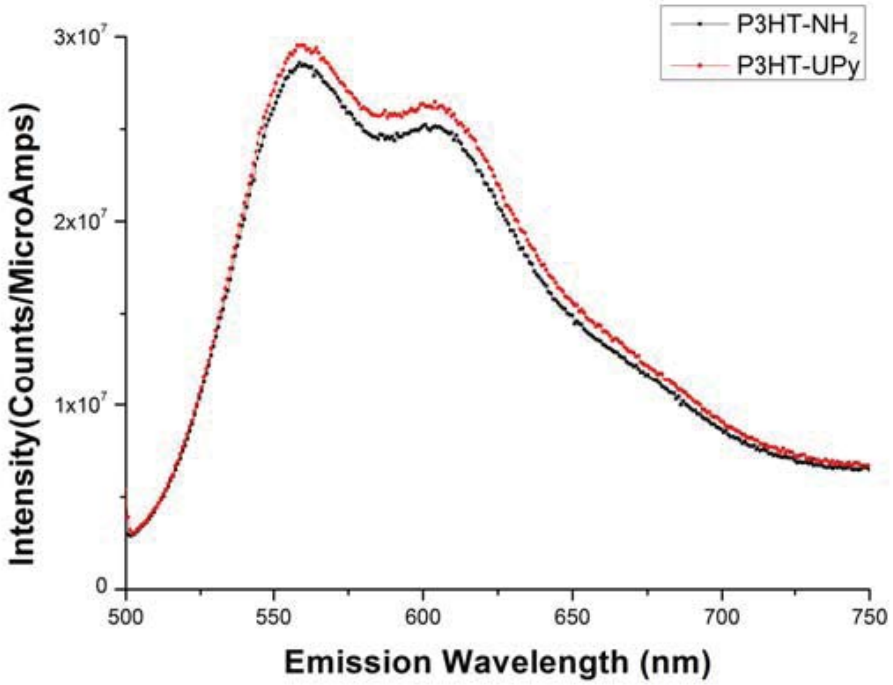

Figure 5.25 – Fluorescence spectrum for P3HT and P3HT-UPy homopolymers at 510 nm excitation wavelength.

The fluorescence spectrum (see Figure 5.25) of pure P3HT and P3HT-UPy solutions shows that the terminal UPy group by itself has a negligible impact on fluorescence quenching. Blends of unmodified polymers show lower fluorescence compared with that of pristine P3HT or P3HT-UPy, indicative of some energy or electron transfer from P3HT to PFO or PFBT, and as expected quenching is more significant for P3HT/PFBT solution blends due to better matching of LUMO energy levels (Figure 5.24b). Furthermore, for both P3HT/PFO and P3HT/PFBT, UPy-modified polymer blends exhibited lower fluorescence compared with that of non-UPy modified polymer

blends. This indicates that UPy-associations increase fluorescence quenching due to decreased average distance between donor and acceptor polymers in solution.

5.4. Conclusions

A series of conjugated and non-conjugated UPy-terminated polymers were synthesized via a one-step reaction with UPy-isocyanate. A combination of AFM, POM, and GIWAXS shows that UPy-mediated quadruple hydrogen bonding interactions can prevent micron-scale phase separation in conjugated polymer blends. UPy modification increases fluorescence quenching in solutions of donor and acceptor polymers, due to hydrogen-bonding associations which reduce the average distance for energy and/or electron transfer. These results show that UPy-mediated interactions can suppress micron-scale phase separation in bulk heterojunction polymer blends at temperatures and processing conditions typically used to prepare bulk-heterojunction OPVs. As a result, UPy functionalization may be a promising route for improving the performance of all-polymer OPVs.

5.5. References

(1) Gunes, S.; Neugebauer, H.; Sariciftci, N. S., *Chem. Rev.* **2007**, *107*, 1324-1338.
(2) Thompson, B. C.; Fréchet, J. M. J., *Angew. Chem. Int. Ed.* **2008**, *47*, 58-77.
(3) Hoppe, H.; Sariciftci, N. S., *J. Mater. Res.* **2004**, *19*, 1924-1945.
(4) Peet, J.; Heeger, A. J.; Bazan, G. C., *Accounts Chem. Res.* **2009**, *42*, 1700-1708.
(5) Veenstra, S. C.; Loos, J.; Kroon, J. M., *Prog. Photovolt.: Res. Appl.* **2007**, *15*, 727-740.
(6) McNeill, C. R.; Greenham, N. C., *Adv. Mater.* **2009**, *21*, 3840-3850.
(7) Kim, J.-S.; Ho, P. K. H.; Murphy, C. E.; Friend, R. H., *Macromolecules* **2004**, *37*, 2861-2871.

(8) McNeill, C. R.; Watts, B.; Thomsen, L.; Ade, H.; Greenham, N. C.; Dastoor, P. C., *Macromolecules* **2007**, *40*, 3263-3270.
(9) McNeill, C. R.; Abrusci, A.; Zaumseil, J.; Wilson, R.; McKiernan, M. J.; Burroughes, J. H.; Halls, J. J. M.; Greenham, N. C.; Friend, R. H., *Appl. Phys. Lett.* **2007**, *90*, 193506-3.
(10) Kietzke, T.; Hörhold, H.-H.; Neher, D., *Chem. Mater.* **2005**, *17*, 6532-6537.
(11) Koetse, M. M.; Sweelssen, J.; Hoekerd, K. T.; Schoo, H. F. M.; Veenstra, S. C.; Kroon, J. M.; Yang, X.; Loos, J., *Appl. Phys. Lett.* **2006**, *88*, 083504.
(12) Granstrom, M.; Petritsch, K.; Arias, A. C.; Lux, A.; Andersson, M. R.; Friend, R. H., *Nature* **1998**, *395*, 257-260.
(13) Holcombe, T. W.; Woo, C. H.; Kavulak, D. F. J.; Thompson, B. C.; Fréchet, J. M. J., *J. Am. Chem. Soc.* **2009**, *131*, 14160-14161.
(14) Segalman, R. A.; McCulloch, B.; Kirmayer, S.; Urban, J. J., *Macromolecules* **2009**, *42*, 9205-9216.
(15) Darling, S. B., *Energy Environ. Sci.* **2009**, *2*, 1266-1273.
(16) Botiz, I.; Schaller, R. D.; Verduzco, R.; Darling, S. B., *J. Phys. Chem.C* **2011**, *115*, 9260-9266.
(17) Mulherin, R. C.; Jung, S.; Huettner, S.; Johnson, K.; Kohn, P.; Sommer, M.; Allard, S.; Scherf, U.; Greenham, N. C., *Nano Lett.* **2011**, *11*, 4846-4851.
(18) Sommer, M.; Komber, H.; Huettner, S.; Mulherin, R.; Kohn, P.; Greenham, N. C.; Huck, W. T. S., *Macromolecules* **2012**, *45*, 4142-4151.
(19) Woody, K. B.; Leever, B. J.; Durstock, M. F.; Collard, D. M., *Macromolecules* **2011**, *44*, 4690-4698.
(20) Wu, S.; Bu, L.; Huang, L.; Yu, X.; Han, Y.; Geng, Y.; Wang, F., *Polymer* **2009**, *50*, 6245-6251.
(21) Lai, Y.-C.; Ohshimizu, K.; Takahashi, A.; Hsu, J.-C.; Higashihara, T.; Ueda, M.; Chen, W.-C., *J. Polym. Sci., Part A: Polym. Chem.* **2011**, *49*, 2577-2587.
(22) Scherf, U.; Gutacker, A.; Koenen, N., *Accounts Chem. Res.* **2008**, *41*, 1086-1097.
(23) Ouhib, F.; Khoukh, A.; Ledeuil, J.-B.; Martinez, H.; Desbrières, J.; Dagron-Lartigau, C., *Macromolecules* **2008**, *41*, 9736-9743.

(24) Ohshimizu, K.; Takahashi, A.; Higashihara, T.; Ueda, M., *J. Polym. Sci., Part A: Polym. Chem.* **2011**, *49*, 2709-2714.
(25) Sun, S.-S.; Zhang, C.; Ledbetter, A.; Choi, S.; Seo, K.; Carl E. Bonner, J.; Drees, M.; Sariciftci, N. S., *Appl. Phys. Lett.* **2007**, *90*, 043117.
(26) Chen, X. L.; Jenekhe, S. A., *Macromolecules* **1996**, *29*, 6189-6192.
(27) Xiao, X.; Fu, Y.; Sun, M.; Li, L.; Bo, Z., *J. Polym. Sci., Part A: Polym. Chem.* **2007**, *45*, 2410-2424.
(28) Verduzco, R.; Botiz, I.; Pickel, D. L.; Kilbey, S. M.; Hong, K.; Dimasi, E.; Darling, S. B., *Macromolecules* **2011**, *44*, 530-539.
(29) Fox, J. D.; Rowan, S. J., *Macromolecules* **2009**, *42*, 6823-6835.
(30) Rehm, T.; Schmuck, C., *Chem. Commun.* **2008**, 801-813.
(31) Yang, S. K.; Ambade, A. V.; Weck, M., *Chem. Soc. Rev.* **2011**, *40*, 129-137.
(32) Feldman, K. E.; Kade, M. J.; de Greef, T. F. A.; Meijer, E. W.; Kramer, E. J.; Hawker, C. J., *Macromolecules* **2008**, *41*, 4694-4700.
(33) Dankers, P. Y. W.; Zhang, Z.; Wisse, E.; Grijpma, D. W.; Sijbesma, R. P.; Feijen, J.; Meijer, E. W., *Macromolecules* **2006**, *39*, 8763-8771.
(34) Huh, J.; Park, H. J.; Kim, K. H.; Park, C.; Jo, W. H., *Adv. Mater.* **2006**, *18*, 624-629.
(35) Takahashi, A.; Rho, Y.; Higashihara, T.; Ahn, B.; Ree, M.; Ueda, M., *Macromolecules* **2010**, *43*, 4843-4852.
(36) Lohmeijer, B. G. G.; Schubert, U. S., *Angew. Chem. Int. Ed.* **2002**, *41*, 3825-3829.
(37) Shokrollahi, P.; Mirzadeh, H.; Huck, W. T. S.; Scherman, O. A., *Polymer* **2010**, *51*, 6303-6312.
(38) Folmer, B. J. B.; Sijbesma, R. P.; Versteegen, R. M.; van der Rijt, J. A. J.; Meijer, E. W., *Adv. Mater.* **2000**, *12*, 874-878.
(39) Beijer, F. H.; Sijbesma, R. P.; Kooijman, H.; Spek, A. L.; Meijer, E. W., *J. Am. Chem. Soc.* **1998**, *120*, 6761-6769.
(40) Lee, K. J.; Lee, D. K.; Kim, Y. W.; Kim, J. H., *Eur. Polym. J.* **2007**, *43*, 4460-4465.
(41) Keizer, H. M.; Gonzalez, J. J.; Segura, M.; Prados, P.; Sijbesma, R. P.; Meijer, E. W.; de Mendoza, J., *Chem.-Eur. J.* **2005**, *11*, 4602-4608.

(42) Wrue, M. H.; McUmber, A. C.; Anthamatten, M., *Macromolecules* **2009**, *42*, 9255-9262.
(43) Wang, S. M.; Yu, M. L.; Ding, J.; Tung, C. H.; Wu, L. Z., *J. Phys. Chem. A* **2008**, *112*, 3865-3869.
(44) Kim, Y. J.; Kim, J. H.; Kang, M. S.; Lee, M. J.; Won, J.; Lee, J. C.; Kang, Y. S., *Adv. Mater.* **2004**, *16*, 1753-1757.
(45) Abbel, R.; Grenier, C.; Pouderoijen, M. J.; Stouwdam, J. W.; Leclere, P.; Sijbesma, R. P.; Meijer, E. W.; Schenning, A., *J. Am. Chem. Soc.* **2009**, *131*, 833-843.
(46) Han, Y.-K. L., Y-J; and Huang, P-C, *J. Electrochem. Soc.* **2009**, *156*, k37-k43.
(47) Zhang, X.; Tian, H.; Liu, Q.; Wang, L.; Geng, Y.; Wang, F., *J. Org. Chem.* **2006**, *71*, 4332-4335.
(48) Jiang, Z.; Li, X. F.; Strzalka, J.; Sprung, M.; Sun, T.; Sandy, A. R.; Narayanan, S.; Lee, D. R.; Wang, J., *J. Synchrot. Radiat.* **2012**, *19*, 627-636.
(49) Jiang, Z., *GIXSGUI is available for download: http://www.aps.anl.gov/Sectors/Sector8/Operations/GIXSGUI.html*.
(50) Herguth, P.; Jiang, X.; Liu, M. S.; Jen, A. K. Y., *Macromolecules* **2002**, *35*, 6094-6100.
(51) Kim, Y.; Cook, S.; Choulis, S. A.; Nelson, J.; Durrant, J. R.; Bradley, D. D. C., *Chem. Mater.* **2004**, *16*, 4812-4818.
(52) Yamauchi, K.; Lizotte, J. R.; Long, T. E., *Macromolecules* **2003**, *36*, 1083-1088.
(53) Yamauchi, K.; Lizotte, J. R.; Hercules, D. M.; Vergne, M. J.; Long, T. E., *J. Am. Chem. Soc.* **2002**, *124*, 8599-8604.
(54) Mather, B. D.; Elkins, C. L.; Beyer, F. L.; Long, T. E., *Macromol. Rapid Commun.* **2007**, *28*, 1601-1606.
(55) Ramanathan, M.; Darling, S. B., *Prog. Polym. Sci.* **2011**, *36*, 793-812.
(56) Anthamatten, M., *J. Polym. Sci., Part B: Polym. Phys.* **2007**, *45*, 3285-3299.
(57) Feng, E. H.; Lee, W. B.; Fredrickson, G. H., *Macromolecules* **2007**, *40*, 693-702.

Chapter 6

Hydrogen Bonding-Mediated Conjugated Polymers for Bulk-Heterojunction Organic Photovoltaics

A major challenge in the optimization of bulk heterojunction photovoltaics (BHJ OPVs) is control over their morphology. In contrast to the simple polymer blend OPVs, we use hydrogen bonding interactions to mediate the morphology and improve power conversion efficiency of all-polymer BHJ OPVs. Poly(3-hexylthiophene) (P3HT) and poly(2,7-(9′,9′-dioctyl-fluorene)-alt-5,5-(4′,7′-di-2-thienyl-2′,1′,3′-benzothiadiazole) (PFTBT) with self-associating, quadruple hydrogen bonding end groups (2-ureido-4[1H]-pyrimidinone, UPy) are used to explore the role of hydrogen bonding associations on blend morphology and photovoltaic performance. We study three different BHJ OPV systems: P3HT/PCBM, PFTBT/PCBM and P3HT/PFTBT and analyze these blends by AFM, impedance spectroscopy, and device characteristics. With hydrogen bonding mediation, the performance is improved from 1.21% to 2.16% in P3HT/PCBM whereas the performance is reduced from 1.84% to 1.08% in PFTBT/PCBM. This contradiction between two systems may be due to enhanced long-range order of semi-crystalline of P3HT but molecular entanglement of non-crystalline PFTBT chains. In P3HT/PFTBT system, the performance is improved from 0.43% to 0.77% because the hydrogen

bonding interaction suppresses the macro-phase separation with maintained uniform films under 155 ^{o}C annealing temperature that better P3HT ordering is expected. Overall, the impedance analysis under short circuit and illumination conditions indicates the faster charge transport (lower bulk resistance, R_1) and reduced charge recombination (higher donor-acceptor interfacial recombination resistance, R_2) within the better performed devices. This study shows that hydrogen bonding interactions can reduce phase separation but not significantly produce better OPV devices in all cases perhaps because of diluted effect of hydrogen bonding on the end groups of polymer chains.

6.1. Introduction

The morphology in the active layer of bulk heterojunction (BHJ) organic photovoltaics (OPVs) is one of the key factors leading to efficient performance. In general, the final structure of active layer is a result of various non-equilibrium processes, including polymer crystallization and phase separation that occur during film casting and annealing.[1,2] A variety of methods have been implemented to control the length scale interface structure and crystallinity of the active layers including the use of processing additives[3-5] and top-down approaches to patterning.[6-8] For OPVs that comprised of all polymers, the morphology and the optimization of devices have been studied by means of composition,[9] casting solvents,[10] annealing temperatures,[11] nanoimprint lithography[6] and block copolymer self-assembly.[12-14] Although all-conjugated block copolymers with p- and n- type blocks are considered an effective way to achieve optimal structures and superior performance, the simplicity of using polymer blends is still widely studied.[10,11,15,16]

In order to enhance intermolecular interaction between donor-acceptor materials, hydrogen bonding is considered as the first choice due to its strength and selectivity.[17-19]

Enhanced performance in BHJ OPVs has been demonstrated with using hydrogen bonding interaction for morphological control in polymer/inorganic molecules blends.[20-24] Previous studies also show that the hydrogen bonding interaction can improve energy transfer between donor-acceptor polymers and dyes.[25,26] Then, improved performances in all-polymer OPVs which are mediated by hydrogen bonding is anticipated. Herein, a quadruple hydrogen bonding group (2-ureido-4[1H]-pyrimidinone, UPy) is introduced as end-functional groups to Poly(3-hexylthiophene) (P3HT) and poly(2,7-(9′,9′-dioctyl-fluorene)-alt-5,5-(4′,7′-di-2-thienyl-2′,1′,3′-benzothiadiazole) (PFTBT) to mediate the morphologies and the BHJ OPVs.

We study the devices in varying donor-acceptor combinations: P3HT/PCBM, PFTBT/PCBM and P3HT/PFTBT. The hydrogen bonding improves performance of P3HT/PCBM (1.21% to 2.16%) and P3HT/PFTBT (0.43% to 0.77%) devices in which P3HT is the electron donor polymer but drops the performance of PFTBT/PCBM (1.84% to 1.08%) devices that PFTBT is the electron donor polymer. Furthermore, AFM indicates that the quadruple hydrogen bonding molecule gives finer morphologies in polymer/PCBM devices and more uniform films even at 155 ^{o}C annealing temperature in P3HT/PFTBT blend devices. Impedance spectroscopy (IS) is performed to analyze the influence of the hydrogen bonding molecule to the electronic properties of OPV devices. Overall, the impedance analysis under short circuit and illumination conditions indicates the faster charge transport (lower bulk resistance, R_1) and reduced charge recombination (higher donor-acceptor interfacial recombination resistance, R_2) within the better performed devices. This study shows that hydrogen bonding interactions can alter the morphology by enhancing miscibility of blends but not significantly produce better OPV devices and can be even detrimental in some cases. Thorough formulation of hydrogen

bonding-modified polymers in regular polymer blends may be important for device optimization.

6.2. Experimental Section

Materials. We used the synthetic method of functionalized initiator for P3HT-OH as reported previously.[27] PFTBT-OH and UPy-terminated polymers were synthesized with similar methods as reported previously.[26] Polystyrene relative M_w of P3HT = 11 kg/mol with polydispersity = 1.05 and regioregularity = 94%. Polystyrene relative M_w of PFTBT = 14 kg/mol with polydispersity = 1.63. Chemical structures of polymers are shown in Figure 6.1.

Cyclic voltammetery (CV). CV measurement was performed using CHI 620C Electrochemical Analyzer, CH Instruments. Sample solutions were prepared by adding trace amount of polymers in anhydrous 0.1 M TBAP electrolyte $CHCl_3$ solution. We used carbon as the working electrode, Pt wire as counter electrode and saturated $AgNO_3$ as reference electrode. Equipment was calibrated with using ferrocence dissolved in 0.1 M TBAP electrolyte $CHCl_3$ solution. Sample solution was purged with N_2 for 10 minutes before measurement. The CV curves and UV-Vis spectra for calculation of energy levels are provided in Figure 6.2-6.4. Calculation for energy levels followed the methods as reported previously.[28] The estimation of HOMO level was done with the equation $E_{HOMO}= [(E_{ox}-E_{1/2(ferrocene)})+4.8]$ eV, where the E_{red} is the onset point of reduction potential and $E_{1/2(ferrocene)}$ is the average of oxidation and reduction potentials from ferrocene. The band gap energy of polymers were calculated from the cross point of onset line and baseline of UV-Vis curves. The LUMO level is E_{HOMO} subtracting the band gap energy.

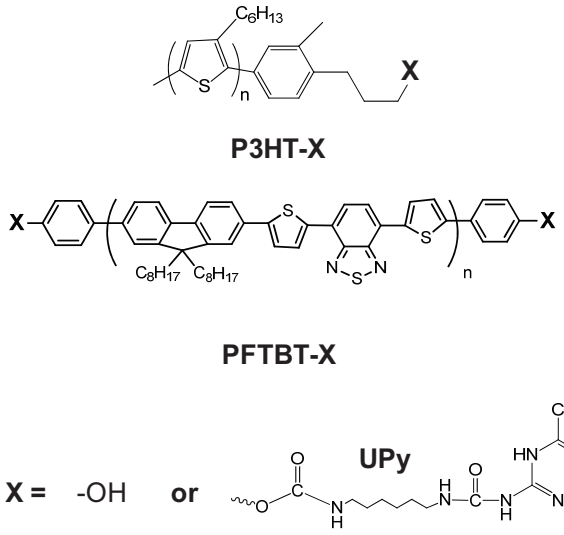

Figure 6.1 – Chemical structures for OH- and UPy-terminated P3HT and PFTBT.

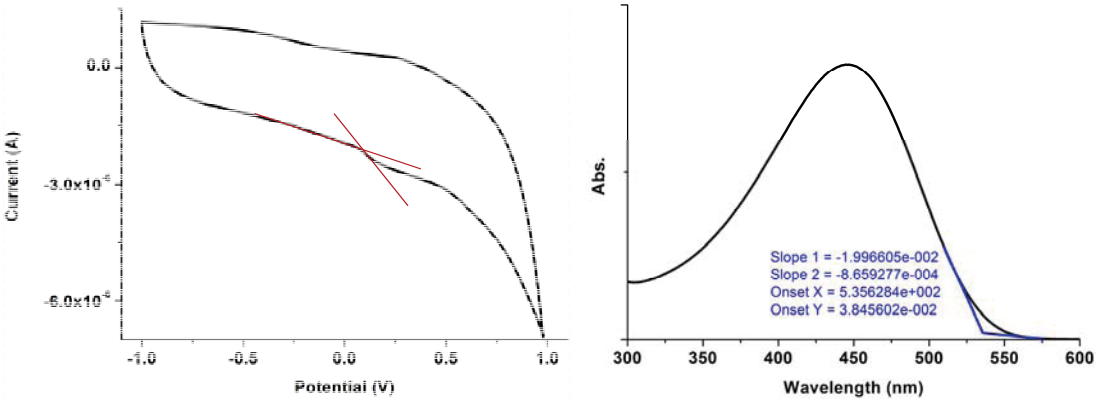

Figure 6.2 – Current-voltage curve and UV-Vis spectrum for P3HT-OH.

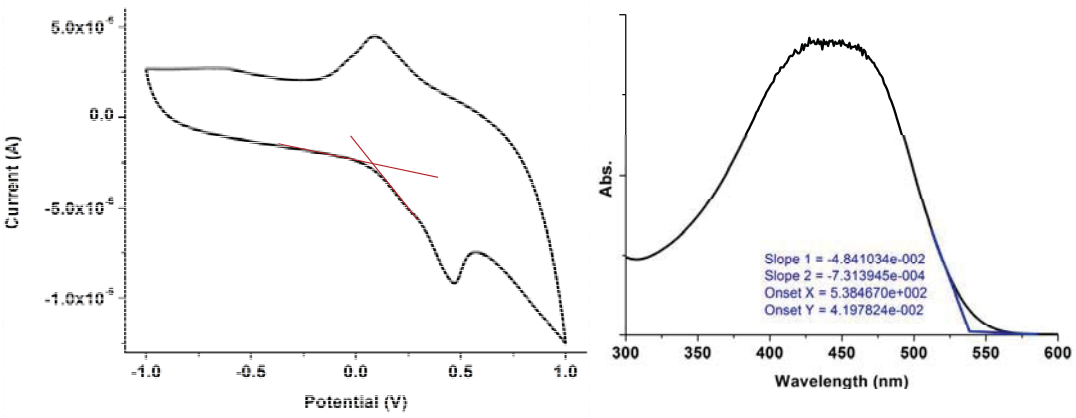

Figure 6.3 – Current-voltage curve and UV-Vis spectrum for P3HT-UPy.

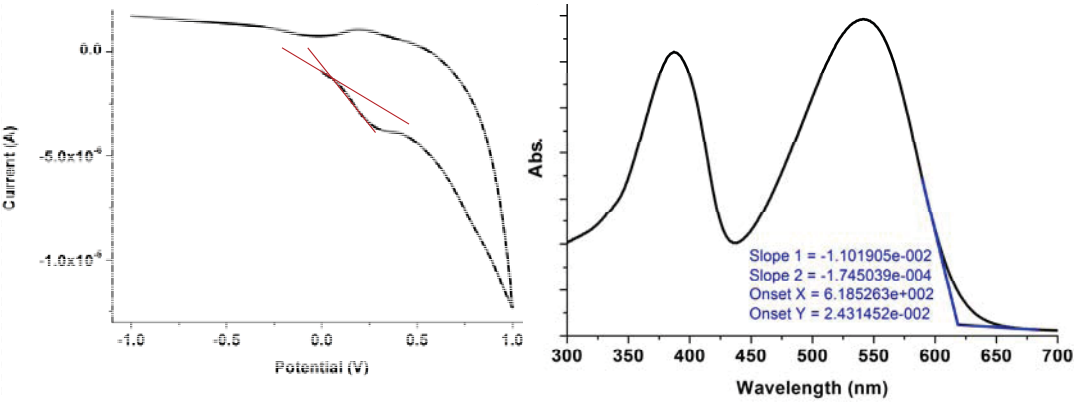

Figure 6.4 – Current-voltage curve and UV-Vis spectrum for P3HT-UPy.

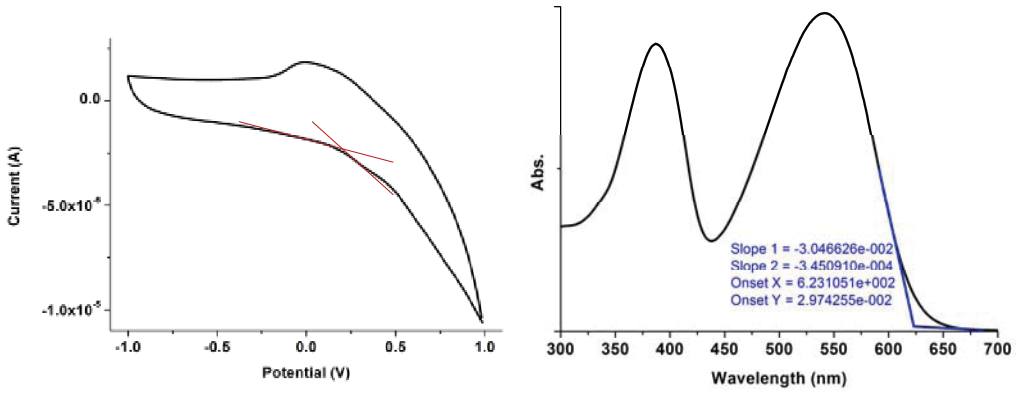

Figure 6.5 – Current-voltage curve and UV-Vis spectrum for PFTBT-UPy.

Photovoltaic device fabrication and measurement. Photovoltaic devices were prepared with conventional structures of ITO/PEDOT:PSS(55 nm)/active layer (80-90 nm)/Al (100 nm). ITO glass substrates (20 ohm/sq, 150 nm, purchased from TFD Inc.) were rinsed with isopropanol, followed by 3 minutes ozone/plasma treatment. PEDOT:PSS (purchased from Sigma Aldrich) was spin-coated on top of ITO at 5000 rpm for 40 seconds giving a film thickness about 55 nm measured by Bruker Dektak XT profilometer. The PEDOT:PSS/ITO substrates were thermal annealed at 120 ^{o}C for 10 minutes in air and then transferred to a argon-filled glovebox. Polymer solutions were prepared with using anhydrous $CHCl_3$ and stirred at room temperature for about 20 hours inside glovebox. After spin-coating active layer films, devices were completed by thermal evaporation of 100 nm Al at 10^{-6} torr on top of the active layer through a shadow mask. The device area is 3.5 mm^2. The integrated devices were further thermal annealed at different temperatures as noted in article. The power conversion efficiency (PCE) of the devices was measured in the air by Class AAA with AM 1.5 filter solar simulator at an intensity of 100 mW/cm^2 (PV Measurements Inc.).

Atomic force microscopy (AFM). AFM analysis was performed using a Veeco Multimode 8 with NanoScope V Controller (instruments located at the Rice University). Sample topography was recorded using ScanAsyst^{TM} mode. 2nd order flattening was used for compensation of sample tilt and enhancement of image contrast.

Impedance spectroscopy (IS). IS measurement was performed using Autolab PGSTAT302N with program NOVA 1.10 on the same devices as device measurement. The frequency was used in the range of 0.1 Hz to 10^6 Hz without applying bias. Fiber-Lite Model 190 was used for illumination. Data were analyzed with using Zview.

6.3. Results and discussions

The quadruple hydrogen bonding 2-ureido-4[1H]-pyrimidinone (UPy) has previously been implemented in the preparation of supramolecular polymers and block copolymers through self-complementary associations to prevent macro-phase separation in polymer blends.[26] In this work, as shown in Figure 6.1, we prepare poly(3-hexylthiophene) (P3HT) and poly(2,7-(9′,9′-dioctyl-fluorene)-alt-5,5-(4′,7′-di-2-thienyl-2′,1′,3′-benzothiadiazole) (PFTBT) polymers modified with UPy end-groups with the methods reported previously.[26,27] The hydrogen bonding interaction can be implemented to tune morphology in polymer/PCBM as well as polymer/polymer BHJ OPVs to impact the performance of solar cells. P3HT is a widely studied p-type polymer in BHJ OPVs. PFTBT is a kind of polyfluorene copolymers with low band gap and being studied as a p-type polymer in BHJ OPVs[29] and a n-type polymer in an P3HT–*b*–PFTBT all-conjugated block copolymer OPVs.[12]

Electrochemical analysis is an important method to obtain the highest occupied molecular orbital (HOMO) and lowest unoccupied molecular orbital (LUMO) energy

levels which are critical parameters for selecting materials for OPVs. We performed electrochemical analysis to examine the influence of UPy functional groups. As shown in Figure 6.6, the energy levels of UPy-terminated polymers slightly decrease by about 0.05 eV due to the hydrogen bonding with strong electron affinity. In the following paragraphs, we will discuss the influence of hydrogen bonding to morphologies, interface and performance of polymer/PCBM and polymer/polymer OPVs.

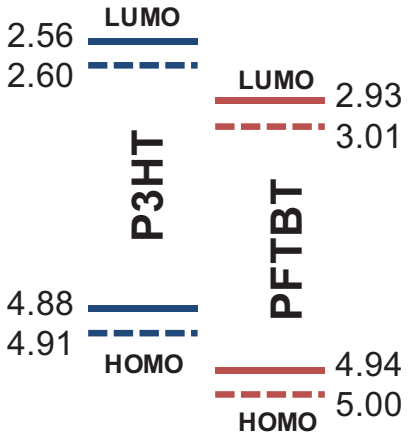

Figure 6.6 – Energy level diagram (in eV) of OH-terminated (solid lines) and UPy-terminated (dash lines) P3HT and PFTBT.

Device characteristics. Both P3HT[30,31] and PFTBT[29,32] have been studied as p-type polymers in blending with PCBM for BHJ OPVs. Several methods such as composition,[33,34] polymer molecular weight,[35,36] solvent effects[37,38] and processing conditions[39,40] have been studied to tune to the film morphology leading to varying device performances. In addition, P3HT and PFTBT have compatible energy levels and have been used for all-polymer OPVs with high open circuit voltage (larger than 1 V) in P3HT/PFTBT blend devices[41] and P3HT–*b*–PFTBT block copolymer devices.[12] Despite of the incentive of high open circuit voltage of polymer/polymer OPV devices, the

control of morphology of polymer blend device remains challenge due to the macro-phase separation. All-conjugated block copolymers can be introduced into polymer blend as an interface compatiblizer to address the macro-phase separation issue.[42] The previous research in supramolecular block copolymers has shown being potential to improve polymer blend OPV due to suppression of macro-phase separation.[26] Here, we use the hydrogen bonding interaction as an unconventional way in tuning film morphology and understand the influences on performances of the three OPV systems: P3HT/PCBM, PFTBT/PCBM and P3HT/PFTBT.

All devices were fabricated from nonpolar chloroform solutions to ensure hydrogen bonding interaction. The I-V curves for all devices are shown in Figure 6.7 and the characteristics of devices are provided in Table 6.1 for polymer/PCBM devices and Table 6.2 for polymer/polymer devices. In P3HT/PCBM (1:0.8 w/w) system under the same thermal annealing at 140 ^{o}C processing condition, P3HT-UPy/PCBM gives power conversion efficiency of 2.16% whereas the efficiency for P3HT-OH/PCBM is 1.21%. This about 78% of efficiency enhancement is attributed to all improved device parameters (V_{oc}, J_{sc} and *FF*). In contrast, in PFTBT/PCBM (1:1w/w) system, PFTBT-UPy/PCBM has efficiency of 1.08% whereas the efficiency for PFTBT-OH is 1.84%. This about 41% drop in efficiency is due to all decreased device parameters.

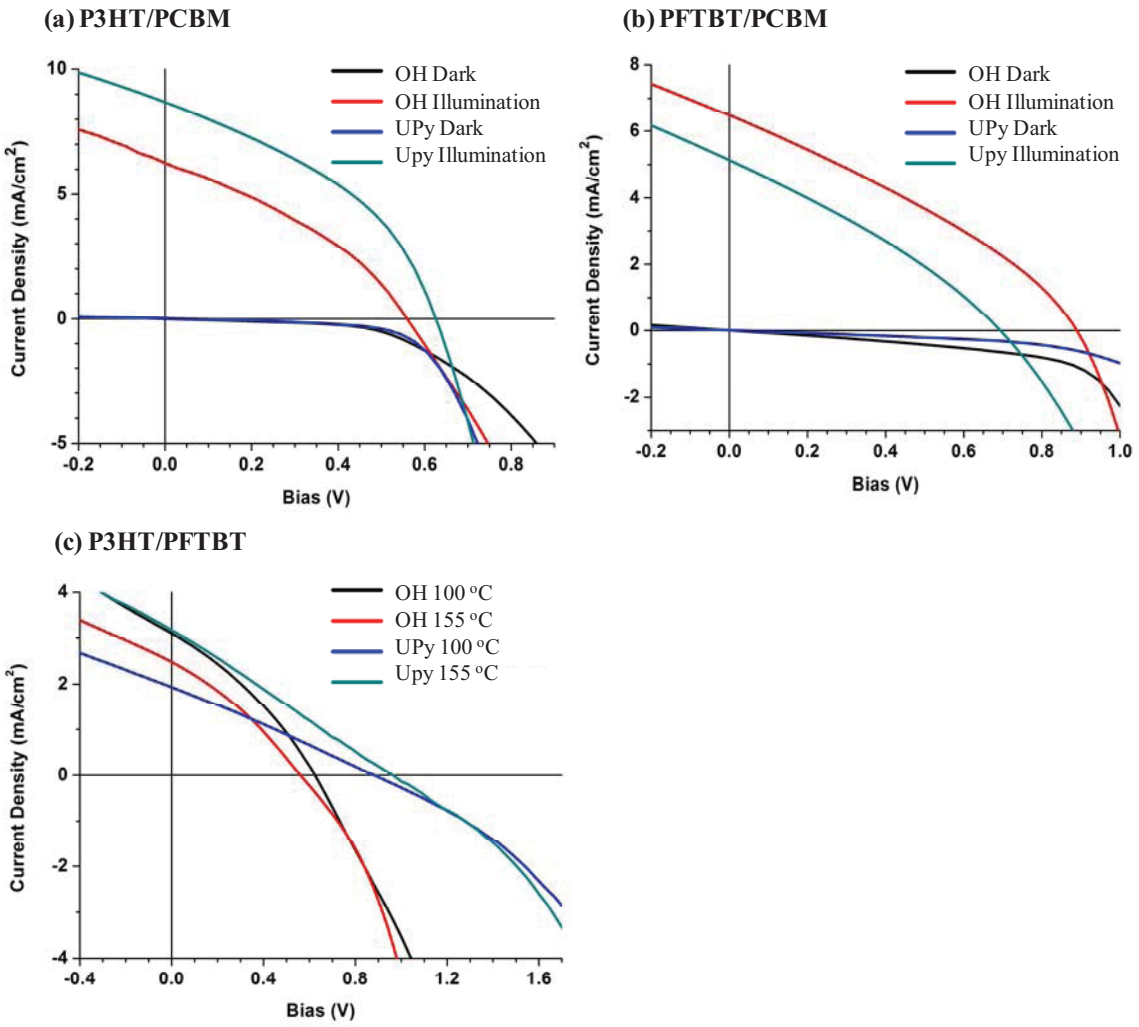

Figure 6.7 – OPV device I-V curves for (a) P3HT/PCBM (1:0.8 w/w) devices with thermal annealing at 140 °C, (b) PFTBT/PCBM (1:1 w/w) with thermal annealing at 120 °C and (c) P3HT/PFTBT(1:1 w/w) with thermal annealing at 100 and 155 °C, respectively. Device I-V curves are plotted for comparison between OH- or UPy-terminated polymers.

Polymers	Efficiency (%)	Short-circuit current (mA/cm^2)	Open-circuit voltage (V)	Fill Factor
P3HT-OH[a]	1.21	6.25	0.56	0.34
P3HT-UPy[a]	2.16	8.68	0.62	0.39
PFTBT-OH[b]	1.84	6.48	0.89	0.32
PFTBT-UPy[b]	1.08	5.13	0.69	0.30

[a]Polymer/PCBM solutions were prepared in ratios of 1:08 w/w and devices were thermal annealed at 140 °C. [b]Polymer/PCBM solutions were prepared in ratios of 1:1 w/w and devices were thermal annealed at 120 °C.

Table 6.1– Device characteristics for polymer/PCBM OPVs.

Active Layer	Efficiency (%)	Short-circuit current (mA/cm^2)	Open-circuit voltage (V)	Fill Factor
P3HT-OH/ PFTBT-OH[a]	0.62	3.10	0.62	0.32
P3HT-UPy/ PFTBT-UPy[a]	0.45	1.93	0.88	0.26
P3HT-OH/ PFTBT-OH[b]	0.43	2.48	0.56	0.31
P3HT-UPy/ PFTBT-UPy[b]	0.77	3.18	0.96	0.25

[a]Samples are annealed under 100 °C for 10 minutes. [a]Samples are annealed under 155 °C for 10 minutes.

Table 6.2 – Device characteristics for polymer/polymer (1:1 w/w) OPVs.

P3HT/PFTBT devices were annealed under two different annealing temperatures, 100 °C and 155 °C, in that increased annealing temperature offer enhanced P3HT order for better hole mobility[43] but may hinder performance due to macro-phase separation giving poor charge generation in polymer/polymer blends.[11,41,42] Furthermore, hydrogen bonding interaction can prevent macro-phase separation with annealing temperature up to 160 °C as reported previously.[26] As shown in Figure 6.7(c) and Table 6.2, P3HT-UPy/PFTBT-UPy devices generally have higher V_{oc} compared with P3HT-OH/PFTBT-OH devices under both annealing conditions due to improved miscibility in polymer/polymer blends (see AFM images at Figure 6.9 and below discussion on morphology). The drop of performance (from 0.62% to 0.43%) of P3HT-OH/PFTBT-OH devices at elevated annealing temperature from 100 °C to 155 °C is attributed to macro-

phase separation. On the other hand, the increase of performance (from 0.43% to 0.77%) and short-circuit current (from 1.93 mA/cm^2 to 3.18 mA/cm^2) in P3HT-UPy/PFTBT-UPy devices at elevated annealing temperature from 100 ^{o}C to 155 ^{o}C can be expected by enhanced long range order of structures with maintained miscibility due to hydrogen bonding interaction. It is worth noting that the fill factor for devices with using UPy-modified polymers is lower than that without using UPy-modified polymers under both annealing conditions. We hypothesize that the introduction of hydrogen bonding may increase the charge transport resistance of device and thorough discussion for this will be provided in impedance spectroscopy section. Although the performance in this research is relatively lower compared with literatures mainly because of smaller molecular weight of polymers, the results still show clear difference in performance with using supramolecular interaction. Closer investigation on the morphologies and the underlying electronic properties are provided in next sections.

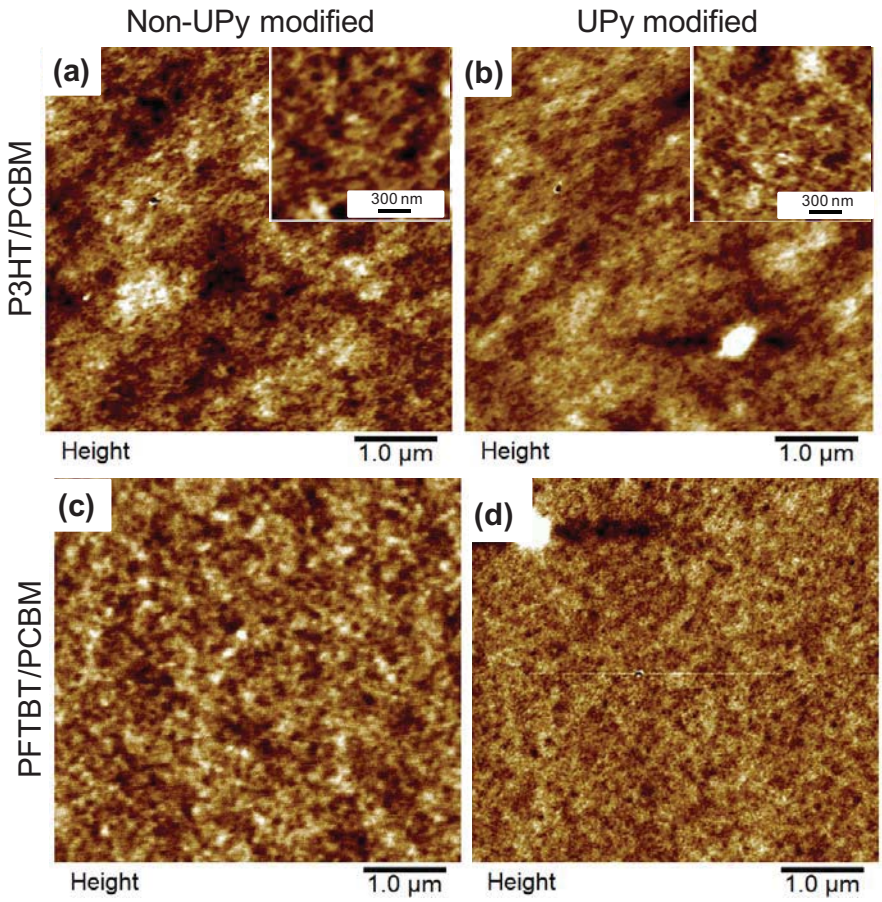

Figure 6.8 – AFM height images on the polymer/PCBM devices: (a) P3HT-OH/PCBM, (b) P3HT-UPy/PCBM, (c) PFTBT-OH/PCBM and (d) PFTBT-UPy/PCBM.

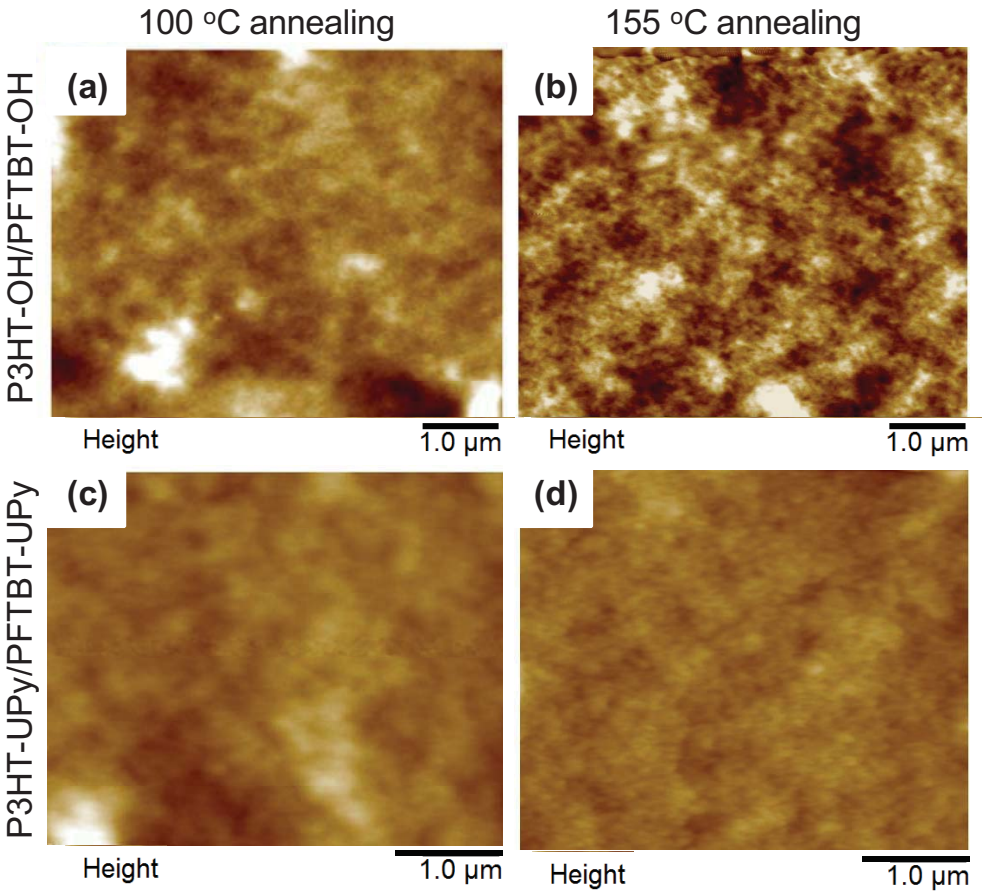

Figure 6.9 – AFM height images on the polymer/polymer devices: (a) P3HT-OH/PFTBT-OH annealed at 100 °C, (b) P3HT-OH/PFTBT-OH annealed at 155 °C, (c) P3HT-UPy/PFTBT-UPy annealed at 100 °C and (d) P3HT-UPy/PFTBT-UPy annealed at 155 °C.

Morphology. The AFM images for the morphologies of three different combinations of BHJ OPVs are shown in Figure 6.8 (P3HT/PCBM and PFTBT/PCBM) and Figure 6.9 (P3HT/PFTBT). In general, both polymers/PCBM systems present improved miscibility of polymers and PCBM with using the UPy-terminated polymers. Both P3HT-UPy/PCBM (Figure 6.8(b)) and PFTBT-UPy/PCBM (Figure 6.8(d)) have relatively smaller PCBM aggregated domains in comparison with P3HT/PCBM (Figure

6.8(a)) and PFTBT/PCBM (Figure 6.8(c)) in that the high molecular weight polymers are expected to reduce the diffusion of PCBM.[44] Previous researches have emphasized the importance of high molecular weight to the performance of OPVs especially in P3HT due to more π stackings.[45,46] The improved efficiency in P3HT-UPy/PCBM also attributes to long-range order of P3HT due to hydrogen bonding association at the P3HT end groups (see embedded images of Figure 6.8(a) and 6.8(b)). Moreover, the molecular weight dependent performance on the non-crystalline PFTBT was also studied and shown to have enhanced efficiency with increasing molecular weight.[36] This inconsistency of our results from PFTBT/PCBM system is perhaps due to the entanglement of high molecular weight of PFTBT-UPy chains because the polymer has UPy functional groups on both end groups.[35]

AFM was also performed to elucidate the morphological difference in non-UPy and UPy-modified P3HT/PFTBT blend devices as well as the effects of annealing temperatures in polymer blends. As shown in Figure 6.9(a) and 6.9(b), 155 ^{o}C annealed film is less uniform in comparison with 100 ^{o}C annealed film for non-UPy modified P3HT/PFTBT blend devices may be mainly driven by macro-phase separation. This reduces amount of interfaces between polymers and hinder the charge transport within the active layer. Therefore, decreased V_{oc} and J_{sc} are found in 155 ^{o}C annealed non-UPy modified polymer blend device. Although the hydrogen bonding interaction improves the miscibility of polymer blends, this may not be favorable to charge transport due to reduced bi-continuous pathways when we compare devices of non-UPy modified and UPy-modified polymer blend devices under 100 ^{o}C annealing temperature (see Figure 6.9(a) and 6.9(c)). However 155 ^{o}C annealed UPy modified polymer blend device not only remains miscibility of two polymers but also improves long range order of structures resulted from higher annealing temperature as shown in Figure 6.9(d). The combination

of miscibility and improved long range order of structures give better performance of 155 ^{o}C annealed UPy modified polymer blend device.

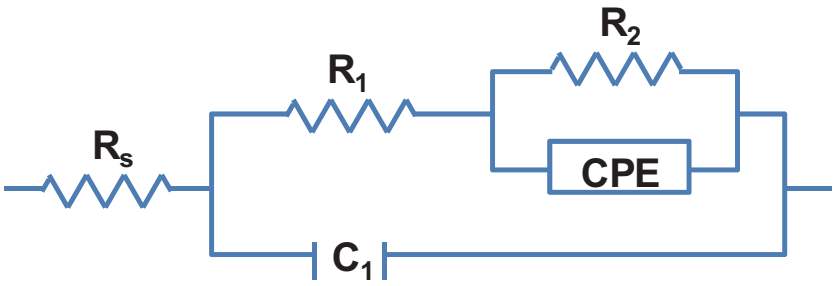

Figure 6.10 – Equivalent circuit elements for donor/acceptor BHJ OPVs. R_s is the resistance loss from the ITO and PEDOT:PSS which is about 90 Ω in our device system. R_1 is the bulk resistance of the film. R_2 is the recombination resistance at the donor-acceptor interface. C_1 is the geometrical capacitance in the film. CPE is the chemical capacitance at the donor-acceptor interface.

Impedance analysis. Impedance spectroscopy is commonly used for electrical devices and applied to study dye-sensitized solar cells by modeling with equivalent circuit elements to understand the internal interface and device components.[47-52] Impedance analysis has also been applied to analyze BHJ OPVs[53,54] and been used to extract by using a simplified equivalent circuit model (see Figure 6.10) as presented previously to correlate impedance behavior of P3HT/PCBM devices with active layer composition and processing history.[55,56] We apply this model to estimate the bulk resistance (R_1) of the active layer by analyzing the high frequency arc and the recombination resistance (R_2) at the donor-acceptor interface by analyzing the low frequency arc from the Cole-Cole plots (see Figure 6.11 and 6.12) for all devices. The short circuit current condition is our particular interest because the bimolecular recombination dominates the mechanism of OPVs.[55,57] We like to find the R_1 and R_2

parameters to reveal how the hydrogen bonding intrinsically influences device characteristics in addition to morphologies.

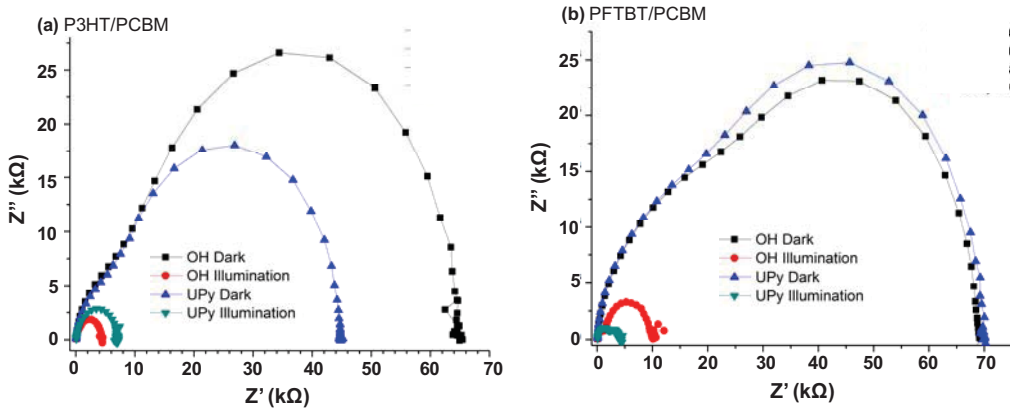

Figure 6.11 – Impedance spectroscopy for (a) P3HT/PCBM and (b) PFTBT/PCBM made from OH- and UPy-terminated polymers under dark and illumination conditions.

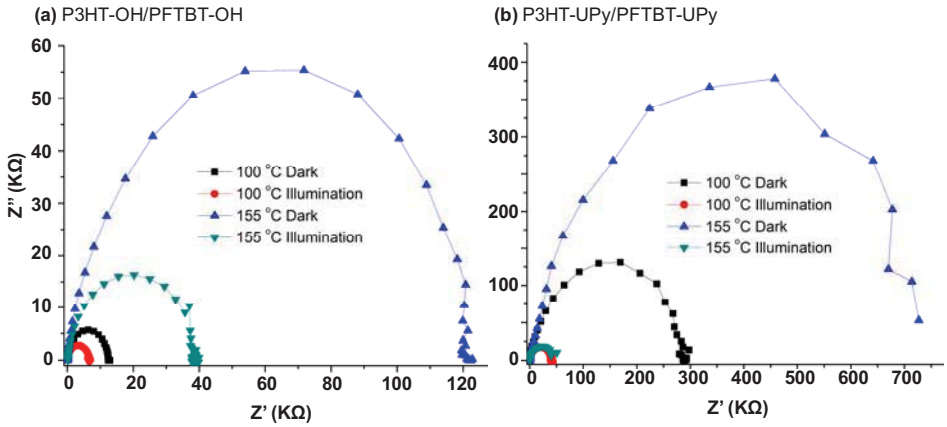

Figure 6.12 – Impedance spectroscopy for (a) P3HT-OH/PFTBT-OH and (b) P3HT-UPy/PFTBT-UPy under 100 °C and 155 °C annealing conditions and dark and illumination conditions.

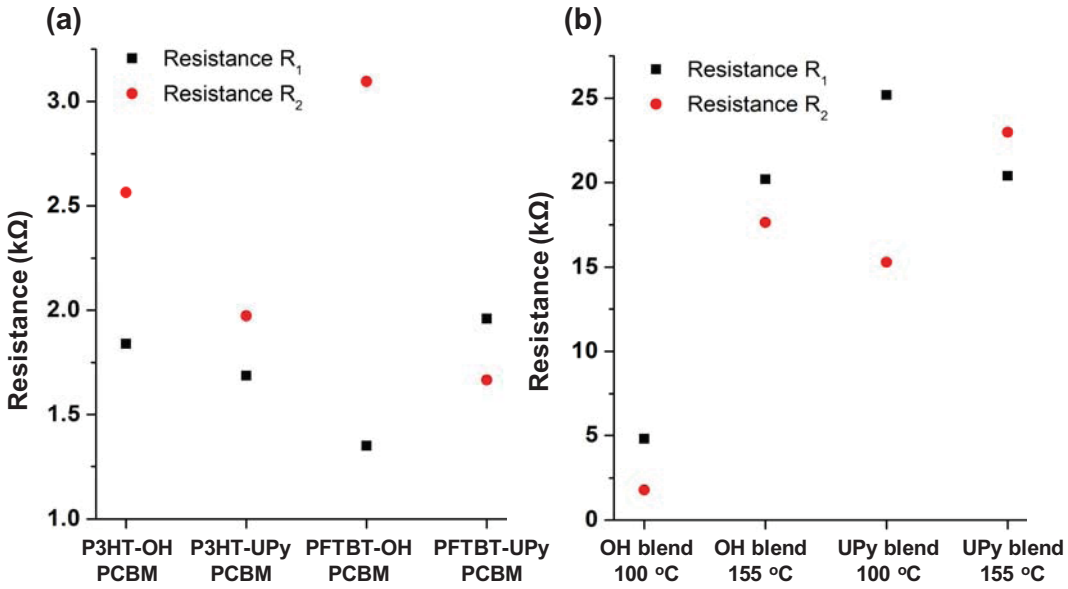

Figure 6.13 – R_1 and R_2, that are extracted from Cole-Cole plots for (a) polymer/PCBM and (b) P3HT/PFTBT devices under illumination condition at 0 V bias.

As shown in Figure 6.13(a), both R_1 and R_2 are lower in P3HT-UPy/PCBM device than that in P3HT-OH/PCBM device under illumination condition. These suggest that the charge transport across the active layer is enhanced and the charge recombination at the donor-acceptor interface is reduced due to less accumulation of trapped charges.[56,58,59] The results match the facts induced from all improved device characteristics in P3HT-UPy/PCBM device and morphologies and the argument that higher degree of polymer crystallinity helps charge pair separation by increasing the probability of escape from the donor-acceptor interface.[57] However, for PFTBT/PCBM system, the R_1 increases but R_2 decreases within hydrogen bonding mediated devices. However, the entanglement of non-crystalline PFTBT slows the charge transport and cause charge accumulation at the PFTBT-PCBM interface which causes more charge recombination happening at donor-acceptor interfaces. The results from the two

polymer/PCBM systems with using hydrogen bonding to tune the morphologies in devices show that faster charge transport plays an important role in efficient charge separation at the donor-acceptor interface.

Impedance analysis was also performed on the P3HT/PFTBT devices for better understandings on their device characteristics as shown in Figure 6.13(b). In the system of P3HT-OH/PFTBT-OH, R_1 for 155 ^oC annealed film is about quadruple of R_1 for 100 ^oC annealed film that could attribute to macro-phase separation in polymer blends. Interestingly, the R_2 for 155 ^oC annealed film under illumination is also higher than R_2 for 100 ^oC annealed film. This may be because of the larger domains at higher annealing temperature so that the charge can be quickly removed from interface.[60] On the other hand, P3HT-UPy/PFTBT-UPy system, R_1 for 155 ^oC annealed film is smaller than R_1 for 100 ^oC annealed film and R_2 for 155 ^oC annealed film is higher than R_2 for 100 ^oC annealed film under illumination. These agree the findings from morphologies that the uniform with long range order of P3HT which improves charge transport (lower R_1 bulk resistance) and prevents charge accumulation (higher R_2 recombination resistance) at interface.

To cross compare these two polymer blends, the addition of hydrogen bonding group indeed increases the bulk resistances 100 ^oC and 155 ^oC annealed devices. Previous research reports that the series resistance including active layer resistances, electrode resistances and contact resistance has pronounced effect on fill factor and limited effect on J_{sc}.[61] The series resistance can be narrowed down to the active layer resistances in our case because all configurations in the studied devices are almost identical. Hence, this enlarged bulk resistance may be the suitable reason why worse fill factor in UPy-modified polymer blend devices as the result of enhanced miscibility from the hydrogen

bonding interaction. Therefore, there are no significant improvements on polymer blend OPV devices with using hydrogen bonding modified polymers.

6.4. Conclusions

We use a quadruple hydrogen bonding group, UPy-terminated P3HT and PFTBT to give an unconventional way to tune the nanostructures in polymer/PCBM and polymer/polymer blend OPV devices. We studied device morphologies as well as impedance analysis to understand how morphology influences device characteristics. In conclusion, superior charge transport across the active layer plays a critical role in efficient charge separation at the donor-acceptor interfaces in all three cases. Hydrogen bonding interaction was shown to be an effective way to suppress macro-phase separation in polymer/polymer blends but give limited improvement for device performance because the improved miscibility indeed enhances the V_{oc} but surrenders the fill factor due to enlarged bulk resistance.

6.5. References

(1) Hoppe, H.; Sariciftci, N. S., *J. Mater. Chem.* **2006**, *16*, 45-61.

(2) Erb, T.; Zhokhavets, U.; Gobsch, G.; Raleva, S.; Stühn, B.; Schilinsky, P.; Waldauf, C.; Brabec, C. J., *Adv. Funct. Mater.* **2005**, *15*, 1193-1196.

(3) Peet, J.; Soci, C.; Coffin, R. C.; Nguyen, T. Q.; Mikhailovsky, A.; Moses, D.; Bazan, G. C., *Appl. Phys. Lett.* **2006**, *89*, 252105-3.

(4) Moon, J. S.; Takacs, C. J.; Cho, S.; Coffin, R. C.; Kim, H.; Bazan, G. C.; Heeger, A. J., *Nano Lett.* **2010**, *10*, 4005-4008.

(5) Perez, L. A.; Chou, K. W.; Love, J. A.; van der Poll, T. S.; Smilgies, D.-M.; Nguyen, T.-Q.; Kramer, E. J.; Amassian, A.; Bazan, G. C., *Adv. Mater.* **2013**, *25*, 6380-6384.

(6) He, X.; Gao, F.; Tu, G.; Hasko, D.; Hüttner, S.; Steiner, U.; Greenham, N. C.; Friend, R. H.; Huck, W. T. S., *Nano Lett.* **2010**, *10*, 1302-1307.

(7) Slota, J. E.; He, X. M.; Huck, W. T. S., *Nano Today* **2010**, *5*, 231-242.
(8) Moungthai, S.; Mahadevapuram, N.; Ruchhoeft, P.; Stein, G. E., *ACS Appl. Mater. Interfaces* **2012**, *4*, 4015-4023.
(9) Kim, Y.; Cook, S.; Choulis, S. A.; Nelson, J.; Durrant, J. R.; Bradley, D. D. C., *Chem. Mater.* **2004**, *16*, 4812-4818.
(10) Mori, D.; Benten, H.; Kosaka, J.; Ohkita, H.; Ito, S.; Miyake, K., *ACS Appl. Mater. Interfaces* **2011**, *3*, 2924-2927.
(11) McNeill, C. R.; Abrusci, A.; Hwang, I.; Ruderer, M. A.; Müller-Buschbaum, P.; Greenham, N. C., *Adv. Funct. Mater.* **2009**, *19*, 3103-3111.
(12) Guo, C.; Lin, Y.-H.; Witman, M. D.; Smith, K. A.; Wang, C.; Hexemer, A.; Strzalka, J.; Gomez, E. D.; Verduzco, R., *Nano Lett.* **2013**, *13*, 2957-2963.
(13) Segalman, R. A.; McCulloch, B.; Kirmayer, S.; Urban, J. J., *Macromolecules* **2009**, *42*, 9205-9216.
(14) Darling, S. B., *Energy Environ. Sci.* **2009**, *2*, 1266-1273.
(15) McNeill, C. R.; Abrusci, A.; Zaumseil, J.; Wilson, R.; McKiernan, M. J.; Burroughes, J. H.; Halls, J. J. M.; Greenham, N. C.; Friend, R. H., *Appl. Phys. Lett.* **2007**, *90*, 193506-3.
(16) Facchetti, A., *Mater. Today* **2013**, *16*, 123-132.
(17) Emsley, J., *Chem. Soc. Rev.* **1980**, *9*, 91-124.
(18) Prins, L. J.; Reinhoudt, D. N.; Timmerman, P., *Angew. Chem. Int. Ed.* **2001**, *40*, 2382-2426.
(19) Glowacki, E. D.; Irimia-Vladu, M.; Bauer, S.; Sariciftci, N. S., *J. Mater. Chem. B* **2013**, *1*, 3742-3753.
(20) Lin, Y.; Wei, Q.; Qian, G.; Yao, L.; Watkins, J. J., *Macromolecules* **2012**, *45*, 8665-8673.
(21) Liu, C.; Li, Y.; Li, C.; Li, W.; Zhou, C.; Liu, H.; Bo, Z.; Li, Y., *J. Phys. Chem.C* **2009**, *113*, 21970-21975.
(22) Patra, D.; Ramesh, M.; Sahu, D.; Padhy, H.; Chu, C.-W.; Wei, K.-H.; Lin, H.-C., *Polymer* **2012**, *53*, 1219-1228.

(23) Sahu, D.; Padhy, H.; Patra, D.; Kekuda, D.; Chu, C.-W.; Chiang, I. H.; Lin, H.-C., *Polymer* **2010**, *51*, 6182-6192.
(24) Hsu, S.-L.; Chen, C.-M.; Cheng, Y.-H.; Wei, K.-H., *J. Polym. Sci., Part A: Polym. Chem.* **2011**, *49*, 603-611.
(25) Schenning, A. P. H. J.; v. Herrikhuyzen, J.; Jonkheijm, P.; Chen, Z.; Würthner, F.; Meijer, E. W., *J. Am. Chem. Soc.* **2002**, *124*, 10252-10253.
(26) Lin, Y.-H.; Darling, S. B.; Nikiforov, M. P.; Strzalka, J.; Verduzco, R., *Macromolecules* **2012**, *45*, 6571-6579.
(27) Smith, K. A.; Pickel, D. L.; Yager, K.; Kisslinger, K.; Verduzco, R., *J. Polym. Sci., Part A: Polym. Chem.* **2014**, *52*, 154-163.
(28) Shafiee, A.; Salleh, M. M.; Yahaya, M., *Sains Malays.* **2011**, *40 (2)*, 173-176.
(29) Svensson, M.; Zhang, F.; Veenstra, S. C.; Verhees, W. J. H.; Hummelen, J. C.; Kroon, J. M.; Inganäs, O.; Andersson, M. R., *Adv. Mater.* **2003**, *15*, 988-991.
(30) Dang, M. T.; Hirsch, L.; Wantz, G., *Adv. Mater.* **2011**, *23*, 3597-3602.
(31) Dennler, G.; Scharber, M. C.; Brabec, C. J., *Adv. Mater.* **2009**, *21*, 1323-1338.
(32) Zhang, F. L.; Gadisa, A.; Inganäs, O.; Svensson, M.; Andersson, M. R., *Appl. Phys. Lett.* **2004**, *84*, 3906-3908.
(33) Baek, W.-H.; Yoon, T.-S.; Lee, H. H.; Kim, Y.-S., *Org. Electron.* **2010**, *11*, 933-937.
(34) Park, S. H.; Roy, A.; Beaupre, S.; Cho, S.; Coates, N.; Moon, J. S.; Moses, D.; Leclerc, M.; Lee, K.; Heeger, A. J., *Nat Photon* **2009**, *3*, 297-302.
(35) Ballantyne, A. M.; Chen, L.; Dane, J.; Hammant, T.; Braun, F. M.; Heeney, M.; Duffy, W.; McCulloch, I.; Bradley, D. D. C.; Nelson, J., *Adv. Funct. Mater.* **2008**, *18*, 2373-2380.
(36) Müller, C.; Wang, E.; Andersson, L. M.; Tvingstedt, K.; Zhou, Y.; Andersson, M. R.; Inganäs, O., *Adv. Funct. Mater.* **2010**, *20*, 2124-2131.
(37) Rispens, M. T.; Meetsma, A.; Rittberger, R.; Brabec, C. J.; Sariciftci, N. S.; Hummelen, J. C., *Chem. Commun.* **2003**, 2116-2118.
(38) Liang, Y.; Yu, L., *Accounts Chem. Res.* **2010**, *43*, 1227-1236.
(39) Kim, J. S.; Lee, J. H.; Park, J. H.; Shim, C.; Sim, M.; Cho, K., *Adv. Funct. Mater.* **2011**, *21*, 480-486.

(40) Ma, W.; Yang, C.; Gong, X.; Lee, K.; Heeger, A. J., *Adv. Funct. Mater.* **2005**, *15*, 1617-1622.
(41) McNeill, C. R.; Halls, J. J. M.; Wilson, R.; Whiting, G. L.; Berkebile, S.; Ramsey, M. G.; Friend, R. H.; Greenham, N. C., *Adv. Funct. Mater.* **2008**, *18*, 2309-2321.
(42) Mulherin, R. C.; Jung, S.; Huettner, S.; Johnson, K.; Kohn, P.; Sommer, M.; Allard, S.; Scherf, U.; Greenham, N. C., *Nano Lett.* **2011**, *11*, 4846-4851.
(43) Mihailetchi, V. D.; Xie, H. X.; de Boer, B.; Koster, L. J. A.; Blom, P. W. M., *Adv. Funct. Mater.* **2006**, *16*, 699-708.
(44) Ma, W.; Kim, J. Y.; Lee, K.; Heeger, A. J., *Macromol. Rapid Commun.* **2007**, *28*, 1776-1780.
(45) Schilinsky, P.; Asawapirom, U.; Scherf, U.; Biele, M.; Brabec, C. J., *Chem. Mater.* **2005**, *17*, 2175-2180.
(46) Wu, M.-C.; Chang, C.-H.; Lo, H.-H.; Lin, Y.-S.; Lin, Y.-Y.; Yen, W.-C.; Su, W.-F.; Chen, Y.-F.; Chen, C.-W., *J. Mater. Chem.* **2008**, *18*, 4097-4102.
(47) Bisquert, J.; Fabregat-Santiago, F.; Mora-Seró, I.; Garcia-Belmonte, G.; Giménez, S., *J. Phys. Chem.C* **2009**, *113*, 17278-17290.
(48) Mora-Seró, I.; Bisquert, J.; Fabregat-Santiago, F.; Garcia-Belmonte, G.; Zoppi, G.; Durose, K.; Proskuryakov, Y.; Oja, I.; Belaidi, A.; Dittrich, T.; Tena-Zaera, R.; Katty, A.; Lévy-Clément, C.; Barrioz, V.; Irvine, S. J. C., *Nano Lett.* **2006**, *6*, 640-650.
(49) Bisquert, J., *Phys. Chem. Chem. Phys.* **2003**, *5*, 5360-5364.
(50) Fabregat-Santiago, F.; Bisquert, J.; Palomares, E.; Otero, L.; Kuang, D.; Zakeeruddin, S. M.; Grätzel, M., *J. Phys. Chem.C* **2007**, *111*, 6550-6560.
(51) Wang, Q.; Moser, J.-E.; Grätzel, M., *J. Phys. Chem. B* **2005**, *109*, 14945-14953.
(52) Longo, C.; Nogueira, A. F.; De Paoli, M.-A.; Cachet, H., *J. Phys. Chem. B* **2002**, *106*, 5925-5930.
(53) Garcia-Belmonte, G.; Boix, P. P.; Bisquert, J.; Sessolo, M.; Bolink, H. J., *Sol. Energy Mater. Sol. Cells* **2010**, *94*, 366-375.
(54) Garcia-Belmonte, G.; Munar, A.; Barea, E. M.; Bisquert, J.; Ugarte, I.; Pacios, R., *Org. Electron.* **2008**, *9*, 847-851.

(55) Leever, B. J.; Bailey, C. A.; Marks, T. J.; Hersam, M. C.; Durstock, M. F., *Adv. Energy Mater.* **2012**, *2*, 120-128.
(56) Aoyama, Y.; Yamanari, T.; Ohashi, N.; Shibata, Y.; Suzuki, Y.; Mizukado, J.; Suda, H.; Yoshida, Y., *Sol. Energy Mater. Sol. Cells* **2014**, *120, Part B*, 584-590.
(57) Keivanidis, P. E.; Clarke, T. M.; Lilliu, S.; Agostinelli, T.; Macdonald, J. E.; Durrant, J. R.; Bradley, D. D. C.; Nelson, J., *J. Phys. Chem. Lett.* **2010**, *1*, 734-738.
(58) Seemann, A.; Sauermann, T.; Lungenschmied, C.; Armbruster, O.; Bauer, S.; Egelhaaf, H. J.; Hauch, J., *Sol. Energy* **2011**, *85*, 1238-1249.
(59) Schafferhans, J.; Baumann, A.; Wagenpfahl, A.; Deibel, C.; Dyakonov, V., *Org. Electron.* **2010**, *11*, 1693-1700.
(60) Groves, C.; Marsh, R. A.; Greenham, N. C., *J. Chem. Phys.* **2008**, *129*, 114903.
(61) Servaites, J. D.; Yeganeh, S.; Marks, T. J.; Ratner, M. A., *Adv. Funct. Mater.* **2010**, *20*, 97-104.

Chapter 7

Proposed Future Works

In addition to the above synthetic works and device works in this thesis research, this chapter gives several other preliminary studies in donor-acceptor polymer interface engineering for OPV device studies that may enable better understanding on key factors toward superior OPVs. Here, we particularly concentrate on the molecular linker of all-conjugated block copolymers to understand how the linking group influences the charge separation and recombination. This chapter also includes several notes for OPV device fabrication.

7.1. Introduction

All-conjugated block copolymers are promising materials for use in solution processed organic photovoltaics (OPVs).[1,2] These materials can produce OPV active layers with well-defined donor and acceptor domains through block copolymer self-assembly, of interest both for the development of high-efficiency OPVs and for achieving a better fundamental understanding of the photoconversion process in organic donor-

acceptor heterojunctions. Recent work reported all-conjugated block copolymers with 3% power conversion efficiencies, demonstrating their feasibility and potential for use in OPVs.[3] However, a clear understanding of the molecular characteristics that govern their performance in photovoltaic devices is lacking.

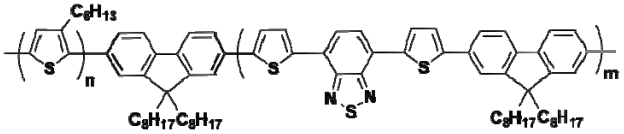

P3HT-F-PTBTF

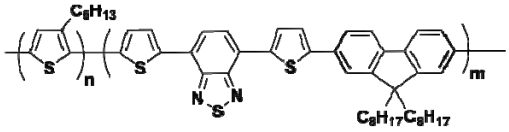

P3HT-PTBTF

Figure 7.1 – Structure of all-conjugated block copolymers. The primary difference in the two conjugated block copolymers is the chemistry of the covalent linking group.

Here, we study the role of the linking group between polymer donor and acceptor blocks in fully conjugated block copolymer systems as shown in Figure 7.1. We analyze conjugated block copolymer systems which differ primarily in the chemistry of the linking group between donor and acceptor polymer blocks. A combination of OPV device studies, grazing incidence X-ray analysis, and transient absorbance spectroscopy is used to understand the potential role on photovoltaic performance and charge separation and recombination. Our results show a clear effect of the linking group on photovoltaic device performance, and we show that charge separation can be suppressed due to the formation of low-energy charge-transfer states at the donor-acceptor interface, depending on the chemistry of the linking group. Our results further show that charge recombination is ultrafast even in high-performance block copolymer OPVs, and

therefore optimization of the linking group may significantly improve the performance of block copolymer OPVs.

7.2. Identical nanostructures and crystallinity between P3HT-PTBTF and P3HT-F-PTBTF

The morphology and crystallinity of the block copolymer films was analyzed by differential scanning calorimetry (DSC) measurements (Figure 7.2) and grazing incidence X-ray scattering (GIXS) (Figure 7.3). DSC measurements reveal P3HT crystallinity in both samples, with a crystal melting temperatures of approximately 220 and 215 °C for P3HT-F-PTBTF and P3HT-PTBTF, respectively. This difference in crystal melting temperatures is attributed to a higher P3HT content in this sample. GIXS measurements provide information on the orientation of crystallites in the block copolymer films, in particular the orientation of the face-to-face π-π stacking of P3HT crystallites. Solution processed P3HT films and P3HT/PCBM blends typically exhibit an in-plane π-π stacking direction.[4-5] A notable feature of this block copolymer system noted in a prior publication is the out-of-plane π-π stacking direction in solution-processed OPV device.[3] It was hypothesized that the out-of-plane stacking may provide improved charge transport to electrodes. As shown in Figure 7.3, both block copolymer films exhibit peaks characteristic of 2-dimensional P3HT crystals. The (010) peak corresponds to the π-π stacking direction in P3HT and is out-of-plane (q_z) in both films, while (100), (200), and (300) peaks correspond to stacking through alkyl side-chains and are oriented along the in-plane (q_x) direction. Thus, GIXS patterns indicate an out-of-plane π-π stacking direction for both samples processed under conditions identical to those for devices. Based on these results, we conclude that crystallinity or film morphology cannot account

for the difference in photovoltaic performance observed for the two block copolymer samples.

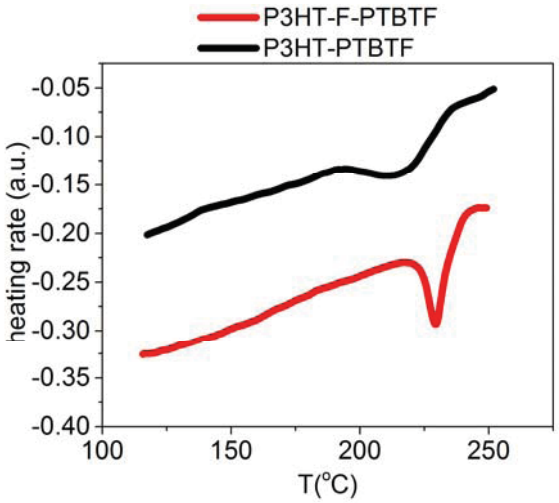

Figure 7.2 – Differential scanning calorimetry (DSC) of all-conjugated block copolymers. Second heating cycle is shown for both samples.

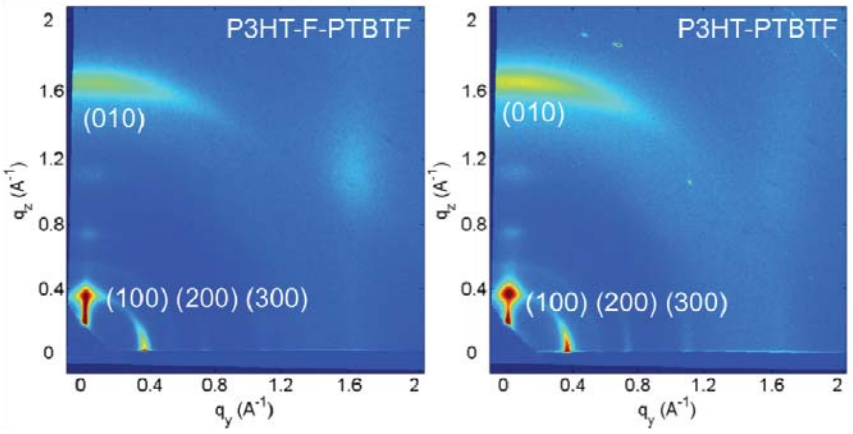

Figure 7.3 – Grazing-incidence wide-angle X-ray analysis of P3HT-PTBTF and P3HT-F-PTBTF films.

7.3. Different behaviors in device characteristics

We investigated the photovoltaic properties of the all-conjugated block copolymers in solar cell structures of ITO/PEDOT:PSS/block copolymer/Ca/Al that were fabricated and tested at Penn State University. The active layers were comprised of pure block copolymer, which were spin cast from either chloroform or a mixture of chloroform and chloronaphthalene (95:5 v/v) at 5 mg/ml concentration, and further annealed at 165 ^{o}C for 15 minutes. Current-voltage (*I-V)* curves of the OPVs solar cells illuminated at AM 1.5 at 100mW/cm^2 are shown in Figure 7.4 and device characteristics are summarized in Table 7.1. P3HT-F-PTBTF block copolymer OPVs have a larger short-circuit current (J_{SC}) by an order of magnitude, and the fill factor (FF) and open-circuit voltage (V_{OC}) are greater for P3HT-F-PTBTF OPV devices. The overall power conversion efficiency is roughly 40 times greater for P3HT-F-PTBTF devices compared with P3HT-PTBTF.

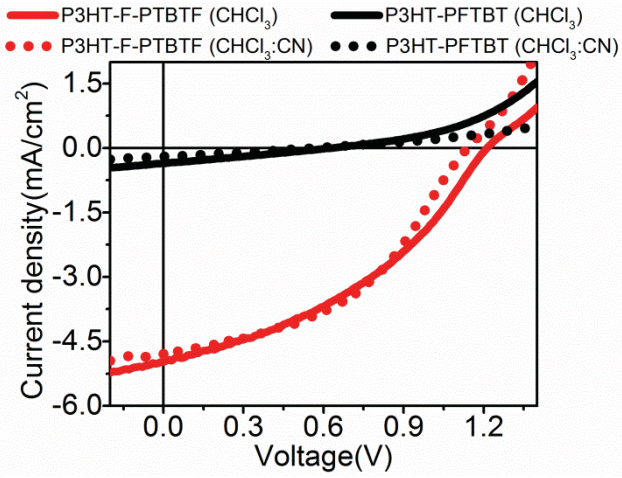

Figure7.4 – I-V curves of OPV solar cells of P3HT-F-PTBTF (red) and P3HT-PTBTF (black) illuminated at AM 1.5 at 100 mW/cm^2.

Active Layer	Efficiency (%)	Short-circuit current (mA/cm^2)	Open-circuit voltage (V)	Fill Factor
P3HT-*F*-PTBTF ($CHCl_3$)	2.01	4.69	1.15	0.378
P3HT-*F*-PTBTF ($CHCl_3$:CN)	2.24	4.73	1.11	0.424
P3HT-PTBTF ($CHCl_3$)	0.052	0.355	0.58	0.267
P3HT-PTBTF ($CHCl_3$:CN)	0.021	0.195	0.39	0.278

Table 7.1 – Device characteristics of block copolymer OPVs, averaged over 6 devices.

Given the similarities in the composition and structure of the two block copolymers the large difference in the photovoltaic performance of the materials is surprising. A number of factors can contribute to power conversion efficiencies, including absorbance, composition, processing history, active layer morphology, charge mobilities, and donor-acceptor interface properties. We can exclude composition and processing history as predominant factors since both systems contain the same polymeric donor and acceptor blocks with similar compositions, and the devices were processed using the same procedures.

7.4. Techniques to understand the differences in device characteristics

The steady-state photoluminescence (PL) and absorbance of block copolymers and P3HT and PTBTF homopolymers are also shown in Figure 7.5. P3HT-F-TBTF exhibits PL spectra that are roughly a combination of the parent P3HT and PTBTF homopolymers. By comparison, P3HT-PTBTF exhibits excitation spectra that are red-shifted relative to P3HT-F-PTBTF and both homopolymers. This redshift indicates the formation of an excited state in P3HT-PTBTF not present in the block copolymer with the F linker or in the homopolymers. We note that the photoluminescence of P3HT-PTBTF is similar to that of a model block copolymer systems studied by Johnson et al., in which a P3HT oligomer was terminated by a single TBTF monomer.[4] We attribute the redshift in the PL of P3HT-PTBTF to the formation of a low energy charge-transfer state at the donor-acceptor interface in P3HT-PTBTF not present in P3HT-F-PTBTF.

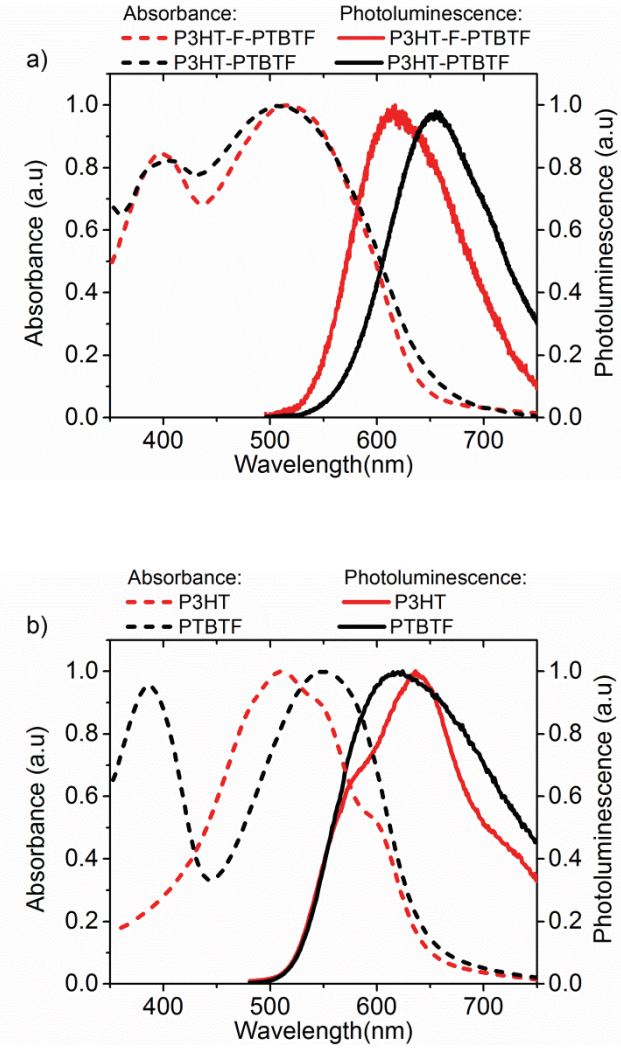

Figure 7.5 – Steady state absportion and photoluminescence spectra of a) block copolymers and b) homopolymers. All materials were spin cast from chloroform and further annealed at device conditions.

To gain direct information on the formation and recombination of charge separated states, ultrafast transient absorption (TA) measurements were carried out on homopolymer and block copolymer films. Analysis of the TA signal can provide direct evidence for the generation of charge separated states and an estimate of their lifetimes. Prior studies have demonstrated that charge separated states (polarons) in regioregular

P3HT exhibit a strong absorption band in the mid-IR range (λ = 650 – 1200 nm).[6-9] Thus, populations and lifetimes of charge-separated states in P3HT can be determined through analysis of the photoinduced absorption signal (PIA) at wavelengths of 650 – 1200 nm. Prior work has also revealed two time scales for charge separation in polymer-fullerene[6-8,10] and polymer-polymer blends.[9] The first timescale is ultrafast and occurs on < 0.1 ps timescales and corresponds to excitons generated near the donor acceptor interface. A second, slower process is observed and is associated with excitons that diffuse to the donor-acceptor interface before charge separation. In polymer-polymer blends, in contrast to typical rates for recombination in polymer-fullerene blends, sub-nanosecond charge recombination has been observed.[11]

TA measurements over timescales of 0.1 – 1000 ps were carried out on P3HT and PTBTF homopolymer films (see Figure 7.6 top), P3HT-F-PTBTF and P3HT-PTBTF films (see Figures 7.6 bottom). P3HT and PTBTF homopolymer films exhibit primarily positive differential transmission, reflective of ground state bleach or stimulated excitation in the pristine films. Some PIA is observed at longer wavelengths in PTBTF, characteristic of some charge separation commonly observed in donor-acceptor conjugated polymers.[9] P3HT-F-PTBTF exhibits a broad PIA from 650 – 800 nm from 0.1 – 1000 ps. The observed PIA signal exhibits similar features to that of a similar polymer photovoltaic blends, P3HT and F8TBT[12], and other P3HT bulk heterojunction OPV systems. This PIA is indicative of the creation of charge-separated states in P3HT-F-PTBTF over timescales of 0.1 – 1000 ps. Similar to polymer-fullerene and polymer polymer blends, charge separation is observed to occur rapidly, within 0.1 ps, and additional charges are created over time due to diffusions of excitons to the donor-acceptor interface. The maximum in the PIA intensity occurs at roughly 30 ps.

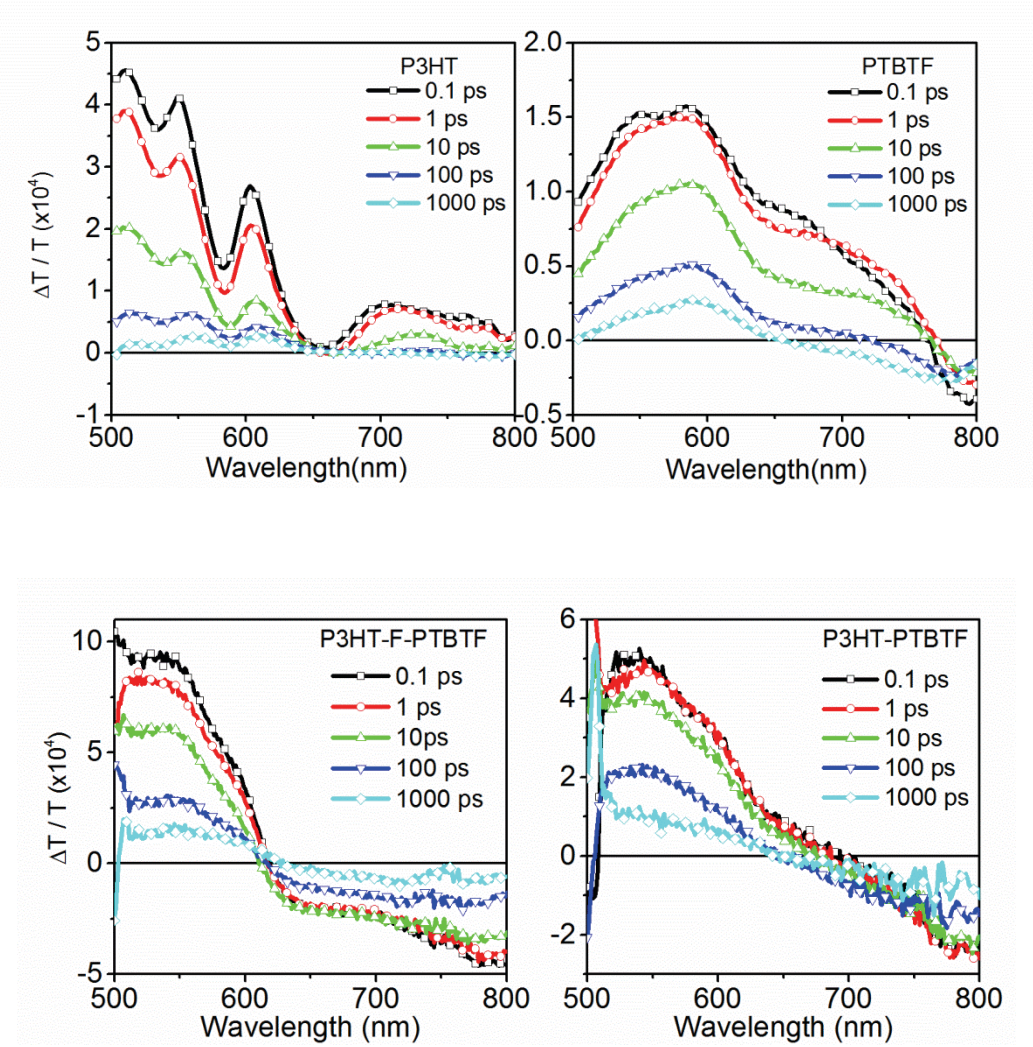

Figure 7.6 – TA measurements of homopolymer (top) and block copolymer (bottom) films excited at 500 nm. Films were annealed at device conditions.

In the case of P3HT-PFTBT (Figure 7.6 bottom right) in contrast to a broad PIA signal, positive differential transmission is observed from 600 – 700 nm at short times (0.1 – 10 ps). This corresponds to stimulated emission in these samples, consistent with the red-shifted PL observed in P3HT-PFTBT films. Stimulated emission is predominant at short times, and at longer times (> 100 ps) the stimulated emission decays to reveal a

broad PIA signal corresponding to charge-separated states. This demonstrates that charge separation is suppressed in P3HT-PTBTF due to the formation of the low-energy charge transfer state at the donor-acceptor interface in P3HT-PTBTF. This result is consistent with the device measurements and shows that the chemistry of the linking group is important to photovoltaic charge generation in block copolymer OPVs. These results are also consistent with the model BCP systems recently reported by Johnson et al.[4]

7.5. Increase length of molecular linker at interface may further improve OPV performance

With clear evidence on the positive influence of fluorene molecule linker at the interface of donor and acceptor polymers, a few extra linking units may further foster effective charge separation. In contrast to the synthetic method for preparation of P3HT–*b*–PF in earlier chapters that usually gives more than 10 fluorene units, we attempt to have shorter PF linker in that larger PF block can be an insulating block and prevent charge transport between donor and acceptor polymers. The proposed synthetic methods are shown in Figure 7.7. The earlier synthesis for P3HT84–*b*–PF13 in Chapter 3 has shown that a dilute reaction concentration in Suzuki reaction can lead to relative short PF block. Therefore, P3HT–*b*–PF–*b*–PFTBT triblock copolymer is expected to be prepared by following an addition Suzuki polycondensation reaction.

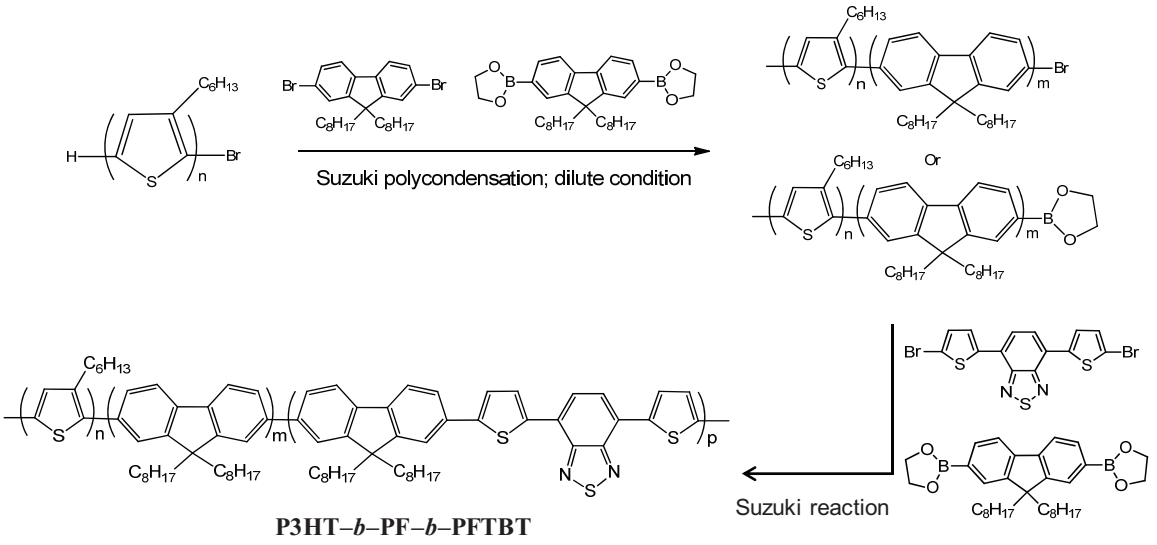

Figure 7.7 – Proposed reaction route for P3HT–*b*–PF–*b*–PFTBT triblock copolymer.

7.6. Notes for OPV fabrication

This section provides several notes for steps during OPV fabrication based on my earlier experiences.

The first step in OPV fabrication is cleaning ITO substrates. I've used glass detergents followed by sonication within DI water, acetone, and isopropyl alcohol. Then, the substrates are treated with UV-ozone to turn the surface into hydrophilic. Also I've used rinsing substrates with isopropyl alcohol followed by ozone-plasma treatment for surface modification. Both methods are good for OPV fabrication. The second method is time-saving.

The second step is PEDOT:PSS film coating. Thermal annealing is required after film casting in order to fully fry the films. My recipe is 120 ^{o}C for 10 minutes.

The third step is to coat active layer. There are a few key notices for solution preparations. The insoluble polymers, especially in the case of PFTBT, are detrimental to devices while defects can form on the spots for following aluminum deposition. Filtration is not recommended because some polymer aggregates may be filtered off and leads to poor devices. Solution preparation with heat can improve solubility of polymers. For example, I stirred the chloroform solution at 100 ^{o}C. Extra attention is necessary when opening caps. Polymer solutions may flush out of vials due to vapor pressures within vials. It is then better to slightly release the pressure before fully open the caps. If the solvent is chlorobenzene or dichlorobenzene, the films after spinning coating are usually not dry enough. It is better to wait several minutes until solvents fully evaporate before loading samples onto masks for aluminum deposition.

The fourth step is aluminum electrode deposition for 100 nm thickness. Slow deposition rate (<1 Å per second) in first 10 nm is important in order to give uniform contact at active layer-electrode interface.

Post annealing on devices is critical to further improve device performance due to enhanced crystallinity of polymers.

7.7. Conclusions

These preliminary results demonstrate that covalently linking donor and acceptor polymers can be both beneficial and detrimental to photovoltaic performance. First, the covalent linkage precludes large-scale phase separation, commonly observed in polymer-blend photovoltaic systems.[13] Large-scale phase separation is detrimental to photovoltaic performance due to the short lifetime of photoexcited states, and therefore eliminating phase separation should improve photovoltaic performance. On the other hand, most

block copolymer OPVs underperform relative to polymer-polymer blends. we demonstrate that the linking group can suppress charge recombination, resulting in very poor photovoltaic devices (<0.1 % PCE). Furthermore, even for the optimal linking group chemistry studied in this report our measurements indicate faster charge recombination compared with polymer-fullerene and polymer-polymer bulk heterojunction systems.

Thus, covalently linking donor and acceptor polymers can be detrimental to performance in at least two ways: through the formation of charge-transfer states that do not produce free charges, or through significantly increasing the rate for charge recombination. In order to address this and improve the photovoltaic performance of block copolymer OPVs, electronic coupling between donor and acceptor polymers should be decreased. Prior studies with donor-acceptor dyads[14] and with polymer-polymer blend systems[13] suggest that this can be accomplished by, for example, increasing the separation between donor and acceptor blocks.

7.8. References

(1) Robb, M. J.; Ku, S.-Y.; Hawker, C. J., *Adv. Mater.* **2013**, *25*, 5686-5700.

(2) Yassar, A.; Miozzo, L.; Gironda, R.; Horowitz, G., *Prog. Polym. Sci.* **2013**, *38*, 791-844.

(3) Guo, C.; Lin, Y.-H.; Witman, M. D.; Smith, K. A.; Wang, C.; Hexemer, A.; Strzalka, J.; Gomez, E. D.; Verduzco, R., *Nano Lett.* **2013**, *13*, 2957-2963.

(4) Johnson, K.; Huang, Y.-S.; Huettner, S.; Sommer, M.; Brinkmann, M.; Mulherin, R.; Niedzialek, D.; Beljonne, D.; Clark, J.; Huck, W. T. S.; Friend, R. H., *J. Am. Chem. Soc.* **2013**, *135*, 5074-5083.

(5) Lin, Y.-H.; Darling, S. B.; Nikiforov, M. P.; Strzalka, J.; Verduzco, R., *Macromolecules* **2012**, *45*, 6571-6579.

(6) Brabec, C. J.; Zerza, G.; Cerullo, G.; De Silvestri, S.; Luzzati, S.; Hummelen, J. C.; Sariciftci, S., *Chem. Phys. Lett.* **2001**, *340*, 232-236.

(7) Barbour, L. W.; Pensack, R. D.; Hegadorn, M.; Arzhantsev, S.; Asbury, J. B., *J. Phys. Chem.C* **2008**, *112*, 3926-3934.
(8) Guo, J.; Ohkita, H.; Benten, H.; Ito, S., *J. Am. Chem. Soc.* **2010**, *132*, 6154-6164.
(9) Etzold, F.; Howard, I. A.; Mauer, R.; Meister, M.; Kim, T.-D.; Lee, K.-S.; Baek, N. S.; Laquai, F., *J. Am. Chem. Soc.* **2011**, *133*, 9469-9479.
(10) Marsh, R. A.; Hodgkiss, J. M.; Albert-Seifried, S.; Friend, R. H., *Nano Lett.* **2010**, *10*, 923-930.
(11) Hodgkiss, J. M.; Campbell, A. R.; Marsh, R. A.; Rao, A.; Albert-Seifried, S.; Friend, R. H., *Phys. Rev. Lett.* **2010**, *104*, 177701.
(12) Zhou, Y.; Kurosawa, T.; Ma, W.; Guo, Y.; Fang, L.; Vandewal, K.; Diao, Y.; Wang, C.; Yan, Q.; Reinspach, J.; Mei, J.; Appleton, A. L.; Koleilat, G. I.; Gao, Y.; Mannsfeld, S. C. B.; Salleo, A.; Ade, H.; Zhao, D.; Bao, Z., *Adv. Mater.* **2014**, *26*, 3767-3772.
(13) McNeill, C. R.; Westenhoff, S.; Groves, C.; Friend, R. H.; Greenham, N. C., *J. Phys. Chem.C* **2007**, *111*, 19153-19160.
(14) Verhoeven, J. W.; van Ramesdonk, H. J.; Groeneveld, M. M.; Benniston, A. C.; Harriman, A., *Chem. Phys. Chem.* **2005**, *6*, 2251-2260.

Appendix A-Publication List

The publications relate to this thesis. Reprints are in Appendix B.

1. Yen-Hao Lin, Kevin G. Yager, Bridget Stewart, Rafael Verduzco, "Lamellar Structures of Solvent Annealed All-Conjugated Block Copolymers," *Soft Matter,* 2014, **4(2)**, 3817-3825.
2. Yen-Hao Lin, Kendall A. Smith, Chloe N. Kempf, Rafael Verduzco, "Synthesis and Crystallinity of All-Conjugated Poly(3-hexylthiophene) Block Copolymers," *Polymer Chemistry,* 2013, **4(2)**, 229-232.
3. Changhe Guo, Yen-Hao Lin, Mathew D. Witman, Kendall A. Smith, Cheng Wang, Alexandar Hexemer, Joseph Strzalka, Enrique D. Gomez, Rafael Verduzco, "Conjugated Block Copolymer Photovoltaics with near 3% Efficiency through Microphase Separation," *Nano Letters,* 2013, **13 (6)**, 2957-2963.
4. Yen-Hao Lin, Seth B. Darling, Maxim P. Nikiforov, Joseph Strzalka, Rafael Verduzco, "Supramolecular Conjugated Block Copolymers," *Macromolecules,* 2012, **45**, 6571-6579.
5. Yen-Hao Lin and Rafael Verduzco, "Synthesis and Process-Dependent Film Structure of All-conjugated Copolymers for Organic Photovoltaics," *The American Chemical Society Symposium of Polymer Composites for Energy Harvesting, Conversion and Storage*, 2014, Chapter 3, 49-70.

Appendix B-Reprints

Soft Matter

PAPER

View Article Online
View Journal

Cite this: DOI: 10.1039/c3sm53090f

Lamellar and liquid crystal ordering in solvent-annealed all-conjugated block copolymers†

Yen-Hao Lin,[a] Kevin G. Yager,[b] Bridget Stewart[a] and Rafael Verduzco*[a]

All-conjugated block copolymers are an emerging class of polymeric materials promising for organic electronic applications, but further progress requires a better understanding of their microstructure including crystallinity and self-assembly through micro-phase segregation. Here, we demonstrate remarkable changes in the thin film structure of a model series of all-conjugated block copolymers with varying processing conditions. Under thermal annealing, poly(3-hexylthiophene)-*b*-poly(9′,9′-dioctylfluorene) (P3HT-*b*-PF) all-conjugated block copolymers exhibit crystalline features of P3HT or PF, depending on the block ratio, and poor π–π stacking. Under chloroform solvent annealing, the block copolymers exhibit lamellar ordering, as evidenced by multiple reflections in grazing incidence wide- and small-angle X-ray scattering (GIWAXS and GISAXS), including an in-plane reflection indicative of order along the π–π stacking direction for both P3HT and PF blocks. The lamellae have a characteristic domain size of 4.2 nm, and this domain size is found to be independent of block copolymer molecular weight and block ratio. This suggests that lamellar self-assembly arises due to a combination of polymer block segregation and π–π stacking of both P3HT and PF polymer blocks. Strategies for predicting the microstructure of all-conjugated block copolymers must take into account intermolecular π–π stacking and liquid crystalline interactions not typically found in flexible coil block copolymers.

Received 12th December 2013
Accepted 26th March 2014

DOI: 10.1039/c3sm53090f

www.rsc.org/softmatter

Introduction

All-conjugated block copolymers are an emerging class of materials comprised of two or more covalently linked conjugated polymer chains. This class of block copolymers is of interest for organic electronic applications because they combine the optoelectronic properties of semiconductive polymers with structure control through micro-phase segregation[1,2] and crystallization.[3,4] As an example, recent work demonstrated significant performance enhancement in block copolymer organic photovoltaics (OPVs) compared with polymer–polymer blends.[5] However, further progress in the development of all-conjugated block copolymers requires a better understanding of the microstructure of all-conjugated block copolymers and how their crystallinity, micro-phase segregation, and domain orientation can be controlled by applying different processing strategies.

Comprehensive theoretical and experimental studies of rod–coil diblock copolymers (containing one conjugated polymer block and one flexible coil polymer block) have revealed an interplay between relative block size, polymer crystallinity, liquid crystal ordering, and micro-phase segregation.[6–11] Processing conditions have been demonstrated to give some control over the microstructure of rod–coil block copolymers, including aligned domains through the application of a magnetic field[12–15] or the formation of micellar assemblies using a selective solvent.[16] This work has led to the development of a quantitative model to describe the phase behavior of rod–coil block copolymers, including self-assembly and liquid crystal ordering.[17] Comparable predictive models are unavailable for all-conjugated block copolymers due in part to limited experimental studies on structure–processing relationships. Previous work with P3HT-based all-conjugated block copolymers have found that P3HT crystallization dominates the film morphology, suppressing micro-phase segregation and crystallization of the second polymer block.[18,19] Evidence for micro-phase segregation in rod–rod all-conjugated block copolymer has been inconclusive, potentially due to polymer crystallization, slow dynamics, stiff polymer backbones, and/or low enthalpic driving force for micro-phase segregation.[20] Improved control over the microstructure of all-conjugated block copolymers and a broader understanding of structure–processing–property relationships could benefit their development for and use in organic electronic devices and applications.

Here, we report remarkable changes in the thin film structure of a model series of all-conjugated block copolymers under different annealing conditions. Thermally annealed

[a]Department of Chemical and Biomolecular Engineering, MS-362, Rice University, 6100 Main Street, Houston, Texas 77005, USA. E-mail: rafaelv@rice.edu
[b]Center for Functional Nanomaterials, Brookhaven National Laboratory, Upton, New York 11973, USA

† Electronic supplementary information (ESI) available: NMR spectra, additional GIWAXS and GISAXS images, and POM images of films. See DOI: 10.1039/c3sm53090f

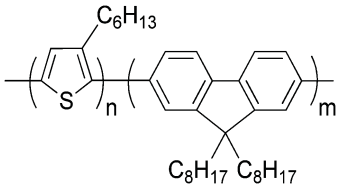

Scheme 1 Chemical structure of poly(3-hexylthiophene)-*b*-poly-(9′,9′-dioctylfluorene) (P3HT-*b*-PF).

poly(3-hexylthiophene)-*b*-poly(9′,9′-dioctylfluorene) (P3HT-*b*-PF) (Scheme 1) all-conjugated block copolymers exhibit crystalline features characteristic of P3HT or PF, but poor order along the π–π stacking direction. The same block copolymers, under solvent annealing, self-assemble into a lamellar phase, as evidenced by multiple reflections in grazing incidence wide- and small-angle X-ray scattering (GIWAXS and GISAXS). The degree of face-to-face π–π stacking substantially increases in solvent-annealed compared with unannealed films. We present a detailed analysis of the structure of P3HT-*b*-PF block copolymer films and the self-assembled lamellar phase, including paracrystallinity measurement, spectroscopic properties, and phase behaviour with temperature. These results indicate that all-conjugated block copolymers have a rich, processing-dependent microstructure determined by a combination of π–π stacking, crystallization, and micro-phase segregation of the polymer blocks.

Experimental section

Synthesis of P3HT-*b*-PF

P3HT-*b*-PF block copolymers were synthesized as reported previously.[21] Characteristics of P3HT-*b*-PF block copolymers reported in this study are listed in Table 1. ^{1}H NMR spectra are provided in the ESI Fig. S1.†

Sample preparation and processing

Sample films were prepared by drop casting from 0.05 wt% chloroform solutions onto silicon substrates and quartz substrates. Evaporation of chloroform under ambient conditions gives films with a thickness of approximately 350 nm as measured by X-ray reflectivity. Samples were solvent annealed in a closed chamber saturated with chloroform at ambient temperature and pressure for 5 days. Samples were dried under vacuum for at least 12 hours prior to measurement.

Grazing incident small- and wide-angle X-ray scattering (GIWAXS and GISAXS)

Grazing incidence small- and wide-angle X-ray scattering measurements were carried out on the X9 beamline at the National Synchrotron Light Source, Brookhaven National Laboratory. The undulator beamline was operated at an energy of 14 keV; two-dimensional images were collected using CCD area detectors. The beam size was 100 μm (h) × 50 μm (v). Sample detector distance was 370 mm for the wide-angle detector and 3091 mm for the small-angle detector. Sample measurements were carried out under vacuum which was in the range of 2–3 × 10^{-6} bar, with a temperature-controlled sample stage interfaced with a Lakeshore 340 unit. Where indicated, measurements were performed on sector 8-ID-E at Advanced Photon Source, Argonne National Laboratory. Details for these measurements are provided in the ESI.†

Differential scanning calorimetry (DSC)

Differential scanning calorimetry measurements were performed using a TA Instrument DSC Q10 with a ramp rate of 5 °C min^{-1} under N_2. Samples were placed in hermetic pans from Thermal Support, Inc. Solvent annealed samples were solvent annealed as described above for one month and dried under vacuum before measurement. All samples were subjected to at least two heating and cooling cycles between 10 °C to 250 °C.

Ultraviolet-visible absorbance spectroscopy (UV-VIS)

UV-VIS measurements were carried out with a Shimadzu UV-3101PC spectrophotometer with scan range of 200–900 nm. All films were cast on quartz substrates.

Polarized optical microscopy

Optical microscopy images of polymer films were acquired using an Axioplan 2 imaging microscope in reflective mode. Films were the same as films for GIXS measurements. Images were processed using Axio Vision version 4.8.

Results and discussions

P3HT-*b*-PF is an all-conjugated block copolymer comprised of two semi-crystalline conjugated polymer blocks (crystal melting temperatures 220 °C and 150 °C for P3HT and PF, respectively). Prior work with P3HT-*b*-PF thin films has found a morphology dominated primarily by crystallization of the P3HT or PF block

Table 1 Characteristics of all-conjugated P3HT-*b*-PF block copolymers

Polymers	P3HT[a] M_w (PDI)	BCP[a] M_w (PDI)	DP ratios[b] (P3HT wt%)
P3HT36-*b*-PF100	6.1 (1.16)	48.4 (1.86)	36 : 100 (13%)
P3HT81-*b*-PF105	13.5 (1.32)	60.6 (1.87)	81 : 105 (25%)
P3HT84-*b*-PF80	14.1 (1.10)	42.5 (1.58)	84 : 80 (33%)
P3HT84-*b*-PF13	14.1 (1.10)	22.8 (1.39)	84 : 13 (74%)

[a] M_w (kg mol^{-1}) and PDI for P3HT and block copolymers determined by comparison to a set of monodisperse polystyrene standards. Head-to-tail regioregularity of P3HT is greater than 93% for all samples as determined from ^{1}H NMR. [b] DP ratios and P3HT content were determined by ^{1}H NMR *via* comparison of the integrated intensity of P3HT aromatic peak (6.9 ppm) and fluorene alkyl peaks (2.2 ppm).

but no evidence for liquid crystal ordering or micro-phase segregation.[19,21–23] We hypothesized that long-term solvent annealing in a good solvent for both blocks would increase chain mobility, yielding improved crystallinity, new phases and/or micro-phase segregation. Similar strategies applied to flexible coil block copolymers can result in improved long-range ordering of block copolymer domains and, in some cases, new phases through micro-phase segregation.[24]

As detailed by prior work, the microstructure of P3HT and PF homopolymers is influenced by processing. Regioregular P3HT organizes into lamellar crystalline domains with face-to-face π–π stacking between chains and lamellar stacking through the hexyl side-chains.[25] In solution processed thin films, the preferred orientation of P3HT crystallites can be dictated to some extent by varying processing conditions.[26] PF exhibits crystalline, liquid crystalline, or amorphous phases depending on its processing history.[27–29]

To investigate the role of processing and annealing conditions, the microstructure of a series of P3HT-*b*-PF films with varying P3HT contents after solvent and/or thermal annealing were analyzed by grazing-incidence X-ray scattering, microscopy, UV-VIS absorbance measurements, and differential scanning calorimetry (DSC). P3HT-*b*-PF all-conjugated block copolymers with varying block ratios were synthesized *via* a combination of Grignard metathesis and Suzuki–Miyaura polycondensation. The P3HT-*b*-PF block copolymers studied have varying compositions ranging from 13 wt% of P3HT to 74 wt% of P3HT, as shown in Table 1. Samples films were drop cast from chloroform and analyzed by grazing-incidence wide- and small-angle scattering (GIWAXS and GISAXS) without annealing (as-cast), after thermal annealing, and with long-time solvent annealing (5 days at room temperature, $CHCl_3$).

Grazing incidence X-ray scattering (GIXS) analysis of P3HT-*b*-PF under varying processing conditions

Small- and wide-angle X-ray scattering (GISAXS and GIWAXS) measurements provide information on both the in-plane (q_{xy}, direction parallel to substrate) and out-of-plane (q_z, direction perpendicular to the substrate) structure of the films. Peaks or reflections in the spectra indicate periodicities in the film microstructure, which may arise due to crystallinity or self-assembly processes. More information on the application of GIWAXS and GISAXS to study block copolymer films is provided by Ree *et al.*[30]

GIWAXS measurements of P3HT-*b*-PF films are shown in Fig. 1 and ESI S2 and S3.† As-cast P3HT-*b*-PF films are amorphous and exhibit a weak in-plane reflection at $q \sim 1.45$ Å^{-1} (see ESI Fig. S2 and S3†). This in-plane reflection matches the π–π stacking reflection observed in PF homopolymer films,[31] and we therefore conclude this reflection indicates some π–π stacking of the PF polymer block in as-cast films. P3HT84-*b*-PF13 additionally exhibits weak scattering peaks characteristic of P3HT crystallites: an in-plane π–π stacking (010) peak at $q \sim 1.65$ Å^{-1} and out-of-plane (100), (200), and (300) peaks.[4,25,32]

After thermal annealing at 220 °C – beyond the crystal melting temperatures for both blocks – and cooling to 100 °C, the films exhibit characteristics of pure P3HT or PF crystallites, or both, depending on the block ratio (Fig. 1a). Thermally annealed P3HT36-*b*-PF100 films exhibit characteristics of PF α-phase crystals[33] while thermally annealed P3HT84-*b*-PF13 films show (100), (200), and (300) P3HT crystal reflections. Block copolymers with intermediate P3HT compositions, P3HT81-*b*-PF105 and P3HT84-*b*-PF80, show primarily reflections consistent with PF α-phase and some crystallization of the P3HT block. In contrast to thermally annealed P3HT homopolymer films, reflections corresponding to π–π stacking ($q \sim 1.45$ Å^{-1} and 1.65 Å^{-1} for PF and P3HT, respectively) are absent for all thermally annealed block copolymer films.

Block copolymer films subjected to 5 days of solvent annealing in a good solvent for both blocks (chloroform) exhibit multiple out-of-plane reflections indicative of long-range, lamellar ordering (Fig. 1b, 2 and 3). A primary GISAXS reflection is observed at ~0.15 Å^{-1}, which corresponds to a spacing between lamellae of approximately 4.2 nm (Fig. 2). As shown in Fig. 3, the observed peaks are separated by integral multiples of q. These reflections reveal long-range lamellar ordering in solvent annealed P3HT-*b*-PF films not present in solvent or thermally annealed pristine P3HT or PF films. By contrast, solvent annealed P3HT homopolymer exhibits a (100) crystal peak while solvent-annealed PF films exhibit a metastable liquid crystal β mesophase[34] (see ESI Fig. S4, S5, and S6†).

Solvent-annealed block copolymer films also display strong in-plane reflections at $q \sim 1.45$ Å^{-1} and $q \sim 1.65$ Å^{-1} (see ESI Fig. S7†). These reflections are characteristic of face-to-face π–π stacking for PF and P3HT, respectively. Other crystal reflections characteristic of PF or P3HT homopolymers are absent in solvent annealed films, except for P3HT84-*b*-PF13. A peak corresponding to the (100) P3HT crystal spacing ($q \sim 0.39$ Å^{-1}) is clearly evident in solvent-annealed P3HT84-*b*-PF13 (see linecut in Fig. 3). A quantitative analysis of crystalline disorder through measurements of a paracrystallinity parameter is provided below.

On heating the solvent-annealed films from room temperature to 150 °C, lamellar GISAXS and GIWAXS reflections disappear and P3HT-*b*-PF films, with the exception of P3HT84-*b*-PF13, show only diffuse scattering, with no sharp reflections or peaks. This is indicative of an amorphous or liquid crystal nematic phase (Fig. 1c). Note that 150 °C is below the crystal melting temperatures for both P3HT and PF blocks.

The presence of nematic liquid crystal ordering is confirmed by inspection of the films by polarized optical microscopy (POM), which reveals a birefringent Schlieren texture characteristic of a nematic phase for P3HT36-*b*-PF100, P3HT81-*b*-PF105, and P3HT84-*b*-PF80 (Fig. 4a–c). The block copolymer with the highest P3HT content, P3HT84-*b*-PF13, (comprised of 85 wt% P3HT) does not exhibit a nematic phase. Instead, as shown in Fig. 1c, some P3HT crystallization is evident. POM analysis of all solvent-annealed and solvent plus thermal-annealed block copolymer films are provided in the ESI Fig. S8.†

P3HT-*b*-PF films, with the exception of P3HT84-*b*-PF13, thus form a nematic phase after solvent annealing followed by heating to 150 °C and slowly cooling to room temperature. PF homopolymers exhibit a nematic phase only at temperatures

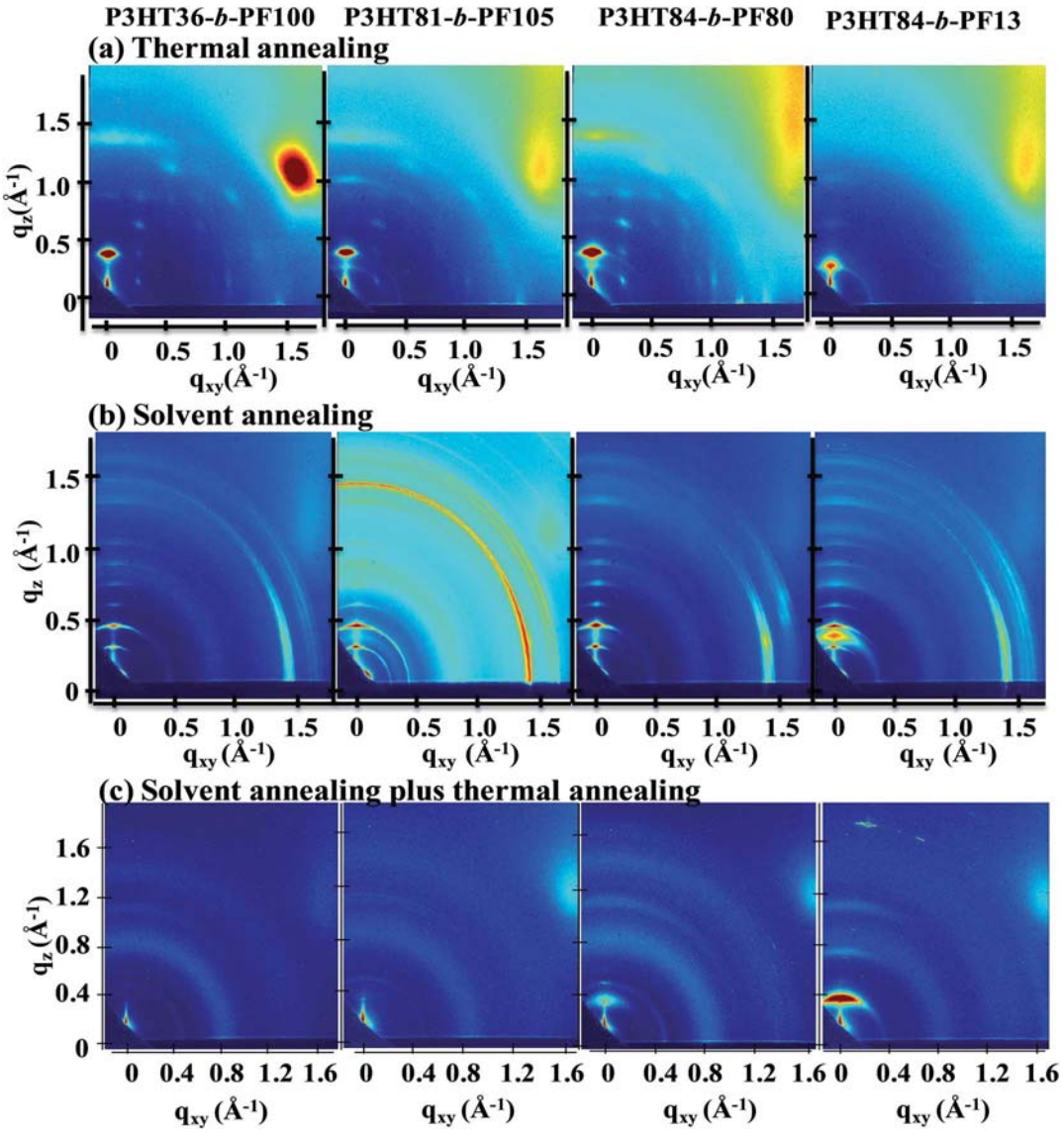

Fig. 1 GIWAXS measurements for P3HT36-*b*-PF100, P3HT81-*b*-PF105, P3HT84-*b*-PF80, P3HT84-*b*-PF13 with varying processing histories, as indicated. (a) and (b) were acquired at room temperature and (c) was acquired at 150 °C. All samples were measured at an incident angle of 0.25° and 30 seconds exposure time.

higher than the crystal melting temperature[35] or at room temperature after rapid quenching.[28,36] The enhanced stability of the nematic phase in block copolymers may be due to poor chain mobility resulting from the rigidity of polymer chains or close π–π stacking in the self-assembled lamellar phase.[37] The results also suggest that the lamellae of P3HT-*b*-PF is metastable and can be affected by elevated temperature as well as the crystallization of P3HT as shown in P3HT84-*b*-PF13.

P3HT-*b*-PF films thus exhibit remarkable changes depending on the processing history. Thermally annealed films show characteristics of P3HT or PF crystallites, but with poor order along the π–π stacking direction. Solvent-annealed films exhibit a self-assembled lamellar phase along with ordering along the π–π stacking direction. Solvent-annealed films subsequently heated to 150 °C transition to a nematic liquid crystal phase, which is stable on cooling back down to room temperature. This phase behaviour is distinct from that of P3HT or PF homopolymers. Below, we provide a proposed structure of the lamellar phase, detail the optical and thermal properties of the materials, and quantify disorder in solvent-annealed films through quantitative analysis of peak spacings and widths.

Schematic for lamellar assembly in solvent-annealed films

A schematic for the film microstructure consistent with the features of GISAXS and GIWAXS is shown in Fig. 5. P3HT and PF lamellar domains are oriented parallel to the substrate, and the primary lamellar peak reflection ($q_z \sim 0.15$ Å^{-1}) (Fig. 2 and inset Fig. 3) corresponds to a domain spacing of 4.2 nm. Peaks at $q \sim 1.45$ Å^{-1} and $q \sim 1.65$ Å^{-1} correspond to face-to-face (π–π) packing for PF and P3HT, respectively, and indicate π–π stacking along the in-plane direction, as shown schematically in

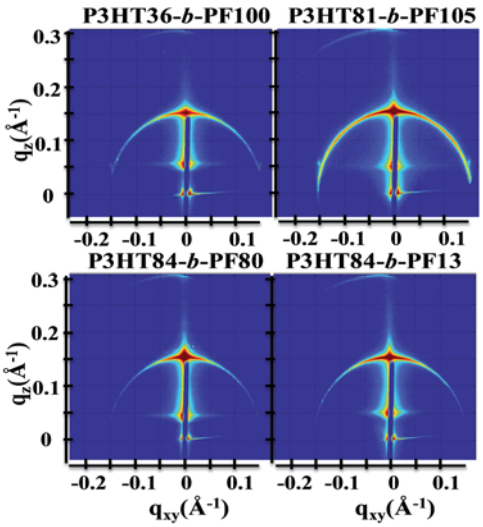

Fig. 2 GISAXS measurements for solvent-annealed P3HT36-*b*-PF100, P3HT81-*b*-PF105, P3HT84-*b*-PF80, P3HT84-*b*-PF13. Samples were analyzed at room temperature.

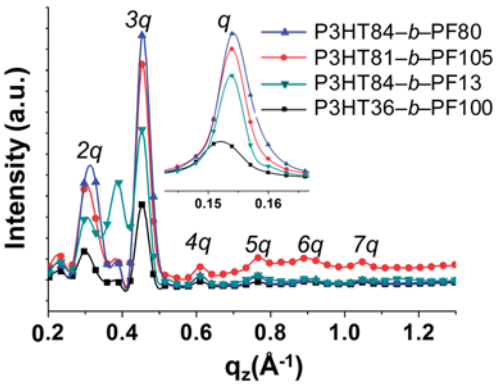

Fig. 3 Linecuts of GISAXS (imbedded figure) and GIWAXS measurements along $q_{xy} \sim 0$ Å^{-1} for solvent annealed samples.

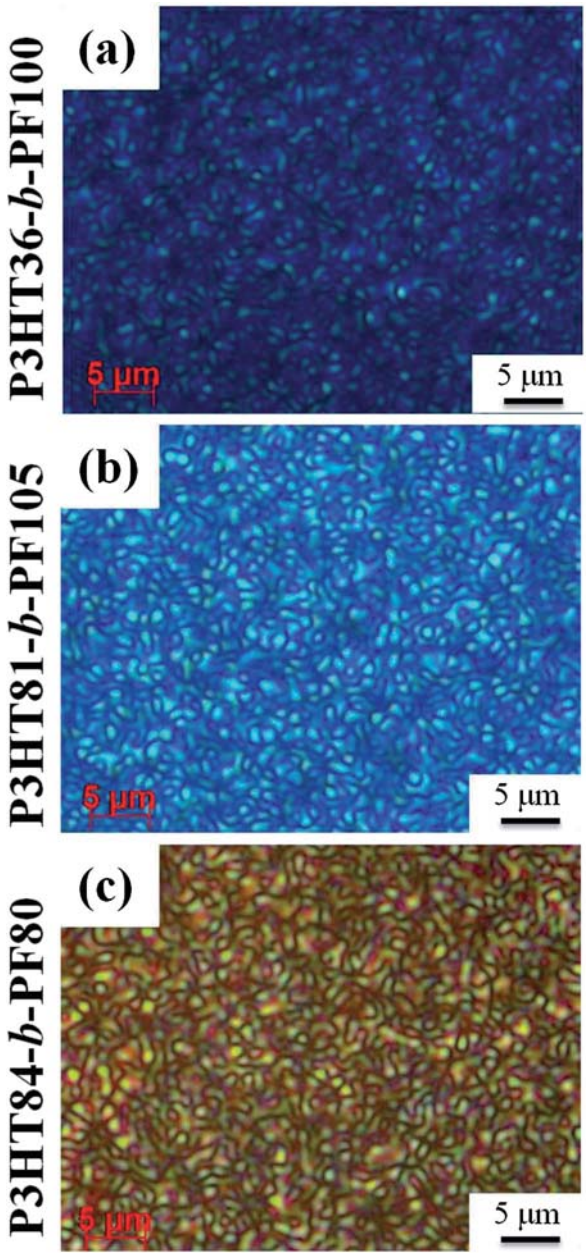

Fig. 4 Polarized optical microscopy images of P3HT-*b*-PF block copolymer thin films subjected to solvent-annealing followed by thermal annealing at 150 °C. Images were acquired at room temperature.

Fig. 5. The orientation of the face-to-face π–π stacking is perpendicular to the lamellar domains but free to rotate 180 degrees within the plane parallel to the substrate. For clarity, only one possible orientation is shown in the schematic.

The size of the lamellar domains formed after solvent annealing is invariant with block copolymer molecular weight and composition. All solvent-annealed block copolymers exhibit lamellar ordering with a characteristic domain spacing of 4.2 nm. The underlying mechanism for the formation of lamellar domains cannot be attributed to conventional microphase segregation as in coil–coil block copolymers, in which the domain spacing is dependent on the block copolymer molecular weight.[38] Instead, we propose that self-assembled lamellae arise due to a combination of polymer block segregation and π–π interactions of both P3HT and PF polymer blocks. The lamellae are expected to consist of both ordered and amorphous regions, consistent with the structure of P3HT and other semicrystalline, conjugated polymers.[39] Prior work has shown that P3HT polymer chains can be folded in amorphous regions and between crystalline domains, even with very sharp turns and folds of the P3HT backbone.[40] This allows for a single chain to occupy both ordered and amorphous domains and pass in and out of relatively small domains. As a result, the lamellar domain size (4.2 nm) is determined primarily by π–π stacking associations and is relatively unaffected by block copolymer molecular weight and composition.

An alternative possibility for the structure of solvent-annealed block copolymer films is shown schematically in the ESI Fig. S9.† In this proposed schematic, polymer backbones

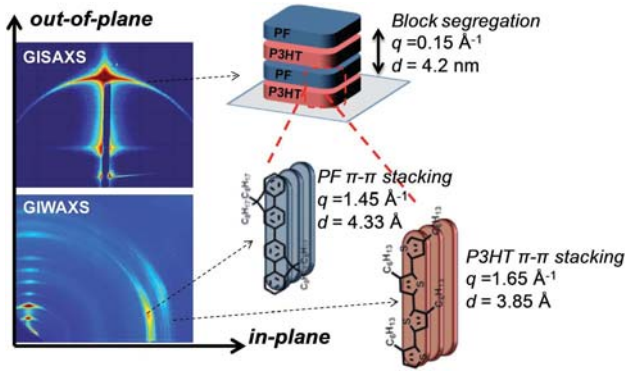

Fig. 5 Representative GISAXS and GIWAXS reflections and schematic for lamellar ordering in solvent-annealed P3HT-*b*-PF all-conjugated block copolymers.

are oriented in-plane rather than out-of-plane. As a result, the domain spacing is determined by the fully extended length of the alkyl side-chains. While this structure is consistent with the features observed by GISAXS and GIWAXS, we believe this type of ordering is unlikely due to the relatively large spacing between polymers, 4.2 nm. This would require stretching of the P3HT and PF alkyl side-chains. Additionally, the hypothetical ordering is not volume conserving due to the large space (4.2 nm) between polymer chains and close π–π stacking. As a result, the structure in Fig. 5 is the more likely possibility, but we acknowledge the potential for an alternative configuration shown in ESI Fig. S9.†

Optical and thermal properties of P3HT-*b*-PF films

UV-VIS absorbance analysis of block copolymer films can provide information about ordering and crystallinity, particularly along the π–π stacking direction. UV-VIS analysis has previously been used to study conformational changes in PF[34,36] and P3HT.[41–43] High-temperature thermally annealed block copolymer films, which exhibit a morphology dominated by crystallinity of either P3HT or PF (Fig. 1a), show only broad absorbance peaks at $\lambda \sim 390$ and 500 nm, indicative of poor π–π stacking (Fig. 6a). Similar broad peaks by UV-VIS are observed in the PF crystalline α-phase[34] and nematic phases.[34]

After solvent annealing, UV-VIS measurements reveal peaks at $\lambda \sim 522$, 560 and 603 nm in the absorption spectra, reflecting P3HT π–π stacking in all solvent annealed films. Regioregular P3HT homopolymer, ordered in the π–π stacking direction, exhibits similar peaks by UV-VIS analysis.[41–43] UV-VIS analysis also reveals peaks at $\lambda \sim 400$ and 435 nm in the absorption spectra for lamellar block copolymer films, similar to what is seen for the PF β phase.[31] This suggests that face-to-face π–π of PF and P3HT polymer blocks is enhanced in solvent-annealed films, compared with thermally annealed films.

After heating to 150 °C resulting in nematic liquid crystal ordering, sharp absorbance features characteristic of π–π stacking disappear. Nematic block copolymer films show only broad peaks in the absorption spectra at $\lambda \sim 390$ and 500 nm, similar to thermally annealed block copolymer films and

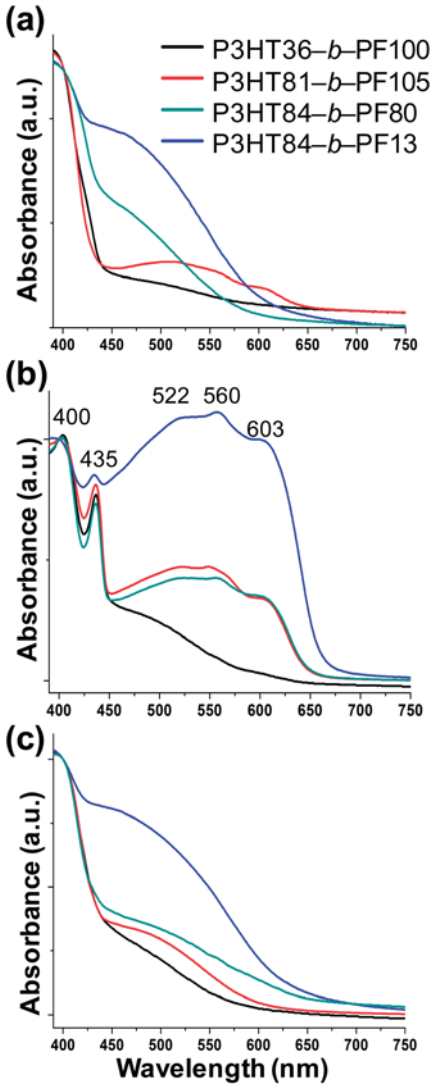

Fig. 6 UV-VIS spectra for P3HT-*b*-PF block copolymers after: (a) high-temperature thermal annealing, (b) long-term solvent annealing, and (c) long-term solvent annealing followed by 150 °C thermal annealing. All spectra were acquired at room temperature.

corresponding to poor face-to-face ordering of PF and P3HT blocks. The observed transformations in the UV-VIS spectra are thus consistent with GIWAXS measurements that indicate poor π–π stacking in crystalline and nematic block copolymer films and enhanced π–π stacking in the lamellar block copolymer phase.

Differential scanning calorimetry (DSC) reveals differences in the crystal melting temperatures for samples with different processing histories. With the exception of P3HT84-*b*-PF13, DSC measurements detect a phase transition at 145 °C in solvent-annealed block copolymer on the first heating cycle (Fig. 7a). This transition temperature is consistent with the transition to the nematic liquid crystal phase observed by GIWAXS.

For thermally annealed samples, melting transitions at roughly 157 °C and 215 °C are detected. These temperatures correspond approximately to the crystal melting temperatures of PF and P3HT, respectively.

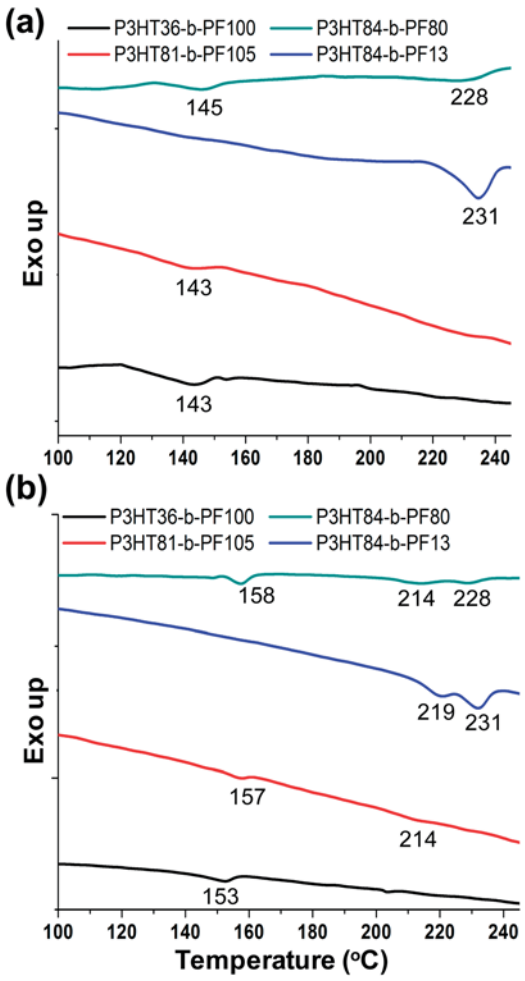

Fig. 7 DSC analysis of P3HT-*b*-PF block copolymers after (a) long-term solvent annealing and (b) thermal annealing above 220 °C.

DSC measurements thus indicate that the self-assembled lamellar phase melts near 150 °C, while thermally annealed samples exhibit crystal melting temperatures comparable to the constituent homopolymers. Similar results for thermally annealed films have been previously reported for P3HT-*b*-PF[4,21] and other all-conjugated block copolymers.[3,18,44–46] For P3HT84-*b*-PF13, only one thermal transition near 220 °C (near the crystal melting temperature of P3HT) is detected by DSC on both first and second heating cycles, suggesting that PF crystallization is suppressed in this sample due to the much higher content of P3HT in the block copolymer.

Paracrystallinity disorder analysis on lamellar ordering

Peak width analysis can provide information on disorder within crystalline or semicrystalline regions. Disorder is quantified through calculation of a paracrystallinity disorder parameter g,[47] calculated using the center (q_0) and breadth (Δq) of a peak, as shown in eqn (1).[39,48] A larger value of g indicates greater disorder. Here, we present an analysis of g for block copolymer films under different processing histories and for P3HT and PF homopolymer films. The paracrystallinity disorder parameter was measured for the out-of-plane primary lamellar spacing (Fig. 2) in GISAXS and the in-plane π–π stacking reflection (Fig. 5) in GIWAXS in solvent-annealed films.

$$g = \sqrt{\Delta q / 2\pi q_0} \quad (1)$$

Table 2 Paracrystallinity disorder (g) analysis on solvent annealed films

Spacings[a]	Samples	g (%)
π–π stacking, P3HT	P3HT36-*b*-PF100	9.68
	P3HT81-*b*-PF105	7.58
	P3HT84-*b*-PF80	9.54
	P3HT84-*b*-PF13	8.42
	Solvent ann. P3HT[b]	8.82
	Thermal ann. P3HT[b]	8.19
π–π stacking, PF	P3HT36-*b*-PF100	8.23
	P3HT81-*b*-PF105	5.18
	P3HT84-*b*-PF80	8.81
	P3HT84-*b*-PF13	7.59
	Solvent ann. PF	17.84
Primary lamellar reflection	P3HT36-*b*-PF100	9.38
	P3HT81-*b*-PF105	9.05
	P3HT84-*b*-PF80	9.44
	P3HT84-*b*-PF13	8.89

[a] π–π stacking of P3HT and PF was analyzed on GIWAXS patterns whereas 1st lamellar ordering was analyzed on GISAXS patterns. [b] Commercially available P3HT homopolymer has $M_w \sim 60$ kg mol^{-1}.

As shown in Table 2, the paracrystallinity disorder parameter g measured for P3HT π–π stacking in thermally-annealed films is in agreement with literature values ($g \sim$ 6–8%[39]). The disorder for π–π stacking of the P3HT block is slightly higher for solvent-annealed P3HT-*b*-PF compared with thermally annealed P3HT homopolymer. This is expected due to connectivity to a PF block which can increase disorder in the P3HT π–π stacking.

The paracrystallinity disorder parameter has similar values, roughly 8–10%, for PF π–π stacking and for ordering of the self-assembled lamellae. We also note that PF is more ordered along π–π direction in solvent-annealed BCPs compared with solvent annealed PF homopolymer β phase ($g \sim$ 17.84%).

Quantitative paracrystallinity disorder analysis thus indicates that ordering along the π–π stacking direction is substantially improved for solvent-annealed films compared with thermally-annealed block copolymers.

Conclusions

A combination of analytical techniques—GIXS, UV-VIS, POM and DSC—reveal novel lamellar ordering in all-conjugated P3HT-*b*-PF block copolymers after long-term solvent annealing. We observe enhanced π–π stacking in the lamella compared with either the crystal or nematic phases. These results demonstrate that all-conjugated block copolymers exhibit a rich, processing-dependent microstructure, and a quantitative description will have to account for various intermolecular

interactions including π–π stacking, steric repulsions of the alkyl side-chains, and chain rigidity. The presence of a liquid crystal phase with enhanced π–π stacking may lead to block copolymer films with superior optoelectronic properties or the use of new processing strategies, such as the application of magnetic fields,[13–15] to achieve improved alignment. The results reported for rod–rod all-conjugated block copolymers contrast with previous studies of coil–coil and rod–coil diblock copolymers. In the case of rod–coil block copolymers, self-assembly can be described through a mean field theory that includes Flory–Huggins interactions and Maier–Saupe parameter to account for liquid crystal ordering.[17] Here, we observe a qualitatively different self-assembly process driven by both π–π stacking interactions and polymer block segregation.

Acknowledgements

This work was supported by the National Science Foundation under Grant no. CBET-1264703 and Louis and Peaches Owen. Research carried out in part at the Center for Functional Nanomaterials and National Synchrotron Light Source, Brookhaven National Laboratory, which is supported by the U.S. Department of Energy, Office of Basic Energy Sciences, under Contract no. DE-AC02-98CH10886. Use of Advanced Photon Source at Argonne National Laboratory was supported by the U.S. Department of Energy, Office of Science, Office of Basic Energy Sciences, under Contract no. DE-AC02-06CH11357. B.S. acknowledges the support of the Department of Homeland Security, Office of Science and Technology, Award # 2009-ST-000031.

Notes and references

1 F. S. Bates and G. H. Fredrickson, *Phys. Today*, 1999, **52**, 32–38.
2 C. Park, J. Yoon and E. L. Thomas, *Polymer*, 2003, **44**, 6725–6760.
3 M. Sommer, H. Komber, S. Huettner, R. Mulherin, P. Kohn, N. C. Greenham and W. T. S. Huck, *Macromolecules*, 2012, **45**, 4142–4151.
4 K. A. Smith, Y.-H. Lin, D. B. Dement, J. Strzalka, S. B. Darling, D. L. Pickel and R. Verduzco, *Macromolecules*, 2013, **46**, 2636–2645.
5 C. Guo, Y.-H. Lin, M. D. Witman, K. A. Smith, C. Wang, A. Hexemer, J. Strzalka, E. D. Gomez and R. Verduzco, *Nano Lett.*, 2013, **13**, 2957–2963.
6 H. C. Moon, D. Bae and J. K. Kim, *Macromolecules*, 2012, **45**, 5201–5207.
7 C. A. Dai, W. C. Yen, Y. H. Lee, C. C. Ho and W. F. Su, *J. Am. Chem. Soc.*, 2007, **129**, 11036–11038.
8 B. D. Olsen and R. A. Segalman, *Macromolecules*, 2005, **38**, 10127–10137.
9 R. H. Lohwasser, G. Gupta, P. Kohn, M. Sommer, A. S. Lang, T. Thurn-Albrecht and M. Thelakkat, *Macromolecules*, 2013, **46**, 4403–4410.
10 S. Y. Choi, J. U. Lee, J. W. Lee, S. Lee, Y. J. Song, W. H. Jo and S. H. Kim, *Macromolecules*, 2011, 1771–1774.
11 Y. J. Lee, S. H. Kim, H. Yang, M. Jang, S. S. Hwang, H. S. Lee and K.-Y. Baek, *J. Phys. Chem. C*, 2011, **115**, 4228–4234.
12 B. McCulloch, G. Portale, W. Bras, J. A. Pople, A. Hexemer and R. A. Segalman, *Macromolecules*, 2013, **46**, 4462–4471.
13 M. Gopinadhan, P. W. Majewski, E. S. Beach and C. O. Osuji, *ACS Macro Lett.*, 2011, **1**, 184–189.
14 M. Gopinadhan, P. W. Majewski, Y. Choo and C. O. Osuji, *Phys. Rev. Lett.*, 2013, **110**, 078301.
15 H. Tran, M. Gopinadhan, P. W. Majewski, R. Shade, V. Steffes, C. O. Osuji and L. M. Campos, *ACS Nano*, 2013, **7**, 5514–5521.
16 Y.-C. Tung, W.-C. Wu and W.-C. Chen, *Macromol. Rapid Commun.*, 2006, **27**, 1838–1844.
17 B. D. Olsen, M. Shah, V. Ganesan and R. A. Segalman, *Macromolecules*, 2008, **41**, 6809–6817.
18 X. Yu, H. Yang, S. Wu, Y. Geng and Y. Han, *Macromolecules*, 2012, **45**, 266–274.
19 R. Verduzco, I. Botiz, D. L. Pickel, S. M. Kilbey, K. Hong, E. Dimasi and S. B. Darling, *Macromolecules*, 2011, **44**, 530–539.
20 M. He, F. Qiu and Z. Lin, *J. Mater. Chem.*, 2011, **21**, 17039–17048.
21 Y.-H. Lin, K. A. Smith, C. N. Kempf and R. Verduzco, *Polym. Chem.*, 2013, **4**, 229–232.
22 U. Scherf, A. Gutacker and N. Koenen, *Acc. Chem. Res.*, 2008, **41**, 1086–1097.
23 G. Tu, H. Li, M. Forster, R. Heiderhoff, L. J. Balk, R. Sigel and U. Scherf, *Small*, 2007, **3**, 1001–1006.
24 C. Sinturel, M. Vayer, M. Morris and M. A. Hillmyer, *Macromolecules*, 2013, **46**, 5399–5415.
25 H. Sirringhaus, P. J. Brown, R. H. Friend, M. M. Nielsen, K. Bechgaard, B. M. W. Langeveld-Voss, A. J. H. Spiering, R. A. J. Janssen, E. W. Meijer, P. Herwig and D. M. de Leeuw, *Nature*, 1999, **401**, 685–688.
26 R. J. Kline, M. D. McGehee, E. N. Kadnikova, J. Liu, J. M. J. Fréchet and M. F. Toney, *Macromolecules*, 2005, **38**, 3312–3319.
27 S. H. Chen, A. C. Su and S. A. Chen, *J. Phys. Chem. B*, 2005, **109**, 10067–10072.
28 M. Grell, D. D. C. Bradley, G. Ungar, J. Hill and K. S. Whitehead, *Macromolecules*, 1999, **32**, 5810–5817.
29 J. Peet, E. Brocker, Y. Xu and G. C. Bazan, *Adv. Mater.*, 2008, **20**, 1882–1885.
30 B. Lee, I. Park, J. Yoon, S. Park, J. Kim, K.-W. Kim, T. Chang and M. Ree, *Macromolecules*, 2005, **38**, 4311–4323.
31 K.-L. Tseng, J. Ruan, Y.-K. Lan, W.-Z. Wang and A.-C. Su, *Macromolecules*, 2013, **46**, 1820–1831.
32 E. Verploegen, R. Mondal, C. J. Bettinger, S. Sok, M. F. Toney and Z. Bao, *Adv. Funct. Mater.*, 2010, **20**, 3519–3529.
33 S. H. Chen, H. L. Chou, A. C. Su and S. A. Chen, *Macromolecules*, 2004, **37**, 6833–6838.
34 S. H. Chen, A. C. Su, C. H. Su and S. A. Chen, *Macromolecules*, 2005, **38**, 379–385.
35 J. Teetsov and M. Anne Fox, *J. Mater. Chem.*, 1999, **9**, 2117–2122.
36 M. Misaki, Y. Ueda, S. Nagamatsu, Y. Yoshida, N. Tanigaki and K. Yase, *Macromolecules*, 2004, **37**, 6926–6931.

37 Y.-H. Lin, S. B. Darling, M. P. Nikiforov, J. Strzalka and R. Verduzco, *Macromolecules*, 2012, **45**, 6571–6579.
38 M. W. Matsen and F. S. Bates, *Macromolecules*, 1996, **29**, 1091–1098.
39 R. Noriega, J. Rivnay, K. Vandewal, F. P. V. Koch, N. Stingelin, P. Smith, M. F. Toney and A. Salleo, *Nat. Mater.*, 2013, **12**, 1038–1044.
40 B. Grévin, P. Rannou, R. Payerne, A. Pron and J. P. Travers, *Adv. Mater.*, 2003, **15**, 881–884.
41 M. He, L. Zhao, J. Wang, W. Han, Y. Yang, F. Qiu and Z. Lin, *ACS Nano*, 2010, **4**, 3241–3247.
42 N. Kiriy, E. Jähne, H.-J. Adler, M. Schneider, A. Kiriy, G. Gorodyska, S. Minko, D. Jehnichen, P. Simon, A. A. Fokin and M. Stamm, *Nano Lett.*, 2003, **3**, 707–712.
43 S. Samitsu, T. Shimomura, S. Heike, T. Hashizume and K. Ito, *Macromolecules*, 2008, **41**, 8000–8010.
44 S.-Y. Ku, M. A. Brady, N. D. Treat, J. E. Cochran, M. J. Robb, E. J. Kramer, M. L. Chabinyc and C. J. Hawker, *J. Am. Chem. Soc.*, 2012, **134**, 16040–16046.
45 J. Wang, M. Ueda and T. Higashihara, *ACS Macro Lett.*, 2013, **2**, 506–510.
46 K. Nakabayashi and H. Mori, *Macromolecules*, 2012, **45**, 9618–9625.
47 A. M. Hindeleh and R. Hosemann, *J. Phys. C: Solid State Phys.*, 1988, **21**, 4155.
48 J. Rivnay, R. Noriega, R. J. Kline, A. Salleo and M. F. Toney, *Phys. Rev. B: Condens. Matter Mater. Phys.*, 2011, **84**, 045203.

Polymer Chemistry

www.rsc.org/polymers

Volume 4 | Number 2 | 21 January 2013 | Pages 197–416

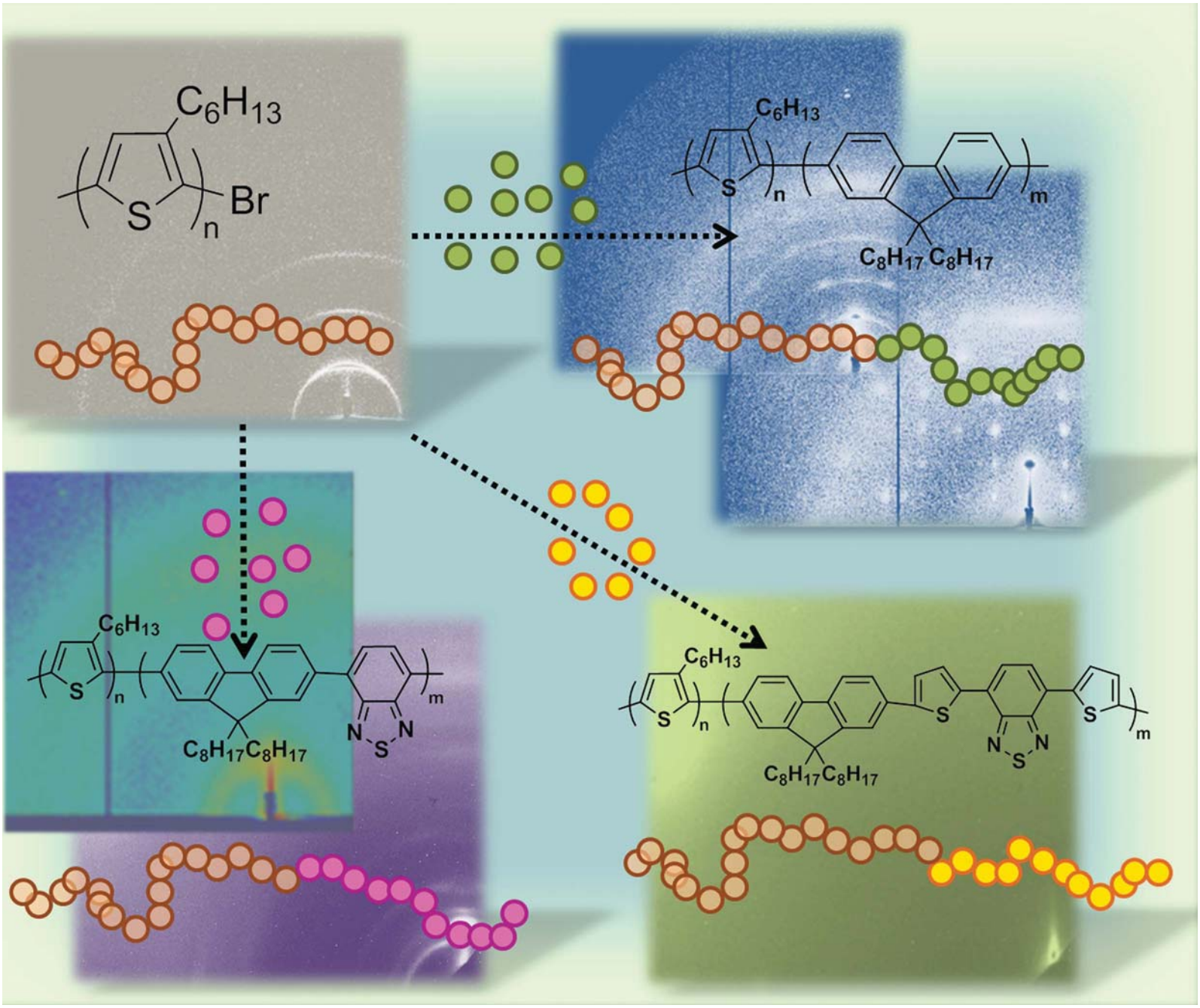

ISSN 1759-9954

RSC Publishing

COMMUNICATION

Rafael Verduzco *et al.*

Synthesis and crystallinity of all-conjugated poly(3-hexylthiophene) block copolymers

Polymer Chemistry

RSC Publishing

COMMUNICATION

Synthesis and crystallinity of all-conjugated poly(3-hexylthiophene) block copolymers†

Cite this: *Polym. Chem.*, 2013, **4**, 229

Yen-Hao Lin, Kendall A. Smith, Chloe N. Kempf and Rafael Verduzco*

Received 7th October 2012
Accepted 19th October 2012

DOI: 10.1039/c2py20830j

www.rsc.org/polymers

A simplified approach towards the synthesis of high molecular weight (M_w > 50 kg mol^{-1}) poly(3-hexylthiophene) (P3HT)-based all-conjugated block copolymers is demonstrated and applied to prepare a series of all-conjugated block copolymers. Grazing-incidence X-ray scattering measurements show that P3HT crystallization is suppressed in all-conjugated block copolymers with low (<25 wt%) P3HT content.

Block copolymers comprised of two-conjugated polymer blocks, known as all-conjugated block copolymers,[1] can potentially improve the performance of organic electronic devices, including bulk heterojunction organic photovoltaics (OPVs) and white-light emitting diodes.[2,3] All-conjugated block copolymers may provide broad absorbance, efficient charge separation, white-light emission, and both hole and electron transport. Additionally, these materials are expected to self-assemble into regular nanostructures due to a reduced entropy of mixing and a balance between nanoscale phase separation, chain stretching, and interfacial energies, and if properly designed may lead to optimal nanostructures for OPV devices.

However, studies on all-conjugated block copolymers are limited, due in large part to synthetic challenges.[1,4–15] Recent work has demonstrated the preparation of block copolythiophenes using Grignard metathesis polymerization (GRIM)[8,9,16–26] resulting in block copolymers with two p-type blocks and similar optoelectronic properties. Most approaches for making donor–acceptor all-conjugated block copolymers, which incorporate both n- and p-type polymer blocks, take advantage of distinct polymerization reactions for each polymer block, including GRIM, Suzuki–Miyaura, and Stille polymerization reactions.[5,6,15,27] A drawback of these methods is that they typically result in relatively low molecular weight block copolymers with significant amounts of homopolymer impurities that can only be removed using tedious column purification techniques.[6,15,26]

In this work, we report an improved route to the synthesis of all-conjugated block copolymers *via* GRIM and Suzuki–Miyaura polycondensation. We show that the use of a LiCl additive during GRIM allows for the preparation of high molecular weight block copolymers with little or no homopolymer impurities. This improved synthetic method is applied to the preparation of three different P3HT block copolymers. The molecular weights, polydispersities, and block ratios are measured using a combination of size-exclusion chromatography with refractive index (SEC-RI) and UV-VIS absorbance (SEC-UVVIS) detection and nuclear magnetic resonance spectroscopy (NMR) (provided in ESI†). The morphology and thermal properties of the materials are characterized using X-ray diffraction (XRD), grazing-incidence wide-angle X-ray scattering (GIWAXS), and differential scanning calorimetry (DSC). In contrast to previous work with P3HT-based block copolymers, we observe suppression of P3HT crystallinity in high molecular weight all-conjugated block copolymers, but at more balanced block ratios crystallization of both blocks is achieved. This work provides an improved synthetic method for preparing high-molecular weight all-conjugated block copolymers and the first examples of all-conjugated block copolymers with crystallinity determined by polymer block ratios.

Our synthetic strategy involves a combination of GRIM and Suzuki–Miyaura polymerizations. GRIM is first carried out to synthesize a Br end-functionalized P3HT (P3HT-Br) macroreagent, and P3HT-Br is subsequently utilized in a Suzuki–Miyaura polymerization reaction to make all-conjugated P3HT block copolymers (Scheme 1). A high degree of end functionalization of the P3HT-Br macroreagent is required to avoid residual P3HT homopolymer impurities, and this was accomplished using LiCl as an additive for the preparation of bromo-chloromagnesio-hexylthiophene monomer. LiCl has been shown to be an effective additive for accelerating Grignard formation and producing P3HT with a high degree of end-group functionality.[28–30] P3HT-Br was prepared using standard methods by the addition of Ni(dppp)Cl_2 catalyst to the monomer solution to initiate GRIM.[31] Three different sizes of P3HT were

Department of Chemical and Biomolecular Engineering, MS-362, Rice University, 6100 Main Street, Houston, Texas 77005, USA. E-mail: rafaelv@rice.edu

† Electronic supplementary information (ESI) available: Experimental methods, ^{1}H NMR spectra of all block polymers, UV-VIS spectra, SEC-UVVIS data, DSC, XRD, and temperature-dependent GIWAXS measurements. See DOI: 10.1039/c2py20830j

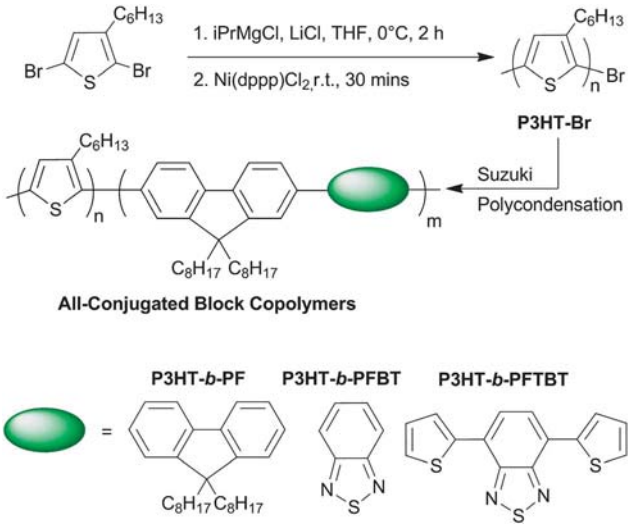

Scheme 1 Preparation of all-conjugated P3HT block copolymers *via* Grignard metathesis polymerization with LiCl additive followed by Suzuki–Miyaura polycondensation. Conditions for Suzuki–Miyaura: $Pd(PPh_3)_4$, toluene, water, 90 °C. An equimolar ratio of 9′,9′-dioctylfluorene-2′,7′-diboronic acid ester and corresponding dibromo monomer is used, as described in the ESI.†

synthesized with relatively low PDI and regioregularity higher than 93%. Next, P3HT-Br was reacted in a Suzuki–Miyaura polycondensation reaction to prepare three different types block copolymers, each with a P3HT block and a second conjugated polymer block: poly(9′,9′-dioctyl fluorene) (PF), poly(9′,9′-dioctyl fluorene-*alt*-benzothiadiazole) (PFBT), and poly(2,7-(9′,9′-dioctyl-fluorene)-*alt*-5,5-(4′,7′-di-2-thienyl-2′,1′,3′-benzothiadiazole) (PFTBT). PF, PFBT, and PFTBT have been previously studied for use in bulk-heterojunction OPVs and OLEDs,[32–34] and PFTBT may be particularly promising for use in block copolymer OPVs because it exhibits a broad absorbance and a low-lying HOMO level.[35,36] A high and low molecular weight P3HT-Br macroreagent was used for each type of block copolymer, resulting in a total of six different block copolymers, as shown in Table 1. The formation of triblock copolymers is unlikely due to a low

Table 1 Characteristics of all-conjugated P3HT block copolymers

Polymers	P3HT[a] M_w (PDI)	BCP[a] M_w (PDI)	DP ratios[b] (P3HT wt%)
P3HT36-*b*-PF100	6.1 (1.16)	48.4 (1.86)	36 : 100 (13%)
P3HT81-*b*-PF105	13.5 (1.32)	60.6 (1.87)	81 : 105 (25%)
P3HT51-*b*-PFBT66	8.5 (1.19)	168 (3.61)	51 : 66 (20%)
P3HT81-*b*-PFBT90	13.5 (1.32)	81.5 (2.24)	81 : 90 (22%)
P3HT51-*b*-PFTBT17	8.5 (1.19)	19.7 (1.49)	51 : 17 (42%)
P3HT81-*b*-PFTBT12	13.5 (1.32)	N/A[c]	81 : 12 (62%)

[a] M_w (kg mol^{-1}) and PDI for P3HT and block copolymers determined by comparison to a set of monodisperse polystyrene standards. Head-to-tail regioregularity of P3HT is greater than 93% for all samples as determined from ^{1}H NMR. [b] DP ratios and P3HT content were determined by ^{1}H NMR *via* comparison of the integrated intensity of P3HT aromatic peak (6.9 ppm) and fluorene alkyl peaks (2.2 ppm). [c] P3HT81-*b*-PFTBT12 contains primarily homopolymer impurities, and therefore an estimate for block copolymer molecular weight is not provided.

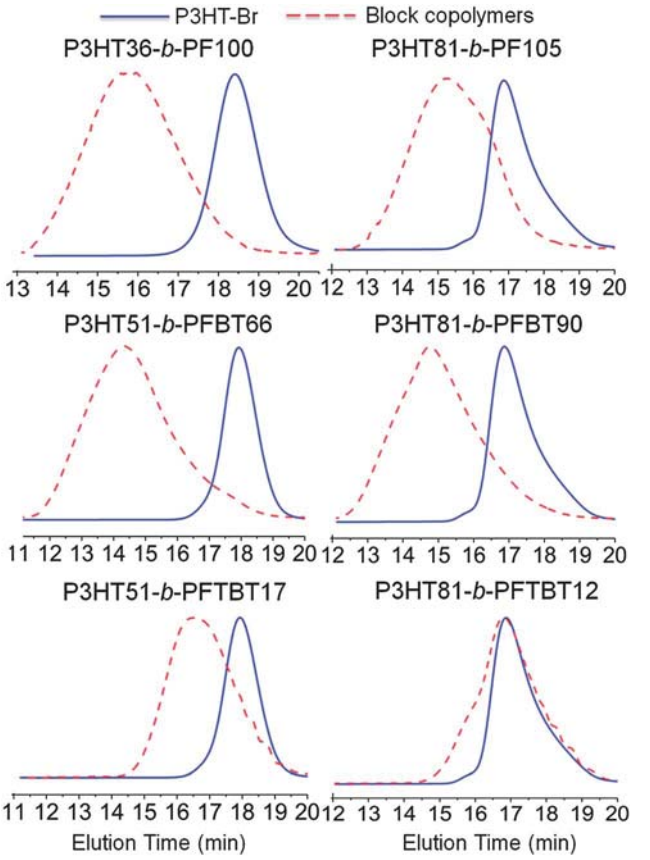

Fig. 1 SEC-RI analysis of block copolymers and corresponding P3HT-Br macroreagents. Intensities are normalized for clarity.

content of P3HT-Br macroreagent used in the Suzuki–Miyaura polycondensation step (roughly 1 mole% relative to monomers).

A comparison of the characteristics of final block copolymer products produced (Fig. 1 and Table 1) with previous reports using similar methods[6,15] indicates that the use of an LiCl additive enables the preparation of much cleaner and higher molecular weight block copolymers. With the exception of P3HT81-*b*-PFTBT12, a clear shift in the molecular weight distribution of the final products is observed relative to the starting P3HT homopolymers. For comparison, our previous attempts at making similar all-conjugated block copolymers using similar methods (but without the LiCl additive) resulted in only modest shifts in the molecular weight distribution along with homopolymer impurities.[15] Other reports using similar synthetic methods report the presence of significant homopolymer impurities or relatively low molecular weights for the second polymer block.[6,26] The clear shift in the molecular weight distributions of the block copolymer products shown in Fig. 1 indicates that little or no residual P3HT homopolymer remains, and all-conjugated block copolymers with a mass-averaged molecular weight M_w as high as 168 kg mol^{-1} (relative to polystyrene) are produced. Number-averaged molecular weights for each block estimated by SEC-RI are in relatively good agreement with ^{1}H NMR estimates of P3HT content of the final block copolymers (see Table 1 and ESI, Fig. S1–S3†). In the case of P3HT81-*b*-PFTBT12, the synthesis failed to produce significant amounts of block copolymer due to poor solubility of the PFTBT block and the resulting block

copolymer. However, the use of a lower molecular weight P3HT macroreagent in the polycondensation reaction of PFTBT resulted in product with majority block copolymer in P3HT51-*b*-PFTBT17.

Analysis of the final product using SEC with UV-VIS absorbance detection (SEC-UVVIS) provides additional information on homopolymer impurities (see ESI, Fig. S4 and S5†). By using two different wavelengths for analysis, the molecular weight distributions for each polymer block can be obtained (see ESI† for details of this analysis). For all BCP samples except for P3HT81-*b*-PFTBT12, SEC-UVVIS analysis indicates clean block copolymer product – a clear shift in the SEC-UVVIS traces corresponding to P3HT is observed as well a good match between SEC-UVVIS traces at both wavelengths. The purity of the final product is better for block copolymers with shorter P3HT blocks; both P3HT36-*b*-PF100 and P3HT51-*b*-PFBT66 exhibit excellent overlap between SEC-UVVIS traces corresponding to both polymer blocks, while some high molecular weight P3HT homopolymer may be present in P3HT81-*b*-PF105 and P3HT81-*b*-PFBT90. In the case of P3HT51-*b*-PFTBT17, some high molecular weight PFTBT homopolymer is present, but the product is primarily block copolymer. Deconvolution of the SEC-RI trace gives an estimate of approximately 15% for PFTBT homopolymer impurities in the final P3HT51-*b*-PFTBT17 product.

Altogether, SEC-RI and SEC-UVVIS indicate the formation of clean all-conjugated block copolymer products. The synthetic method enables the preparation of all-conjugated block copolymers with high molecular weights (M_w up to 168 kg mol^{-1}) and with varying molecular weight of the P3HT block. Importantly, the synthetic method is straightforward to implement, scalable, and provides the final product in good overall yield.

Prior studies on P3HT block copolymers have found that P3HT crystallization can dominate the morphology, suppressing microphase segregation and crystallization of the second block.[18,37–39] Here, we are able to test whether this holds true in large (M_w > 50 kg mol^{-1}) all-conjugated block copolymers with a semi-crystalline polymer block attached to a minority P3HT block. For all block copolymers, DSC indicates that the crystallization of P3HT is suppressed or shifted to lower temperatures, and as expected the effect is more pronounced in block copolymers with lower P3HT block ratios (Fig. S6†). For block copolymers with larger P3HT blocks, P3HT81-*b*-PF105 and P3HT81-*b*-PFBT90, a crystallization transition is observed at approximately 214 °C, a roughly 10 °C decrease in the crystallization temperature relative to the corresponding P3HT-Br macroreagent. P3HT crystallization is not observed for P3HT51-*b*-PFBT66 while the decrease in the crystallization temperature is approximately 15 and 20 °C for P3HT36-*b*-PF100 and P3HT51-*b*-PFTBT17, respectively. P3HT81-*b*-PFTBT12 exhibits a transition near 224 °C matching that of the corresponding P3HT-Br homopolymer, as expected due to the presence of P3HT homopolymer impurities. In the case of P3HT36-*b*-PF100, as discussed below, GIWAXS analysis indicates that the observed transition at 153 °C corresponds primarily to crystallization of the PF block. Only P3HT81-*b*-PF105 exhibits two transitions; one at 214 °C corresponding to P3HT crystallization and a second near 150 °C, corresponding to PF crystallization.

XRD (Fig. S7†) and GIWAXS (Fig. 2 and Fig. S8†) analysis confirms the low content of P3HT crystallinity in the block copolymer samples. P3HT-*b*-PFBT and P3HT-*b*-PFTBT block

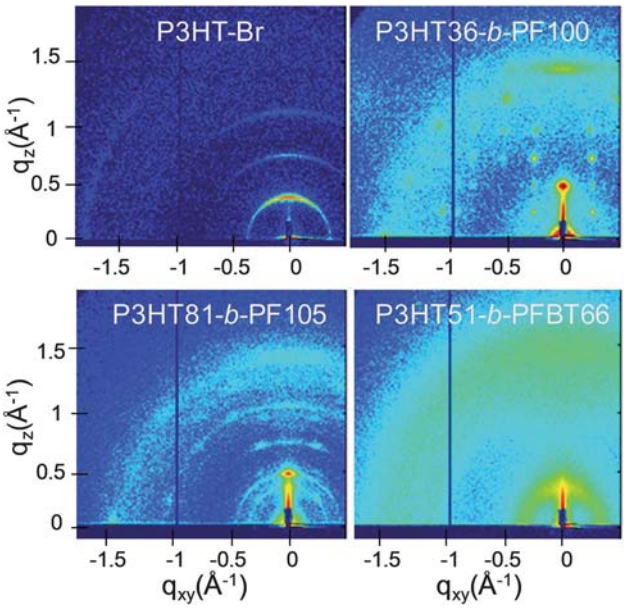

Fig. 2 GIWAXS measurement for P3HT-Br, P3HT36-*b*-PF100, P3HT81-*b*-PF105, and P3HT51-*b*-PFBT66. All samples were thermally annealed at 230 °C and measured at 80 °C. Samples were measured at an incident angle of 0.25° and 20 seconds exposure time. All images plotted using the same color scale for the scattered intensity.

copolymers show only broad scattering peaks, while P3HT-*b*-PF block copolymers exhibit crystalline peaks corresponding primarily to PF crystallites. Highly oriented crystallites are observed in P3HT36-*b*-PF100 films with features characteristic of the PF phase,[40] confirming that the DSC transition near 150 °C reflects PF crystallization. In the case of P3HT81-*b*-PF105, both P3HT and PF crystallinities are observed, but P3HT crystallite peaks are less pronounced. Quantitative analysis of the GIWAXS pattern for P3HT81-*b*-PF105 shows scattering peaks at $q_z = 0.38$, 0.75, and 1.12 Å^{-1} corresponding to the (100), (200), and (300) reflections for P3HT crystallites and a scattering peak at $q_z = 0.50$ Å^{-1} corresponding to PF crystallites (see ESI, Fig. S8b†). This is consistent with DSC measurements that show both a PF and a P3HT crystallization transition for P3HT81-*b*-PF105, the latter which is shifted to lower temperatures relative to the corresponding P3HT-Br macroreagent. Altogether, DSC, XRD, and GIWAXS results show that P3HT crystallization is reduced or suppressed in high molecular weight all-conjugated P3HT block copolymers, and at more balanced block ratios both blocks can crystallize.

In conclusion, we demonstrate a straightforward, versatile, and scalable synthetic route to prepare block copolymers comprised of a poly(alkyl thiophene) block and second polymer block made *via* Suzuki–Miyaura polycondensation, and block copolymers with M_w > 50 kg mol^{-1} are achieved. Analysis of different all-conjugated block copolymers indicates that P3HT crystallinity is reduced or completely suppressed in all-conjugated P3HT block copolymers. These results indicate that proper balance of block ratios is important for the development of all-conjugated block copolymers for use in OPVs.

Acknowledgements

This work was carried out with support from the Welch Foundation for Chemical Research (Grant #C-1750), the Shell Center for Sustainability, and Louis and Peaches Owen. Use of the Center for Nanoscale Materials and Advanced Photon Source at Argonne National Laboratory was supported by the U. S. Department of Energy, Office of Science, Office of Basic Energy Sciences, under Contract no. DE-AC02-06CH11357. Research carried out in National Synchrotron Light Source, Brookhaven National Laboratory, which is supported by the U.S. Department of Energy, Office of Basic Energy Sciences, under Contract no. DE-AC02-98CH10886.

Notes and references

1 U. Scherf, A. Gutacker and N. Koenen, *Acc. Chem. Res.*, 2008, **41**, 1086–1097.
2 R. A. Segalman, B. McCulloch, S. Kirmayer and J. J. Urban, *Macromolecules*, 2009, **42**, 9205–9216.
3 S. B. Darling, *Energy Environ. Sci.*, 2009, **2**, 1266–1273.
4 I. Botiz, R. D. Schaller, R. Verduzco and S. B. Darling, *J. Phys. Chem. C*, 2011, **115**, 9260–9266.
5 R. C. Mulherin, S. Jung, S. Huettner, K. Johnson, P. Kohn, M. Sommer, S. Allard, U. Scherf and N. C. Greenham, *Nano Lett.*, 2011, **11**, 4846–4851.
6 M. Sommer, H. Komber, S. Huettner, R. Mulherin, P. Kohn, N. C. Greenham and W. T. S. Huck, *Macromolecules*, 2012, **45**, 4142–4151.
7 K. B. Woody, B. J. Leever, M. F. Durstock and D. M. Collard, *Macromolecules*, 2011, **44**, 4690–4698.
8 S. Wu, L. Bu, L. Huang, X. Yu, Y. Han, Y. Geng and F. Wang, *Polymer*, 2009, **50**, 6245–6251.
9 Y.-C. Lai, K. Ohshimizu, A. Takahashi, J.-C. Hsu, T. Higashihara, M. Ueda and W.-C. Chen, *J. Polym. Sci., Part A: Polym. Chem.*, 2011, **49**, 2577–2587.
10 F. Ouhib, A. Khoukh, J.-B. Ledeuil, H. Martinez, J. Desbrières and C. Dagron-Lartigau, *Macromolecules*, 2008, **41**, 9736–9743.
11 K. Ohshimizu, A. Takahashi, T. Higashihara and M. Ueda, *J. Polym. Sci., Part A: Polym. Chem.*, 2011, **49**, 2709–2714.
12 S.-S. Sun, C. Zhang, A. Ledbetter, S. Choi, K. Seo, C. E. Bonner, Jr, M. Drees and N. S. Sariciftci, *Appl. Phys. Lett.*, 2007, **90**, 043117.
13 X. L. Chen and S. A. Jenekhe, *Macromolecules*, 1996, **29**, 6189–6192.
14 X. Xiao, Y. Fu, M. Sun, L. Li and Z. Bo, *J. Polym. Sci., Part A: Polym. Chem.*, 2007, **45**, 2410–2424.
15 R. Verduzco, I. Botiz, D. L. Pickel, S. M. Kilbey, K. Hong, E. Dimasi and S. B. Darling, *Macromolecules*, 2011, **44**, 530–539.
16 A. Gutacker, S. Adamczyk, A. Helfer, L. E. Garner, R. C. Evans, S. M. Fonseca, M. Knaapila, G. C. Bazan, H. D. Burrows and U. Scherf, *J. Mater. Chem.*, 2010, **20**, 1423–1430.
17 S.-Y. Ku, M. A. Brady, N. D. Treat, J. E. Cochran, M. J. Robb, E. J. Kramer, M. L. Chabinyc and C. J. Hawker, *J. Am. Chem. Soc.*, 2012, **134**, 16040–16046.
18 X. Yu, H. Yang, S. Wu, Y. Geng and Y. Han, *Macromolecules*, 2012, **45**, 266–274.
19 P.-T. Wu, G. Ren, F. S. Kim, C. Li, R. Mezzenga and S. A. Jenekhe, *J. Polym.Sci., Part A: Polym. Chem.*, 2010, **48**, 614–626.
20 A. E. Javier, S. R. Varshney and R. D. McCullough, *Macromolecules*, 2010, **43**, 3233–3237.
21 J. Hollinger, A. A. Jahnke, N. Coombs and D. S. Seferos, *J. Am. Chem. Soc.*, 2010, **132**, 8546–8547.
22 J. Ge, M. He, F. Qiu and Y. Yang, *Macromolecules*, 2010, **43**, 6422–6428.
23 Y. Zhang, K. Tajima and K. Hashimoto, *Macromolecules*, 2009, **42**, 7008–7015.
24 P.-T. Wu, G. Ren, C. Li, R. Mezzenga and S. A. Jenekhe, *Macromolecules*, 2009, **42**, 2317–2320.
25 Y. Zhang, K. Tajima, K. Hirota and K. Hashimoto, *J. Am. Chem. Soc.*, 2008, **130**, 7812–7813.
26 C.-C. Chueh, T. Higashihara, J.-H. Tsai, M. Ueda and W.-C. Chen, *Org. Electron.*, 2009, **10**, 1541–1548.
27 G. Tu, H. Li, M. Forster, R. Heiderhoff, L. J. Balk, R. Sigel and U. Scherf, *Small*, 2007, **3**, 1001–1006.
28 R. H. Lohwasser and M. Thelakkat, *Macromolecules*, 2011, **44**, 3388–3397.
29 W. M. Kochemba, S. M. Kilbey and D. L. Pickel, *J. Polym. Sci., Part A: Polym. Chem.*, 2012, **50**, 2762–2769.
30 A. Takahashi, Y. Rho, T. Higashihara, B. Ahn, M. Ree and M. Ueda, *Macromolecules*, 2010, **43**, 4843–4852.
31 R. S. Loewe, P. C. Ewbank, J. S. Liu, L. Zhai and R. D. McCullough, *Macromolecules*, 2001, **34**, 4324–4333.
32 P. Herguth, X. Jiang, M. S. Liu and A. K. Y. Jen, *Macromolecules*, 2002, **35**, 6094–6100.
33 Y. Kim, S. Cook, S. A. Choulis, J. Nelson, J. R. Durrant and D. D. C. Bradley, *Chem. Mater.*, 2004, **16**, 4812–4818.
34 A. Calabrese, G. Schimperna, R. Po, T. Yohannes, S. E. Debebe, F. Tinti and N. Camaioni, *J. Appl. Phys.*, 2011, **110**, 113106.
35 W.-Y. Lee, K.-F. Cheng, T.-F. Wang, C.-C. Chueh, W.-C. Chen, C.-S. Tuan and J.-L. Lin, *Macromol. Chem. Phys.*, 2007, **208**, 1919–1927.
36 W.-Y. Lee, K.-F. Cheng, T.-F. Wang, W.-C. Chen and F.-Y. Tsai, *Thin Solid Films*, 2010, **518**, 2119–2123.
37 S. Y. Choi, J. U. Lee, J. W. Lee, S. Lee, Y. J. Song, W. H. Jo and S. H. Kim, *Macromolecules*, 2011, 1771–1774.
38 C. A. Dai, W. C. Yen, Y. H. Lee, C. C. Ho and W. F. Su, *J. Am. Chem. Soc.*, 2007, **129**, 11036–11038.
39 Y. J. Lee, S. H. Kim, H. Yang, M. Jang, S. S. Hwang, H. S. Lee and K.-Y. Baek, *J. Phys. Chem. C*, 2011, **115**, 4228–4234.
40 S. H. Chen, H. L. Chou, A. C. Su and S. A. Chen, *Macromolecules*, 2004, **37**, 6833–6838.

NANO LETTERS

Letter

pubs.acs.org/NanoLett

Conjugated Block Copolymer Photovoltaics with near 3% Efficiency through Microphase Separation

Changhe Guo,[†,¶] Yen-Hao Lin,[§,¶] Matthew D. Witman,[†] Kendall A. Smith,[§] Cheng Wang,[∥] Alexander Hexemer,[∥] Joseph Strzalka,[⊥] Enrique D. Gomez,*[,†,‡] and Rafael Verduzco*[,§]

[†]Department of Chemical Engineering and [‡]Materials Research Institute, The Pennsylvania State University, University Park, Pennsylvania 16802, United States

[§]Department of Chemical and Biomolecular Engineering, Rice University, Houston, Texas 77005, United States

[∥]Advanced Light Source, Lawrence Berkeley National Laboratory, Berkeley, California 94720, United States

[⊥]X-ray Science Division, Argonne National Laboratory, Argonne, Illinois 60439, United States

S *Supporting Information*

ABSTRACT: Organic electronic materials have the potential to impact almost every aspect of modern life including how we access information, light our homes, and power personal electronics. Nevertheless, weak intermolecular interactions and disorder at junctions of different organic materials limit the performance and stability of organic interfaces and hence the applicability of organic semiconductors to electronic devices. Here, we demonstrate control of donor−acceptor heterojunctions through microphase-separated conjugated block copolymers. When utilized as the active layer of photovoltaic cells, block copolymer-based devices demonstrate efficient photoconversion well beyond devices composed of homopolymer blends. The 3% block copolymer device efficiencies are achieved without the use of a fullerene acceptor. X-ray scattering results reveal that the remarkable performance of block copolymer solar cells is due to self-assembly into mesoscale lamellar morphologies with primarily face-on crystallite orientations. Conjugated block copolymers thus provide a pathway to enhance performance in excitonic solar cells through control of donor−acceptor interfaces.

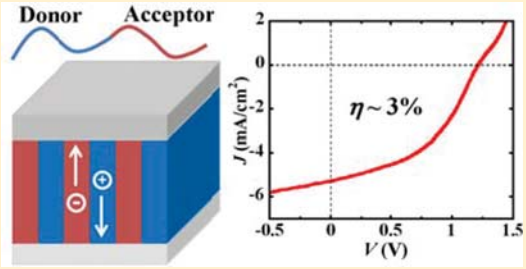

KEYWORDS: *Self-assembly, organic solar cells, all-conjugated block copolymers, RSOXS, GIWAXS*

Excitonic photovoltaics are a class of devices where donor−acceptor interfaces are critical for photogeneration of charges and efficient device performance.[1−4] In contrast to many inorganic semiconductors where optical excitations generate delocalized free charge carriers, current generation in organic photovoltaics depends on dissociation of tightly bound charge transfer states near donor−acceptor interfaces. For instance, a recent model by Giebink et al. suggests that tuning the electronic coupling at donor/acceptor interfaces is crucial to minimizing the recombination rate of charge transfer states while maintaining yields of exciton dissociation near unity.[5] It follows that tuning the chemical structure and local order at organic heterojunctions is a requirement to access the full potential of organic solar cell materials. Unfortunately, organic solar cells rely on kinetically trapped, partially phase-separated structures of donor/acceptor mixtures to create a high surface area for exciton dissociation and networks of bicontinuous phases for charge extraction.[6−12] As a consequence, molecular control of the interface in state-of-the-art organic photovoltaics is nearly impossible.

Microphase-separated block copolymers comprised of electron donor and electron acceptor polymers can address many of the current challenges in morphology and interfacial structure control for photovoltaics. The equilibrium self-assembly of block copolymers into mesoscale (5−500 nm) well-ordered morphologies where interfaces are governed by moieties near the junction between blocks[13,14] is ideal for the active layer of organic solar cells. While several examples of block copolymers with donor and acceptor blocks have been reported, the majority contain a nonconjugated insulating backbone in at least one polymer block and consequently do not directly control donor/acceptor interfaces.[15−20] Recent work has demonstrated significant progress in the design, synthesis, and characterization of fully conjugated block copolymers,[21−23] but it remains a challenge to achieve efficient charge photogeneration in photovoltaic device architectures.

We demonstrate that poly(3-hexylthiophene)−*block*−poly((9,9-dioctylfluorene)-2,7-diyl-alt-[4,7-bis(thiophen-5-yl)-2,1,3-benzothiadiazole]-2′,2″-diyl) (P3HT-*b*-PFTBT) block copolymers can be utilized as the active layer for efficient photovoltaic device operation. These block copolymers self-assemble to form in-plane lamellar morphologies with alternating electron donor and acceptor domains and a dominant face-on orientation in the crystalline P3HT block. Even without the

Received: April 20, 2013
Revised: May 14, 2013
Published: May 20, 2013

   dx.doi.org/10.1021/nl401420s | *Nano Lett.* 2013, 13, 2957−2963

use of fullerene, we obtain efficiencies near 3%, remarkable open-circuit voltages of 1.2 V, and short-circuit currents above 5 mA/cm^2 from block copolymer devices. These results demonstrate that conjugated block copolymers are a viable strategy for morphology and interfacial control for high performance organic solar cells.

The structure of P3HT, PFTBT, and P3HT-*b*-PFTBT are shown in Figure 1a. P3HT-*b*-PFTBT is roughly symmetric in composition with 56 wt % P3HT and a total weight-averaged molecular weight of 29 kg/mol. The energy levels of PFTBT as an electron acceptor are well aligned with those of P3HT as an electron donor, such that the difference between the lowest unoccupied molecular orbital of PFTBT (~ 3.5 eV)[24] and the highest occupied molecular orbital of P3HT (~ 4.9 eV)[25] can yield open-circuit voltages above 1 V. High open-circuit voltages have indeed been demonstrated for solar cells where the active layer is comprised of blends of P3HT and other dioctylfluorene bisthienyl-benzothiadiazole alternating copolymers,[25] ternary blends composed of similar conjugated block copolymers as P3HT-*b*-PFTBT with donor and acceptor homopolymers,[26] or polymer blends with fluorene benzothiadiazole alternating copolymers as acceptor molecules.[27−29]

Solar cell devices with P3HT/PFTBT blends as active layers are compared with devices comprised of P3HT-*b*-PFTBT block copolymers in Figure 1b. All devices have an active layer thickness of 60−70 nm and were thermally annealed after deposition of the cathode (Al). As shown in Table 1, devices made from P3HT/PFTBT blends exhibit a maximum power conversion efficiency of 1.0%, which is comparable to the performance reported previously for devices that utilize blends of P3HT and PFTBT-based polymers as the active layer.[25] Solar cells made from P3HT/PFTBT blends are optimized at 1:2 weight ratios of P3HT/PFTBT after annealing at 100 °C for 20 min. Longer annealing times or higher annealing temperatures lead to a drop in performance, potentially due to macroscopic phase separation.

If the active layer is comprised of P3HT-*b*-PFTBT block copolymers, devices yield average efficiencies of 1.5% under annealing conditions optimal for polymer blend devices (100 °C for 20 min) and higher efficiencies of around 1.7% with an extended annealing time of 90 min at 100 °C (Table 1). Optimal performance, however, is achieved at higher annealing temperatures. After annealing for 10 min at 165 °C, average power conversion efficiencies of 2.7 ± 0.4% with short-circuit currents (J_{sc}) of 5.0 ± 0.3 mA/cm^2, open-circuit voltages (V_{oc}) of 1.14 ± 0.08 V and fill factors of 0.45 ± 0.02 were measured for devices under simulated solar conditions made from block copolymers. The nearly 3-fold increase in device performance with respect to optimized devices comprised of polymer blends is due to enhancements of the short-circuit currents and fill factors. Nevertheless, fill factors in all of our devices do not exceed 0.5, a result of the inflection point near open-circuit conditions visible in the current−voltage characteristics shown in Figure 1. We attribute the presence of an inflection point to problems in charge extraction due to either an imbalance in charge transport or accumulation of charge at an interface.[30,31] As shown in Table 2, the best overall efficiency among our devices was recorded at 3.1% with an open-circuit voltage of 1.23 V. This device performance is remarkable for solar cells based on donor−acceptor block copolymers[15−17,32,33] and for nonfullerene solution-processed organic solar cells.[34−37]

The absorption spectrum of pristine P3HT-*b*-PFTBT films and external quantum efficiency (EQE) of P3HT-*b*-PFTBT devices annealed at 165 °C are shown in Figure 1c. The absorption profiles of P3HT-*b*-PFTBT films preserve the features of the constituent homopolymers and a similar optical bandgap (~2 eV) as P3HT is deduced from the absorption edge (see Figure S1 in the Supporting Information). Optimized

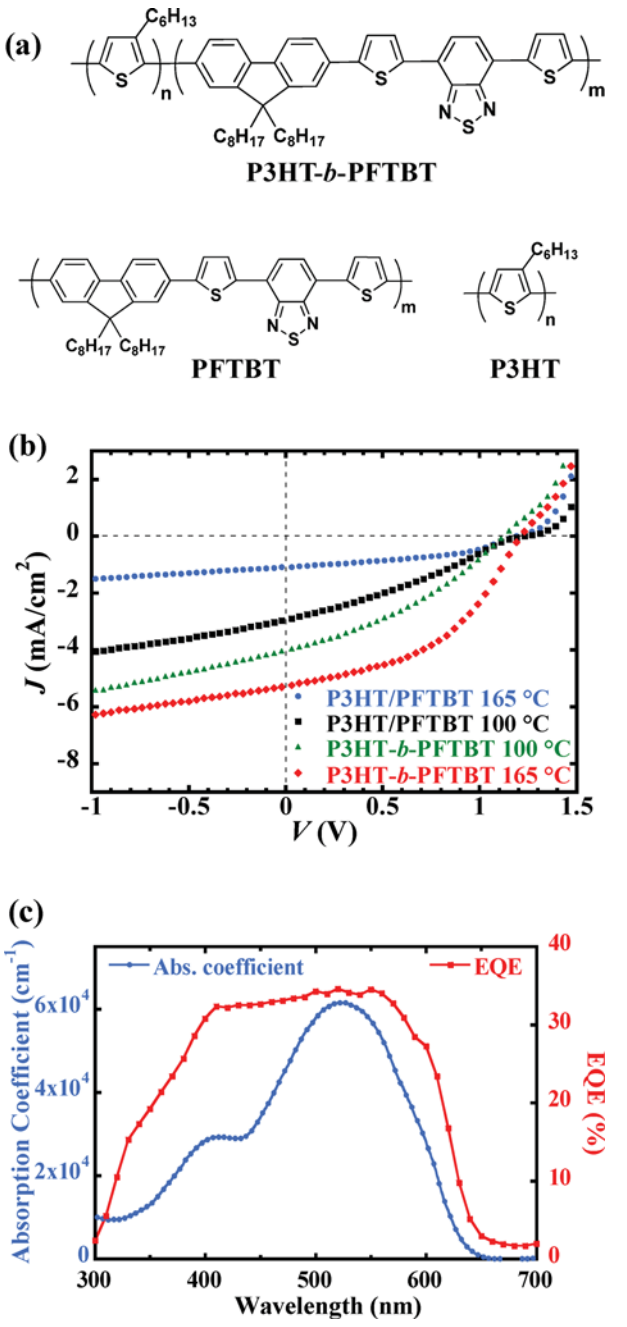

Figure 1. Photovoltaic device performances of block copolymer P3HT-*b*-PFTBT and polymer blend P3HT/PFTBT solar cells at different annealing temperatures. (a) Chemical structures of P3HT-*b*-PFTBT, PFTBT, and P3HT. (b) Current−voltage characteristics of P3HT/PFTBT (1:2 by mass) and P3HT-*b*-PFTBT photovoltaic devices annealed at 100 °C for 20 min and 165 °C for 10 min, respectively. P3HT/PFTBT solar cells are optimized at 100 °C for 20 min, while P3HT-*b*-PFTBT devices are optimized at 165 °C for 10 min. Devices were measured under simulated AM 1.5G irradiation with intensity of 97 mW/cm^2. (c) UV−visible absorption spectrum of a P3HT-*b*-PFTBT film and EQE characteristics of a P3HT-*b*-PFTBT solar cell annealed at optimized conditions (165 °C for 10 min).

dx.doi.org/10.1021/nl401420s | *Nano Lett.* 2013, 13, 2957−2963

Table 1. Device Characteristics[a] of P3HT/PFTBT Blend and P3HT-*b*-PFTBT Block Copolymer Solar Cells at Different Annealing Conditions

	efficiency (%)	short-circuit current (mA/cm^2)	open-circuit voltage (V)	fill factor
100 °C 20 min polymer blend	1.0 ± 0.1	2.6 ± 0.3	1.22 ± 0.02	0.33 ± 0.02
165 °C 10 min polymer blend	0.5 ± 0.1	1.0 ± 0.1	1.16 ± 0.03	0.42 ± 0.02
100 °C 20 min block copolymer	1.5 ± 0.1	3.7 ± 0.2	1.13 ± 0.04	0.35 ± 0.01
100 °C 90 min block copolymer	1.7 ± 0.1	4.1 ± 0.1	1.14 ± 0.02	0.35 ± 0.01
165 °C 10 min block copolymer	2.7 ± 0.4	5.0 ± 0.3	1.14 ± 0.08	0.45 ± 0.02

[a]Under simulated AM 1.5G irradiation with intensity of 97 mW/cm^2.

Table 2. Device Characteristics[a] of P3HT/PFTBT Polymer Blend and P3HT-*b*-PFTBT Block Copolymer Solar Cells with Highest Efficiencies

	efficiency (%)	short-circuit current (mA/cm^2)	open-circuit voltage (V)	fill factor
best device, block copolymer	3.1	5.2	1.23	0.47
best device, blend	1.1	2.9	1.22	0.30

[a]Under simulated AM 1.5G irradiation with intensity of 97 mW/cm^2.

block copolymer devices display relatively high photoconversion efficiencies over a broad range of wavelengths (namely 350−610 nm) with EQE values of 20−35%, which are significant for thin-film photovoltaics based on only polymeric materials. Interestingly, an EQE value of 31% was recorded at 400 nm where the exciton generation is mostly attributed to the optical absorption of PFTBT, suggesting efficient exciton dissociation from photoexcitations in the acceptor domains. Integrating the EQE results predicts a J_{sc} of 4.7 mA/cm^2 with an AM 1.5G reference spectrum. This is consistent with a measured J_{sc} of 5.0 mA/cm^2 under AM 1.5G simulated solar conditions for the same device (~5% error). We attribute the small discrepancy to degradation in air, as EQE measurements took place in ambient. Indeed, devices that have undergone EQE measurements exhibit reduced J_{sc}'s (<4 mA/cm^2) when tested under 1 sun conditions in a N_2 atmosphere.

Resonant soft X-ray scattering (RSOXS) and grazing-incidence X-ray scattering measurements were carried out to elucidate the basis for the enhanced performance of block copolymer devices compared to devices made from polymer blends. RSOXS is a powerful tool for characterizing the phase separation in polymer thin films with limited phase contrast or in complicated multiphase systems.[38−41] Differences in the core electronic transitions of organic materials in the soft X-ray regime greatly enhance scattered intensities over hard X-ray scattering, enabling transmission X-ray scattering experiments of thin polymer films. As shown in Figure S2 of the Supporting Information, the X-ray absorptions of P3HT and PFTBT differ at 285.4 eV, which enables RSOXS experiments.

Figure 2 presents RSOXS intensities as a function of scattering vector, q ($q = 4\pi \sin(\theta/2)/\lambda$, λ is the X-ray wavelength and θ is the scattering angle), taken at 285.4 eV X-ray energy for P3HT/PFTBT polymer blend and P3HT-*b*-PFTBT block copolymer thin films annealed at 100 and 165 °C, respectively. The film annealing conditions match the optimum for the active layer of devices. Scattering data from polymer blends show little structure. Scattering profiles from P3HT-*b*-PFTBT block copolymer films are distinct from scattering data from polymer blends (Figure 2 and Figure S3 of the Supporting Information) or polymer/fullerene mixtures.[10,42] A primary scattering peak at $q^* = 0.035$ Å^{-1} and a weak second-order peak at $2q^* = 0.070$ Å^{-1} are evident in data from thin films of block copolymers annealed at 165 °C. The positions of the scattering peaks at q^* and $2q^*$ are a signature of self-assembly into block copolymer lamellar microdomains[43,44] with a domain spacing of approximately 18 nm. The individual domain sizes are therefore roughly 9 nm, comparable to the exciton diffusion length in organic semiconductors (~10 nm).[45]

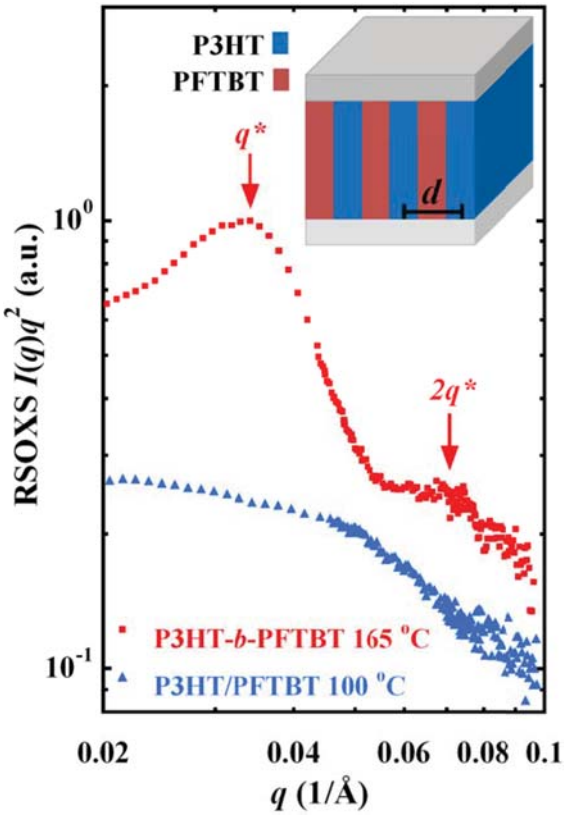

Figure 2. Comparison of the morphology in the active layers of optimized P3HT-*b*-PFTBT and P3HT/PFTBT photovoltaic devices using RSOXS. RSOXS data were acquired at the carbon absorption edge (285.4 eV) of a P3HT-*b*-PFTBT film annealed at 165 °C and a P3HT/PFTBT (1:2 by mass) blend annealed at 100 °C. RSOXS intensities are offset for clarity. Scattering data are presented as a Kratky plot of $I(q)q^2$ vs q, where $I(q)$ is the scattering intensity and q is the scattering vector. In optimized P3HT-*b*-PFTBT samples, a well-defined primary peak, q^* (~0.035 Å^{-1}), and second-order reflection, $2q^*$, are identified. Schematic illustration of the lamellar morphology is shown in the inset with the average domain spacing indicated as d.

RSOXS experiments in the transmission geometry exclusively explore the in-plane film structure and consequently demonstrate the presence of P3HT-*b*-PFTBT lamellae oriented perpendicular to the substrate, as shown in the inset of Figure 2. Grazing incidence small-angle X-ray scattering (GISAXS) measurements shown in Figure S4 of the Supporting Information similarly suggest in-plane microdomains with

dx.doi.org/10.1021/nl401420s | Nano Lett. 2013, 13, 2957−2963

roughly 16 nm spacing (q^* = 0.04 Å^{-1}), in reasonable agreement with the length scales extracted from RSOXS data. Consequently, RSOXS and GISAXS data demonstrate a thin-film lamellar morphology that not only establishes an equilibrium microstructure amenable for exciton dissociation but also provides pathways for electron and hole transport to the corresponding electrodes. We note that the appearance of a lamellar microstructure in P3HT-*b*-PFTBT films only occurs at 165 °C and not 100 °C (see Figure S3 of the Supporting Information), and device efficiencies exhibit a roughly 2-fold increase when films are annealed at 165 °C versus 100 °C (Table 1). Thus, we attribute the significant improvement in photovoltaic device performance to the self-assembly of block copolymers into well-defined mesostructures in the active layer.

We examined the molecular order in block copolymer thin films using conventional X-ray diffraction (XRD) and grazing-incidence wide-angle X-ray scattering (GIWAXS). Measurements were performed on P3HT-*b*-PFTBT films deposited on top of PEDOT:PSS-coated Si substrates and processed in an analogous manner to optimized devices (165 °C annealing for 10 min). XRD results show that PFTBT is amorphous while P3HT forms crystalline structures in both blend and block copolymer films with the same (100) spacing as that in pristine P3HT films (Figure 3a). Complementary 2D GIWAXS measurements provide the preferred orientation of these crystallites through analysis of both the in-plane (along q_y) and out-of-plane (along q_z) scattering data. As shown in Figure 3b, the (100), (200), and (300) reflections of P3HT ($q \sim 0.4$, 0.8, and 1.2 Å^{-1}, respectively), corresponding to spacing between the polymer backbone through the alkyl side-chains, are strongly in-plane with the substrate (along q_y). The (010) peak ($q \sim 1.65$ Å^{-1}), which corresponds to $\pi-\pi$ stacking between chains, is only evident in the out-of-plane direction (along q_z). This indicates that P3HT assumes a predominantly face-on orientation with π-stacking primarily out-of-plane with the substrate. Face-on P3HT crystallites likely enhance the hole extraction efficacy because the fast charge transport direction is along the $\pi-\pi$ stacking direction.[46] The orientation of P3HT crystals in P3HT-*b*-PFTBT block copolymer films differs qualitatively from previously reported studies on P3HT crystallization in homopolymers,[47] polymer/fullerene mixtures,[48,49] or polymer/polymer blends[50] where edge-on orientations are strongly preferred. To first order, there is no reason for the lamellar block copolymer morphology to constrain the P3HT block into either a face-on or edge-on orientation. Instead, we hypothesize that interactions between PFTBT and the substrate lead to preferred face-on orientations for the PFTBT block at the substrate interface. Consequently, the connectivity between blocks nucleates crystals with face-on orientations within the P3HT domains.

The combination of our device results and structural characterization on multiple length scales demonstrates the unique strengths of block copolymer architectures for efficient organic photovoltaics. In addition to controlling the mesoscale structure, conjugated block copolymers provide control of the donor–acceptor interface and of crystallite orientations. Covalent bonding across the donor–acceptor interface has the potential to control charge separation and charge recombination rates,[51,52] opening the possibility of achieving the near unit efficiencies for charge separation from charge transfer states observed in photosynthetic systems.[53] In our studies, the device performance increases when the active layer is composed of block copolymers instead of polymer blends

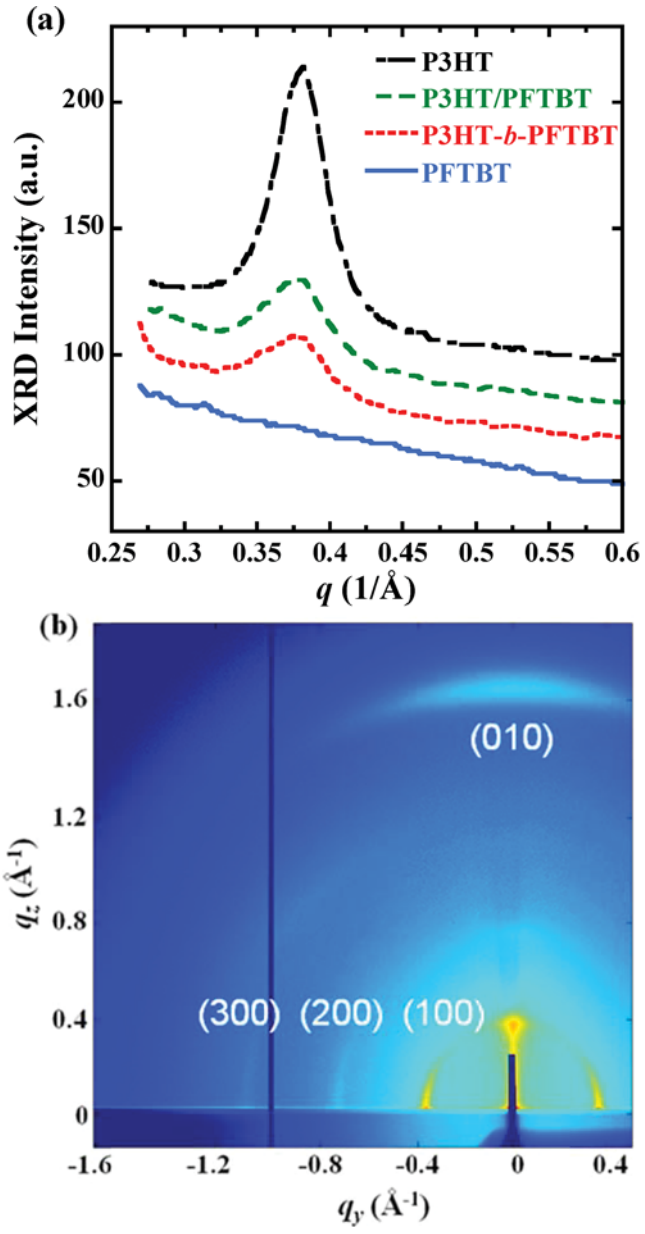

Figure 3. Molecular organization in P3HT-*b*-PFTBT thin films. (a) X-ray diffraction (XRD) patterns of neat P3HT, neat PFTBT, P3HT/PFTBT blend, and P3HT-*b*-PFTBT block copolymer films annealed at 165 °C. (b) Two-dimensional GIWAXS pattern for thin films of P3HT-*b*-PFTBT annealed at optimized conditions (165 °C) for device performance. The (100), (200), and (300) diffraction peaks of regioregular P3HT are strongly biased in the in-plane direction (q_y) and the (010) peak is apparent in the out-of-plane direction (q_z), suggesting face-on crystallites.

even when the morphology is roughly invariant between the two systems; for example, after annealing at 100 °C the device efficiencies improve by 50% when block copolymers are used as active layers even though the RSOXS data and mesoscale structures are similar for block copolymer and blend films (Table 1 and Figure S3 of the Supporting Information). A possible explanation for the difference in the device performance between blend and block copolymer devices is that the connectivity between blocks provides donor/acceptor interfaces within length scales of the order of chain dimensions (ca. 10 nm) and consequently promotes charge separation. The size

dx.doi.org/10.1021/nl401420s | *Nano Lett.* 2013, 13, 2957–2963

of domains, however, in P3HT/PFTBT blends at optimum conditions is near 10−20 nm, as evident from the inflection point in the scattering data from blends shown in Figure 2 or RSOXS data in ref 54. Another possible explanation, changes in charge extraction efficacy, is ruled out given that the current at reverse bias scales with the short-circuit current in Figure 1b.[42] Thus, we hypothesize that conjugation across the donor−acceptor interface is responsible for enhancing device performance in block copolymer devices even when the microstructure of the active layer is similar to blends, suggesting that covalent control of donor−acceptor interfaces is a route for controlling interfacial molecular order, exciton dissociation and charge recombination to enhance excitonic solar cell performance.

Establishing exceptional performance in P3HT-*b*-PFTBT solar cells provides a clear pathway for enhancing efficiencies in fully conjugated block copolymers devices. The choice of P3HT and PFTBT as constituent blocks is motivated by previous work on optimizing polymer blends composed of P3HT and PFTBT derivatives for the active layer of solar cells.[25,55−58] As a consequence, combinations of polymer blocks with complementary absorbance could lead to significant enhancements in short-circuit currents beyond P3HT-*b*-PFTBT because the absorption spectra of P3HT and PFTBT overlap significantly (Figure S1 of the Supporting Information). Broad-band light absorption can be achieved in combination with open-circuit voltages beyond 1 V with careful design of the HOMO/LUMO levels of the constituent blocks, as demonstrated with P3HT-*b*-PFTBT. Previous work has also demonstrated the presence of exciplex or bound charge transfer states at polymer−polymer interfaces that are unlikely to contribute to the photocurrent at room temperature.[59−61] These strongly bound states are localized, in many cases intermolecularly to the benzothiadiazole group in the acceptor polymer.[62,63] Nevertheless, recent photophysical studies of conjugated donor−acceptor molecules have shown that the presence of localized charge transfer states and consequently the degree of recombination depend strongly on the linking chemistry.[64] As such, fully conjugated block copolymers provide a path to achieve unprecedented combinations of light absorption, high photovoltages, and control of electronic coupling at donor−acceptor interfaces in single-component active layers of organic solar cells.

Materials and Methods. Regioregular P3HT (96% H-T regioregular, M_n = 26 kg/mol, polydispersity = 2.0) was purchased from Merck. All other reagents and solvents were purchased from Sigma-Aldrich and used as received. P3HT-*b*-PFTBT block copolymers were synthesized using a procedure similar to that previously described[23] and the synthesis is briefly discussed in the Supporting Information (Section 4, Synthesis of Block Copolymers).

Photovoltaic devices were prepared with the conventional architecture of ITO/PEDOT/:PSS (65 nm)/active layer (60−70 nm)/Al (75 nm). ITO-coated glass substrates (20 ohm/sq, Xin Yan Technology, Hong Kong) were cleaned by soap, followed by 20 min of sonication in acetone, then isopropanol, and finally 15 min of ultraviolet light ozonation. Poly(3,4-ethylenedioxythiophene) poly(styrenesulfonate), PEDOT:PSS (Clevios P, Heraeus), was spin-coated on top of ITO at 4000 rpm for 2 min yielding a thickness of about 65 nm. The PEDOT:PSS/ITO substrates were dried for 10 min at 165 °C in air and then transferred to a nitrogen-filled glovebox. Solutions of P3HT/PFTBT mixtures (15 mg/mL, weight ratio 1:2) and P3HT-*b*-PFTBT (5 mg/mL) were made with anhydrous chloroform (≥ 99%, amylenes as stabilizer, Sigma-Aldrich) and stirred at 95 °C for about 20−22 h in a tightly sealed container prior to casting in a N_2 glovebox. The active layers of P3HT/PFTBT and P3HT-*b*-PFTBT devices were cast onto PEDOT:PSS layers from prepared hot solutions (95 °C) at various spin speeds for 1 min to maintain thicknesses around 60−70 nm. The film thicknesses were determined on a TENCOR P-10 surface profiler. Samples were then transferred immediately onto a calibrated digital hot plate at 100 or 165 °C and dried for 5 min. The devices were completed by vacuum thermal evaporation of 75 nm aluminum at 10^{-6} Torr on top of the active layer through a shadow mask. The device area is 16.2 mm^2. Integrated solar cells were further annealed at 100 or 165 °C for various annealing times.

Photovoltaic measurements were performed in a N_2 atmosphere under simulated AM 1.5G illumination (97 mW/cm^2) from a xenon lamp solar simulator (Newport Model SP92250A-1000). The illumination intensity was calibrated using an optical power meter and NREL certified Si reference photocell (Newport). A Keithley 2636A Sourcemeter was used to measure the current−voltage characteristics of solar cells. External quantum efficiencies (EQE) were measured in air. The photocurrents as a function of wavelength were recorded by a multifunction optical power meter (Model 70310) using 300 W xenon lamp and Cornerstone monochromator (Newport Model 74100) illumination. The absorption spectra of films were measured using an ultraviolet/visible/near-infrared spectrophotometer (Beckman DU Series 500).

Samples for RSOXS, XRD, GISAXS, and GIWAXS measurements were prepared on PEDOT:PSS/Si substrates in the same manner as for device fabrication. For RSOXS experiments, as-cast films were floated-off in deionized water and picked up with 5 mm × 5 mm silicon frames supporting a 1 mm × 1 mm, 100 nm thick Si_3N_4 window. Samples were then dried for 24 h at room temperature under vacuum and subsequently annealed on a hot plate in the N_2 glovebox. RSOXS measurements were carried out at beamline 11.0.1.2 at the Advanced Light Source, Lawrence Berkeley National Laboratory.[65] Scattering was performed in the transmission geometry in vacuum at the carbon absorption edge X-ray energies (285.4 eV) with linearly polarized X-rays. Data were corrected for dark currents and azimuthally integrated.

XRD experiments were conducted at the Materials Characterization Lab of the Pennsylvania State University on a Rigaku DMAX Rapid Microdiffractometer. The X-ray wavelength, λ, was 1.54 Å. Rocking curves were obtained by rocking the sample (±0.5°) around the Bragg angle and images were collected with a curved image plate detector. Data were azimuthally integrated. GISAXS and GIWAXS measurements were carried out at Beamline 8-ID-E of the Advanced Photon Source, Argonne National Laboratory (λ = 1.6868 Å).[66] Scattering data were acquired at an incident angle of 0.2°. Data were corrected for X-ray polarization, detector sensitivity, and geometrical solid-angle.

■ ASSOCIATED CONTENT

Supporting Information

Details on device characteristics, optical and X-ray absorption spectra, GISAXS and RSOXS data, synthetic details of block copolymers, and size-exclusion chromatography traces. This material is available free of charge via the Internet at http://pubs.acs.org.

AUTHOR INFORMATION

Corresponding Author

*E-mail: (E.D.G.) edg12@psu.edu; (R.V) rafaelv@rice.edu.

Author Contributions

¶C.G. and Y.H.L. contributed equally to this work.

Notes

The authors declare no competing financial interests.

ACKNOWLEDGMENTS

C.G., M.D.W., and E.D.G. acknowledge financial support from NSF under Award DMR-1056199. The Advanced Light Source is supported by the Director, Office of Science, Office of Basic energy Sciences, of the U.S. Department of Energy under Contract No. DE-AC02-05CH11231. Use of the Advanced Photon Source is supported by the U.S. Department of Energy, Office of Science, Office of Basic Energy Sciences, under Contract No. DE-AC02-06CH11357. R.V., K.A.S., and Y.H.L. acknowledge support from the Welch Foundation for Chemical Research (Grant C-1750), the Shell Center for Sustainability, and Louis and Peaches Owen. The authors acknowledge John Asbury at the Pennsylvania State University for use of his UV−vis spectrometer.

REFERENCES

(1) Brédas, J.-L.; Norton, J. E.; Cornil, J.; Coropceanu, V. *Acc. Chem. Res.* **2009**, *42* (11), 1691−1699.

(2) Forrest, S. R. *Nature* **2004**, *428* (6986), 911−918.

(3) Shaheen, S. E.; Ginley, D. S.; Jabbour, G. E. *MRS Bull.* **2005**, *30* (1), 10−19.

(4) Mayer, A. C.; Scully, S. R.; Hardin, B. E.; Rowell, M. W.; McGehee, M. D. *Mater. Today* **2007**, *10* (11), 28−33.

(5) Giebink, N. C.; Wiederrecht, G. P.; Wasielewski, M. R.; Forrest, S. R. *Phys. Rev. B* **2010**, *82* (15), 155305.

(6) Thompson, B. C.; Fréchet, J. M. J. *Angew. Chem., Int. Ed.* **2008**, *47* (1), 58−77.

(7) Chen, W.; Nikiforov, M. P.; Darling, S. B. *Energy Environ. Sci.* **2012**, *5* (8), 8045−8074.

(8) Kim, J. B.; Allen, K.; Oh, S. J.; Lee, S.; Toney, M. F.; Kim, Y. S.; Kagan, C. R.; Nuckolls, C.; Loo, Y. L. *Chem. Mater.* **2010**, *22* (20), 5762−5773.

(9) Vakhshouri, K.; Kozub, D. R.; Wang, C.; Salleo, A.; Gomez, E. D. *Phys. Rev. Lett.* **2012**, *108* (2), 026601.

(10) Kozub, D. R.; Vakhshouri, K.; Orme, L. M.; Wang, C.; Hexemer, A.; Gomez, E. D. *Macromolecules* **2011**, *44* (14), 5722−5726.

(11) Brabec, C. J.; Gowrisanker, S.; Halls, J. J. M.; Laird, D.; Jia, S.; Williams, S. P. *Adv. Mater.* **2010**, *22* (34), 3839−3856.

(12) Xin, H.; Reid, O. G.; Ren, G. Q.; Kim, F. S.; Ginger, D. S.; Jenekhe, S. A. *ACS Nano* **2010**, *4* (4), 1861−1872.

(13) Bates, F. S.; Fredrickson, G. H. *Phys. Today* **1999**, *52* (2), 32−38.

(14) Leibler, L. *Macromolecules* **1980**, *13* (6), 1602−1617.

(15) Sary, N.; Richard, F.; Brochon, C.; Leclerc, N.; Leveque, P.; Audinot, J. N.; Berson, S.; Heiser, T.; Hadziioannou, G.; Mezzenga, R. *Adv. Mater.* **2010**, *22* (6), 763−768.

(16) Zhang, Q. L.; Cirpan, A.; Russell, T. P.; Emrick, T. *Macromolecules* **2009**, *42* (4), 1079−1082.

(17) Tao, Y. F.; McCulloch, B.; Kim, S.; Segalman, R. A. *Soft Matter* **2009**, *5* (21), 4219−4230.

(18) Sivula, K.; Ball, Z. T.; Watanabe, N.; Frechet, J. M. J. *Adv. Mater.* **2006**, *18* (2), 206−210.

(19) Sun, S. S.; Zhang, C.; Ledbetter, A.; Choi, S.; Seo, K.; Bonner, C. E.; Drees, M.; Sariciftci, N. S. *Appl. Phys. Lett.* **2007**, *90*, 043117.

(20) Hadziioannou, G. *MRS Bull.* **2002**, *27*, 456−460.

(21) Ku, S.-Y.; Brady, M. A.; Treat, N. D.; Cochran, J. E.; Robb, M. J.; Kramer, E. J.; Chabinyc, M. L.; Hawker, C. J. *J. Am. Chem. Soc.* **2012**, *134* (38), 16040−16046.

(22) Sommer, M.; Komber, H.; Huettner, S.; Mulherin, R.; Kohn, P.; Greenham, N. C.; Huck, W. T. S. *Macromolecules* **2012**, *45* (10), 4142−4151.

(23) Lin, Y.-H.; Smith, K. A.; Kempf, C. N.; Verduzco, R. *Polym. Chem.* **2013**, *4* (2), 229−232.

(24) Zhang, F. L.; Perzon, E.; Wang, X. J.; Mammo, W.; Andersson, M. R.; Inganas, O. *Adv. Funct. Mater.* **2005**, *15* (5), 745−750.

(25) McNeill, C. R.; Halls, J. J. M.; Wilson, R.; Whiting, G. L.; Berkebile, S.; Ramsey, M. G.; Friend, R. H.; Greenham, N. C. *Adv. Funct. Mater.* **2008**, *18* (16), 2309−2321.

(26) Mulherin, R. C.; Jung, S.; Huettner, S.; Johnson, K.; Kohn, P.; Sommer, M.; Allard, S.; Scherf, U.; Greenham, N. C. *Nano Lett.* **2011**, *11* (11), 4846−4851.

(27) Ramsdale, C. M.; Barker, J. A.; Arias, A. C.; MacKenzie, J. D.; Friend, R. H.; Greenham, N. C. *J. Appl. Phys.* **2002**, *92* (8), 4266−4270.

(28) Barker, J. A.; Ramsdale, C. M.; Greenham, N. C. *Phys. Rev. B* **2003**, *67* (7), 075205.

(29) Snaith, H. J.; Greenham, N. C.; Friend, R. H. *Adv. Mater.* **2004**, *16* (18), 1640−1645.

(30) Tress, W.; Petrich, A.; Hummert, M.; Hein, M.; Leo, K.; Riede, M. *Appl. Phys. Lett.* **2011**, *98* (6), 063301.

(31) Wang, J. C.; Ren, X. C.; Shi, S. Q.; Leung, C. W.; Chan, P. K. L. *Org. Electron.* **2011**, *12* (6), 880−885.

(32) Miyanishi, S.; Zhang, Y.; Tajima, K.; Hashimoto, K. *Chem. Commun.* **2010**, *46* (36), 6723−6725.

(33) Topham, P. D.; Parnell, A. J.; Hiorns, R. C. *J. Polym. Sci., Part B: Polym. Phys.* **2011**, *49* (16), 1131−1156.

(34) Anthony, J. E. *Chem. Mater.* **2011**, *23* (3), 583−590.

(35) Sonar, P.; Lim, J. P. F.; Chan, K. L. *Energy Environ. Sci.* **2011**, *4* (5), 1558−1574.

(36) Mikroyannidis, J. A.; Suresh, P.; Sharma, G. D. *Synth. Met.* **2010**, *160* (9−10), 932−938.

(37) Ahmed, E.; Ren, G. Q.; Kim, F. S.; Hollenbeck, E. C.; Jenekhe, S. A. *Chem. Mater.* **2011**, *23* (20), 4563−4577.

(38) Virgili, J. M.; Tao, Y.; Kortright, J. B.; Balsara, N. P.; Segalman, R. A. *Macromolecules* **2007**, *40* (6), 2092−2099.

(39) Wang, C.; Lee, D. H.; Hexemer, A.; Kim, M. I.; Zhao, W.; Hasegawa, H.; Ade, H.; Russell, T. P. *Nano Lett.* **2011**, *11* (9), 3906−3911.

(40) Swaraj, S.; Wang, C.; Yan, H. P.; Watts, B.; Jan, L. N.; McNeill, C. R.; Ade, H. *Nano Lett.* **2010**, *10* (8), 2863−2869.

(41) Guo, C.; Kozub, D. R.; Vajjala Kesava, S.; Wang, C.; Hexemer, A.; Gomez, E. D. *ACS Macro Lett.* **2013**, *2*, 185−189.

(42) Kozub, D. R.; Vakhshouri, K.; Kesava, S. V.; Wang, C.; Hexemer, A.; Gomez, E. D. *Chem. Commun.* **2012**, *48* (47), 5859−5861.

(43) Bendejacq, D.; Ponsinet, V.; Joanicot, M.; Loo, Y. L.; Register, R. A. *Macromolecules* **2002**, *35* (17), 6645−6649.

(44) Hamley, I. W. *The Physics of Block Copolymers*; Oxford University Press: Oxford, 1998.

(45) Haugeneder, A.; Neges, M.; Kallinger, C.; Spirkl, W.; Lemmer, U.; Feldmann, J.; Scherf, U.; Harth, E.; Gugel, A.; Mullen, K. *Phys. Rev. B* **1999**, *59* (23), 15346−15351.

(46) Sirringhaus, H.; Brown, P. J.; Friend, R. H.; Nielsen, M. M.; Bechgaard, K.; Langeveld-Voss, B. M. W.; Spiering, A. J. H.; Janssen, R. A. J.; Meijer, E. W.; Herwig, P.; de Leeuw, D. M. *Nature* **1999**, *401* (6754), 685−688.

(47) Yang, H. C.; Shin, T. J.; Yang, L.; Cho, K.; Ryu, C. Y.; Bao, Z. N. *Adv. Funct. Mater.* **2005**, *15* (4), 671−676.

(48) Woo, C. H.; Thompson, B. C.; Kim, B. J.; Toney, M. F.; Frechet, J. M. J. *J. Am. Chem. Soc.* **2008**, *130* (48), 16324−16329.

(49) Li, G.; Yao, Y.; Yang, H.; Shrotriya, V.; Yang, G.; Yang, Y. *Adv. Funct. Mater.* **2007**, *17* (10), 1636−1644.

(50) Nam, S.; Shin, M.; Park, S.; Lee, S.; Kim, H.; Kim, Y. *Phys. Chem. Chem. Phys.* **2012**, *14* (43), 15046−15053.

(51) Bu, L.; Guo, X.; Yu, B.; Qu, Y.; Xie, Z.; Yan, D.; Geng, Y.; Wang, F. *J. Am. Chem. Soc.* **2009**, *131* (37), 13242−13243.

(52) Guo, Z. Y.; Jenekhe, S. A.; Prezhdo, O. V. *Phys. Chem. Chem. Phys.* **2011**, *13* (17), 7630−7636.
(53) Blankenship, R. E. *Molecular Mechanisms of Photosynthesis*; Blackwell Science: Oxford, U.K., 2002.
(54) Yan, H. P.; Collins, B. A.; Gann, E.; Wang, C.; Ade, H.; McNeill, C. R. *ACS Nano* **2012**, *6* (1), 677−688.
(55) McNeill, C. R.; Abrusci, A.; Zaumseil, J.; Wilson, R.; McKiernan, M. J.; Burroughes, J. H.; Halls, J. J. M.; Greenham, N. C.; Friend, R. H. *Appl. Phys. Lett.* **2007**, *90* (19), 193506−3.
(56) McNeill, C. R.; Westenhoff, S.; Groves, C.; Friend, R. H.; Greenham, N. C. *J. Phys. Chem. C* **2007**, *111* (51), 19153−19160.
(57) McNeill, C. R.; Abrusci, A.; Hwang, I.; Ruderer, M. A.; Müller-Buschbaum, P.; Greenham, N. C. *Adv. Funct. Mater.* **2009**, *19* (19), 3103−3111.
(58) McNeill, C. R.; Greenham, N. C. *Adv. Mater.* **2009**, *21* (38−39), 3840−3850.
(59) Morteani, A. C.; Dhoot, A. S.; Kim, J. S.; Silva, C.; Greenham, N. C.; Murphy, C.; Moons, E.; Cina, S.; Burroughes, J. H.; Friend, R. H. *Adv. Mater.* **2003**, *15* (20), 1708−1712.
(60) Friend, R. H.; Phillips, M.; Rao, A.; Wilson, M. W. B.; Li, Z.; McNeill, C. R. *Faraday Discuss.* **2012**, *155*, 339−348.
(61) Yin, C. H.; Kietzke, T.; Kumke, M.; Neher, D.; Horhold, H. H. *Sol. Energy Mater. Sol. Cells* **2007**, *91* (5), 411−415.
(62) Huang, Y. S.; Westenhoff, S.; Avilov, I.; Sreearunothai, P.; Hodgkiss, J. M.; Deleener, C.; Friend, R. H.; Beljonne, D. *Nat. Mater.* **2008**, *7* (6), 483−489.
(63) Bakulin, A. A.; Rao, A.; Pavelyev, V. G.; van Loosdrecht, P. H. M.; Pshenichnikov, M. S.; Niedzialek, D.; Cornil, J.; Beljonne, D.; Friend, R. H. *Science* **2012**, *335* (6074), 1340−1344.
(64) Johnson, K.; Huang, Y.-S.; Huettner, S.; Sommer, M.; Brinkmann, M.; Mulherin, R.; Niedzialek, D.; Beljonne, D.; Clark, J.; Huck, W. T. S.; Friend, R. H. *J. Am. Chem. Soc.* **2013**, *135* (13), 5074−5083.
(65) Gann, E.; Young, A. T.; Collins, B. A.; Yan, H.; Nasiatka, J.; Padmore, H. A.; Ade, H.; Hexemer, A.; Wang, C. *Rev. Sci. Instrum.* **2012**, *83* (4), 045110.
(66) Jiang, Z.; Li, X.; Strzalka, J.; Sprung, M.; Sun, T.; Sandy, A. R.; Narayanan, S.; Lee, D. R.; Wang, J. *J. Synchrotron Radiat.* **2012**, *19*, 627−636.

Macromolecules

Article

pubs.acs.org/Macromolecules

Supramolecular Conjugated Block Copolymers

Yen-Hao Lin,[†] Seth B. Darling,[‡,∥] Maxim P. Nikiforov,[‡] Joseph Strzalka,[§] and Rafael Verduzco.*[,†]

[†]Department of Chemical and Biomolecular Engineering, MS 362, Rice University, 6100 Main Street, Houston, Texas 77005, United States

[‡]Center for Nanoscale Materials, Argonne National Laboratory, 9700 South Cass Avenue, Argonne, Illinois 60439, United States

[§]X-ray Science Division, Advanced Photon Source, Argonne National Laboratory, Argonne, Illinois 60439, United States

[∥]Institute for Molecular Engineering, The University of Chicago, 5747 South Ellis Avenue, Chicago, Illinois 60637, United States

Supporting Information

ABSTRACT: While the performance of polymer−polymer bulk heterojunction organic photovoltaics (OPVs) is poor compared with polymer−fullerene OPVs, reducing or eliminating micrometer-scale phase separation in all-polymer OPVs may dramatically improve performance. Herein, we demonstrate that 2-ureido-4[1*H*]-pyrimidinone (UPy) quadruple hydrogen bonding interactions can be used to prevent micrometer-scale phase separation at temperatures and processing conditions typically used to prepare bulk heterojunction OPVs. UPy-terminated polymers are synthesized by coupling hydroxyl or primary amine terminated polymers to a reactive isocyanate−UPy group in a one-step reaction. Polymer blend films are subsequently prepared by solution blending, casting onto a surface, and thermal and/or solvent annealing. Film microstructure including the presence of phase-separated domains and polymer crystallinity is analyzed by optical microscopy, atomic force microscopy (AFM), and grazing-incidence wide-angle X-ray scattering (GIWAXS). In contrast to unmodified polymer blends, blends of UPy-terminated polymers do not exhibit micrometer-scale phase separation after extended thermal annealing. AFM reveals the presence of crystalline nanofibers and, in some cases, 100−300 nm phase-separated domains in UPy-mediated polymer blends. Fluorescence measurements indicate that UPy modification increases fluorescence quenching in solutions of donor and acceptor polymers, due to hydrogen-bonding associations which reduce the average distance for energy and/or electron transfer. These results show that UPy-mediated interactions can suppress micrometer-scale phase separation in bulk heterojunction polymer blends at temperatures and processing conditions typically used to prepare bulk-heterojunction OPVs. As a result, UPy functionalization may be a powerful route for improving the performance of all-polymer OPVs.

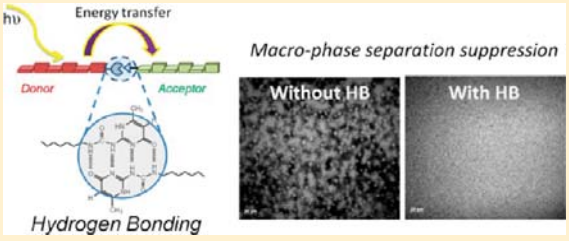

INTRODUCTION

The nanoscale structure of the active layer plays a key role in determining the efficiency of photon-to-electricity conversion in bulk heterojunction (BHJ) organic photovoltaics (OPVs), which are typically comprised of a blend of p-type (hole-conductive) and n-type (electron-conductive) organic semiconductors. While some degree of phase separation is desired for creating continuous charge transport pathways, micrometer-scale phase separated domains are unfavorable due to reduced interfacial area and decreased charge separation efficiencies.[1−4] This presents significant challenges for all-polymer OPVs, which are made up of a blend of a p-type and n-type conjugated polymers; micrometer-scale phase separation is commonly observed due to the reduced entropy of mixing for polymer blends.[5−8] While the best performance in all-polymer OPVs (∼2%)[9−13] is significantly lower compared with state-of-the art polymer-fullerene BHJs, reducing or eliminating large-scale phase separation in all-polymer OPVs may dramatically improve performance. Advantages of all-polymer OPVs over polymer-fullerene OPVs include a typically higher V_{oc}, broader absorbance, and tunability of the absorption profile due to the presence of two polymeric semiconductors in the active layer.

All-conjugated block copolymers with p- and n-type blocks represent a promising approach to improving the performance of all-polymer OPVs. Phase separation can be avoided and block copolymer self-assembly may lead to ideal structures for charge dissociation and transport.[14,15] However, studies on donor−acceptor all-conjugated block copolymers are limited, due in large part to synthetic challenges,[16−28] and noncovalent interactions may provide a more accessible approach to construct materials that exhibit the desirable properties of all-conjugated block copolymers.[29−31] Noncovalent associations such as hydrogen bonds,[32,33] ionic bonds,[34,35] and metal−ligand coordination[36] give rise to persistent intermolecular associations between monomeric or polymeric units resulting in supramolecular polymers. These associations potentially provide a straightforward method to reduce phase separation in all-polymer OPVs, resulting in improved performance and model materials for understanding the structure of conjugated polymer blends.

Received: April 24, 2012
Revised: July 15, 2012
Published: July 31, 2012

   dx.doi.org/10.1021/ma300829u | *Macromolecules* 2012, 45, 6571−6579

The ureidopyrimidone (UPy) group forms self-complementary quadrupole hydrogen bonding interactions with high dimerization constants (up to 10^7 M^{-1} in nonpolar solvents such as chloroform).[37−39] Supramolecular polymers based on UPy interactions have been widely studied, and recent work with coil-like (nonconjugated) polymers has shown that hydrogen bonding interactions can reduce phase separation in polymer blends.[32,38,40−42] The UPy group is also effective in mediating the microstructure and optoelectronic properties of organic semiconductors. For example, UPy hydrogen bonding interactions can enhance energy transfer between electron donor and acceptor molecules[43] and improve interfacial contact and ionic conductivity when incorporated in the polymer electrolyte of a dye-sensitized solar cell.[44] Also, white-light emitting diodes have been demonstrated using UPy-mediated supramolecular interactions between semiconductive oligomers.[45]

Herein, we present a study of the structure, optoelectronic properties, and crystallization of blends of polymers modified with UPy groups. Conjugated and nonconjugated polymers are functionalized with UPy in a one-step coupling reaction and solution blended to form supramolecular conjugated block copolymers. A practical advantage of UPy interactions compared with all-conjugated block copolymers is a greatly simplified synthetic route and straightforward preparation through solution blending. The structure of blend films is analyzed under a variety of annealing conditions using a combination of polarized optical microscopy (POM), atomic force microscopy (AFM), and grazing-incidence wide-angle X-ray scattering (GIWAXS). We find that UPy quadruple hydrogen bonding interactions can prevent micrometer-scale phase separation in polymer blend thin films and increase fluorescence quenching in solution due to a reduced average distance between donor and acceptor polymers.

EXPERIMENTAL SECTION

Materials. Methyl isocytosine (MIC) was purchased from Sigma-Aldrich and dried under vacuum at 100 °C overnight before use. Styrene (purchased from Sigma-Aldrich) was purified by passing through an Al_2O_3 column. Poly(ethylene glycol) methyl ether (PEG−OH, 5000 g/mol) was purchased from Sigma-Aldrich. 2-(6-Isocyanatohexylaminocarbonylamino)-6-methyl-4[1*H*]-pyrimidinone (UPy-isocyanate),[38] 2,5-dibromo-3-hexylthiophene,[46] 9′,9′-dioctylfluoren-2′,7′-diboronic pinacol ester, and 7′-bromo-9′,9′-dioctylfluoren-2′-yl-4,4,5,5-tetramethyl[1,3,2]dioxaborolane[47] were synthesized as previously described. Tetrahydrofuran (THF) and chloroform ($CHCl_3$) were dried over molecular sieves (4 Å). All other reagents were purchased from Sigma-Aldrich and used as received. Silicon wafers were purchased from El-Cat, washed by sonication in DI water and isopropyl alcohol, and dried under a stream of compressed air before use.

Aniline-End Functionalized Poly(3-hexylthiophene), P3HT−NH_2. P3HT−NH_2 was prepared using a procedure adapted from a previous report.[35] In a 50 mL flask purged with nitrogen gas, 2,5-dibromo-3-hexylthiophene (1.9 g, 5.82 mmol) was dissolved in anhydrous THF (5 mL), and the solution was stirred under nitrogen at 0 °C for 15 min. A solution of isopropyl magnesium chloride and LiCl (1.3 M) in THF (4.48 mL, 5.82 mmol) was added, and the mixture was stirred for 2 h. Then, 25 mL of THF was then added before adding Ni(dppp)Cl_2 (105.15 mg, 0.194 mmol), and the mixture was stirred for 15 min. The reaction was quenched by adding a 1 M THF solution of 3-[bis(trimethylsilyl)amino] phenylmagnesium chloride (6 mL, 6 mmol) and stirring for 15 min. Then 5 M HCl (8 mL, 40 mmol) was added, and the solution was stirred for another 15 min. The final mixture was collected by precipitation in cold methanol and water and then by washing with $CHCl_3$ in a Soxhlet apparatus. The $CHCl_3$ solution was stirred with 2 M Na_2CO_3 solution to neutralize the aniline end group. The resulting product was precipitated in cold methanol and dried at 50 °C under vacuum. Yield: 0.86 g (88%). M_w (GPC): 4986 g/mol, d*n*/d*c* = 0.250, polydispersity (PDI) = 1.17, Degree of polymerization (DP) (NMR) = 30. ^{1}H NMR (400 MHz, $CDCl_3$), δ (ppm): 6.95 (30H; Aryl-*H*), 3.75 (2H; NH_2), 2.82 (60H; C−CH_2−C_5H_{11}), 1.70 (60H; CH_2−CH_2−C_4H_9), 1.35 (180H; CH_2−C_3H_6−CH_3), 0.92 (90H; CH_2−CH_3).

Hydroxyl-End Functionalized Poly(9,9-dioctylfluorenyl-2,7-diyl), PFO−OH. 7′-Bromo-9′,9′-dioctylfluoren-2′-yl-4,4,5,5-tetramethyl[1,3,2]dioxaborolane (1 g, 1.68 mmol), 4-(Hydroxymethyl)phenylboronic acid pinacol ester (19.6 mg, 0.08 mmol), Tetrakis(triphenylphosphine)palladium(0) (75 mg, 0.065 mmol), and Aliquat 336 (3 drops) were added to a Schlenk tube loaded with nitrogen-purged toluene (25 mL) and 2 M Na_2CO_3 aqueous solution (10 mL). The reaction was stirred in 90 °C oil bath for 1 day. 4-(Hydroxymethyl)phenylboronic acid pinacol ester (157 mg, 0.67 mmol) was added to the reaction tube and the solution was stirred for 1 day at 90 °C. Bromobenzene (large excess) was added to the reaction and stirred for an additional day before collecting the product by precipitation in methanol. The polymer was subsequently washed with copious amounts of methanol and acetone and dried under vacuum. Yield: 520 mg (84%). M_w (GPC): 5860 g/mol, d*n*/d*c* = 0.234, PDI = 1.31, DP (NMR) = 13. ^{1}H NMR (400 MHz, $CDCl_3$), δ (ppm): 7.5−7.8 (87H; −Ph), 4.78 (2H; Ar−CH_2−OH), 2.1 (52H; CH_2−C_7H_{15}), 1.13 (260H; CH_2−C_5H_{10}−CH_3), 0.80 (78H; C_7H_{14}−CH_3).

Hydroxyl-End Functionalized Poly(9,9-dioctylfluorenyl-2,7-diyl)-*co*-(2,3,5-benzothiadiazole), PFBT−OH. 9′,9′-Dioctylfluorene-2′,7′-diboronic pinacol ester (812 mg, 1.265 mmol), 4,7-dibromobenzo[1,2,5]thiadiazole (370 mg, 1.265 mmol), 4-(hydroxymethyl)phenylboronic acid pinacol ester (14.8 mg, 0.063 mmol), tetrakis(triphenylphosphine)palladium(0) (75 mg, 0.065 mmol), and Aliquat 336 (3 drops) were added to a Schlenk tube loaded with nitrogen-purged toluene (25 mL) and 2 M Na_2CO_3 aqueous solution (10 mL). The reaction was stirred in 90 °C oil bath for 1 day. 4-(Hydroxymethyl)phenylboronic acid pinacol ester (118 mg) was added to the reaction tube, and the solution was stirred for 1 day at 90 °C. 4-bromobenzyl alcohol (283 mg) was added to the reaction, and the solution was stirred for 1 day at 90 °C. The polymer was recovered by precipitation in methanol, washed with copious amounts of methanol and acetone, and dried under vacuum. Yield: 620 mg (81%). M_w (GPC): 15320 g/mol, d*n*/d*c* = 0.263, PDI = 1.37, DP (NMR) = 22. ^{1}H NMR (400 MHz, $CDCl_3$), δ (ppm): 7.3−8.2 (184H; −Ph), 4.78 (4H; Ar−CH_2−OH), 2.1 (88H; CH_2−C_7H_{15}), 1.13 (440H; CH_2−C_5H_{10}−CH_3), 0.80 (132H; C_7H_{14}−CH_3).

Hydroxyl-End Functionalized Polystyrene, PS−OH. Bromine-terminated polystyrene (PS-Br) was first synthesized by mixing styrene (12 g, 115.2 mmol), Cu^IBr (200 mg, 1.38 mmol), PMDETA (0.29 mL), and ethyl α-bromoisobutyrate (0.127 mL, 0.86 mmol) under nitrogen and reacting at 65 °C. The polystyrene product was precipitated in cold methanol and dried at 50 °C under vacuum. Next, PS−Br (M_w ∼ 10 000, 1.6 g, 0.16 mmol), ethanolamine (0.5 mL), and Et_3N (1 mL) were dissolved in DMF (25 mL) and stirred at room temperature overnight. The product was precipitated in cold methanol and dried at 50 °C under vacuum. Yield: 5 g (50%). M_w (GPC): 9851, d*n*/d*c* = 0.173, PDI = 1.04. DP (NMR) = 97. ^{1}H NMR (400 MHz, $CDCl_3$), δ (ppm): 6.45−7.08 (490H; −Ph), 3.42 (2H; O−CH_2−CH_3), 3.36 (2H; −CH_2−OH), 3.10 (1H; NH−C*H*−Ph), 2.10 (2H; NH−CH_2−CH−OH), 1.84 (194H; CH_2−CH−Ph), 1.42 (97H; CH_2−C*H*−Ph), 0.99(6H; C−(CH_3)$_2$), 0.83 (3H; O−CH_2−CH_3).

General Procedure for the Preparation of UPy-End Functionalized Polymers. All UPy-end terminated polymers were prepared using the same procedure, except where indicated otherwise. In a representative procedure, P3HT−NH_2 (300 mg, 0.075 mmol), UPy−isocyanate (65.9 mg, 0.225 mmol), and 3 drops of dibutyltin dilaurate (DBDTL) were dissolved in dry $CHCl_3$ and stirred at 50 °C for 24 h. Silica gel (240 mesh, 10 mg) was subsequently added, and the solution was stirred at 60 °C for 24 h. The crude product was precipitated in cold methanol (PEG−UPy was precipitated from cold

dx.doi.org/10.1021/ma300829u | *Macromolecules* 2012, 45, 6571−6579

diethyl ether), loaded into a Soxhlet apparatus, and washed with $CHCl_3$ to collect the final product, which was concentrated under reduced pressure and dried under vacuum. Recovered yield: 261 mg, 87%. ^{1}H NMR data for each polymer is provided in the text below and in the Supporting Information.

UPy-Functionalized Polystyrene (PS−UPy). Yield (recovered): 90%. ^{1}H NMR (500 MHz, $CDCl_3$), δ (ppm): 13.15 (1H; −N*H*), 11.88 (1H; −N*H*), 10.18 (1H, −N*H*), 5.82 (1H; −C*H*), 6.45−7.08 (490H; −Ph), 3.42 (2H; O−CH_2−CH_3), 3.21 (2H; −CH_2−O− isocyanate−UPy), 3.10 (1H; NH−C*H*−Ph), 2.10 (2H; NH−CH_2−CH−OH), 1.84 (194H; CH_2−CH−Ph), 1.42 (97H; CH_2−C*H*−Ph), 0.99(6H; C−(CH_3)$_2$), 0.83 (3H; O−CH_2−CH_3).

UPy-Functionalized Poly(ethylene glycol) (PEG−UPy). Yield (recovered): 92%. ^{1}H NMR (400 MHz, $CDCl_3$), δ (ppm): 13.15 (1H; −N*H*), 11.88 (1H; −N*H*), 10.18 (1H, −N*H*), 5.82 (1H; −C*H*), 3.4−3.8 (452H; O−CH_2−CH_2−O−), 3.35 (3H; O−CH_3), 3.21 (4H; NH−CH_2), 2.20 (3H; NH−C−CH_3); 1.63 (4H; −CH_2−CH_2−), 1.35 (4H; NH−CH_2−CH_2).

UPy-Functionalized Poly(3-hexyl thiophene) (P3HT−UPy). Yield (recovered): 87%. ^{1}H NMR (500 MHz, $CDCl_3$), δ (ppm): 13.15 (1H; −N*H*), 11.88 (1H; −N*H*), 10.18 (1H, −N*H*), 5.82 (1H; −C*H*), 6.95 (30H; Aryl-*H*), 3.75 (1H; N*H*−UPy), 2.82 (60H; C−CH_2−C_5H_{11}), 1.70 (60H; CH_2−CH_2−C_4H_9), 1.35 (180H; CH_2−C_3H_6−CH_3), 0.92 (90H; CH_2−CH_3).

UPy-Functionalized Poly(9,9-dioctyl fluorene) (PFO−UPy). Yield (recovered): 85%. ^{1}H NMR (500 MHz, $CDCl_3$), δ (ppm): 13.15 (1H; −N*H*), 11.88 (1H; −N*H*), 10.18 (1H, −N*H*), 5.82 (1H; −C*H*), 7.5−7.8 (87H; −Ph), 5.12 (2H; Ar−CH_2−O−UPy), 2.1 (52H; CH_2−C_7H_{15}), 1.13 (260H; CH_2−C_5H_{10}−CH_3), 0.80 (78H; C_7H_{14}−CH_3).

UPy-Functionalized Poly(9,9-dioctyl fluorene-*alt*-benzothiadiazole) (PFBT−UPy). Yield (recovered): 87%. ^{1}H NMR (500 MHz, $CDCl_3$), δ (ppm): 13.15 (2H; −N*H*), 11.88 (2H; −N*H*), 10.18 (2H, −N*H*), 5.82 (2H; −C*H*), 7.3−8.2 (184H; −Ph), 5.12 (4H; Ar−CH_2−OH), 2.1 (88H; CH_2−C_7H_{15}), 1.13 (440H; CH_2−C_5H_{10}−CH_3), 0.80 (132H; C_7H_{14}−CH_3).

Instrumentation. Size Exclusion Chromatography (SEC). Molecular weights and polydispersities were obtained by SEC using an Agilent 1200 module equipped with three PSS SDV columns in series (100, 1000, and 10000 Å pore sizes), an Agilent variable wavelength UV/vis detector, a Wyatt Technology HELEOS II multiangle laser light scattering (MALLS) detector (λ = 658 nm), and a Wyatt Technology Optilab reX RI detector. This system enables SEC with simultaneous refractive index (SEC−RI), UV/vis (SEC−UV/vis), and MALLS detection. THF was used as the mobile phase at a flow rate of 1 mL/min at 40 °C.

Nuclear Magnetic Resonance (NMR). ^{1}H NMR spectroscopy was performed on Bruker 400 MHz spectrometers for all OH- and NH_2-terminated polymers and Varian 500 MHz for all UPy-terminated polymers. Samples were placed in 5 mm o.d. tubes with sample concentrations of about 5 mg/mL. Solvents contain 0.05% TMS as an internal standard.

Polarizing Optical Microscopy. Optical microscopy images of polymer blend films were acquired using an Axioplan 2 imaging microscope in reflective mode. Films were prepared by spin-casting 6 mg/mL solutions onto a silicon wafer cleaned by sonication in DI water and isopropyl alcohol. Images were processed using Axio Vision version 4.8.

Fourier Transform Infrared (FTIR). FTIR analysis was carried out using a Thermo-Nicolet Nexus 670 instrument operated via the OMNIC program. Samples were prepared by depositing approximately 1 mg of bulk polymer on the sample holder.

Atomic Force Microscopy (AFM). AFM analysis was performed using a Veeco Multimode 8 with NanoScope V Controller (instruments located at the Center for Nanoscale Materials at Argonne National Laboratory and the Center for Functional Nanomaterials at Brookhaven National Laboratory) and a Multimode with Nanoscope IIIA controller at Rice University. Sample topography was recorded using Tapping and PeakForce modes. second order flattening has been used for compensation of sample tilt and enhancement of image contrast. Sample films were prepared by spin-casting a 6 mg/mL solution onto a silicon substrate and thermally annealing on a temperature controlled hot plate.

Ultraviolet−visible (UV−vis) absorbance and Luminescence spectrometer. UV−vis absorbance measurements were carried out with a Varian Cary 50 spectrophotometer with scan range of 190−1100 nm, and fluorescence quenching measurements were carried out on a Jobin-Yvon Horiba NanoLog spectrofluorimeter. Samples for fluorescence measurements were prepared by stirring 1 mg/mL solutions in $CHCl_3$ overnight before diluting to a concentration of approximately 1 μg/mL P3HT or P3HT−UPy. The actual P3HT or P3HT−UPy concentration in the sample was estimated by measuring the optical density at 510 nm, and normalized fluorescence data were obtained by scaling the raw fluorescence measurement by the actual concentration of P3HT or P3HT−UPy in solution.

Grazing Incidence Wide-Angle X-ray Scattering (GIWAXS). Grazing incidence wide-angle X-ray scattering measurements were carried out on Sector 8-ID-E at Advanced Photon Source, Argonne National Laboratory.[48] Beamline 8-ID-E operates at an energy of 7.35 keV and images were collected from a Pilatus 1MF camera (Dectris), with two exposures for different vertical position of the detector. After flatfield correction for detector nonuniformity, the images are combined to fill in the gaps for rows at the borders between modules, leaving dark only the columns of inactive pixels at the center. Using the GIXSGUI package[49] for Matlab (Mathworks), data are corrected for X-ray polarization, detector sensitivity and geometrical solid-angle. The beam size is 200 μm (h) × 20 μm (v). Sample detector distance is 204 mm. Sample measurement and thermal annealing were carried out under vacuum which is in the range of 2−3 × 10^{-6} bar, with the sample stage interfaced with a Lakeshore 340 unit.

RESULTS AND DISCUSSION

Synthesis of UPy-Functionalized Polymers. Supramolecular block polymers can be prepared by blending UPy-functionalized homopolymers. UPy is a self-complementary group, and as a result the blend is expected to consist of A−A, A−B, and B−B associations (Figure 1b). To investigate phase-separation, crystallinity, and optoelectronic properties of supramolecular block copolymers, both conjugated and non-conjugated UPy-functionalized polymers were prepared. Specifically, three conjugated polymers—poly(3-hexylthiophene) (P3HT), poly(9,9-dioctyl fluorene) (PFO), and poly(9,9-dioctyl fluorene-*alt*-benzothiadiazole) (PFBT)—and two coil-like polymers—poly(ethylene glycol) (PEG) and polystyrene (PS)—were studied. P3HT is a widely studied p-type polymer in bulk-heterojunction OPVs. PFO has been utilized in both OPVs and OLEDs, and a variety of PFO copolymers exhibit broad absorbance, low bandgap, and, in some cases, electron transport.[50] PFBT has measurable electron mobility,[42] and bulk heterojunction blends of PFBT and P3HT exhibit a 0.13% power conversion efficiency.[51] PS and PEG are chosen as model coil-like polymers for their ease of preparation and relevance to a number of block copolymer systems.

As shown schematically in Figure 1a, UPy-terminated polymers can be prepared through a one-step coupling reaction involving hydroxyl or primary amine-functionalized polymers and isocyanate-functionalized UPy.[38] As evidenced by ^{1}H NMR and FTIR, this enables the preparation of UPy-terminated polymers with a high degree of functionalization due to the reactivity of isocyanate groups toward primary hydroxyl and amine functionalities (Figures 2 and 3). All UPy-functionalized polymers prepared exhibited four distinct NMR peaks corresponding to the terminal UPy group - δ (ppm) =13.15 (-N*H*), 11.88 (-N*H*), 10.18 (-N*H*), and 5.82 (−C*H*) (Figure 2a and S5−S9). PS, PFO, and PFBT also exhibit a clear shift in the ^{1}H NMR peak corresponding to CH_2 adjacent to the terminal hydroxyl group (Figure 2). For PS−OH, the ^{1}H NMR peak

dx.doi.org/10.1021/ma300829u | *Macromolecules* 2012, 45, 6571−6579

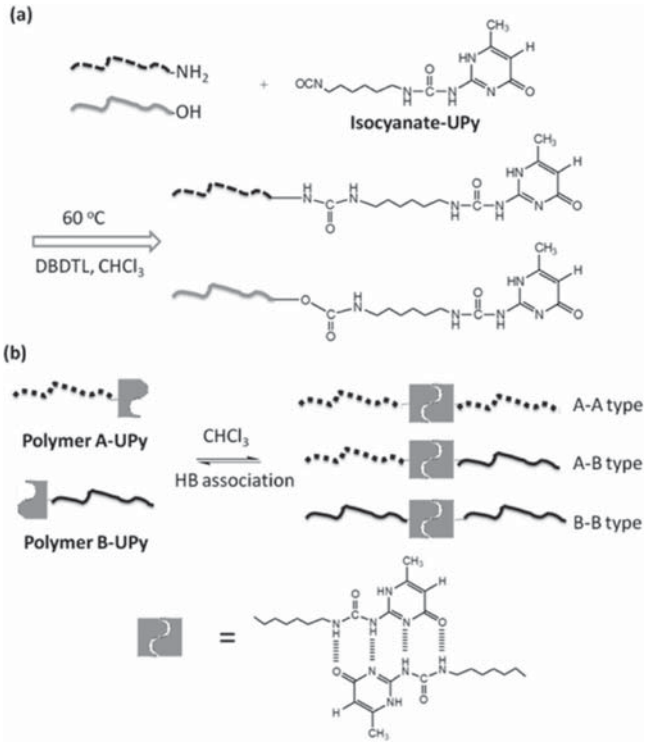

Figure 1. Schematic of (a) the synthetic scheme for preparation of UPy-terminated polymers and (b) quadruple hydrogen bonding (HB) associations between different UPy-terminated polymers to form supramolecular block copolymers.

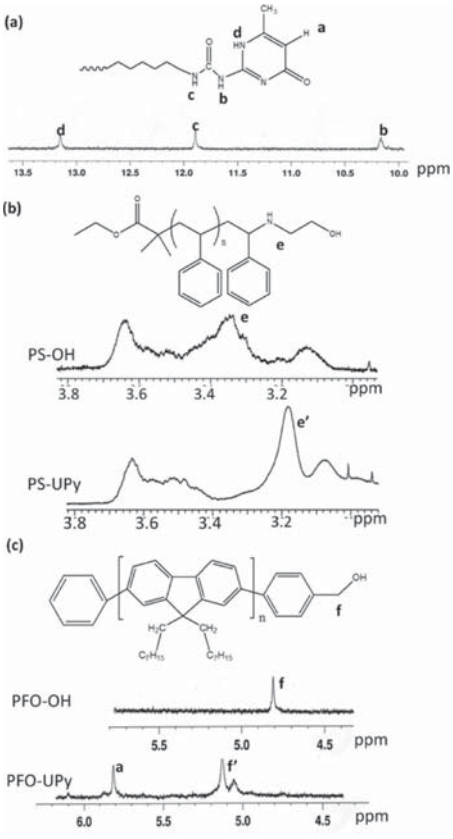

Figure 2. ^{1}H NMR data for (a) the UPy end group, (b) polystyrene before and after coupling to UPy, and (c) poly(9,9-dioctyl fluorene) before and after coupling to UPy.

corresponding to terminal CH_2 shifts from δ (ppm) = 3.36 to 3.21 after the coupling reaction (Figure 2b). In the case of PFO−OH and PFBT−OH (see Supporting Information, Figures S2 and S3), the terminal CH_2 ^{1}H NMR peak shifts from δ (ppm) = 4.78 to 5.12 (Figure 2c).

FTIR spectroscopy (Figure 3) provides further evidence for UPy functionalization of P3HT and PFO. MIC, a precursor to the UPy end group, exhibits a sharp primary amine ($-NH_2$) peak at 3330 cm^{-1} and a peak at 1655 cm^{-1} corresponding to the carbonyl group (C═O). After reaction with hexyl diisocyanate, the primary amine peak vanishes and a peak at 2282 cm^{-1} corresponding to free isocyanate (N═C═O) appears. A new peak near 3235 cm^{-1} corresponding to a secondary amine also appears, and split peaks at 1655 cm^{-1} reflect hydrogen bonding interactions between the carbonyl group and the secondary amine functionality. P3HT-NH_2 exhibits two weak signals at around 3400 and 3500 cm^{-1}, and after functionalization with UPy a broad peak at 3380 cm^{-1} appears, indicative of a secondary amine functional group. PFO−OH has a small peak at around 3450 cm^{-1} corresponding to the primary hydroxyl group, and the peak disappears after functionalization with UPy. FTIR was less reliable for analyzing end-group functionalization of PEG−OH, PS−OH, and PFBT−OH (see Supporting Information, Figure S10).

Phase Behavior of Polymer Blends in Thin Films. In order to test the effect of UPy associations on phase behavior, blend films were cast on a surface and analyzed by optical microscopy and AFM. Samples were thermally annealed near but below the highest crystallization temperatures (180 and 110 °C for 5K P3HT and PFO, respectively) before analysis by POM. These annealing conditions were chosen because a clear difference was observed in the phase behavior of UPy and non-UPy polymer blends. POM analysis shows that UPy-mediated hydrogen bonding interactions suppress micrometer-scale phase separation at these annealing conditions (Figure 4). For example, in the case of P3HT/PS blends mixed at a 50/50 ratio by mass, clear evidence for micrometer-scale phase separation is observed after annealing overnight at 160 °C (Figure 4a). By contrast, no micrometer-scale phase separation is observed for P3HT-UPy/PS-UPy blend films (Figure 4b). Similar results are observed for PFO/PEG blend films annealed at 100 °C (Figures 4c and 4d), P3HT/PEG blend films annealed at 160 °C (see Supporting Information, Figure S11), and P3HT/PFO blend annealed at 160 °C (Figures 4e and 4f). Results for PS/PFO blend films were inconclusive since no phase separation was observed for both PS/PFO and PS−UPy/PFO−UPy blends (Supporting Information, Figure S12). Altogether, these results indicate that UPy-functionalized conjugated polymer blends have a reduced tendency for micrometer-scale phase separation.

While a clear difference between UPy and non-UPy-terminated polymers was observed for the specific annealing conditions described above, higher temperature treatment conditions were tested to explore the limit of miscibility of UPy-terminated polymer blends. All blend films studied, including UPy polymer blends, showed micrometer-scale phase separation when solvent annealed at 170 °C in the presence of dichlorobenzene (see Supporting Information, Figure S13) or when thermally annealed (without solvent present) at 190 °C (higher than the crystalline temperature of the present P3HT sample) (see Supporting Information, Figure S14). On the other hand, no phase separation was observed by

dx.doi.org/10.1021/ma300829u | Macromolecules 2012, 45, 6571−6579

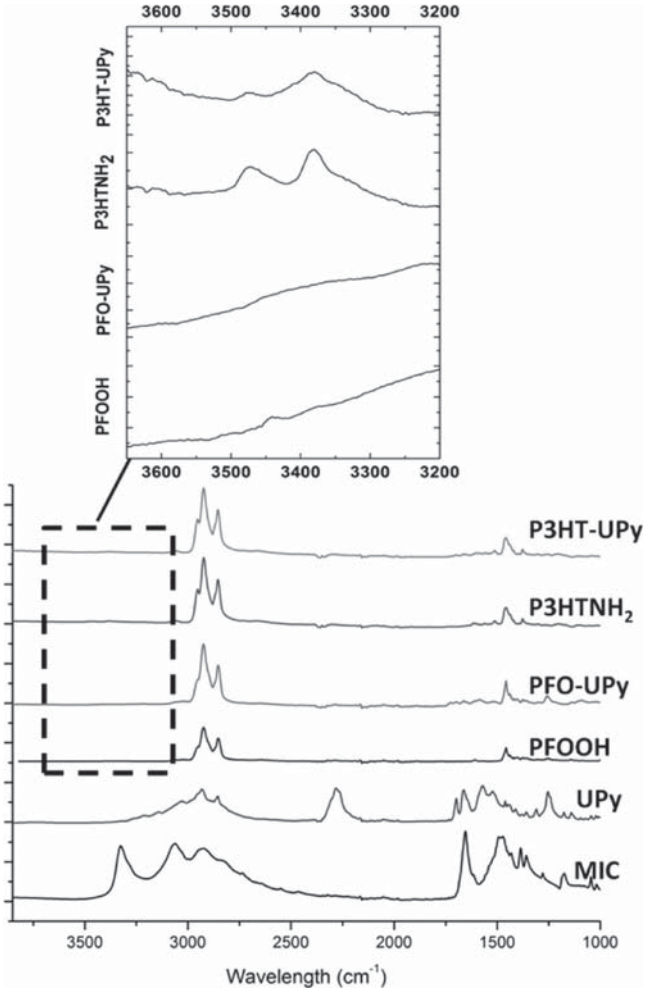

Figure 3. FTIR spectra for various end-functionalized polymers as well as the reactive UPy–isocyanate group (UPy) and methyl isocytosine (MIC).

POM after annealing overnight at 100 °C for any polymer blend (see Supporting Information, Figure S12, for an example). These results indicate that thermal annealing at 190 °C or at 170 °C in the presence of dichlorobenzene is required to induce micrometer-scale phase separation in P3HT–UPy blends. By comparison, other studies on UPy-functionalized molecules have shown that associations are disrupted at a temperature of approximately 80 °C when solvent is present,[52,53] and a report on star-shaped UPy end-functionalized polymers found associations persist only to temperatures as high as 130 °C.[54] A recent study on UPy-functionalized nonconjugated polymers reported micrometer-scale phase separation in polymer blend films thermally annealed at just 100 °C.[32] Thus, the results in the present study indicate that blends consisting of one or more conjugated polymers can increase the temperature required for phase separation. This may be due to a combination of thermodynamic and kinetic effects, as discussed below.

GIWAXS measurements were carried out on pristine P3HT–UPy films, P3HT films, and P3HT blend films to investigate crystallization in UPy-modified polymers and polymer blends (Figures 5 and 6). In the case of P3HT–UPy, as-cast films show little or no crystallinity, but on heating to 80 °C characteristic P3HT-crystallite peaks appear and persist up to temperatures of 160 °C (Figure 5). The positions and intensity of crystalline peaks is qualitatively similar to those of P3HT films prepared similarly and measured at an elevated temperature (Figure 6a). Furthermore, thermally annealed (160 °C, 16 h) P3HT–UPy/PFO–UPy and P3HT–UPy/PS–UPy blend films exhibit similar crystalline peaks (Figure 6, parts b and c), but the intensity of the crystal peaks is significantly weaker for blend films compared with pristine P3HT films. These measurements indicate that crystallization is still present but reduced in UPy-modified polymer blend films.

AFM measurements were carried out to investigate the mesoscale structure of UPy polymer blend films.[55] AFM images show clear evidence for crystallization in pristine P3HT, pristine PFO, and their blend films with UPy-mediated interactions. For example, AFM topography images of P3HT–UPy/PS–UPy blend films reveals crystalline nanowires characteristic of P3HT with fiber dimensions approximately 10 nm in width and lengths up to 100 nm after 16 h of thermal

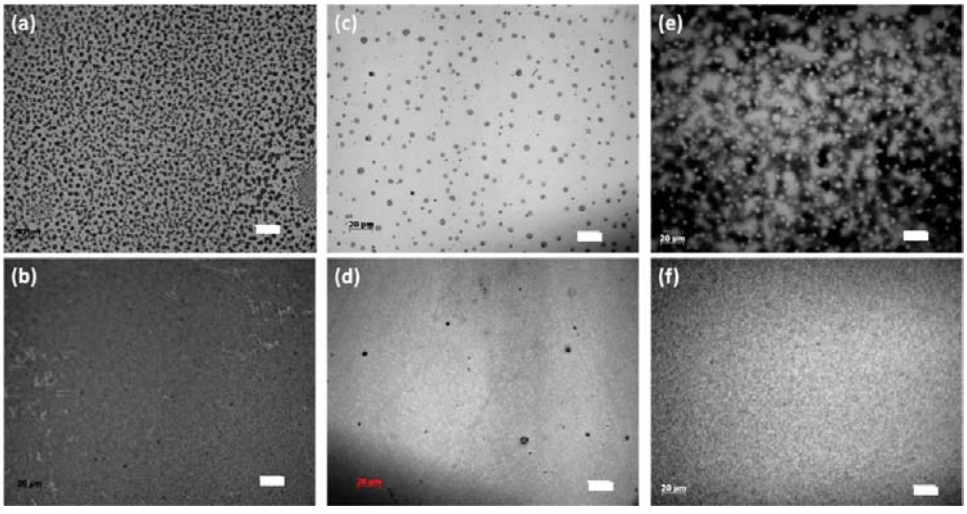

Figure 4. Optical microscopy images of thermally annealed polymer blends: (a) 50/50 wt % P3HT/PS, (b) 50/50 wt % P3HT–UPy/PS–UPy, (c) 50/50 wt % PFO/PEG, (d) 50/50 wt % PFO–UPy/PEG–UPy, (e) 50/50 wt % P3HT/PFO, and (f) 50/50 wt % P3HT-UPy/PFO-UPy. Scale bar: (a) 50 μm, and (b–f) 20 μm. Thermal annealing conditions: (a, b, e, and f) 160 °C, 16 h; (c and d) 100 °C, 16 h.

dx.doi.org/10.1021/ma300829u | *Macromolecules* 2012, 45, 6571–6579

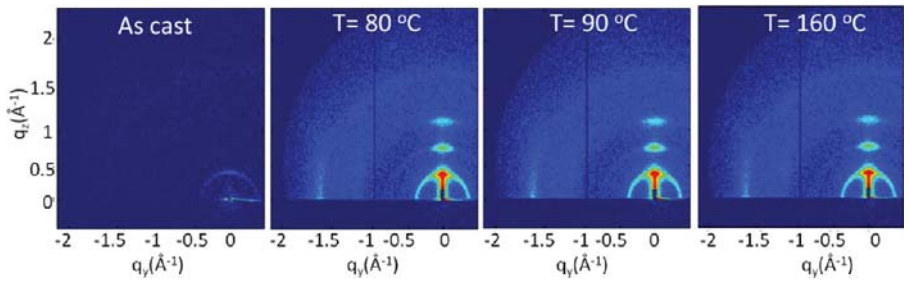

Figure 5. GIWAXS patterns of a P3HT−UPy thin films cast at room temperature and thermally annealed in situ. All samples were measured at an incident angle of 0.25° and 20 s exposure time, and all images have the same color scale.

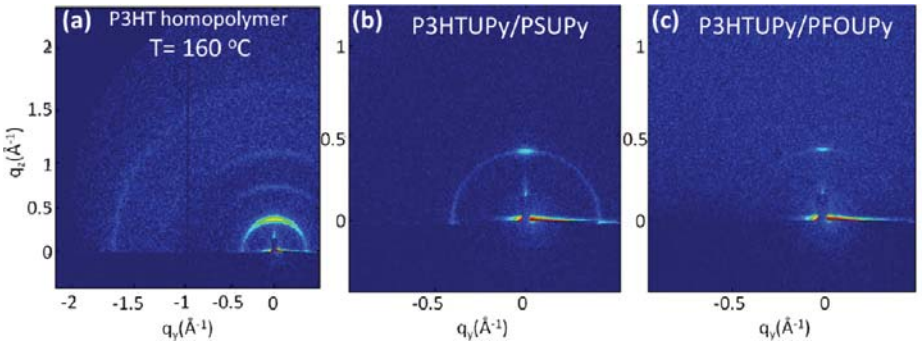

Figure 6. GIWAXS patterns of (a) P3HT homopolymer annealed in situ at 160 °C, (b) P3HT−UPy/PS−UPy, and (c) P3HT−UPy/PFO−UPy measured at room temperature after thermal annealing for 16 h at 160 °C. All samples were measured at an incident angle of 0.25° and 20 s exposure time, and all images have the same color scale.

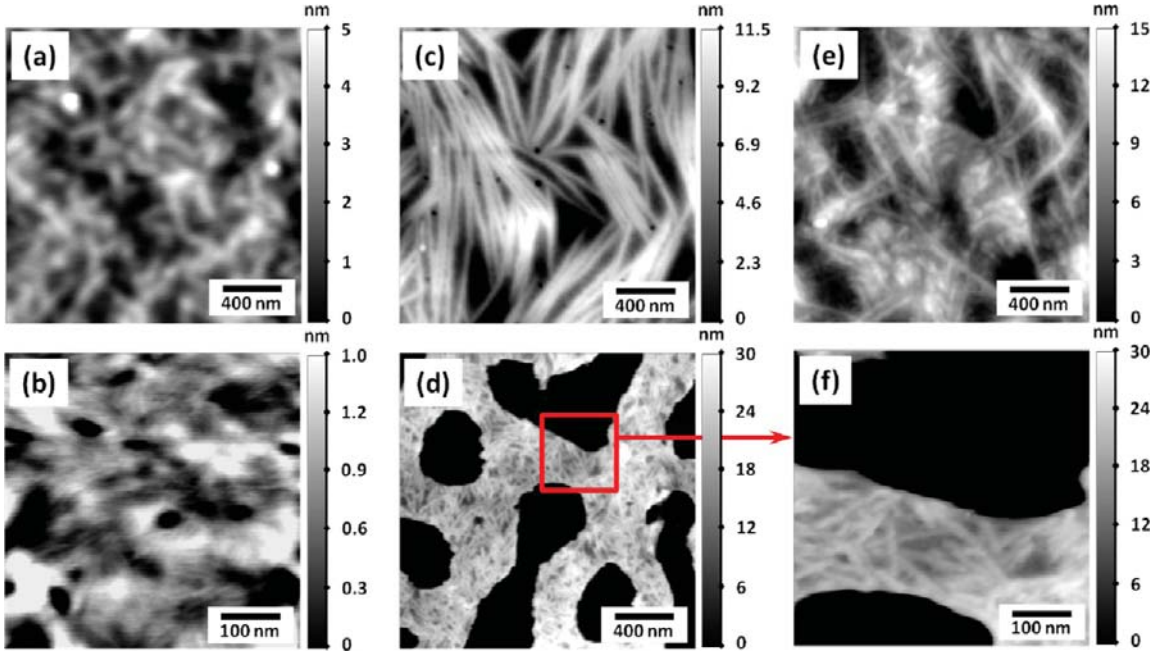

Figure 7. Atomic force microscopy height images of thermally annealed polymer films: (a) pristine P3HT−NH_2, (b) 50/50 wt % P3HT−UPy/PS−UPy, (c) PFO, (d) 50/50 wt % PFO−UPy/PEG−UPy, (f) 50/50 wt % PFO−UPy/PEG−UPy in smaller scale, and (e) 50/50 wt % P3HT−UPy/PFO−UPy. Thermal annealing conditions: (a, b, and e) 160 °C, 16 h; (c, d, and f) 100 °C, 16 h.

annealing at 160 °C (Figure 7b). Pristine PFO films also exhibit crystalline fibers after thermal annealing at 100 °C for 16 h (Figure 7c), with fiber dimensions of about 50 nm in width and lengths up to 1 μm. In the case of PFO−UPy/PEG−UPy annealed at 100 °C for 16 h, both crystallization and submicrometer-scale phase separation are observed, with phase-separated domains roughly 300 nm in size (Figure 7d,e). Crystalline fibers are only present in the PFO-rich domains and have fiber dimensions approximately 20 nm in width and lengths up to 200 nm. Similar fibril structures with dimensions of about 30 nm in width and 700 nm in length were observed in P3HT−UPy/PFO−UPy blends annealed at 160 °C for 16 h with no evidence of phase separation. Submicrometer phase separation was also observed in

dx.doi.org/10.1021/ma300829u | *Macromolecules* 2012, 45, 6571−6579

P3HT−UPy/PEG−UPy and PFO−UPy/PS−UPy blends (Supporting Information, Figure S16). Furthermore, for P3HT−UPy/PFO−UPy and P3HT−UPy/PS−UPy, solvent annealing at room temperature for 4 days gives rise to nanoscale phase-separated domains with P3HT crystallinity (see Supporting Information, Figure S18).

Altogether, AFM and POM measurements of thermally annealed polymer blend films indicate that UPy-mediated interactions can suppress micrometer-scale phase separation in conjugated polymer blend films thermally annealed at temperatures up to 160 °C. The reduced tendency for micrometer-scale phase separation may be due to a combination of thermodynamic and kinetic effects. Previous work indicates that UPy-mediated hydrogen bonding interactions are weak above 100 °C,[52,53] but crystallization in P3HT−UPy blends persists up to 180 °C and may lead to reduced chain mobility and slower kinetics for phase-separation. This is consistent with the GIWAXS data that show significant crystallinity present in P3HT−UPy at 160 °C and AFM images, which indicate that phase separation occurs at a reduced length scale in some UPy-terminated polymer blend films (e.g., PFO−UPy/PEG−UPy). On the other hand, UPy-modification may also affect the thermodynamics of polymer blends, resulting in a homogeneous phase for some UPy−polymer blends. This is supported by mean-field theories for supramolecular block copolymers that indicate complete miscibility under some conditions[56,57] and may explain the absence of microphase segregated structures in UPy polymer blends.

Fluorescence Quenching in Conjugated Polymer Blends. Fluorescence measurements were carried out on P3HT/PFO and P3HT/PFBT solution blends to determine if UPy-mediated interactions between donor and acceptor polymers affect fluorescence quenching. UPy associations are expected to decrease the average distance between polymers compared with unmodified polymer blends, resulting in increased fluorescence quenching. PFBT has a more compatible LUMO level for energy transfer with P3HT and is therefore expected to exhibit more significant quenching compared with PFO.[28]

Fluorescence quenching measurements were carried out by selectively exciting P3HT; this is accomplished by choosing an excitation wavelength greater than 510 nm, above which PFO and PFBT exhibit no absorbance (Figure 8a). The measurements therefore probe energy and/or electron transfer from P3HT to PFO or PFBT, and a quantitative comparison can be made by preparing solutions with approximately the same P3HT content (1−5 μg/mL) and normalizing fluorescence spectra by the overall P3HT concentration, estimated by the measured absorbance at 510 nm.

The fluorescence spectrum (see Supporting Information, Figure S17) of pure P3HT and P3HT-UPy solutions shows that the terminal UPy group by itself has a negligible impact on fluorescence quenching. Blends of unmodified polymers show lower fluorescence compared with that of pristine P3HT or P3HT-UPy, indicative of some energy or electron transfer from P3HT to PFO or PFBT, and as expected quenching is more significant for P3HT/PFBT solution blends due to better matching of LUMO energy levels (Figure 8b). Furthermore, for both P3HT/PFO and P3HT/PFBT, UPy-modified polymer blends exhibited lower fluorescence compared with that of non-UPy modified polymer blends. This indicates that UPy-associations increase fluorescence quenching due to decreased average distance between donor and acceptor polymers in solution.

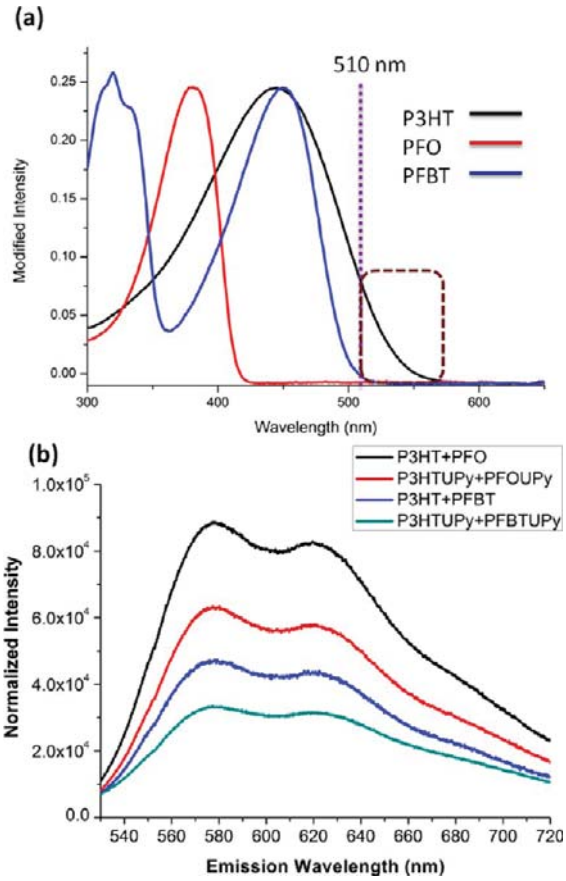

Figure 8. (a) UV−vis absorbance spectra of P3HT, PFO, and PFBT. The dotted line indicates the excitation wavelength used for fluorescence measurements; note that only P3HT exhibits significant absorbance at 510 nm. (b) Fluorescence spectra for conjugated polymer blends in solution under 525 nm excitation wavelength.

CONCLUSION

A series of conjugated and nonconjugated UPy-terminated polymers were synthesized via a one-step reaction with UPy-isocyanate. A combination of AFM, POM, and GIWAXS shows that UPy-mediated quadruple hydrogen bonding interactions can prevent micrometer-scale phase separation in conjugated polymer blends. UPy modification increases fluorescence quenching in solutions of donor and acceptor polymers, due to hydrogen-bonding associations which reduce the average distance for energy and/or electron transfer. These results show that UPy-mediated interactions can suppress micrometer-scale phase separation in bulk heterojunction polymer blends at temperatures and processing conditions typically used to prepare bulk-heterojunction OPVs. As a result, UPy functionalization may be a promising route for improving the performance of all-polymer OPVs.

ASSOCIATED CONTENT

Supporting Information

^{1}H NMR spectra of polymers prepared, POM images of polymer blend films, AFM images of polymer blend films, fluorescence data, and GIWAXS data. This material is available free of charge via the Internet at http://pubs.acs.org.

dx.doi.org/10.1021/ma300829u | Macromolecules 2012, 45, 6571−6579

AUTHOR INFORMATION

Corresponding Author

*E-mail: rafaelv@rice.edu.

Notes

The authors declare no competing financial interest.

ACKNOWLEDGMENTS

This work was carried out with support from the Welch Foundation for Chemical Research (Grant #C-1750), the Shell Center for Sustainability, and Louis and Peaches Owen. We gratefully acknowledge Tao Sun for assistance with the GIWAXS measurements. Use of the Center for Nanoscale Materials and Advanced Photon Source at Argonne National Laboratory was supported by the U.S. Department of Energy, Office of Science, Office of Basic Energy Sciences, under Contract No. DE-AC02-06CH11357. Research carried out in part at the Center for Functional Nanomaterials, Brookhaven National Laboratory, which is supported by the U.S. Department of Energy, Office of Basic Energy Sciences, under Contract No. DE-AC02-98CH10886.

REFERENCES

(1) Gunes, S.; Neugebauer, H.; Sariciftci, N. S. *Chem. Rev.* **2007**, *107*, 1324−1338.
(2) Thompson, B. C.; Fréchet, J. M. J. *Angew. Chem., Int. Ed.* **2008**, *47*, 58−77.
(3) Hoppe, H.; Sariciftci, N. S. *J. Mater. Res.* **2004**, *19*, 1924−1945.
(4) Peet, J.; Heeger, A. J.; Bazan, G. C. *Acc. Chem. Res.* **2009**, *42*, 1700−1708.
(5) Veenstra, S. C.; Loos, J.; Kroon, J. M. *Prog. Photovolt.: Res. Appl.* **2007**, *15*, 727−740.
(6) McNeill, C. R.; Greenham, N. C. *Adv. Mater.* **2009**, *21*, 3840−3850.
(7) Kim, J.-S.; Ho, P. K. H.; Murphy, C. E.; Friend, R. H. *Macromolecules* **2004**, *37*, 2861−2871.
(8) McNeill, C. R.; Watts, B.; Thomsen, L.; Ade, H.; Greenham, N. C.; Dastoor, P. C. *Macromolecules* **2007**, *40*, 3263−3270.
(9) McNeill, C. R.; Abrusci, A.; Zaumseil, J.; Wilson, R.; McKiernan, M. J.; Burroughes, J. H.; Halls, J. J. M.; Greenham, N. C.; Friend, R. H. *Appl. Phys. Lett.* **2007**, *90*, 193506−3.
(10) Kietzke, T.; Hörhold, H.-H.; Neher, D. *Chem. Mater.* **2005**, *17*, 6532−6537.
(11) Koetse, M. M.; Sweelssen, J.; Hoekerd, K. T.; Schoo, H. F. M.; Veenstra, S. C.; Kroon, J. M.; Yang, X.; Loos, J. *Appl. Phys. Lett.* **2006**, *88*, 083504.
(12) Granstrom, M.; Petritsch, K.; Arias, A. C.; Lux, A.; Andersson, M. R.; Friend, R. H. *Nature* **1998**, *395*, 257−260.
(13) Holcombe, T. W.; Woo, C. H.; Kavulak, D. F. J.; Thompson, B. C.; Fréchet, J. M. J. *J. Am. Chem. Soc.* **2009**, *131*, 14160−14161.
(14) Segalman, R. A.; McCulloch, B.; Kirmayer, S.; Urban, J. J. *Macromolecules* **2009**, *42*, 9205−9216.
(15) Darling, S. B. *Energy Environ. Sci.* **2009**, *2*, 1266−1273.
(16) Botiz, I.; Schaller, R. D.; Verduzco, R.; Darling, S. B. *J. Phys. Chem.C* **2011**, *115*, 9260−9266.
(17) Mulherin, R. C.; Jung, S.; Huettner, S.; Johnson, K.; Kohn, P.; Sommer, M.; Allard, S.; Scherf, U.; Greenham, N. C. *Nano Lett.* **2011**, *11*, 4846−4851.
(18) Sommer, M.; Komber, H.; Huettner, S.; Mulherin, R.; Kohn, P.; Greenham, N. C.; Huck, W. T. S. *Macromolecules* **2012**, *45*, 4142−4151.
(19) Woody, K. B.; Leever, B. J.; Durstock, M. F.; Collard, D. M. *Macromolecules* **2011**, *44*, 4690−4698.
(20) Wu, S.; Bu, L.; Huang, L.; Yu, X.; Han, Y.; Geng, Y.; Wang, F. *Polymer* **2009**, *50*, 6245−6251.
(21) Lai, Y.-C.; Ohshimizu, K.; Takahashi, A.; Hsu, J.-C.; Higashihara, T.; Ueda, M.; Chen, W.-C. *J. Polym. Sci., Part A: Polym. Chem.* **2011**, *49*, 2577−2587.
(22) Scherf, U.; Gutacker, A.; Koenen, N. *Acc. Chem. Res.* **2008**, *41*, 1086−1097.
(23) Ouhib, F.; Khoukh, A.; Ledeuil, J.-B.; Martinez, H.; Desbrières, J.; Dagron-Lartigau, C. *Macromolecules* **2008**, *41*, 9736−9743.
(24) Ohshimizu, K.; Takahashi, A.; Higashihara, T.; Ueda, M. *J. Polym. Sci., Part A: Polym. Chem.* **2011**, *49*, 2709−2714.
(25) Sun, S.-S.; Zhang, C.; Ledbetter, A.; Choi, S.; Seo, K.; Carl, E.; Bonner, J.; Drees, M.; Sariciftci, N. S. *Appl. Phys. Lett.* **2007**, *90*, 043117.
(26) Chen, X. L.; Jenekhe, S. A. *Macromolecules* **1996**, *29*, 6189−6192.
(27) Xiao, X.; Fu, Y.; Sun, M.; Li, L.; Bo, Z. *J. Polym. Sci., Part A: Polym. Chem.* **2007**, *45*, 2410−2424.
(28) Verduzco, R.; Botiz, I.; Pickel, D. L.; Kilbey, S. M.; Hong, K.; Dimasi, E.; Darling, S. B. *Macromolecules* **2011**, *44*, 530−539.
(29) Fox, J. D.; Rowan, S. J. *Macromolecules* **2009**, *42*, 6823−6835.
(30) Rehm, T.; Schmuck, C. *Chem. Commun.* **2008**, 801−813.
(31) Yang, S. K.; Ambade, A. V.; Weck, M. *Chem. Soc. Rev.* **2011**, *40*, 129−137.
(32) Feldman, K. E.; Kade, M. J.; de Greef, T. F. A.; Meijer, E. W.; Kramer, E. J.; Hawker, C. J. *Macromolecules* **2008**, *41*, 4694−4700.
(33) Dankers, P. Y. W.; Zhang, Z.; Wisse, E.; Grijpma, D. W.; Sijbesma, R. P.; Feijen, J.; Meijer, E. W. *Macromolecules* **2006**, *39*, 8763−8771.
(34) Huh, J.; Park, H. J.; Kim, K. H.; Park, C.; Jo, W. H. *Adv. Mater.* **2006**, *18*, 624−629.
(35) Takahashi, A.; Rho, Y.; Higashihara, T.; Ahn, B.; Ree, M.; Ueda, M. *Macromolecules* **2010**, *43*, 4843−4852.
(36) Lohmeijer, B. G. G.; Schubert, U. S. *Angew. Chem., Int. Ed.* **2002**, *41*, 3825−3829.
(37) Shokrollahi, P.; Mirzadeh, H.; Huck, W. T. S.; Scherman, O. A. *Polymer* **2010**, *51*, 6303−6312.
(38) Folmer, B. J. B.; Sijbesma, R. P.; Versteegen, R. M.; van der Rijt, J. A. J.; Meijer, E. W. *Adv. Mater.* **2000**, *12*, 874−878.
(39) Beijer, F. H.; Sijbesma, R. P.; Kooijman, H.; Spek, A. L.; Meijer, E. W. *J. Am. Chem. Soc.* **1998**, *120*, 6761−6769.
(40) Lee, K. J.; Lee, D. K.; Kim, Y. W.; Kim, J. H. *Eur. Polym. J.* **2007**, *43*, 4460−4465.
(41) Keizer, H. M.; Gonzalez, J. J.; Segura, M.; Prados, P.; Sijbesma, R. P.; Meijer, E. W.; de Mendoza, J. *Chem.—Eur. J.* **2005**, *11*, 4602−4608.
(42) Wrue, M. H.; McUmber, A. C.; Anthamatten, M. *Macromolecules* **2009**, *42*, 9255−9262.
(43) Wang, S. M.; Yu, M. L.; Ding, J.; Tung, C. H.; Wu, L. Z. *J. Phys. Chem. A* **2008**, *112*, 3865−3869.
(44) Kim, Y. J.; Kim, J. H.; Kang, M. S.; Lee, M. J.; Won, J.; Lee, J. C.; Kang, Y. S. *Adv. Mater.* **2004**, *16*, 1753−1757.
(45) Abbel, R.; Grenier, C.; Pouderoijen, M. J.; Stouwdam, J. W.; Leclere, P.; Sijbesma, R. P.; Meijer, E. W.; Schenning, A. *J. Am. Chem. Soc.* **2009**, *131*, 833−843.
(46) Han, Y.-K. L.; Y-J; Huang, P-C. *J. Electrochem. Soc.* **2009**, *156*, k37−k43.
(47) Zhang, X.; Tian, H.; Liu, Q.; Wang, L.; Geng, Y.; Wang, F. *J. Org. Chem.* **2006**, *71*, 4332−4335.
(48) Jiang, Z.; Li, X. F.; Strzalka, J.; Sprung, M.; Sun, T.; Sandy, A. R.; Narayanan, S.; Lee, D. R.; Wang, J. *J. Synchrot. Radiat* **2012**, *19*, 627−636.
(49) Jiang, Z., *GIXSGUI is available for download:* http://www.aps.anl.gov/Sectors/Sector8/Operations/GIXSGUI.html.
(50) Herguth, P.; Jiang, X.; Liu, M. S.; Jen, A. K. Y. *Macromolecules* **2002**, *35*, 6094−6100.
(51) Kim, Y.; Cook, S.; Choulis, S. A.; Nelson, J.; Durrant, J. R.; Bradley, D. D. C. *Chem. Mater.* **2004**, *16*, 4812−4818.
(52) Yamauchi, K.; Lizotte, J. R.; Long, T. E. *Macromolecules* **2003**, *36*, 1083−1088.

(53) Yamauchi, K.; Lizotte, J. R.; Hercules, D. M.; Vergne, M. J.; Long, T. E. *J. Am. Chem. Soc.* **2002**, *124*, 8599−8604.
(54) Mather, B. D.; Elkins, C. L.; Beyer, F. L.; Long, T. E. *Macromol. Rapid Commun.* **2007**, *28*, 1601−1606.
(55) Ramanathan, M.; Darling, S. B. *Prog. Polym. Sci.* **2011**, *36*, 793−812.
(56) Anthamatten, M. *J. Polym. Sci., Part B: Polym. Phys.* **2007**, *45*, 3285−3299.
(57) Feng, E. H.; Lee, W. B.; Fredrickson, G. H. *Macromolecules* **2007**, *40*, 693−702.

Chapter 3

Synthesis and Process-Dependent Film Structure of All-Conjugated Copolymers for Organic Photovoltaics

Yen-Hao Lin and Rafael Verduzco*

Department of Chemical and Biomolecular Engineering, MS-362, Rice University, 6100 Main Street, Houston, Texas 77005
***E-mail: rafaelv@rice.edu.**

Donor-acceptor all-conjugated block copolymers can be used to build organic photovoltaics (OPVs) with improved interfacial structure, broader light absorption, and enhanced performance. The past decade has seen significant progress in the synthesis and structure analysis of all-conjugated block copolymers. One system in particular – Poly(3–alkylthiophene)–*b*–poly(9′,9′–dioctylfluorene) (P3AT–*b*–PF) – has served as a model system for developing new synthetic techniques and analyzing the microstructure in thin films, in the melt, and in the solutions. This article reviews work with P3AT–*b*–PF block copolymers, emphasizing both material synthesis and analysis of crystallinity, micro-phase segregation in films, and aggregation in solutions. This overview demonstrates significant advances in the preparation and characterization of all-conjugated block copolymers and emphasizes remaining challenges in the application of all-conjugated block copolymers for OPVs.

In Polymer Composites for Energy Harvesting, Conversion, and Storage; Li, L., et al.;
ACS Symposium Series; American Chemical Society: Washington, DC, 2014.

1. Introduction

Conjugated polymers have received enormous attention since their discovery in the late 70s, recognized by the Nobel Prize in Chemistry awarded in 2000 (*1*). Conjugated polymers are currently being investigated for organic electronic applications, including light emitting diodes (OLEDs) (*2–7*), field-effect transistors (OFETs) (*8–11*), photovoltaics (OPVs) (*12–15*), sensors (*16*, *17*), and electrochromic devices (*18*) and they offer potentially low-cost solution processing strategies other benefits such as flexibility and transparency (*19–21*).

Achieving efficient solution-processed polymer OPVs is a significant challenge and a current area of research emphasis (*22–31*). Conjugated polymer OPVs are made by depositing one or more conjugated organic molecules or polymers in a thin film of few hundred nanometers. The large absorption coefficients of conjugated polymer enables ~ 100 nm thin photovoltaic active layers (*32*). This active layer is sandwiched between anode and cathode electrodes (as shown in Figure 1). The absorption of a photon results in an electron/hole pair known as an exciton which must be separated into distinct charges to generate a useful current. This is in contrast to inorganic photovoltaics where free charges are created upon light absorption (*33*). Generating a useful current requires separating the exciton into distinct charges, which must occur within the short lifetime of the photoexcited state (*34–37*). The exciton is most efficiently separated at the interface between donor and acceptor semiconductors, therefore optimizing the active layer structure is important for achieving efficient OPV performance.

Figure 1. Representative configuration of an OPV device. The active layer is comprised of a blend of electron-donor and electron-acceptor organic semiconductors.

A schematic for bulk-heterojunction OPVs consisting of both conjugated polymer and fullerene is shown in Figure 2a. In general, the final active layer structure is a result of various non-equilibrium processes, including polymer crystallization and phase separation, that occur during film casting and annealing (*24*, *38*). A variety of methods have been implemented to control the length scale interface structure and crystallinity of the active layers including the use of processing additives (*39–41*) and top-down approaches to patterning (*42–44*).

In Polymer Composites for Energy Harvesting, Conversion, and Storage; Li, L., et al.;
ACS Symposium Series; American Chemical Society: Washington, DC, 2014.

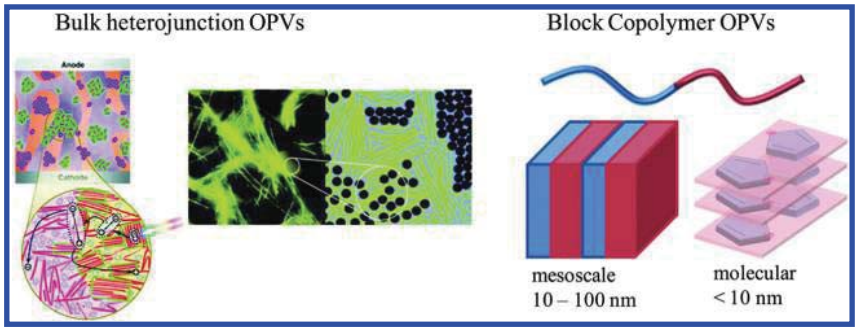

Figure 2. Schematics for the active layer morphologies of bulk heterojunction OPVs (left) and all-conjugated block copolymer OPVs (right). (Reproduced with permission from references (22) and (31). Copyright 2011 American Chemical Society.)

Block copolymers comprised of two-conjugated polymer blocks, known as all-conjugated block copolymers (*45*), can potentially address many of the current challenges in morphology and interfacial structure control for OPVs. All-conjugated block copolymers are an emerging class of materials comprised of two or more conjugated polymer chains. Such block copolymers combine the optoelectronic properties of semiconductive polymers with structure control through micro-phase segregation (*46–48*) and crystallization (*49*, *50*). Donor-acceptor all-conjugated block copolymers comprised of both hole-conductive (*p*-type) and electron-conductive (*n*-type) polymer blocks are of particular interest for OPVs (*51*, *52*). Selected examples of all-conjugated block copolymers are shown in Scheme 1 (*45*, *49*, *53–63*). The micro-phase segregation of diblock copolymer typically leads to domain sizes of 5-100 nm with various morphologies, depending on the volume fraction of block (*64*, *65*). As shown in Figure 2, all-conjugated block copolymers can potentially self-assemble into well-defined donor and acceptor domains with controlled size and orientation.

Recent work has demonstrated significant progress in the design, synthesis, and characterization of all-conjugated block copolymers (*49*, *66–69*). All-conjugated block copolymers have recently demonstrated efficienties near 3 % in a block copolymer device (*70*). However, further progress requires advances in both the synthesis and processing-structure-property relationships. Here, we review the synthesis and characterization of all-conjugated block copolymers with a specific emphasis on conjugated block copolymers that incorporate both poly(alkylthiophene) (P3AT) and poly(dialkylfluorene) (PF) polymer blocks. P3AT-*b*-PF block copolymers were among the first all-conjugated block copolymers reported (*45*), and significant progress has been made in the synthesis and characterization of these materials. Progress with P3AT-*b*-PF can provide valuable lessons for other systems and fundamental insight into the properties of all-conjugated block copolymers. The structure of P3AT-*b*-PF along with other all-conjugated block copolymers reported is shown in Scheme 1.

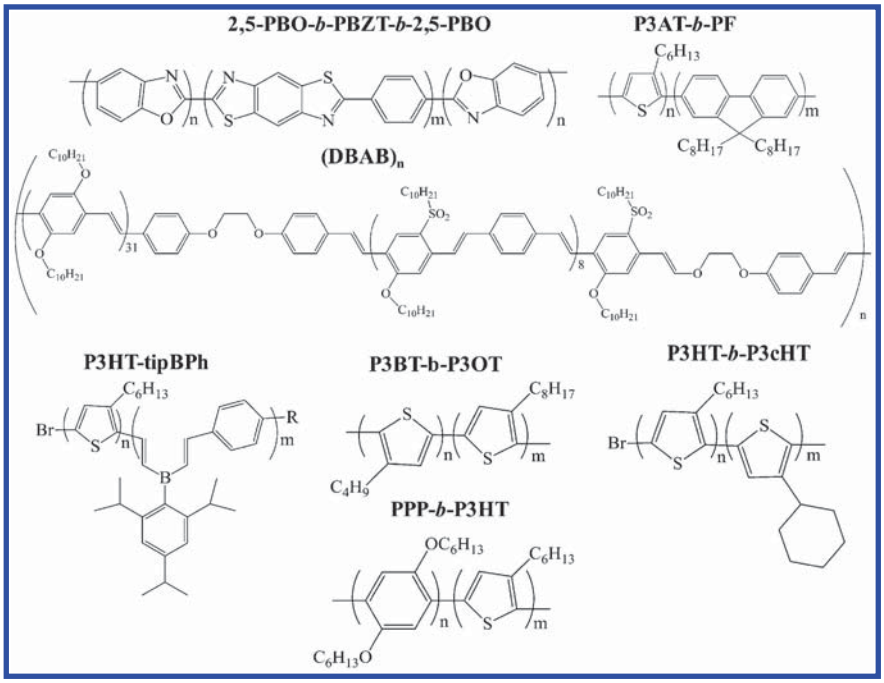

Scheme 1. Different all-conjugated block copolymer structures reported in the literature. 2,5-PBO-b-PBZT-b-2,5-PBO (61), P3HT-b-PF (45), $(DBAB)_n$ (71), P3HT-tipBPh (72), P3BT-b-P3OT (73), P3HT-b-P3cHT (74) and PPP-b-P3HT (75).

Below, we review synthetic approaches and processing-structure-property relationships in all-conjugated block copolymers, emphasizing results with P3AT-*b*-PF block copolymers. The synthesis of well-defined, all-conjugated block copolymers has been a significant challenge in the field, and over the past several years new synthetic approaches have emerged based on copper-catalyzed click chemistry and stepwise polymerizations. Understanding the microstructure of all-conjugated block copolymer films is crucial to their application, and distinguishing between crystallization and micro-phase segregation requires characterization using a variety of techniques. We show that varying processing conditions results in dramatic changes to the film morphology on a model series of poly(3-alkylthiophene)–*b*-poly(9′,9′-dioctyl fluorene) (P3AT-*b*-PF). We present work from our group and also others that have synthesized and characterized P3AT-*b*-PF. While we focus primarily on work with P3AT-*b*-PF, there have been significant advances in the synthesis and processing of other conjugated block polymer films as can be found in other publications (*49*, *76*) and recent reviews (*37*, *51*, *77–80*).

2. Synthesis of P3AT-*b*-PF All-Conjugated Block Copolymers

Most approaches for making donor-acceptor all-conjugated block copolymers, which incorporate both *n*- and *p*-type polymer blocks, rely on distinct polymerization reactions for each polymer block, including GRIM, Suzuki-Miyaura, and Stille polymerization reactions (*45*, *49*, *54*, *63*, *83*, *84*). All-conjugated block copolymers are generally synthesized from two general strategies depicted schematically in Figure 3: (a) through a macro-reagent approach involving sequential polymerization reactions; and (b) through the coupling of two conjugated polymers with controlled end-functionalities. Both strategies have advantages and limitations. While the macro-reagent approach is generally more straightforward and versatile, the coupling approach gives better control over the molecular weight of each polymer block separately. However, the coupling approach requires good end-group control for two separate conjugated polymer blocks. Below, we review recent applications and advances in these synthetic approaches applied to the synthesis of P3AT-*b*-PF (*45*, *81–83*).

Alternative approaches to the two mentioned above are limited but include the "all-GRIM" approach which has been applied for the synthesis of block copolythiophenes (*56*, *57*, *68*, *73–75*, *81*, *85–91*) and P3HT-*b*-PF (*85*). The advantage of "all-GRIM" is potentially improved control over the polymerization reaction of both blocks. However, "all-GRIM" is limited in terms of applicability to different monomeric repeat units. The reader is referred to recent reviews for more information on this synthetic approach (*92–94*).

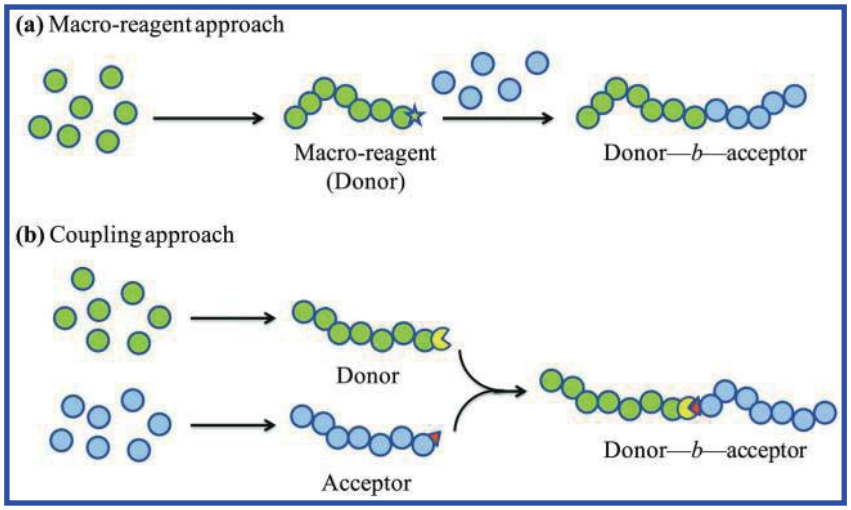

Figure 3. Approaches for synthesis of all-conjugated block copolymers via (a) macro- reagent and (b) covalent/supramolecular coupling.

In Polymer Composites for Energy Harvesting, Conversion, and Storage; Li, L., et al.;
ACS Symposium Series; American Chemical Society: Washington, DC, 2014.

2.1. All-Conjugated Block Copolymer Synthesis Using a Macroreagent Approach

The first example of a macro-reagent approach applied to the synthesis of P3AT-*b*-PF all-conjugated block copolymers was reported by the Scherf group (*83*). Their synthetic method involved the synthesis of a poly(3-hexylthiophene) (P3HT) macro-reagent followed by a Suzuki-Miyaura polycondensation reaction to synthesize the PF block. Several subsequent studies have taken advantage of this general approach to synthesize all-conjugated block copolymers, using Suzuki-Miayaura or other polycondensation reactions for the synthesis of the second polymer block (*45*, *49*, *53*, *63*, *66*, *68*, *84*, *95*). The versatility of this general approach is reflected in the variety of block copolymers reported using this scheme. However, a drawback of these methods is that they typically result in relatively low molecular weight block copolymers with significant amounts of homopolymer impurities that can only be removed using tedious column purification techniques (*26*, *49*, *63*).

An improved approach for synthesizing all-conjugated block copolymers using Suzuki-Miyaura and GRIM with little or no homopolymer approaches was recently demonstrated by our group (*67*). GRIM is first carried out to synthesize an end-functionalized P3HT (P3HT-Br) macroreagent, and P3HT-Br is subsequently utilized in a Suzuki-Miyaura polymerization reaction to make all-conjugated P3HT block copolymers (Scheme 2). A high degree of end functionalization of the P3HT-Br macroreagent is required to avoid residual P3HT homopolymer impurities, and this was accomplished using LiCl as an additive for the preparation of bromo-chloromagnesio -hexylthiophene monomer. LiCl has been shown to be an effective additive for accelerating Grignard formation and producing P3HT with a high degree of end-group functionality (*96–98*). P3HT-Br was prepared using standard methods by the addition of $Ni(dppp)Cl_2$ catalyst to the monomer solution to initiate GRIM (*99*). Three different P3HT macroreagents were prepared using this approach, as shown in Table I.

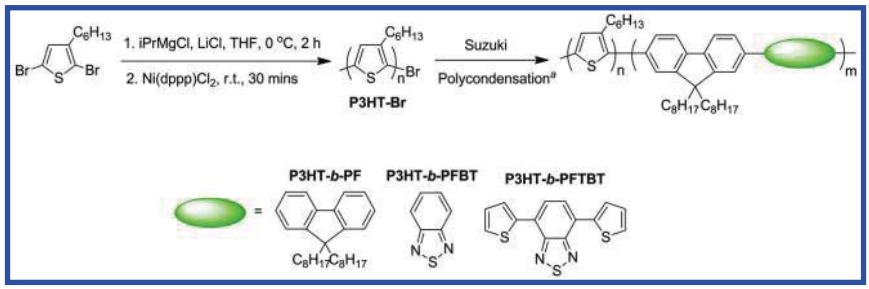

Scheme 2. Preparation of all-conjugated P3HT block copolymers via Grignard metathesis polymerization with LiCl additive followed by Suzuki-Miyaura Polycondensation. [a]conditions for Suzuki-Miyaura: $Pd(PPh_3)_4$, toluene, water, 90 °C. An equimolar ratio of 9',9'-dioctylfluorene-2',7'-diboronic acid ester and corresponding dibromo monomer is used. (Adapted with permission from reference (67). Copyright 2013 Royal Society of Chemistry.)

In Polymer Composites for Energy Harvesting, Conversion, and Storage; Li, L., et al.;
ACS Symposium Series; American Chemical Society: Washington, DC, 2014.

Next, P3HT-Br was reacted in a Suzuki-Miyaura polycondensation reaction to prepare three different types block copolymers, each with a P3HT block and a second conjugated polymer block: poly(9′,9′-dioctyl fluorene) (PF), poly(9′,9′-dioctyl fluorene-*alt*-benzo- thiadiazole) (PFBT), and poly(2,7-(9′,9′-dioctyl-fluorene)-*alt*-5,5-(4′,7′-di-2-thienyl-2′,1′,3′, benzothiadiazole) (PFTBT). PF, PFBT, and PFTBT have been previously studied for use in bulk-heterojunction OPVs and OLEDs (*100–102*), and PFTBT is promising for use in block copolymer OPVs because it exhibits a broad absorbance and a low-lying HOMO level (*103*, *104*). A high and low molecular weight P3HT-Br macroreagent was used for each type of block copolymer, resulting in a total of six different block copolymers, as shown in Table I. The formation of triblock copolymers is unlikely due to a low content of P3HT-Br macroreagent used in the Suzuki-Miyaura polycondensation step (roughly 1 mole % relative to monomers).

Table I. Characteristics of All-Conjugated P3HT Block Copolymers SOURCE: Reproduced with permission from reference (*67*). Copyright 2013 Royal Society of Chemistry.

Polymers	*P3HT[a] M_w (PDI)*	*BCP[a] M_w (PDI)*	*DP ratios[b] (P3HT wt%)*
P3HT13-*b*-PF87	6.1 (1.16)	48.4 (1.86)	36:100 (13%)
P3HT25-*b*-PF75	13.5 (1.32)	60.6 (1.87)	81:105 (25%)
P3HT20-*b*-PFBT80	8.5 (1.19	168 (3.61)	51:66 (20%)
P3HT22-*b*-PFBT78	13.5 (1.32)	81.5 (2.24)	81:90 (22%)
P3HT42-*b*-PFTBT58	8.5 (1.19)	19.7 (1.49)	51:17 (42%)
P3HT62-*b*-PFTBT38	13.5 (1.32)	N/A[c]	81:12 (62%)

[a] M_w (kg/mol) and PDI for P3HT and block copolymers determined by comparison to a set of monodisperse polystyrene standards. Head-to-tail regioregularity of P3HT is greater than 93% for all samples as determined from ^{1}H NMR. [b] DP ratios and P3HT content were determined by ^{1}H NMR *via* comparison of the integrated intensity of P3HT aromatic peak (6.9 ppm) and fluorene alkyl peaks (2.2 ppm). [c] P3HT81-*b*-PFTBT12 contains primarily homopolymer impurities, and therefore an estimate for block copolymer molecular weight is not provided.

The molecular weight distributions for each polymer block and corresponding homopolymer impurities can be obtained by size exclusion chromatography with UV/VIS analysis (SEC-UV/VIS) at two distinct wavelengths. The molecular weight distribution for one block was obtained by using a wavelength specific to one polymer block. 450 nm (specific to P3HT), 500 nm (specific to P3HT), and 550 nm (specific to PFTBT) were used for P3HT-*b*-PF, P3HT-*b*-PFBT, and P3HT-*b*-PFTBT, respectively. PF and PFBT exhibit no measureable absorbance at 450 and 500 nm, respectively, while P3HT exhibits no measureable absorbance at 550 nm. A comparison of the characteristics SEC-refractive index trace

(SEC-RI) of final block copolymer products produced (Figure 4 and Table I) with previous reports using similar methods (*49*, *63*) indicates that the use of an LiCl additive enables the preparation of much cleaner and higher molecular weight block copolymers. With the exception of P3HT62-*b*-PFTBT38, a clear shift in the molecular weight distribution of the final products is observed relative to the starting P3HT homopolymers. For comparison, our previous attempts at making similar all-conjugated block copolymers using similar methods (but without the LiCl additive) resulted in only modest shifts in the molecular weight distribution along with homopolymer impurities (*63*). Other reports using similar synthetic methods report the presence of significant homopolymer impurities or relatively low molecular weights for the second polymer block (*6*, *26*). The clear shift in the molecular weight distributions of the block copolymer products shown in Figure 4 indicates that little or no residual P3HT homopolymer remains, and all-conjugated block copolymers with a mass-averaged molecular weight M_w as high as 168 kg/mol (relative to polystyrene) are produced. Number-averaged molecular weights for each block estimated by SEC-RI are in relatively good agreement with ^{1}H NMR estimates of P3HT content of the final block copolymers (Table I). In the case of P3HT62-*b*-PFTBT38, the synthesis failed to produce significant amounts of block copolymer due to poor solubility of the PFTBT block and the resulting block copolymer. However, the use of a lower molecular weight P3HT macroreagent in the polycondensation reaction of PFTBT resulted in product with majority block copolymer in P3HT42-*b*-PFTBT58.

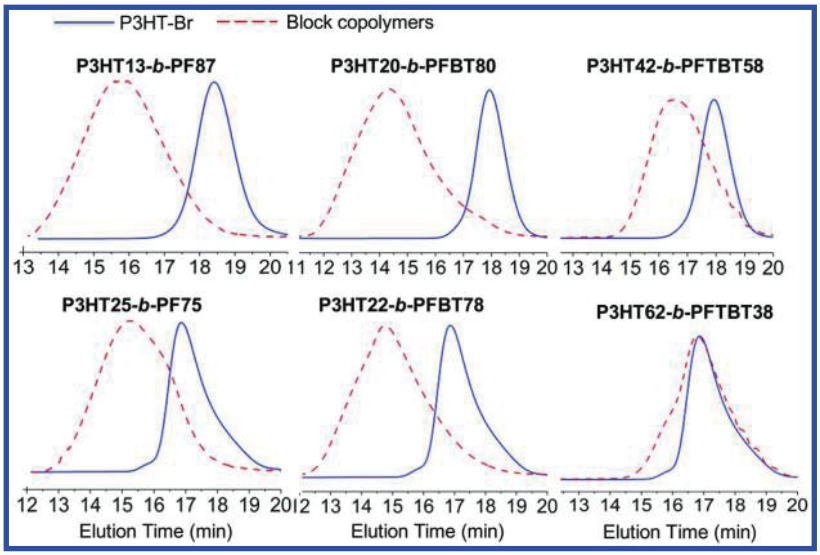

Figure 4. SEC-RI analysis of block copolymers and corresponding P3HT-Br macroreagents. Intensities are normalized for clarity. (Adapted with permission from reference (67). Copyright 2013 Royal Society of Chemistry.)

In summary, the combination of GRIM and Suzuki-Miyaura polymerization reactions can produce all-conjugated block copolymers with some degree of controllable molecular weight and block ratios. GRIM with LiCl additive provides polythiophenes with controlled end-group functionality and molecular weight while the Suzuki-Miyaura reaction has poor control over the molecular weight of the second block. Nonetheless, polycondensation reactions can be qualitatively controlled by varying reaction conditions such as concentration of reagents and reaction time as long as the resulting materials are soluble. The advantage of this strategy is that it can bypass many tedious purification steps such as column chromatography. One drawback to this method is that is limited to polymers that can be prepared by GRIM and by Suzuki-Miyaura. Thus far we have only investigated polythiophene-based all-conjugated block copolymers, but other *p*-type polymer blocks are possible through GRIM (*56*, *59*).

2.2. Synthesis of All-Conjugated Block Copolymers Using Click Coupling Reaction

While the macro-reagent approach has several practical advantages, the relative size of each polymer block cannot be precisely controlled. An alternative route to conjugated block copolymers is to couple two conjugated polymers, which have been independently synthesized, by an efficient chemical reaction. This gives better control over block lengths since each block is synthesized, purified, and characterized prior to coupling. The first donor-acceptor all-conjugated block copolymer reported in the literature was prepared by a coupling approach (*60*, *71*). In addition to material synthesis, work by Sun et al. study demonstrated all-conjugated block copolymer OPVs with near 1 % PCEs. Their synthetic route also produced all-conjugated block copolymers joined by a non-conjugated linker, which the authors hypothesized could reduce the rate of charge recombination. However, few subsequent examples of such an approach have been reported due to the challenge in the synthesis and coupling of conjugated polymers with controlled end-functionality.

Recently, our group investigated the use of copper(I)-catalyzed azide-alkyne "click" coupling to produce P3AT-*b*-PF block copolymers (*50*). Click coupling reactions, in particular copper(I) catalyzed cycloadditions, have been successfully applied as post-polymerization coupling reactions to make rod-coil block copolymers (*105–110*) and block copolythiophenes (*111*) but not previously for the preparation of all-conjugated block copolymers. This synthetic route also produces all-conjugated block copolymers joined by a flexible, non-conjugated linker.

Using a click chemistry approach for the synthesis of P3HT-*b*-PF enables systematic variation of the molecular weight of each polymer block. As shown in scheme 3, P3HT-*b*-PF is synthesized by click coupling of P3HT-alkyne and PF-N_3 in THF in the presence of Cu(I)Br and PMDETA. Details on the preparation of end-functionalized polymeric macroreagents is given in our previous publication (*50*). An excess of the PF macroreagent (20 mol % based on ^{1}H NMR ratio of repeat unit to end group) was added to ensure full reaction of the P3HT-alkyne and

to compensate for any errors in estimates of functionalization. After the reaction was complete, typically less than 8 h or overnight, the product was run through an alumina column, precipitated in hexanes, and washed with boiling hexanes to remove unreacted PF.

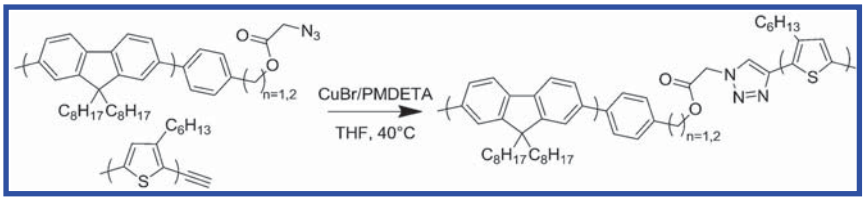

Scheme 3. Preparation of P3HT-b-PF via copper-catalyzed azide-alkyne click chemistry. (Reproduced with permission from reference (50). Copyright 2013 American Chemical Society.)

Table II. P3HT-*b*-PF Conjugated Block Copolymer Samples *via* Click Coupling Reaction. SOURCE: Adapted with permission from reference (*50*). Copyright 2013 American Chemical Society.

Sample	*Mass % P3HT by NMR*	*M_w by SEC-MALLS (kg/mol)*	*PDI*
P3HT79-*b*-PF21	79	19.0	1.22
P3HT64-*b*-PF36	64	17.0	1.27
P3HT52-*b*-PF48	52	17.0	1.53
P3HT32-*b*-PF68	32	18.0	1.38
P3HT23-*b*-PF77	23	19.0	1.50

The click chemistry reaction was carried out with 5 different combinations of P3HT-alkyne and PF-N_3 to yield a series of P3HT-*b*-PF block copolymers (Table II). Similar to the analysis for all-conjugated block copolymers *via* macro-initiator route, the composition, purity, and molecular weight distributions of the final block copolymer products can be determined by ^{1}H NMR and SEC with both MALLS and UV/VIS detection. In all cases, SEC-RI revealed a shift in the molecular weight distribution of the polymeric product relative to the starting macroreagents (see Figure 5a and Supporting Information in the original article (*50*)). A representative example of SEC-UV/VIS analysis is shown for P3HT64-*b*-PF36 in Figure 5b and 5c, and a good match in the molecular weight distributions and at two distinct wavelengths indicates pure block copolymer product with little or no residual homopolymer.

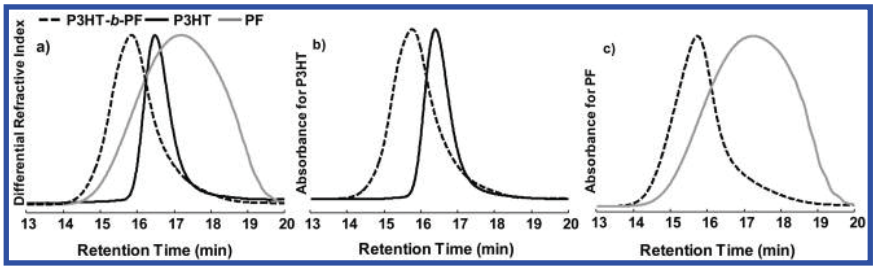

Figure 5. SEC analysis of P3HT64-b-PF36 and corresponding P3HT and PF macroreagents. a) SEC-RI analysis showing a shift in the molecular weight distribution of the final block copolymer relative to the P3HT and PF macroreagents. b) SEC-UV/VIS analysis at 450 nm showing a shift in the molecular weight distribution of the P3HT block relative to the starting P3HT macroreagent. c) SEC-UV/VIS analysis at 300 nm (corrected for the absorbance of the P3HT block) showing a shift in the molecular weight distribution of the PF block relative to starting PF-OH macroreagent. (Reproduced with permission from reference (50). Copyright 2013 American Chemical Society.)

The principle advantage of this synthetic route is the ability to characterize and/or purify the starting materials fully before the coupling reaction, and a single starting polymer may be coupled with multiple different products to give a variety of materials. However, obtaining block copolymer products free of homopolymer impurities is difficult using this route, and requires that both polymeric macroreagents have a high degree of chain-end functionality. For the P3HT-*b*-PF series above, we relied on the differential solubility of each polymer to extract homopolymer impurities, but this is not possible for many block copolymer materials. More recently, this approach was improved through the use of functionalized initiators for the synthesis of both polymer blocks (*112*). The use of functionalized initiators improves the end-group fidelity of both blocks, reducing homopolymer impurities present after coupling (*110*, *113*, *114*).

The work reviewed above demonstrates that versatile synthetic strategies exist to prepare all-conjugated block copolymers. However, challenges remain, including the preparation of block copolymers free of homopolymer impurities and the development of controlled polymerization reactions which will allow for control of the molecular weight and polydispersity of each polymer block. The majority of studies have focused on all-conjugated block copolymers with a poly(3-alkylthiophene) block, but the best performance in bulk heterojunction OPVs has been reported for alternating copolymers produced through polycondensation reactions (*115*). To improve the performance of all-conjugated block copolymer OPV, future work must focus on the development of strategies for incorporating non-thiophene polymer blocks into block copolymers.

3. Process-Dependent Nanostructures for All-Conjugated Block Copolymers

Self-assembly processes in all-conjugated block copolymers remain poorly understood. In particular, unlike for traditional coil-like polymers, crystallization and high glass-transition temperatures can impede the formation of ordered domains through micro-phase segregation. Distinguishing between micro-phase segregation and polymer crystallization in thin films requires a combination of characterization techniques. Below, we review studies exploring processing-structure relationships in P3AT-*b*-PF all-conjugated block copolymers, including their structure in solution, in the bulk, and in thin films.

3.1. Self-Assembly of Amphiphilic P3AT-*b*-PF in Solution

P3AT-*b*-PF block copolymers with one hydrophobic block and one hydrophilic block can self-assemble in solution to form micelles and vesicles. The Scherf and Advincula groups reported the first example of this in P3AT-*b*-PF block copolymers, shown in Figure 6. The P3AT side-chain was modified with a phosphonate group to make the polythiophene block hydrophilic, giving all-conjugated block copolymers that migrate to the air-water interface. The vesicles shown in Figure 6 using both a Langmuir-Blodgett (LB) method and drop casting indicate the formation of micelles and vesicles. The structures result from hydrophobic/hydrophilic interactions and π- π interaction of the hydrophobic segment PF in solutions. This is the first example reporting the self-assembly of an all-conjugated block copolymers in water. All-conjugated block copolymers with one hydrophilic block may be useful for the development of amplifying fluorescent sensors (*116*).

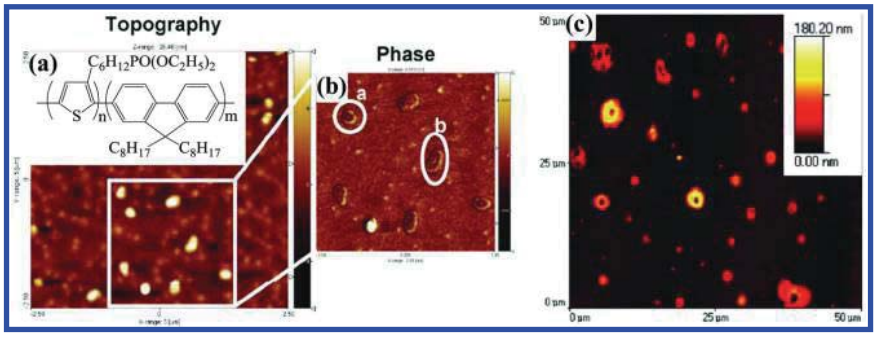

Figure 6. (a) AFM topography, (b) phase image on P3PHT-b-PF films prepared from Langmuir-Blodgett (LB) method at 5mN/m and (c) AFM contact mode image on P3PHT-b-PF films drop-cast from methanol. (Reproduced with permission from reference (45). Copyright 2008 American Chemical Society.)

In Polymer Composites for Energy Harvesting, Conversion, and Storage; Li, L., et al.;
ACS Symposium Series; American Chemical Society: Washington, DC, 2014.

3.2. Crystallinity in Thermally Treated P3HT-*b*-PF

Polymer crystallinity has a direct impact on properties relevant to performance in OPVs, such as charge-transfer mobility (*117*, *118*). For example, previous literatures report that the performance of OPVs is enhanced with increasing crystallinity of P3HT (*119*, *120*). Thus, for the application of all-conjugated block copolymers in OPVs, crystallization of both blocks may be preferred. P3HT-*b*-PF represents an excellent model system for investigating the crystallinity of both polymer blocks as a function of block ratio, molecular weight, and processing conditions. Both polymer blocks are crystalline, with a crystallization temperature of 220 °C for P3HT and 150 °C for PF. Moreover, regioregular P3HT organizes into lamellar crystalline domains with face-to-face π-π stacking between chains and lamellar stacking through the hexyl side-chains (*121*). In solution processed thin films, the preferred orientation of these crystallites can be dictated to some extent by varying processing conditions (*122*). PF exhibits crystalline, liquid crystalline, or amorphous phases depending on its processing history (*123–125*).

We explored the role of polymer block ratio, molecular weight, and processing through solvent and thermal annealing on a model series of P3HT-*b*-PF. Under thermal annealing, all samples show crystalline features which change depending on the majority block of the block copolymers. As shown in Figure 7, for a series of 5 P3HT-*b*-PF block copolymers made through click chemistry, block copolymers with high PF content show crystallinity characteristic of highly ordered PF α phase crystallites while block copolymers with a high P3HT content show exclusively P3HT crystallites with distinct (*h00*) reflection peaks. P3HT52-*b*-PF48 and P3HT32-*b*-PF68 films show some evidence for co-existence of both P3HT and PF crystallites. GISAXS patterns do not show any reflection peak for any sample in the series. These results indicate no self-assembly of P3HT-*b*-PFs under thermal annealing condition and suggest competitive crystallization is predominant. Other studies on P3HT-*b*-PF block copolymers have found similar results (*112*), including for P3HT-*b*-PF bulk powders (*63*).

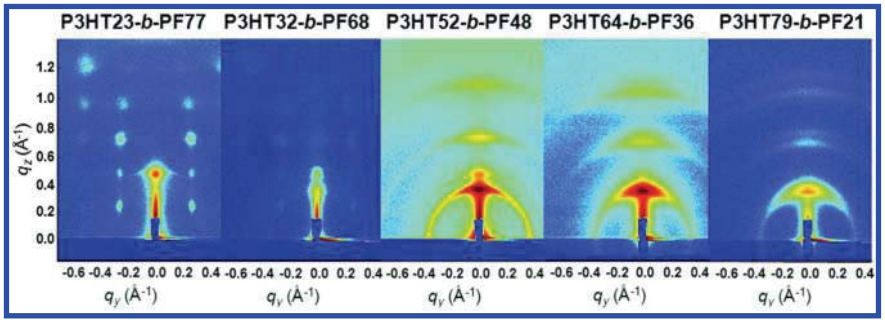

Figure 7. GIWAXS patterns for P3HT-b-PF block copolymer films after thermally annealed at 230 °C and measured at room temperature. (Reproduced with permission from reference (50). Copyright 2013 American Chemical Society.)

In Polymer Composites for Energy Harvesting, Conversion, and Storage; Li, L., et al.;
ACS Symposium Series; American Chemical Society: Washington, DC, 2014.

3.3. Lamellar Structures of Solvent-Treated P3HT-*b*-PFs

The study described in section 3.2 showed that polymer block crystallization was the predominant feature in thermally annealed P3HT-*b*-PF. Thermally annealed films did not show evidence for micro-phase segregation under GISAXS analysis. Prior work with block copolymers has demonstrated that solvent annealing can lead to qualitatively different microstructure and improved long-range ordering (*126*, *127*). Solvent vapor annealing is an effective method for encouraging micro-phase separation of both polymer blocks through increased block mobility.

In recent work, we explored solvent-annealing of a series of P3HT-*b*-PF block copolymers (*128*). We hypothesized that both thermally induced crystallite formation and the poor polymer chain mobility on rigid conjugated polymers within films hindered the self-assembly process. P3HT-*b*-PF films were annealed with chloroform vapor at room temperature. Chloroform is a good solvent for both P3HT and PF and therefore may increase polymer chain mobility during annealing. As shown in Figure 8, highly ordered reflection peaks were observed in out-of-plan direction (q_z) in both GIWAXS and GISAXS of solvent-vapor annealed films. The first order reflection peak of the structure is at $q \sim 0.15$ Å^{-1} (as shown in embedded GISAXS patterns) with a d spacing ~ 4.2 nm for all samples. This indicates the formation of lamellae which is parallel to substrate surface. Surprisingly, the spacing of lamellae is not affected by the relative ratio of polymer block sizes, which contrasts with microphase segregation observed in coil-like block copolymers (*129*). In addition, two in-plane reflection peaks at $q_y \sim 1.45$ Å^{-1} and $q_y \sim 1.63$ Å^{-1} are for planar π-π stacking of PF and P3HT, respectively. The sample with 74 wt% of P3HT shows that P3HT crystallite co-exists with self-assembled lamellae. The result supports our hypothesis that annealing with appearance of a good solvent for both blocks enhances self-assembly of all-conjugated block copolymers.

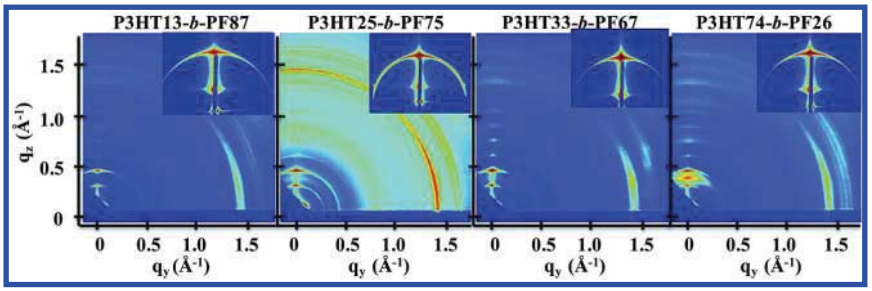

Figure 8. GIWAXS patterns and GISAXS patterns (embedded figures) for P3HT-b-PF block copolymer films after extensive chloroform vapor annealing at room temperature. All of the GISAXS patterns show the first order reflection peak at q ~ 0.15 Å-1.

In Polymer Composites for Energy Harvesting, Conversion, and Storage; Li, L., et al.;
ACS Symposium Series; American Chemical Society: Washington, DC, 2014.

We further explored variations of the processing conditions, specifically: 1) casting samples from 90 °C boiling chloroform solution followed by chloroform annealing and 2) casting samples from room temperature solution followed by thermal annealing in the presence of solvent. As shown in Figure 9, P3HT13-*b*-PF87 film cast from boiling solution shows only PF β phase (*130*) and no P3HT crystzllitazion, but P3HT crystallites form in films with increased P3HT content. In the case of thermally annealed samples, shown in Figure 10, all films show either disorganized crystallites of P3HT and PF or co-existence of two crystallites depending on the block ratios. These tests suggest high-temperature solution casting disrupts crystalline aggregates in solution, resulting in a less-crystalline, disordered film morphology. Conversely, thermal annealing after film casting enhances film crystallinity, with the predominance of P3HT or PF crystals dependent primarily on the relative block ratio.

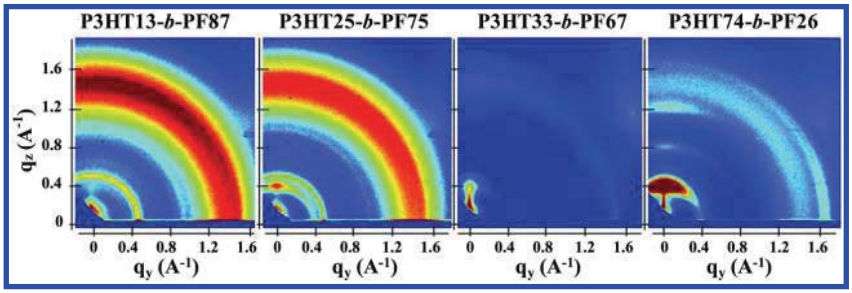

Figure 9. GIWAXS patterns for P3HT-b-PF block copolymer films cast from boiling chloroform solution and measured after extensive chloroform vapor annealing at room temperature.

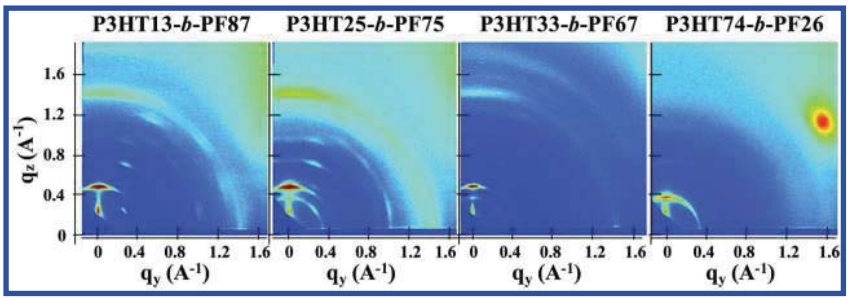

Figure 10. GIWAXS patterns for P3HT-b-PF block copolymer films after thermal annealing at 175 °C in the presence of dichlorobenzene vapor.

In summary, varying solution-casting and annealing conditions has significant impacts on the morphology of all-conjugated block copolymer films. Similar to coil-like polymers, solvent annealing can enhance self-assembly in all-conjugated block copolymers due presumably to enhanced polymer mobility. However,

thermally induced crystallites on P3HT and PF can dominate entire morphologies and suppress or compete with self-assembly processes. Also, casting from hot solvents may disrupt solution crystalline aggregates that form in solution (*131*).

While the majority of prior studies on processing dependent structure of all-conjugated BCPs have focused on the P3HT-*b*-PF system, future work will undoubtedly focus on donor-acceptor systems relevant to OPVs. Other processing approaches that have not been applied to all-conjugated block copolymers include include electrospinning, the use of textured or patterned surfaces, and ink-jet printing.

Conclusion

This article summarized recent progress in the synthesis and processing-dependent structure of P3HT-*b*-PF all-conjugated block copolymers. Both macro-reagent approaches and click coupling approaches have been applied to the synthesis of P3HT-*b*-PF. Future works will likely focus on the application of these approaches to donor-acceptor systems and on the development of controlled polymerization approaches applicable to conjugated polymer systems.

Work analyzing the processing-dependent structure of all-conjugated block copolymers has shown that P3HT-*b*-PF can self-assemble into micelles and vesicles in solution, similar to traditional block copolymer systems. In thin films, P3HT-*b*-PF exhibits competitive crystallization, with one block suppressing the crystallization of the second. The block ratio is the primary variable in determining the crystallinity of the final material. Under solvent annealing, a qualitatively different film structure is observed. P3HT-*b*-PF block copolymers self-assemble into lamellae with 4.2 nm spacing, independent of block ratio. This type of self-assembly has not been reported in any other all-conjugated BCP system, and future work will undoubtedly explore similar processing approaches to different all-conjugated block copolymer systems. Finally, varying casting and annealing conditions has a significant impact on crystalline orientation. Crystalline orientation is randomized under high-temperature solvent casting or solvent annealing.

These results provide a wealth of information on P3HT-*b*-PF and indicate potential approaches for directing the structure of all-conjugated block copolymer systems. In particular, long-term solvent annealing may lead to qualitatively different structures in other all-conjugated block copolymer systems compared with just thermal annealing. Block ratio is likely an important variable for balancing crystallinity of both blocks. However, it is unclear how all-conjugated block copolymers with one or more non-crystalline blocks will be affected by thermal and/or solvent annealing. Furthermore, variation of the side-chain structure to enhance enthalpic interaction between polymer blocks (characterized by the Flory-Huggins χ-parameter) may lead to more exotic nanostructures or a stronger driver for self-assembly.

Finally, relationships between film morphology and photovoltaic performance in block copolymer photovoltaics are only beginning to be explored. A recent study reported near 3% PCE in a block copolymer OPV and found crystallization

In Polymer Composites for Energy Harvesting, Conversion, and Storage; Li, L., et al.;
ACS Symposium Series; American Chemical Society: Washington, DC, 2014.

of the P3HT polymer block along with an edge-on orientation of polymer crystallites (*70*). Future work with BCP OPVs should aim to provide further insight on the relationship between film morphology and electronic properties, including photovoltaic performance.

Acknowledgments

This work was supported by the National Science Foundation under Grant No. CBET-1264703 and the ACS Petroleum Research Fund (Grant # 52345-DNI7). R. Verduzco acknowledges support form Louis and Peaches Owen. Research carried out in part at the Center for Functional Nanomaterials and National Synchrotron Light Source, Brookhaven National Laboratory, which is supported by the U.S. Department of Energy, Office of Basic Energy Sciences, under Contract No. DE-AC02-98CH10886. Use of Advanced Photon Source at Argonne National Laboratory was supported by the U. S. Department of Energy, Office of Science, Office of Basic Energy Sciences, under Contract No. DE-AC02-06CH11357.

References

1. Shirakawa, H.; Louis, E. J.; MacDiarmid, A. G.; Chiang, C. K.; Heeger, A. J. *J. Chem. Soc., Chem. Commun.* **1977**, 578–580.
2. Gustafsson, G.; Cao, Y.; Treacy, G. M.; Klavetter, F.; Colaneri, N.; Heeger, A. J. *Nature* **1992**, *357*, 477–479.
3. Gross, M.; Muller, D. C.; Nothofer, H.-G.; Scherf, U.; Neher, D.; Brauchle, C.; Meerholz, K. *Nature* **2000**, *405*, 661–665.
4. Yang, Y.; Heeger, A. J. *Appl. Phys. Lett.* **1994**, *64*, 1245–1247.
5. Gao, J.; Heeger, A. J.; Lee, J. Y.; Kim, C. Y. *Synth. Met.* **1996**, *82*, 221–223.
6. Carter, S. A.; Angelopoulos, M.; Karg, S.; Brock, P. J.; Scott, J. C. *Appl. Phys. Lett.* **1997**, *70*, 2067–2069.
7. Scott, J. C.; Carter, S. A.; Karg, S.; Angelopoulos, M. *Synth. Met.* **1997**, *85*, 1197–1200.
8. Sirringhaus, H.; Tessler, N.; Friend, R. H. *Science* **1998**, *280*, 1741–1744.
9. Hangarter, C. M.; Bangar, M.; Mulchandani, A.; Myung, N. V. *J. Mater. Chem.* **2010**, *20*, 3131–3140.
10. Janata, J.; Josowicz, M. *Nat. Mater.* **2003**, *2*, 19–24.
11. Facchetti, A. *Chem. Mater.* **2010**, *23*, 733–758.
12. Gunes, S.; Neugebauer, H.; Sariciftci, N. S. *Chem. Rev.* **2007**, *107*, 1324–1338.
13. Thompson, B. C.; Fréchet, J. M. J. *Angew. Chem., Int. Ed.* **2008**, *47*, 58–77.
14. Hoppe, H.; Sariciftci, N. S. *J. Mater. Res.* **2004**, *19*, 1924–1945.
15. Peet, J.; Heeger, A. J.; Bazan, G. C. *Acc. Chem. Res.* **2009**, *42*, 1700–1708.
16. Zhang, X.; Wei, S.; Haldolaarachchige, N.; Colorado, H. A.; Luo, Z.; Young, D. P.; Guo, Z. *J. Phys. Chem. C* **2012**, *116*, 15731–15740.
17. Zhang, X.; Zhu, J.; Haldolaarachchige, N.; Ryu, J.; Young, D. P.; Wei, S.; Guo, Z. *Polymer* **2012**, *53*, 2109–2120.

18. Wei, H.; Yan, X.; Li, Y.; Gu, H.; Wu, S.; Ding, K.; Wei, S.; Guo, Z. *J. Phys. Chem. C* **2012**, *116*, 16286–16293.
19. Krebs, F. C.; Gevorgyan, S. A.; Alstrup, J. *J. Mater. Chem.* **2009**, *19*, 5442–5451.
20. Nielsen, T. D.; Cruickshank, C.; Foged, S.; Thorsen, J.; Krebs, F. C. *Sol. Energy Mater. Sol. Cells* **2010**, *94*, 1553–1571.
21. Krebs, F. C.; Jørgensen, M.; Norrman, K.; Hagemann, O.; Alstrup, J.; Nielsen, T. D.; Fyenbo, J.; Larsen, K.; Kristensen, J. *Sol. Energy Mater. Sol. Cells* **2009**, *93*, 422–441.
22. Chen, W.; Xu, T.; He, F.; Wang, W.; Wang, C.; Strzalka, J.; Liu, Y.; Wen, J.; Miller, D. J.; Chen, J.; Hong, K.; Yu, L.; Darling, S. B. *Nano Lett.* **2011**, *11*, 3707–3713.
23. Scharber, M. C.; Mühlbacher, D.; Koppe, M.; Denk, P.; Waldauf, C.; Heeger, A. J.; Brabec, C. J. *Adv. Mater.* **2006**, *18*, 789–794.
24. Erb, T.; Zhokhavets, U.; Gobsch, G.; Raleva, S.; Stühn, B.; Schilinsky, P.; Waldauf, C.; Brabec, C. J. *Adv. Funct. Mater.* **2005**, *15*, 1193–1196.
25. Zhokhavets, U.; Erb, T.; Gobsch, G.; Al-Ibrahim, M.; Ambacher, O. *Chem. Phys. Lett.* **2006**, *418*, 347–350.
26. Vandewal, K.; Himmelberger, S.; Salleo, A. *Macromolecules* **2013**, *46*, 6379–6387.
27. Guo, X.; Zhou, N.; Lou, S. J.; Smith, J.; Tice, D. B.; Hennek, J. W.; Ortiz, R. P.; Navarrete, J. T. L.; Li, S.; Strzalka, J.; Chen, L. X.; Chang, R. P. H.; Facchetti, A.; Marks, T. J. *Nat. Photonics* **2013**, *7*, 825–833.
28. Chen, H.-Y.; Hou, J.; Zhang, S.; Liang, Y.; Yang, G.; Yang, Y.; Yu, L.; Wu, Y.; Li, G. *Nat. Photonics* **2009**, *3*, 649–653.
29. Son, H. J.; He, F.; Carsten, B.; Yu, L. *J. Mater. Chem.* **2011**, *21*, 18934–18945.
30. Botiz, I.; Darling, S. B. *Macromolecules* **2009**, *42*, 8211–8217.
31. Yin, W.; Dadmun, M. *ACS Nano* **2011**, *5*, 4756–4768.
32. Kietzke, T. *Adv. OptoElectron.* **2007**, 1–15.
33. Gregg, B. A.; Hanna, M. C. *J. Appl. Phys.* **2003**, *93*, 3605–3614.
34. Nayak, P. K.; Narasimhan, K. L.; Cahen, D. *J. Phys. Chem. Lett.* **2013**, *4*, 1707–1717.
35. McNeill, C. R.; Greenham, N. C. *Adv. Mater.* **2009**, *21*, 3840–3850.
36. Hoppe, H.; Sariciftci, N. S.; Meissner, D. *Mol. Cryst. Liq. Cryst.* **2002**, *385*, 113–119.
37. Chen, W.; Nikiforov, M. P.; Darling, S. B. *Energy Environ. Sci.* **2012**, *5*, 8045–8074.
38. Hoppe, H.; Sariciftci, N. S. *J. Mater. Chem.* **2006**, *16*, 45–61.
39. Peet, J.; Soci, C.; Coffin, R. C.; Nguyen, T. Q.; Mikhailovsky, A.; Moses, D.; Bazan, G. C. *Appl. Phys. Lett.* **2006**, *89*, 252105–3.
40. Moon, J. S.; Takacs, C. J.; Cho, S.; Coffin, R. C.; Kim, H.; Bazan, G. C.; Heeger, A. J. *Nano Lett.* **2010**, *10*, 4005–4008.
41. Perez, L. A.; Chou, K. W.; Love, J. A.; van der Poll, T. S.; Smilgies, D.-M.; Nguyen, T.-Q.; Kramer, E. J.; Amassian, A.; Bazan, G. C. *Adv. Mater.* **2013**, *24*, 6305.

42. He, X.; Gao, F.; Tu, G.; Hasko, D.; Huüttner, S.; Steiner, U.; Greenham, N. C.; Friend, R. H.; Huck, W. T. S. *Nano Lett.* **2010**, *10*, 1302–1307.
43. Slota, J. E.; He, X. M.; Huck, W. T. S. *Nano Today* **2010**, *5*, 231–242.
44. Moungthai, S.; Mahadevapuram, N.; Ruchhoeft, P.; Stein, G. E. *ACS Appl. Mater. Interfaces* **2012**, *4*, 4015–4023.
45. Scherf, U.; Gutacker, A.; Koenen, N. *Acc. Chem. Res.* **2008**, *41*, 1086–1097.
46. Tseng, Y.-C.; Darling, S. B. *Polymers* **2010**, *2*, 470–489.
47. Bates, F. S.; Fredrickson, G. H. *Phys. Today* **1999**, *52*, 32–38.
48. Park, C.; Yoon, J.; Thomas, E. L. *Polymer* **2003**, *44*, 6725–6760.
49. Sommer, M.; Komber, H.; Huettner, S.; Mulherin, R.; Kohn, P.; Greenham, N. C.; Huck, W. T. S. *Macromolecules* **2012**, *45*, 4142–4151.
50. Smith, K. A.; Lin, Y.-H.; Dement, D. B.; Strzalka, J.; Darling, S. B.; Pickel, D. L.; Verduzco, R. *Macromolecules* **2013**, *46*, 2636–2645.
51. Sommer, M.; Huettner, S.; Thelakkat, M. *J. Mater. Chem.* **2010**, *20*, 10788–10797.
52. Darling, S. B. *Energy Environ. Sci.* **2009**, *2*, 1266–1273.
53. Botiz, I.; Schaller, R. D.; Verduzco, R.; Darling, S. B. *J. Phys. Chem.C* **2011**, *115*, 9260–9266.
54. Mulherin, R. C.; Jung, S.; Huettner, S.; Johnson, K.; Kohn, P.; Sommer, M.; Allard, S.; Scherf, U.; Greenham, N. C. *Nano Lett.* **2011**, *11*, 4846–4851.
55. Woody, K. B.; Leever, B. J.; Durstock, M. F.; Collard, D. M. *Macromolecules* **2011**, *44*, 4690–4698.
56. Wu, S.; Bu, L.; Huang, L.; Yu, X.; Han, Y.; Geng, Y.; Wang, F. *Polymer* **2009**, *50*, 6245–6251.
57. Lai, Y.-C.; Ohshimizu, K.; Takahashi, A.; Hsu, J.-C.; Higashihara, T.; Ueda, M.; Chen, W.-C. *J. Polym. Sci., Part A: Polym. Chem.* **2011**, *49*, 2577–2587.
58. Ouhib, F.; Khoukh, A.; Ledeuil, J.-B.; Martinez, H.; Desbrières, J.; Dagron-Lartigau, C. *Macromolecules* **2008**, *41*, 9736–9743.
59. Ohshimizu, K.; Takahashi, A.; Higashihara, T.; Ueda, M. *J. Polym. Sci., Part A: Polym. Chem.* **2011**, *49*, 2709–2714.
60. Sun, S.-S.; Zhang, C.; Ledbetter, A.; Choi, S.; Seo, K.; Carl, E.; Bonner, J.; Drees, M.; Sariciftci, N. S. *Appl. Phys. Lett.* **2007**, *90*, 043117.
61. Chen, X. L.; Jenekhe, S. A. *Macromolecules* **1996**, *29*, 6189–6192.
62. Xiao, X.; Fu, Y.; Sun, M.; Li, L.; Bo, Z. *J. Polym. Sci., Part A: Polym. Chem.* **2007**, *45*, 2410–2424.
63. Verduzco, R.; Botiz, I.; Pickel, D. L.; Kilbey, S. M.; Hong, K.; Dimasi, E.; Darling, S. B. *Macromolecules* **2011**, *44*, 530–539.
64. Orilall, M. C.; Wiesner, U. *Chem. Soc. Rev.* **2011**, *40*, 520–535.
65. Matsen, M. W.; Bates, F. S. *Macromolecules* **1996**, *29*, 7641–7644.
66. Nakabayashi, K.; Mori, H. *Macromolecules* **2012**, *45*, 9618–9625.
67. Lin, Y.-H.; Smith, K. A.; Kempf, C. N.; Verduzco, R. *Polym. Chem.* **2013**, *4*, 229–232.
68. Ku, S.-Y.; Brady, M. A.; Treat, N. D.; Cochran, J. E.; Robb, M. J.; Kramer, E. J.; Chabinyc, M. L.; Hawker, C. J. *J. Am. Chem. Soc.* **2012**, *134*, 16040–16046.
69. Wang, J.; Ueda, M.; Higashihara, T. *ACS Macro Lett.* **2013**, *2*, 506–510.

70. Guo, C.; Lin, Y.-H.; Witman, M. D.; Smith, K. A.; Wang, C.; Hexemer, A.; Strzalka, J.; Gomez, E. D.; Verduzco, R. *Nano Lett.* **2013**, *13*, 2957–2963.
71. Zhang, C.; Choi, S.; Haliburton, J.; Cleveland, T.; Li, R.; Sun, S.-S.; Ledbetter, A.; Bonner, C. E. *Macromolecules* **2006**, *39*, 4317–4326.
72. Hinkens, D. M.; Chen, Q.; Siddiki, M. K.; Gosztola, D.; Tapsak, M. A.; Qiao, Q.; Jeffries-El, M.; Darling, S. B. *Polymer* **2013**, *54*, 3510–3520.
73. Wu, P.-T.; Ren, G.; Li, C.; Mezzenga, R.; Jenekhe, S. A. *Macromolecules* **2009**, *42*, 2317–2320.
74. Wu, P.-T.; Ren, G.; Kim, F. S.; Li, C.; Mezzenga, R.; Jenekhe, S. A. *J. Polym. Sci., Part A: Polym. Chem.* **2010**, *48*, 614–626.
75. Yu, X.; Yang, H.; Wu, S.; Geng, Y.; Han, Y. *Macromolecules* **2012**, *45*, 266–274.
76. Wu, Z.-Q.; Liu, D.-F.; Wang, Y.; Liu, N.; Yin, J.; Zhu, Y.-Y.; Qiu, L.-Z.; Ding, Y.-S. *Polym. Chem.* **2013**, *4*, 4588–4595.
77. Yassar, A.; Miozzo, L.; Gironda, R.; Horowitz, G. *Prog. Polym. Sci.* **2013**, *38*, 791–844.
78. Topham, P. D.; Parnell, A. J.; Hiorns, R. C. *J. Polym. Sci., Part B: Polym. Phys.* **2011**, *49*, 1131–1156.
79. Segalman, R. A.; McCulloch, B.; Kirmayer, S.; Urban, J. J. *Macromolecules* **2009**, *42*, 9205–9216.
80. Botiz, I.; Darling, S. B. *Mater. Today* **2010**, *13*, 42–51.
81. Gutacker, A.; Adamczyk, S.; Helfer, A.; Garner, L. E.; Evans, R. C.; Fonseca, S. M.; Knaapila, M.; Bazan, G. C.; Burrows, H. D.; Scherf, U. *J. Mater. Chem.* **2010**, *20*, 1423–1430.
82. Yokozawa, T.; Suzuki, R.; Nojima, M.; Ohta, Y.; Yokoyama, A. *Macromol. Rapid Commun.* **2011**, *32*, 801–806.
83. Tu, G.; Li, H.; Forster, M.; Heiderhoff, R.; Balk, L. J.; Sigel, R.; Scherf, U. *Small* **2007**, *3*, 1001–1006.
84. Scherf, U.; Adamczyk, S.; Gutacker, A.; Koenen, N. *Macromol. Rapid Commun.* **2009**, *30*, 1059–1065.
85. Javier, A. E.; Varshney, S. R.; McCullough, R. D. *Macromolecules* **2010**, *43*, 3233–3237.
86. Hollinger, J.; Jahnke, A. A.; Coombs, N.; Seferos, D. S. *J. Am. Chem. Soc.* **2010**, *132*, 8546–8547.
87. Ge, J.; He, M.; Qiu, F.; Yang, Y. *Macromolecules* **2010**, *43*, 6422–6428.
88. Zhang, Y.; Tajima, K.; Hashimoto, K. *Macromolecules* **2009**, *42*, 7008–7015.
89. Zhang, Y.; Tajima, K.; Hirota, K.; Hashimoto, K. *J. Am. Chem. Soc.* **2008**, *130*, 7812–7813.
90. Chueh, C.-C.; Higashihara, T.; Tsai, J.-H.; Ueda, M.; Chen, W.-C. *Org. Electron.* **2009**, *10*, 1541–1548.
91. He, M.; Zhao, L.; Wang, J.; Han, W.; Yang, Y.; Qiu, F.; Lin, Z. *ACS Nano* **2010**, *4*, 3241–3247.
92. Kiriy, A.; Senkovskyy, V.; Sommer, M. *Macromol. Rapid Commun.* **2011**, *32*, 1503–1517.
93. Okamoto, K.; Luscombe, C. K. *Polym. Chem.* **2011**, *2*, 2424–2434.

94. Verswyvel, M.; Verstappen, P.; De Cremer, L.; Verbiest, T.; Koeckelberghs, G. *J. Polym. Sci., Part A: Polym. Chem.* **2011**, *49*, 5339–5349.
95. Mori, D.; Benten, H.; Ohkita, H.; Ito, S.; Miyake, K. *ACS Appl. Mater. Interfaces* **2012**, *4*, 3325–3329.
96. Lohwasser, R. H.; Thelakkat, M. *Macromolecules* **2011**, *44*, 3388–3397.
97. Kochemba, W. M.; Kilbey, S. M.; Pickel, D. L. *J. Polym. Sci. Part A: Polym. Chem.* **2012**, *50*, 2762–2769.
98. Takahashi, A.; Rho, Y.; Higashihara, T.; Ahn, B.; Ree, M.; Ueda, M. *Macromolecules* **2010**, *43*, 4843–4852.
99. Loewe, R. S.; Ewbank, P. C.; Liu, J. S.; Zhai, L.; McCullough, R. D. *Macromolecules* **2001**, *34*, 4324–4333.
100. Herguth, P.; Jiang, X.; Liu, M. S.; Jen, A. K. Y. *Macromolecules* **2002**, *35*, 6094–6100.
101. Kim, Y.; Cook, S.; Choulis, S. A.; Nelson, J.; Durrant, J. R.; Bradley, D. D. C. *Chem. Mater.* **2004**, *16*, 4812–4818.
102. Calabrese, A.; Schimperna, G.; Po, R.; Yohannes, T.; Debebe, S. E.; Tinti, F.; Camaioni, N. *J. Appl. Phys.* **2011**, *110*, 113106.
103. Lee, W.-Y.; Cheng, K.-F.; Wang, T.-F.; Chueh, C.-C.; Chen, W.-C.; Tuan, C.-S.; Lin, J.-L. *Macromol. Chem. Phys.* **2007**, *208*, 1919–1927.
104. Lee, W.-Y.; Cheng, K.-F.; Wang, T.-F.; Chen, W.-C.; Tsai, F.-Y. *Thin Solid Films* **2010**, *518*, 2119–2123.
105. Tao, Y.; McCulloch, B.; Kim, S.; Segalman, R. A. *Soft Matter* **2009**, *5*, 4219–4230.
106. Kamps, A. C.; Fryd, M.; Park, S.-J. *ACS Nano* **2012**, *6*, 2844–2852.
107. Benanti, T. L.; Kalaydjian, A.; Venkataraman, D. *Macromolecules* **2008**, *41*, 8312–8315.
108. Urien, M.; Erothu, H.; Cloutet, E.; Hiorns, R. C.; Vignau, L.; Cramail, H. *Macromolecules* **2008**, *41*, 7033–7040.
109. Wu, Z.-Q.; Ono, R. J.; Chen, Z.; Li, Z.; Bielawski, C. W. *Polym. Chem.* **2011**, *2*, 300–302.
110. Kempf, C. N.; Smith, K. A.; Pesek, S. L.; Li, X.; Verduzco, R. *Polym. Chem.* **2013**, *4*, 2158–2163.
111. Smeets, A.; Willot, P.; De Winter, J.; Gerbaux, P.; Verbiest, T.; Koeckelberghs, G. *Macromolecules* **2011**, *44*, 6017–6025.
112. Smith, K. A.; Pickel, D. L.; Yager, K.; Kisslinger, K.; Verduzco, R. *J. Polym. Sci., Part A: Polym. Chem.* **2014**, *52*, 154–163.
113. Yokozawa, T.; Yokoyama, A. *Chem. Rev.* **2009**, *109*, 5595–5619.
114. Bronstein, H. A.; Luscombe, C. K. *J. Am. Chem. Soc.* **2009**, *131*, 12894–12895.
115. Carlé, J. E.; Krebs, F. C. *Sol. Energy Mater. Sol. Cells* **2013**, *119*, 309–310.
116. Thomas, S. W.; Joly, G. D.; Swager, T. M. *Chem. Rev.* **2007**, *107*, 1339–1386.
117. Darling, S. B.; Sternberg, M. *J. Phys. Chem. B* **2009**, *113*, 6215–6218.
118. Noriega, R.; Rivnay, J.; Vandewal, K.; Koch, F. P. V.; Stingelin, N.; Smith, P.; Toney, M. F.; Salleo, A. *Nat. Mater.* **2013**, *12*, 1038.

119. Abu-Zahra, N.; Algazzar, M. *J. Sol. Energy Eng.* **2013**, *136*, 021023–021023.
120. Chen, D.; Nakahara, A.; Wei, D.; Nordlund, D.; Russell, T. P. *Nano Lett.* **2010**, *11*, 561–567.
121. Sirringhaus, H.; Brown, P. J.; Friend, R. H.; Nielsen, M. M.; Bechgaard, K.; Langeveld-Voss, B. M. W.; Spiering, A. J. H.; Janssen, R. A. J.; Meijer, E. W.; Herwig, P.; de Leeuw, D. M. *Nature* **1999**, *401*, 685–688.
122. Kline, R. J.; McGehee, M. D.; Kadnikova, E. N.; Liu, J.; Fréchet, J. M. J.; Toney, M. F. *Macromolecules* **2005**, *38*, 3312–3319.
123. Chen, S. H.; Su, A. C.; Chen, S. A. *J. Phys. Chem. B* **2005**, *109*, 10067–10072.
124. Grell, M.; Bradley, D. D. C.; Ungar, G.; Hill, J.; Whitehead, K. S. *Macromolecules* **1999**, *32*, 5810–5817.
125. Peet, J.; Brocker, E.; Xu, Y.; Bazan, G. C. *Adv. Mater.* **2008**, *20*, 1882–1885.
126. Sinturel, C.; Vayer, M.; Morris, M.; Hillmyer, M. A. *Macromolecules* **2013**, *46*, 5399–5415.
127. Darling, S. B. *Prog. Polym. Sci.* **2007**, *32*, 1152–1204.
128. Lin, Y.-H.; Yager, K. G.; Stewart, B.; Verduzco, R. *Soft Matter* **2014**, *10*, 3817.
129. Register, R. A. *Nat. Nanotechnol.* **2013**, *8*, 618–619.
130. Chen, S. H.; Su, A. C.; Su, C. H.; Chen, S. A. *Macromolecules* **2005**, *38*, 379–385.
131. Kiriy, N.; Jähne, E.; Kiriy, A.; Adler, H.-J. *Macromol. Symp.* **2004**, *210*, 359–367.